Fine-tuning of solid-state thermoresponsive behaviour of various LCST showing organic-inorganic hybrid systems

Surabhi Gupta

Japan Advanced Institute of Science and Technology

Doctoral Dissertation

Fine-tuning of solid-state thermoresponsive behaviour of various LCST showing organic-inorganic hybrid systems

Surabhi Gupta

Supervisor: Professor Noriyoshi Matsumi

Graduate School of Advanced Science and Technology
Japan Advanced Institute of Science and Technology
Material Science
September 2019

Fine-tuning of solid-state thermoresponsive behaviour of various LCST showing organic-inorganic hybrid systems

Abstract

Stimuli responsive properties of smart polymers have gained much attention in the recent past. Over the top, thermosensitive materials have already rendered much applications in the field of biomedical and chemistry with highly importance projected in the future than it has ever been in the past. Nowadays, environmentally benign "green" solvents ionic liquids with their enormous database of distinguished cationic and anionic counterparts have enabled the researchers over the globe to invest more time into their future applications. There have been reports about ionic liquids showing thermoresponsive properties as well, in addition to polymers. Considering the vitality of these smart materials, the present research will be addressing synthesis and study of thermoresponsive properties of various polymer-based/ ionic liquid based/ and their copolymer based materials and their tunability over critical solution temperatures.

The primary aim of this thesis work is to focus on the thermosensitivity and tunability of various polymer and ionic liquid system. In the present thesis, thermoresponsive property is examined on three kinds of states: (1) Solid-supported LCST showing materials, (2) LCST showing hydrogels and (3) LCST in liquid-liquid equilibria-Phase transitions of imidazolium based ionic liquids in water. LCST showing hydrogels- Further, dimensionally controlled plasmonic nanoparticles will be embedded into thermoresponsive PNIPAM copolymerized with polymerizable ionic liquids. Au and Ag both acts as tuning agents for phase transitions of these hydrogels. **Chapter 1** opens up to the introduction of thermoresponsive property with respect to polymers and ionic liquids in detail. With a brief introduction about thermoresponsive phase transitions and its types, mechanism to critical solution temperature (CST) and applications corresponding to CST have been discussed.

In **Chapter 2**, the research is directed towards improving the tuning of LCST behaviour of oxazoline based thermoresponsive copolymer and creating a solid-supported hybrid material from it. The chapter describes the synthesis of novel sol-gel hybrids using thermoresponsive copolymer of 2-ethyl-2-oxaoline and 2-isoporopyl-2-oxazoline with tetramethylorthosilicate as the silicate compound. It also reports the method to fine-tune the thermoresponsive property of these hybrids.

Chapter 3 describes another method to form solid-supported LCST showing materials utilizing silicon wafers and polyoxazoline as the thermoresponsive material. In this work, silicon wafers were exposed to extreme acidic conditions to covalently bind with the thermosensitive polymer of 2-ethyl-

2-oxazoline. The system works as a solid-supported phase gradient.

Next, focus was made to target the applications shown by the formation of hydrogels and nanoparticles along with the thermosensitivity due to polymers. Hence, PNIPAM was copolymerized with different imidazolium based ionic liquids such as 1-allyl-3-octylimidazolium bromide and 1-hexyl-3-methyl imidazolium acrylate with tunable properties in **chapter 4** and the corresponding in-situ polymerization was done using Ag and Au nanoparticles. How the size of nanoparticles and structure of IL play a major role in LCST tunability was investigated.

Further, attention was made to study liquid-liquid phase systems in **chapter 5**. Hence, room temperature imidazolium-based ionic liquids was found to exhibit LCST and UCST properties. A more advance, superior and informative technique which is electrochemical impedance spectroscopy was used as the diagnostic tool to evaluate the phase transition temperature as clear visualization of the separation cannot be observed optically. Factors affecting the CST in ionic liquids and its mechanism was scrutinized using Kamlet-Taft parameter studies. Also, COSMO-RS simulations were carried out which suggested a procedure to predict the occurrence of phase transitions, and if so, what type in ILs

Lastly, **chapter 6** chapter summarized the findings of each chapter. It also gave an outlook towards future for the utilization of these materials.

Keywords: Thermoresponsive polymers, Lower Critical Solution Temperature (LCST), Ionic Liquids (ILs), sol-gel materials, plasmonic nanoparticles, nanoparticles, organic-inorganic hybrids, ionic liquids

Preface

The present dissertation is submitted for the Degree of Doctor of Philosophy at Japan Advanced Institute of Science and Technology, Japan. The dissertation is consolidation of results of the works on the topic "Fine-tuning of solid-state thermoresponsive behaviour of various LCST showing organic-inorganic hybrids" under the direction of Prof. Noriyoshi Matsumi at the School of Materials Science, Japan Advanced Institute of Science and Technology during October 2016-September 2019.

Thermoresponsive polymers have a distinctive property to undergo reversible phase transition on the application of heat. The property has its widespread applications ranging from biomedical fields like drug delivery, tissue engineering or sensing to physical separation and purification media to energy storage devices like electrolytes in batteries. The property hence, needs to be tuned for its temperature to be used in varied application by tuning agents. The author's main focus is to fine-tune the phase transitions of thermoresponsive polymers like polyoxazoline and poly(N-isopropylacrylamide) by preparing sol-gel materials and adding metal nanoparticles, respectively. Also, "green solvents" ionic liquids are capable to show the transitions. The authors also studied the factors effecting the transition for imidazolium based ionic liquids and found out a simulative way to predict the property. Successful completion of this research would help in understanding the interface of these systems with water for thermal management of devices.

The work presented in this thesis covers the synthesis and characterization of thermoresponsive polymer system and materials used like ionic liquids, gold nanoparticles, and inorganic silicate hybrids for their fine-tuning of phase transition behavior for thermal management of devices. Finally the conclusions and future prospects of the studies are summarized in the final chapter. To the best of my knowledge, the work is original and no part of the thesis has been plagiarized.

Advanced School of Science and Technology Surabhi Gupta

Japan Advanced Institute of Science and Technology

September 2019

Acknowledgement

Firstly, the author expresses her sincere gratitude to the supervisor *Prof. Noriyoshi Matsumi*, School of Materials Science, Japan Advanced Institute of Science and Technology, for his kind guidance, valuable suggestions and heartfelt encouragements throughout this work. I am thankful to him for his patience, motivation and immense knowledge.

I would also like to thank the members of my Review committee *Assoc. Prof. Kazuaki Matsumura* (JAIST), *Assoc. Prof. Shun Nishimura* (JAIST), *Assoc. Prof. Yuki Nagao* (JAIST) and *Prof. Toshiyuki Oyama* (Yokohama National University), who have spent their valuable time to read my thesis and gave valuable comments and remarks to enhance the quality of my thesis from various perspectives.

The author is thankful to *Assos. Prof. Keiko Miyabayashi*, Faculty of Engineering - Department of Applied Chemistry and Biochemical Engineering, Shizuoka University (Hamamatsu Campus), Japan. for giving her an opportunity to join their team as intern and carry out experiments in the field of fuel cells during minor research.

The author also takes an opportunity to thank *Ass. Prof. Raman Vedarajan* (now working as Scientist in ARCI, Centre for fuel cell technology, India) for his guidance and encouragement at a professional and personal level. I am also grateful to other lab members and friends, for their valuable inputs, cooperation and stimulating discussions throughout my time at JAIST.

I dedicate this thesis to my father *Mr. Harish Gupta (Father-in-law Mr. Mahendra Pal Singh*) and my mother *Mrs. Rajni Gupta (mother-in-law Mrs. Sheela Singh*), whose blessings have helped me to achieve success in my life. Even being far away, they were always morally, mentally and spiritually with me, supporting and encouraging every step of this journey.

I also dedicate this degree to my husband *Dr. Ankit Singh*, for his constant support, relentless encouragement and his love & care at all times. Finally, the author expresses his humble gratitude to the Almighty for all the good things.

Advanced School of Science and Technology Surabhi Gupta

Japan Advanced Institute of Science and Technology

September 2019

Thesis Outline

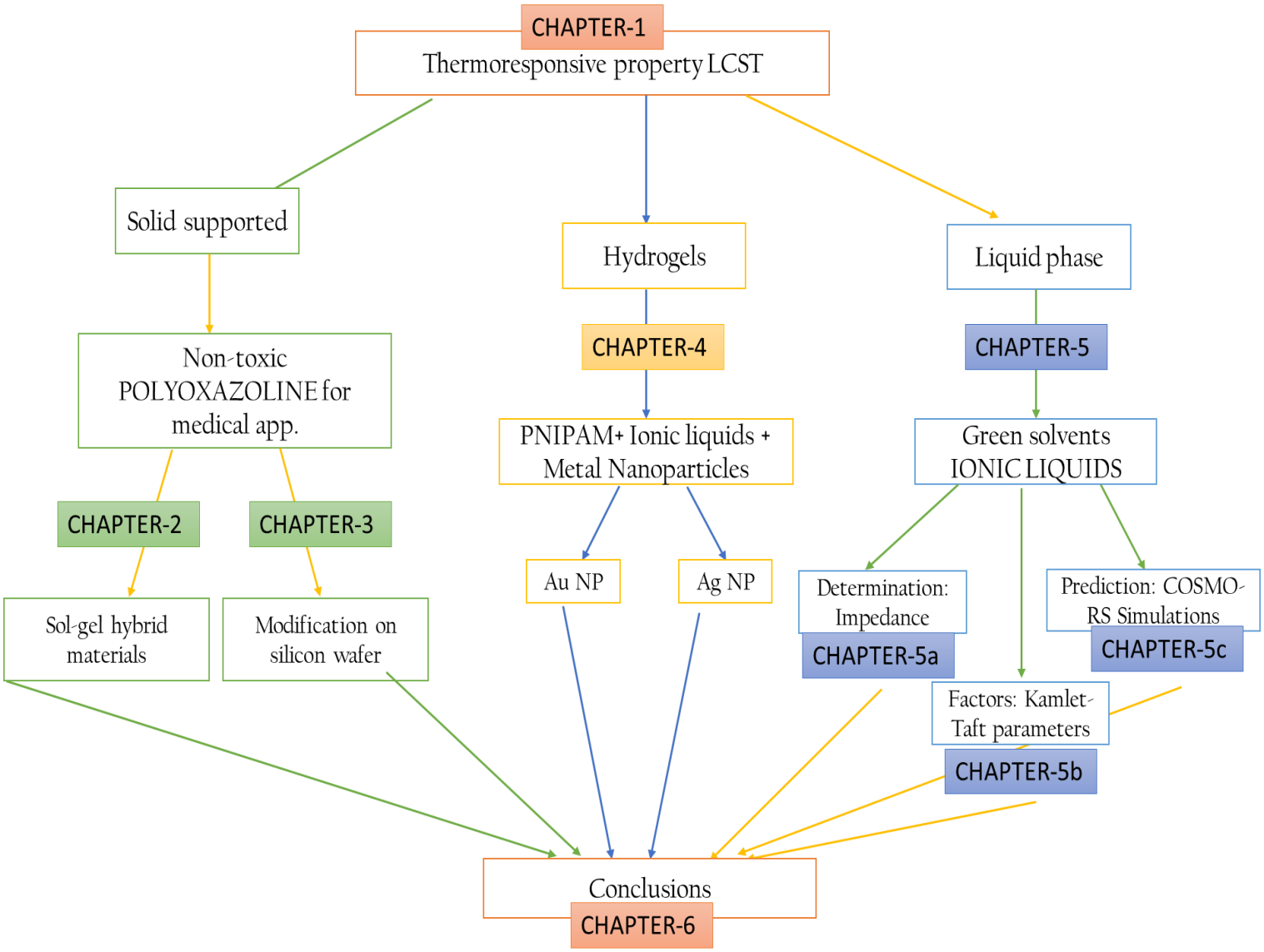

Table of Contents

List of Figures

CHAPTER 1: INTRODUCTION TO THERMORESPONSIVE PROPERTY

CHAPTER 2: FINE-TUNING OF LCST BEHAVIOR OF OXAZOLINE COPOLYMER BASED ORGANIC-INORGANIC HYBRIDS AS SOLID-SUPPORTED SOL-GEL MATERIALS

CHAPTER 3: SILICON WAFER MODIFICATION WITH THERMORESPONSIVE OXAZOLINE BASED COPOLYMER AS SOLID-SUPPORTED PHASE GRADIENTS

Fig. 2. Schematic representation of the formation of modified silicon wafers.

Fig. 3. FT-IR spectra for bare Si (black), Si wafer exposed to Piranha solution (red) and polymer modified silicon wafer (blue).

Fig. 4. Deconvoluted XPS spectra for (a) Si and (b) N for the polymer modified silicon wafer.

Fig. 5. DSC profile of the silyl-terminated polyoxazoline.

Fig. 6. Contact angle measurements of uncoated silicon wafer (Bare Si), and polymer modified Si surface sonicated for minutes 2, 5, 10 and 20 after film formation.

Fig. 7. Graphical illustration showing solid-supported thermoresponsive polymer modified silicon wafer for thermal devices.

CHAPTER 4: CONTROLLED PHASE BEHAVIOUR OF THERMALLY SENSITIVE POLY(N-ISOPROPYLACRYLAMIDE/IONIC LIQUID) HYDROGELS WITH EMBEDDED Au AND Ag NANOPARTICLES

Fig 1. TEM analysis and size distributions for gold nanoparticles (a-f: sample 1-6)

Fig 2. TEM analysis and size distributions for silver nanoparticles (g-i: sample 7-9)

Fig 3. ^{1}H-NMR spectrum of (a) Au@PNIPAM-co-AMImCl, (b) Au@PNIPAM-co-HMImAcr, (c) Au@PNIPAM-co-AOImBr and (d) Au@PNIPAM-co-AOImTFSI.

Fig 4. ^{1}H-NMR spectrum of (a) Ag@PNIPAM-co-AMImCl

Fig 5. (a) Images of the Au@PNIPAM-co-AMImCl when the Au NP size is 17.45 nm, 20.00 nm, 23.44 nm, 24.33 nm. (b) TEM analysis of Au-17.45@PNIPAM-co-AMImCl

Fig 6. Visual images for LCST determination of Au@PNIPAM-co-AMImCl. (a) 50 w/v % aqueous solution after sonication at room temperature, (b) heated at 75 ^{o}C for 10 minutes, (c) decreased the temperature to 40 ^{o}C, (d) solution cooled completely to room temperature.

Fig 7. DSC profiles for LCST determination of (a) Au@PNIPAM-co-AOImTFSI, (b) Au@PNIPAM-co-AOImBr, (c) Au@PNIPAM-co-HMImAcr and (d) Au@PNIPAM-co-AMImCl. (in graph - Au is plotted by varying the size of nanoparticles)

Fig 8. DSC profiles for LCST determination of Ag@PNIPAM-co-IL where Ag size is (a) 31.36 nm, (b) 41.00 nm and (c) 45.76 nm

Fig 9. 3-D plot depicting the simultaneous dependence of type of IL in copolymers and size of Au on LCST of Au NP induced copolymers.

Fig 10. 3-D plot depicting the simultaneous dependence of type of IL in copolymers and size of Ag on LCST of Au NP induced copolymers.

Fig. 11. Images of swelling/de-swelling of Au-20.00@PNIPAM-co-AMImCl at different time intervals.

Fig. 12. Swelling/shrinking abilities of Au-23.66@PNIPAM-co-HMImAcr

Fig. 13. SEM images of de-swelling (a-Au-24.33@PNIPAM-co-HMImAcr; c- Au-24.33@PNIPAM-co-AOImTFSI) and swelling (b-Au-24.33@PNIPAM-co-HMImAcr; d- Au-24.33@PNIPAM-co-AOImTFSI) after 24 hours.

Fig. 14. Swelling/ shrinking images of Au-24.33@PNIPAM-co-AOImBr below/ above LCST.

Fig. 15. Images of swelling and shrinking of Ag-31.36@PNIPAM-co-HMImAcr below and above its LCST.

Fig. 16. Graphical abstract representing the role of nanoparticle size in the nanoparticles embedded PNIPAM based hydrogels using polymerized ionic liquids.

CHAPTER 5: CAN WE PREDICT THE CRITICAL SOLUTION TEMPERATURE (CST) FOR IMIDAZOLIUM-BASED IONIC LIQUIDS?

Fig. 1. FT-IR spectrum of HMImBr.

Fig. 2. ^{1}H-NMR of HMImBr.

Fig. 3. Schematic representation of the cell-setup for the impedance spectroscopy

Fig. 4 (a) Image of 50% w/w HMImBr/water at room temperature (b) image of 50% w/w HMImBr/water after 2 days at 4 ^{o}C.

Fig. 5. UV-Visible spectroscopic analysis for 50% w/w HMImBr in water.

Fig 6. Bode phase for PEIS experiment for 50 wt% HMImBr-water electrolyte system.

Fig. 7. Circuit obtained by curve fitting for PEIS experiment for 50 wt% HMImBr-water electrolyte system. The green color represents the total solution resistance, red stands for ionic liquid and blue portrays water layer.

Fig. 8. Change in Double layer capacitance with Temperature for 50wt% HMImBr-water electrolyte system.

Fig 9. PEIS Spectroscopic analysis for 50 wt% AMImBr in water. The experiment was carried out in the range 5 ^{o}C to 45 ^{o}C. There appeared no change in the phase angle in this range. Hence, AMImBr showed no CST in the range of 5-45 ^{o}C

Fig. 10. Change in Double layer capacitance with temperature for 50 wt% AMImBr-water system. The circuit used for curve-fitting was R(Q(R(CR)))(CR).

Fig 11. PEIS Spectroscopic analysis for 50% w/w OMImBr in water.

Fig. 12. PEIS Spectroscopic analysis for 50 wt% HDMImBr in water.

Fig. 13. PEIS Spectroscopic analysis for 50 wt% OMImPF_6 in water.

Fig. 14. PEIS Spectroscopic analysis for 50 wt% HMImPF_6 in water.

Fig. 15. Graphical representation of $E_T(30)$ parameter with respect to 1000/T in kelvin for HMImBr.

Fig. 16. Graphical representation of E_T^N parameter with respect to 1000/T in kelvin for HMImBr

Fig. 17. Graphical representation of π* parameter with respect to 1000/T in kelvin for HMImBr.

Fig. 18. Graphical representation of α parameter with respect to 1000/T in kelvin for HMImBr.

Fig. 19. Graphical representation of β parameter with respect to 1000/T in kelvin for HMImBr.

Fig. 20. Graphical representation of E_T^{30} parameter with respect to 1000/T in kelvin for OMImBr.

Fig. 21. Graphical representation of E_T^N parameter with respect to 1000/T in kelvin for OMImBr.

Fig. 22. Graphical representation of π* parameter with respect to 1000/T in kelvin for OMImBr.

Fig. 23. Graphical representation of α parameter with respect to 1000/T in kelvin for OMImBr.

Fig. 24. Graphical representation of β parameter with respect to 1000/T in kelvin for OMImBr.

Fig. 25. Graphical illustration showing high electrochemical aspects of synthesized gel electrolyte.

CHAPTER 6: CONCLUSIONS

Fig. 1. Graphical illustration of fine-tuning of LCST of polyoxazoline based copolymer using inorganic silicate material.

Fig 2. Graphical illustration showing solid-supported thermoresponsive polymer modified silicon wafer for thermal devices.

Fig 3. Graphical abstract representing the role of nanoparticle size in the nanoparticles embedded PNIPAM based hydrogels using polymerized ionic liquids.

Fig 4. Graphical illustration showing high electrochemical aspects of synthesized gel electrolyte.

Chapter-1

Introduction to Thermoresponsive property

1.1 Introduction to Thermoresponsive polymers

Stimuli-responsive polymers [1-6], also known as "smart polymers" have become indispensable class of materials in our present lives. As we know, these high-performance materials are able to change physical or chemical parameters with the change to external stimuli such as physical (light, temperature), chemical (pH, metal ions) or biochemical (enzyme, proteins) (Fig. 1). They can alter various properties like their colour, electrical conductivities, and permeability to water and even shape (shape-memory polymers), which can be utilized in highly specialized applications like sensors, production of artificial muscles, biodegradable packing and biomedical engineering [7-10].

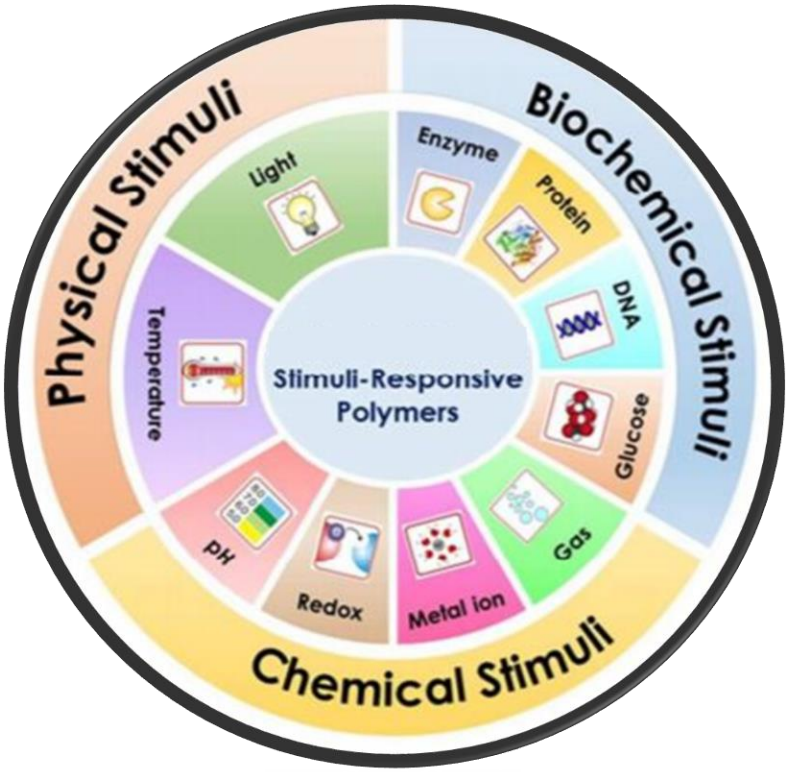

Fig. 1. Schematic diagram representing various external stimuli for stimuli-responsive polymers. (Adapted from *Polym. Chem.*, 2018, **9**, 1257-1287)

Amongst others, temperature-responsive or thermoresponsive polymers have achieved a much wider attention because not only the stimuli is one of the most easily available limitless change, which is temperature (sun), but also due to the facility to finely tune the polymers' solubility in a solution [11]. Hence, these exhibit a miscibility gap in their temperature-composition diagram, which is the resultant of the phase change of the polymer in the solution [12-15]. The macroscopic conformational changes can readily happen over a small change in temperature, which aids in the production of intelligent polymers and attracts more scientific interest [15-20].

1.1.1 Thermoresponsive phase transitions and its types

As the important parameter for thermoresponsive polymers is solubility, these materials are capable of showing a volume phase transition at a certain temperature represented as Critical Solution Temperature (CST). This causes a change in solvation state of the polymers in the solution. By closely examining the phase separation of some of the polymers/solvent systems, it was found that, there are two temperature driven phase transitions: Lower Critical Solution Temperature (LCST)-type and Upper Critical Solution Temperature (UCST)-type phase transitions as represented in Fig. 2. LCST and UCST are critical temperatures below and above which the polymers, or for that matter, any class of material and solvent are completely miscible respectively. That is, a polymer/solvent mixture is homogenously uniform below LCST and appears biphasic or cloudy above LCST. For UCST, it is the opposite phenomenon. This change in phase occurs due to the change of the inter- and intra-molecular hydrogen bonding of polymer molecules, with respect to the solvation energy of water [16, 21-24].

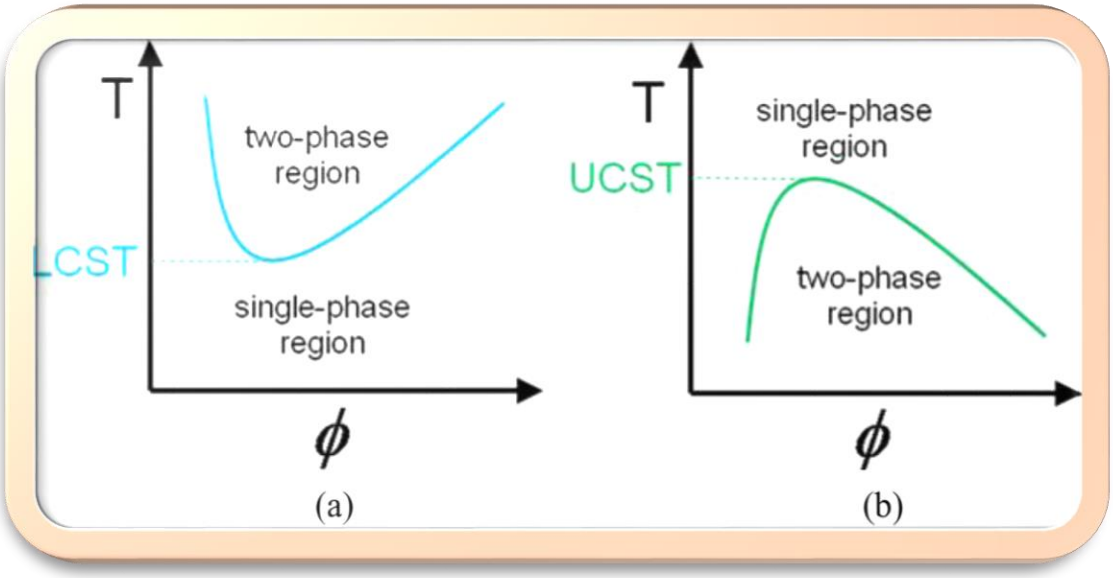

Fig. 2 Temperature (T) vs concentration (ϕ) phase diagrams showing (a) LCST and (b) UCST of biphasic mixtures.

Miscibility gaps [23] are often encountered for polymer systems due to low entropy of mixing. Thus, many polymers tend to exhibit LCST or UCST in organic solvents as well [25].

For example, UCST showing polymers in organic solvents:

- Polyethylene in diphenylether [26].
- Polystyrene in cyclohexane [27].

- LCST showing polymers in organic solvents:
  - Polypropylene in n-hexane [28].
  - Polystyrene in butyl acetate [29].

Water is the universal solvent. Many biological activities and chemical systems work in aqueous systems. It has unique physiochemical properties due to hydrogen bonding. Therefore, choosing water as the other component in a mixture gives several advantages

over other solvents. These mixtures can act as functional fluids in bioscience. Much research on the importance of these mixtures, is being carried out today. Hence, thermoresponsive behaviour of many polymer systems has been already studied and yet, still are being extensively examined to be used in biological applications like drug delivery systems, bioseparation and tissue engineering. One of the vital polymer is Poly(*N*-isopropylacrylamide) (PNIPAM) (Fig. 3), which is known to be exhibit an LCST of 31 °C, close to the human physiological temperature [30-32]. Other typical examples have been represented in the Fig. 3 below.

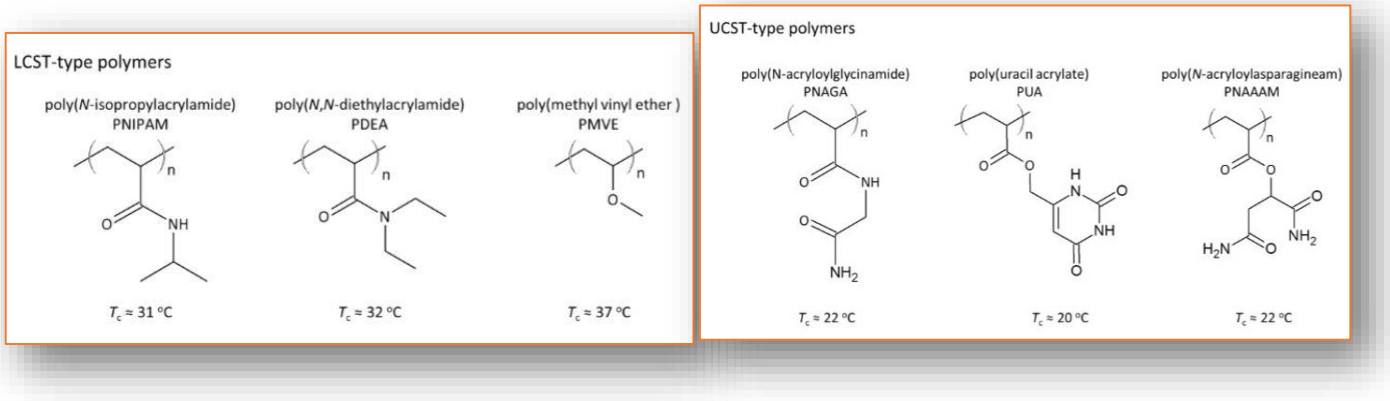

Fig. 3. Selected polymers which LCST type- and UCST type- behaviour in water.

In addition to temperature, diverse factors like molecular weight of the polymer, salt concentration and copolymerization also influence the solubility of the polymer in aqueous mixtures.

Thus, in this thesis work, I will study the systems in aqueous media and find out how different factors affect the LCST of different materials and how these can be tuned for their critical behaviour in water.

1.1.2 Mechanism and Thermodynamics of phase transition

Mechanism of phase transition:

Polymers are believed to undergo a coil-globule transition at the critical temperature. The mechanism of LCST type-phase transitions [33-37] can be understood if we consider it to take place in the following 3 steps, as represented in Fig. 4 :

1. Below LCST: The polymer chains takes the hydrated-coiled structures which are uniformly dissolved in water, providing a transparent solution.
2. During LCST: On increasing the temperature to the critical temperature, hydrogen bonds tend to dissociate, which forces the polymer chains to collapse to the polymer globules. This is called the coil-globule transition and the temperature is called LCST.
3. Above LCST: Due to the dominant hydrophobic interactions and free mutual diffusion in water, the tiny polymer globules are joined to form a large aggregate, thereby producing a polymer rich- and a water-rich domains. These micro-domains can be easily detected by light scattering as the system becomes turbid in colour.

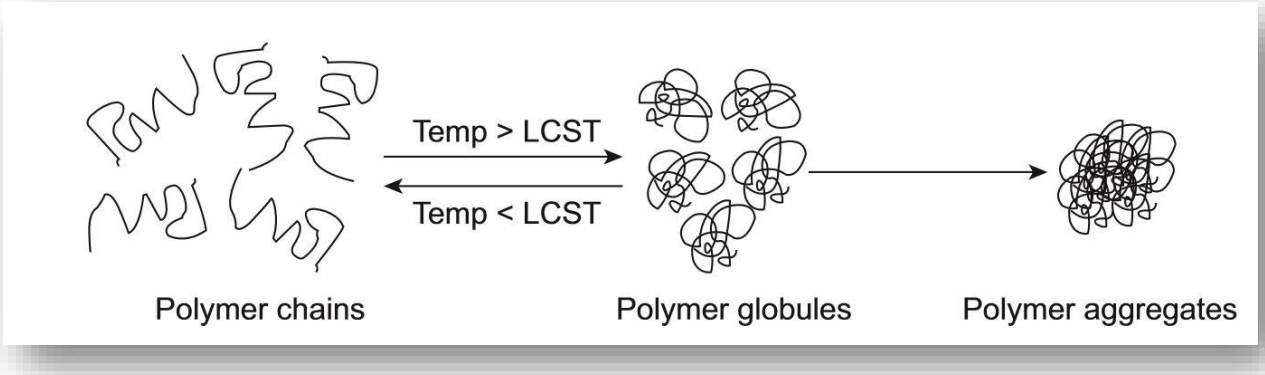

Fig. 4. Mechanism temperature-driven phase transitions of thermos-responsive polymer chains.

In the case of UCST type- phase transitions, the solution forms the globules below the critical temperature, which is insoluble in nature and hence, they appears as turbid. Above the critical temperature, the solution forms the coiled-structured and the polymer chains are soluble in water.

Thermodynamics of phase transitions:

From the Legendre transformation of the Gibbs-Helmholtz equation, we know that the change Gibbs energy of mixing (ΔG_{mix}) is determined by change in enthalpy of mixing (ΔH_{mix}) and the change in entropy of mixing (ΔS_{mix}), as written below:

$$\Delta G_{mix} = \Delta H_{mix} - T.\,\Delta S_{mix}$$

It is also known that the when ΔG_{mix} decreases, polymer dissolves in a solution,. If there are no interactions between the polymer and water molecules, there will be no ΔH_{mix} and the ΔS_{mix} will be ideal. In this case, the $T.\,\Delta S_{mix}$ is a negative term in the case of mixing, and thus, the ΔG_{mix} will always remain positive that means that the system will be in a separated state always. But as we observe the dissolution, this means the interactions do play an important role. Thus, Flory and Huggins developed the theory of thermoresponsive polymers in 1940s [38-40] by considering these interactions between the polymer and water molecules. They independently acknowledged the similar theoretical modulations for organic polymers in solutions with varying temperature and developed polymer phase diagrams. Represented below is the resultant equation for the ΔG_{mix} containing a term which described the sum of all interactions.

$$\frac{\Delta Gmix}{RT} = \frac{\varphi 1}{m1}\ln \varphi 1 + \frac{\varphi 2}{m2}\ln \varphi 2 + \chi \varphi 1 \varphi 2$$

where R is the gas constant, ϕ is the volume fraction of the polymer (1) and solvent (2), respectively, m is the number of occupied lattice sites per molecules (m1 = degree of polymerization and m2 = 1) and χ is the interaction parameter. In simple terms, they postulated that LCST is an entropic change, while the UCST is driven by enthalpy change.

When LCST occurs, the hydrophilic part of the polymer interacts with the water molecules and its solubility increases. The hydrophobic part contributes to the negative ΔH_{mix} and the hydrophobic attraction helps in minimizing the entropic loss of the system. On heating, the total negative entropy becomes larger than the enthalpy of the hydrogen bonding, which causes the ΔG_{mix} to become positive. This can be portrayed as the polymer shrinking caused by the change in phase. Therefore, on heating, the balance between the hydrophobic-hydrophilic energy modifies which leads to the dehydration of the polymer. This hydrophilic part for solubility and hydrophobic part for aggregation are the key factors to exhibit LCST-type phenomenon. Therefore, non-ionic polymers amphiphilic in nature tends to show LCST easily like PNIAPM, PMVE or PDEA.

When UCST occurs, polymers show strong polymer-polymer interactions as the intra-molecular hydrogen bonding is dominant. According to the theory, to show UCST type phenomenon, polymers should have positive ΔH_{mix} and ΔS_{mix} values. So, for positive ΔH_{mix}, stronger inter-molecular interactions like polymer-polymer and solvent-solvent are necessary and available. As the hydrophobic part is less dominant in these type of polymers, this makes ΔS_{mix} also positive. Thus, UCST-type phase transitions are displayed by polymers bearing strong hydrogen-bond forming groups like carboxylic acid, amide, ureido and uracil. These electrostatic interactions and hydrogen-bonds interactions between the polymer chains are therefore, more stabilized in less polar solvents, as polar solvents destabilized the interactions due to presence of water and salts. Therefore, UCST

is not a general tendency to be seen in aqueous systems. This is why, LCST-type systems are being studied extensively with compared to UCST-type systems as the former can be utilized in physiological conditions.

1.1.3 Applications of CST

LCST-type polymers are already being used in various biological and non-biological applications. Some of them are mentioned below with their examples.

- **Drug Delivery**: It is important to deliver drugs for therapeutic effect to the right location, with the right concentration at the correct time. Thus, smart thermoresponsive polymers can be used to deliver the drug as needed in response to the external stimuli. For example, expansion of the polymer chains can lead to release of drug molecules in response to increase in temperature [41].
- **Bio-separation**: Thermoresponsive polymers can be modified using functionalities that can bind to specific biomolecules without much changes to their CST behaviour. On changing the temperature, the polymer-biomolecule conjugate can be precipitated from the solution, which can be ultimately recovered using centrifugation, chromatography or isolation [42].
- **Gene-delivery**: This technique aims to correct the defective genes which causes genetic problems. So, it is important to deliver therapeutic DNA into the cells which can replace/repair or rejuvenate the defective ones. The current problem is that the DNA is a hydrophilic, negatively charged species whose delivery needs to be done in via nucleus of the cell, which is hydrophobic and negatively charged, making is difficult for DNA to pass. Herein, many researchers have already seen that thermoresponsive polymers can play a vital role as the temperature makes

the delivery possible on the basis of hydrophobic-hydrophilic environment, as needed. The DNA can make a complex with a cationic polymer, enabling its release after complex traversing the cell membrane to the cytoplasm and its eventiual release into the nucleus [43].

- **Tissue engineering**: This technique is applied to enhance or repair tissue functions, when required. In this field, thermoresponsive polymers are being used in two current scenarios: (i) they act as the substrates that helps in the cell growth, to regulate the attachment and detachment of the cells from a surface and (ii) they act as injectable gels, as then, cells can be encapsulated into 3D structures in the human body (one such example is formation of a physical gel for in situ formation of a scaffold) [44].
- **Chromatography**: In liquid chromatography, thermoresponsive polymers can be utilized as the stationary phase, whose polarity can be changed with changing temperature. This reduces the need to alter the composition column or solvent itself. This technique has already gained popularity and is slowly increasing to size exclusion chromatography, ion-exchange chromatography and hydrophobic interaction chromatography [45].

Not only these smart materials are identified as superior life-changing materials based on their properties, they can also be acknowledged based on the physical state/structure and architecture of the polymers, widening the applications to other scientific platforms as mentioned below:

- Hydrogels: Hydrogels are semi-solid state polymer network which can contain as much as 1000 % water w/w to polymer. When thermoresponsive polymers are made as hydrogels via covalent linking networks, they swell and shrink in water

with the change in temperature. As PNIPAM is one of the most rigorously studied polymer in the field of biomedical applications, many groups are creating PNIPAM-based hydrogels. The strategy is to release the encapsulated drug faster and in a more controlled manner, when a rapid decrease in the volume of the gel take place at the phase transition [46-47]. Okuyama et al., [48] prepared hydrogels of PNIPAM-co-PBUMA and studied their swelling mechanistics. They found out that a controlled released of the drug can be achieved after the burst release from the outer part of the hydrogel. Grafting of PNIPAM and PVC-HEMA has been achieved by Zhuo et al., [49] onto a dextran chain which yielded injectable and biodegradable hydrogels. These are able to deliver drugs over a period of several days and showed negligible cytotoxicity. High tensile strength and non-toxic hydrogels of PNIPAM, poly(HEMA) and lactic acid to be used in tissue engineering were synthezied by Ma et al., [50] which showed long-lasting degradation mechanistics with no cytotoxicity. Stabenfeldt et al., [51] produced conjugated methylcellulose-laminin protein based hydrogel superior enough to create a desired environment in the cells for neural tissue growth.

- Interpenetrating networks (IPN): These networks is another class of cross-linked hydrogels that have the ability to swell above their UCST due to disruption caused in the hydrogen bonding at the higher temperatures [52]. Wang et al., [53] created an IPN with grafted β-cyclodextrin which showed UCST at 35 ^{o}C and faster rate kinetics. They infused ibuprofen and were able to achieve a positive drug release at required temperature (above and below UCST) in a sustained manner. Kim et al., [54] have produced injectable and photodegradable IPNs of PNIPAM-co-PAAc

crosslinked with peptide chains and obtained the non-cytotoxic degradation by-products enabling their use in tissue engineering.

- Micelles: Ordered structures of block copolymers comprising of both hydrophilic and hydrophobic monomers constitutes micelles. These are highly advantangeous in drug delivery of hydrophobic drugs in physiological environments. Akimoto et al., [55] synthesized a copolymer of PNIPAM-co-PDMAAc and then, created a micelle by block copolymerization with poly lactic acid. This system can be used to internalize into the cells above the critical temperatures. Wei et al., [56] produced a star block copolymer of PNIPAM-co- L- Lactide capable of forming self-assemblies of larger micellar structures to exhibit fast switch on/off type drug release in body.

- Films: PNIPAM-co-BuAAm copolymer films were invented by Wilson et al., [57] which showed a drug release in a controlled manner over a specific amount of time. Ito et al., [58] created a copolymer film of polystyrene grafted with PNIPAM to produce a micro-patterned surface to achieve cell proliferation and selected cell detachment. Poon et al., [59] devised a 3D cell culture method by preparing grafted films of chitosan-PEG-MAc.
- Particles: Zhang et al., [60] coated PNIPAM with insoluble nanoparticles making the particles stable in aqueous media. These can be further expected to be used in biological sensing and drug deliveries. Fundueanue et al., [61] produced nanoparticles of crosslinked PNIPAM-co-AAm. Wang et al., [62] prepared micellar nanoparticles using PVC and polyphosphoester which formed aggregates above LCST in a reversible way.

1.1.4 Importance of phase-tuning of polymers (Motivation of Thesis)

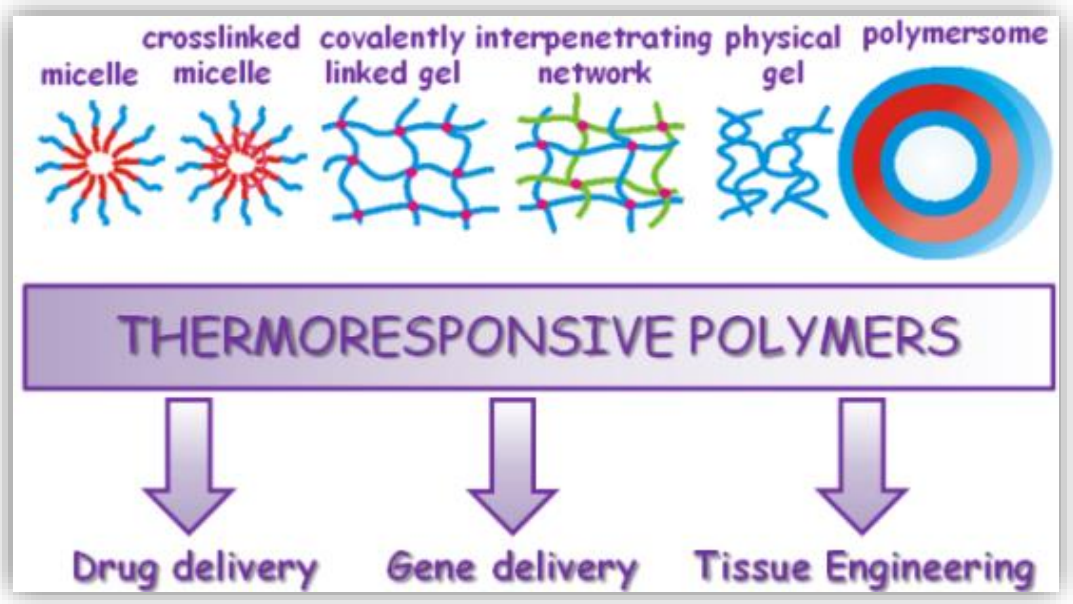

Fig. 5. Illustration depicting various states of polymers used to be used for various biomedical applications. (Adapted from *Polymers* **2011**, *3*(3), 1215-1242)

As seen, there are discrete varieties of polymer structures exposing different utilities (Fig. 5) [63]. Thus, depending on the requirements, the structures, hydrophilicity, polarity and chosen solvent needs to be designed accordingly. Thus, there is a strong urge to study the mechanistics and tuning-abilities of the critical temperatures, enabling the design of the systems with required CST characteristics (LCST/UCST at desired temperatures). Thus, this thesis work mainly focusses on the fine-tuning and control of critical phase behaviour of various architecture and structures like hydrogels, solid-supported and liquid phase to be exploited for various other biomedical and operational chemistry. I have studied tuning agents such as Gold and Silver nanoparticles, and incorporated them to PNIPAM-co-IL copolymers to produce hydrogels. Also, solid supported systems using silicon wafers and inorganic silicate matrix have been prepared separately utilizing polyoxazolines, whose non-toxic nature has already been approved by FDA. Furthermore, how and what factors affect the CST in greener solvents imidazolium-based ionic liquids were found out which lead to a creation of prediction theory of their phase behaviour.

1.2 Solid-supported LCST showing materials

Most thermosensitive polymer classes dissolve in aqueous solutions leading the LCST to manifest in the binary form of liquid-liquid equilibria. However, for versatile applications like drug delivery, tissue engineering, sensors or electronic batteries (automated shut-down after overheating), there is an obligatory demand of solid-liquid phase equilibria. Hence, this part of the study was carried out to design materials which displayed LCST over a solid-support via (i) formation of inorganic-organic hybrid materials and (ii) polymer attached to the silicon wafer using a non-toxic class of polymers known as poly(2-oxazolines). How the phase behaviour of these smart materials can be tuned made the further point of analysis in the work.

1.2.1 Poly(2-oxazolines) (POx) for biomedical applications

It has been a major breakthrough since the class of biocompatible polymers were introduced. This opens a whole new and innovative avenues in the fields of implant design, drug delivery, tissue engineering for cancer treatments, gene therapy and regenerative medicine.

Currently, mostly used bio-stable and bio-degradable class of polymers in medicine is poly(ethylene glycol) (PEG) [64]. The polymer is able to form bioconjugates in a process called PEGylation, to treat diseases like anaemia, hepatitis C and neutropenia. This class became superior owing to its low dispersity, possession of stealth behaviour (not recognized as antigens by the immune system) and biocompatibility [65]. Due to the amphipathic properties, protein PEGylated conjugates are known to enhance the retention effect, thereby increasing the bio-distribution of the drug over the target area. However, to remain site-selective, intensive use of the PEGylated systems is necessary

leading to decreased bio-activity and ultimately, loss of therapeutic efficacy. Recently, anti-PEG antibodies have been observed in many patients, including the ones never treated with PEGylated conjugates. This leads to accelerated blood clearance of these bioconjugates after injection of multiple doses. In addition, PEG polymer backbone is prone to oxidative degradation whose products showed cytotoxity in humans. This diminishes the use of this class of polymer for long-term applications such as induction of PEGylated complement activation and antifouling surfaces for implants [66].

A more superior class of non-toxic, highly efficient with tunable properties is poly(2-oxazolines) or POx [67,68]. They not only possess the biocompatible and beneficial properties of PEG such as low dispersity and stealth behaviour, but also provides higher stability and non-ionic nature. This class of polymer was developed with the purpose of food additive in early 1980s but soon, scientists discovered its use in multiple medical and pharmaceutical applications [69,70]. Polyoxazolines are prepared by living cationic ring-opening polymerization (CROP), and therefore are often viewed as the analogues of proteins (polyamide backbone) (Fig. 6). The presence of these polyamide functionalities suppress the recognition by immune system, thereby incorporating the stealth behaviour and excellent biocompatibility due to its structural similarity. The polymerization is initiated using an electrophilic initiator (like alkyl halides, tosylates: the green circle in Fig. 6) and termination is done by any nucleophilic terminating agent (like carboxylates, amines: the red square in Fig. 6). Introducing a 2-fold functionality, thus enables profound modifications on the architecture and composition in the polymer system.

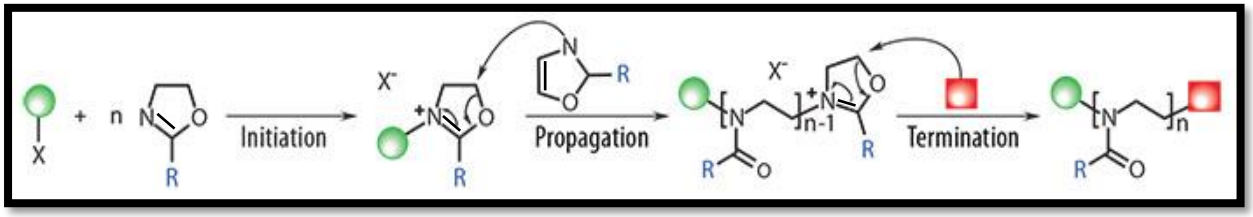

Fig. 6. Scheme for polymerization of POx. (Adapted from *Material Matters, 2016, 11.3*)

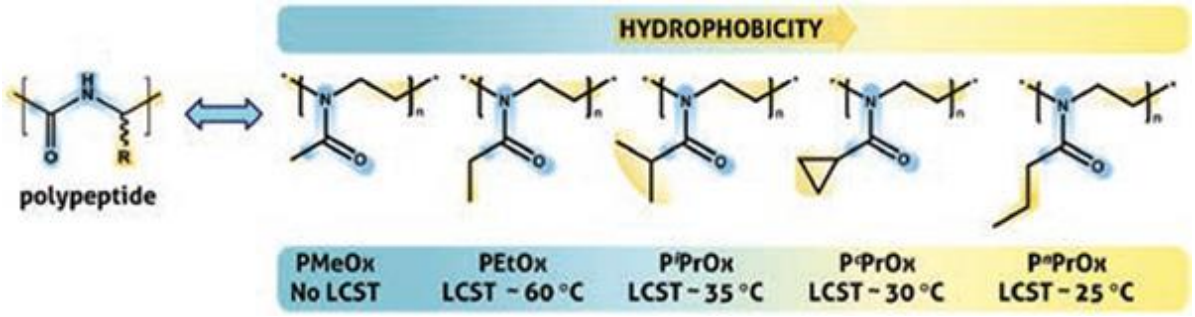

Fig. 7. Types of POx discovered with their LCST. (Adapted from *Material Matters, 2016, 11. 3*)

In addition, the side-chain of the oxazoline molecule (-R group in the Fig. 6) can be substituted and tuned for its hydrophilicity (PEtOx), hydrophobicity (PnPrOx) and thermoresponsive nature. The viscosity, thermosensitivity and hemocompatibility can be supervised by controlling the molecular weight (polymer chain length) or by modelling into the block copolymers from combination of any two homopolymers. The designed architecture can help homopolymers/copolymers to be widen its miscibility in various aqueous/ organic solvents. It is also seen that LCST of POx can selected between 0 ^{o}C and 100 ^{o}C by careful design of the polymer composition (Fig. 7). As a result of this synthetic versatility, many strategies are being employed in the literature:

(i) Excipient in Drug Formulation: A study done by Geest et al., [71] using Aquazol developed tablet formulations of PETOx-based excipients, whose drug release profiles can be increased or decreased depending on the molecular weight of the polymer.

(ii) Micelles with better therapeutic activity: Zhao et al., [72] polymerized ε-caprolactone using PEtOx-based initiator with folate terminal groups. This produced micelles are able to load doxorubicin with 10 wt% higher capacities,

better therapeutic efficacy and lower toxicity than pure doxorubixin in mice infected by KB tumor cells.

(iii) Micelles for cancer drug delivery: Kabanov et al., [73] created a triblockpolymer utilizing PMeOx-PBuOx-PMeOx, which yielded stable micelles below 100 nm of diameter and showed superior anti-cancer drug loading capacities and water insolubility.

(iv) Hydrogels for biomedicine: PEtOx-PEI based copolymers were designed by Lecommandoux et al., [74] whose cross-linking with bis-glycidyl ether produced a hydrogel qualified to be biocompatible nanogels with size-dependent drug-deliveries.

(v) POx-based bioconjugates: Hoogenboom et al., [75] demonstrated the strategy to prepare novel POX-based drug conjugates. They suggested the introduction of various methyl ester functionalities across the backbone chain of EtOx-MestOx copolymer simply by direct amidation with amines.

(vi) POx-based Nanoparticles for anti-fouling behaviour: Koshkina et al., [76] produced a polyorganosiloxane based fluorescent nanoparticles functionalized with Pi-PrOx, which displayed an enhanced anti-fouling activity below the LCST of 31 ^{o}C when dispersed in a medium containing serum.

(vii) POx-based Nanoparticles for enhanced permeation: Alkyne-terminated PEtOx was functionalized with thiolated silica nanoparticles which was as skilful to exhibit enhanced permeation in ex *vivo* through porcine mucosa as the PEGylated nanoparticles[77].

1.2.2 Fine-tuning of POx

As already seen, poly(2-oxazolines) can undergo phase transitions in a wide temperature range in aqueous solutions ranging from 65 °C (as shown by PEtOx) to 25 °C (as shown by PnPrOx) depending on the hydrophobicity/hydrophilicity of the alkyl side-chain of the 2-oxazoline molecule. Not to forget, the LCST of these species depend on molecular weight and concentration of the monomer molecules and the type of initiator and terminal groups, unlike PNIPAM. Over the world, scientists have already studied and demonstrated how the incorporation of a co-monomer can tune the properties and LCST of the required material. Copolymerizing 2-n-propyl-2-oxazoline with 2-ethyl-2-oxazoline decreased the LCST of pure PEtOx to a temperature similar to that of PNIPAM's LCST, making the copolymer work at physiological temperatures. Also, 2-isopropyl-2-oxazoline molecule is structurally similar to N-isopropylacrylamide, and also exhibit LCST of 37 °C, prudent copolymerization of which with 2-ethyl-2-oxazoline can accurately tune and widen the copolymer's LCST range (23-75 °C). Thus, fine-tuning of phase behaviour of variety of POx can be done by meticulously pondering over the factors effecting the LCST like, hydrophobic/hydrophilic nature of the alkyl side chain, molecular weight of the copolymer produced, initiators used, solvents and polymerization temperatures and the concentration of the co-monomers used to obtain a sharp transition temperature. Careful control of the above factors can also lead to construction of block/triblock/graft and gradient polymers which qualify to be used in bio-related fields.

In this thesis work, copolymer of 2-ethyl-2-oxazoline and 2-isopropyl-2-oxazoline was used since that copolymer can be tuned to a wide temperature range.

1.2.3 Organic-inorganic hybrids

As mentioned already, with controlled demanding and flowing disadvantages of liquids, it is sagacious to work on solid-supported systems for assorted applications due to liquid-solid equilibria like in biomedicine and energy storage devices. To initiate such phenomenon, fabrication of organic-inorganic hybrids materials can be one of its kind ideology. Sol-gel materials or organic-inorganic composites [78,79] came into existence in late 1940s and since then, science has experienced a wholesome of new avenue in terms of boundless opportunities. Ranging from health to housing, energy to environment, micro-electronics to automotive [80-83], these magnificent materials can find their way. Such paramount significance lies in the design of these species.

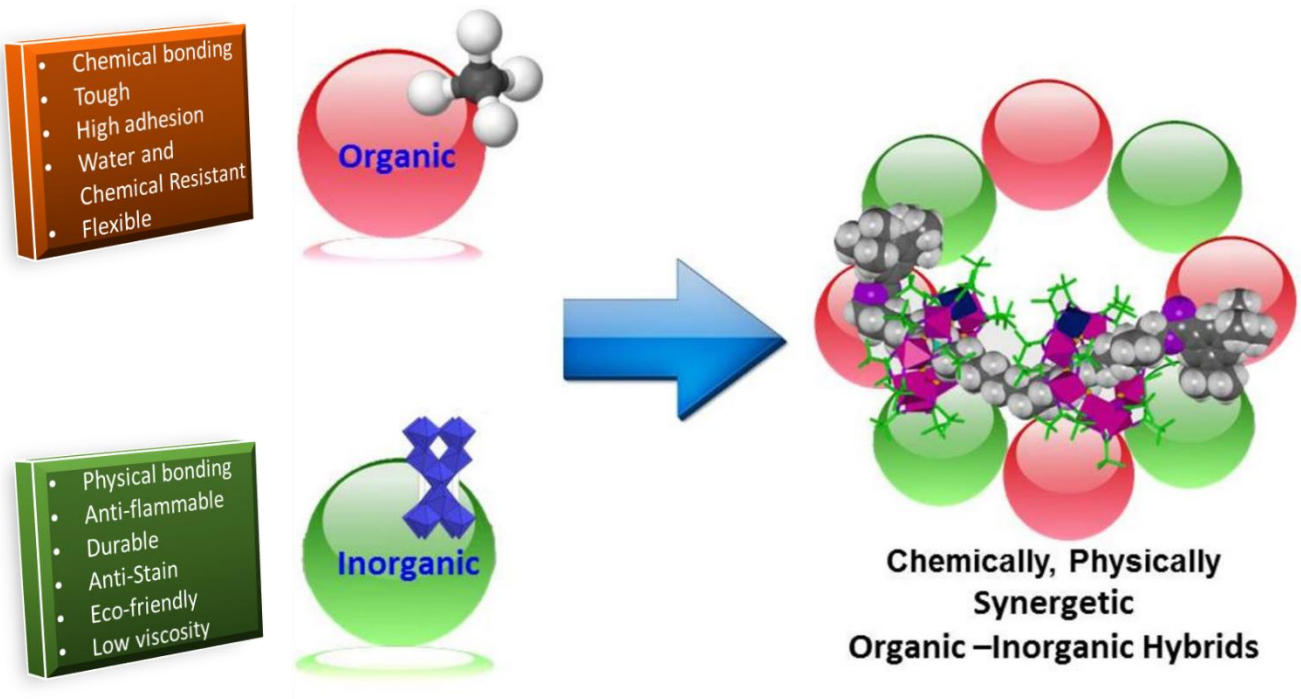

Fig. 8. Development of organic-inorganic hybrids. (Adapted from https://sites.google.com/site/smleeresearch/research-intere

These materials are composed of two discrete categories (Fig. 8), (1) an organic part- generally modified networks of polymers or macromolecules which impart toughness, elasticity and chemical stability and (2) an inorganic part- generally silanes, (esp., tetramethoxysilane or tetraethoxysilane) or other metal oxides that caters for hardness, stiffness and thermal stability. Cooperatively, the hybrids can bag those synergistic properties which either component alone cannot. Synthesis of tailor-made products with desired mechanical, electrical and optical properties can be achieved projecting to their use in inexhaustible applications.

Principally employed method of synthesis of these functionalized materials is to perform sol-gel condensation. Organic-inorganic interface is accomplished using polymers and alkoxysilanes by hydrolysis and sol-gel condensation to form stable Si-O-Si and/or Si-OH bridges. Owing to its mild conditions during synthesis, sol-gel derived silica glass fibers/nanostructures are apparently being widely utilized as organic dyes [85], biomolecules [86], smart coatings [87], membranes [88], sensors [89], catalysts [90] and what not. Hence, it becomes obligatory to study the phase behavior of these smart hybrid composites when a thermoresponsive polymer is incorporated in the hybrid matrix, owing to its widespread need. Chujo et al., [91] prepared hybrids of PMeOx and tetraethylorthosilicate gel and incorporated various transition metal salt like $CuCl_2$, $NiCl_2.6H_20$ and $Cu(OAc)_2$ to be used as colored ceramics. Further, they have also designed a new class of hybrids (CubePOZO) using PMeOx and polyhedral oligomeric silsesquioxane (POSS) with tetramethylorthosilicate which are capable of forming micelles in aqueous systems [92].

1.2.3.1 Motivation for Chapter 2

After studying various literatures as mentioned, it was visualized that if we take the thermoresponsive nature of polyoxazolines and transform the system into inorganic-organic hybrids using silicates, we may be able to prepare a superior tunable thermoresponsive system capable of showing LCST. Thus, for the first work of the thesis, a copolymer of 2-ethyl-2-oxazoline and 2-isopropyl-2-oxazoline was prepared according to the literature which showed the thermoresponsive phase transition at 77 ^{o}C. The initiator chosen was methyltosylate and the terminal end group functionalization was done by methanolic NaOH solution. Further, the copolymer was transformed into novel organic-inorganic hybrids via sol-gel condensation using tetramethylorthosilicate. Various molar ratios of copolymer concentration and inorganic silane moiety was added to obtain smart solid hard materials whose LCST can be tuned for desired applications.

Why copolymer of 2-ethyl-2-oxazline and 2-isopropyl-2-oxazoline?

Both are the monomer species with highly hydrophilic nature in the alkyl side chain and 2-isopropyl-2-oxazoline is structurally similar to N-isopropylacrylamide.

Why transformation of copolymers into organic-inorganic hybrids advantageous?

Transforming the copolymers into sol-gel hybrids enables the system to display solid-supported LCST.

Why will the fine-tuning of LCST of these materials be possible?

Phase transition temperature is highly dependent on the composition of copolymer used with silane moiety giving us a chance to fine-tune of the LCST over a wide range.

Novelty of the work?

Novel hybrids materials were designed using PEtOx-n-P-iso-propOx and TMOS whose LCST cane be tuned by composition of the copolymer used in the hybrid.

1.2.4 Silicon wafer modifications

Most prevalent form of substrate material for immobilization of biomolecules is silicon [93]. However, the metal can be spontaneously oxidized by moisture and air to form a non-reactive amorphous layer incapable of any use. Thus, polymeric smart materials are being deposited on the silicon surfaces for the modification of its physical and chemical properties. These customized and modified silicon substrates [94-98] can be then used for cell cultivation, immobilization of biomolecules and for fabrication of on-chip biosensors.

Most significant method of silicon surface modification broadly being employed in the scientific world is the covalent immobilization/covalent bonding done by the formation of self-assembled monolayers (SAMs) [99,100] of an organosilane moiety for superior physiosorption and bioaffinity immobilization. Studies are being carried out on SAMs extensively in the past few decades for fabrication of devices [101-103]. This technique is highly appreciable when there is a need to tune the desired surface properties of the substrate. These monolayers, which can be seen as thin films, are constituted by the following major parts as represented in the Fig. 9.

1) The head group: This group is vital as it reacts with the silicon substrate and engage in tight covalent bonding with silicon, leading to greater stability of the assembled structure. Examples: trialkoxysilanes.
2) The spacer: This comprises of large polymeric (aliphatic or aromatic) which provides a well-defined thickness to the thin layers.
3) The terminal group: Due to the presence of this terminal chemical functional groups, one is able to determine the surface energy, topography and other surficial properties. This reactivity of this group can also lead to the attachment of biomolecules for biomedical applications. Examples: halides, amino, carboxyl etc.

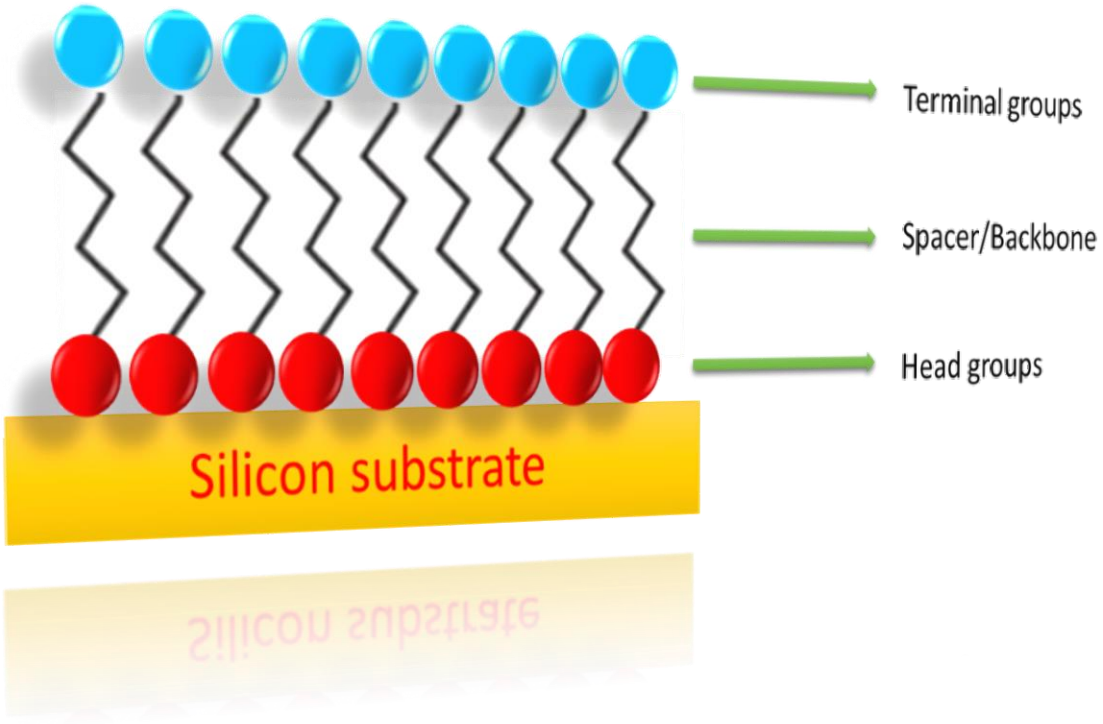

Fig. 9. Schematic illustration representing the structure of SAMs

The formation of SAMs over a silicon substrate is done by silanization process [104] wherein, the molecules corresponding to monolayers are first, chemisorbed on the exposed surface of the substrate which ultimately and spontaneously, orient themselves in the form of large-range ordered structural domains [102,105]. The process can be visualized in the following steps [104,106]:

- At first, reactive silanol groups are formed after the hydrolysis of the silicon substrate.
- Next, these silanol groups are condensed to form siloxane linkages all over the surface.
- Further, these siloxane linkage form hydrogen bonds with the substrate polymer.
- Lastly, formation of a covalent bond (Si-O-Si) takes place between the silicon substrate and organosilane with subsequent loss of small molecules like water or alcohol.

The above procedure can be modified based on the experimental conditions of silane concentration, reaction temperature and type of solvent used to alter the film thickness, its architecture and morphologies. Formation of multilayers is avoided since they are generally unstable and inhomogeneous, leading to decreased biomolecule immobilization. Hence, formation of stable, thin and uniform layers of silane is highly recommended.

Aminosilanes (amino-terminated silanes) [107] are the widely used organosilane-based coupling agents for silicon substrates due to their bifunctional nature, allowing them to form chemical bonds with most classes of organic and inorganic materials. They can be utilized for applications such as fabrication of biosensors [108], chromatography [109] and detection of specific gases [110]. Structures of some aminosilanes like (3-aminopropyl)dimethylethoxysilane (APDMES) and (3-aminopropyl)triethoxysilane (APTES) have been portrayed in Fig. 10.

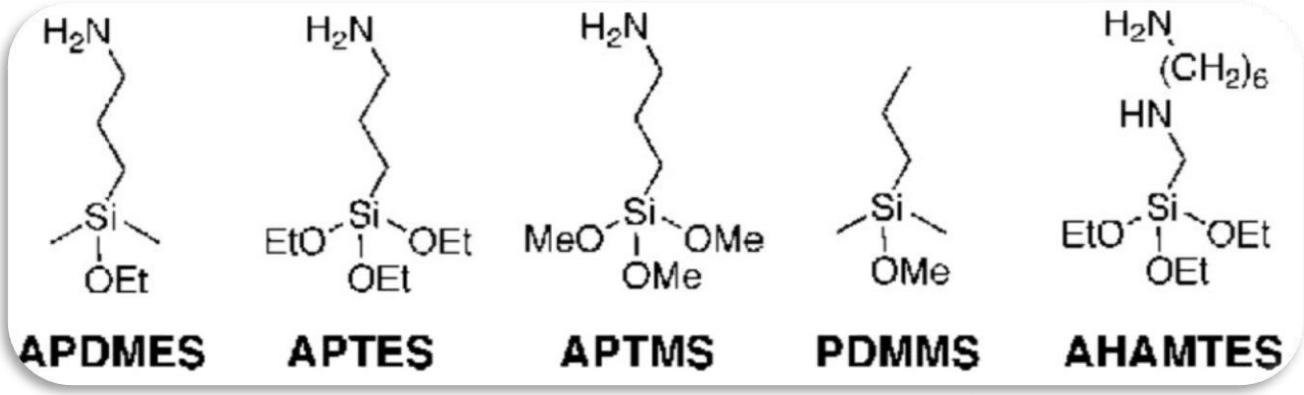

Fig. 10. Chemical structures of some aminosilanes generally used as the silane coupling agents.

Of which, APTES [111] is being extensively employed in the field of silicon substrate modifications owing to a ease of potential hydrolysable groups leading to high chances of covalent attachments to form organic films or homogeneous monolayers.

The bonding of aminosilanes with the silicon wafer or silicon substrate can be seen as in Fig. 11 [104,106]. Initially, silicon substrates are exposed to vigorous oxidative environments to form silanol group. The presence of –OH groups makes the process of chemical attachment easier for aminosilanes by the removal of alcohol molecules. It has already been observed that presence of amine groups makes the silanization easier as they are able to catalyse the hydrolysis of siloxane bonds at the ambient temperatures. It also binds to the silicon atoms of the neighbour aminosilane molecules by involving into inter- and intra-molecular interactions to form some cyclic intermediates. These intermediates are very reactive towards nucleophiles like water. This gives us the idea to coat a thermoresponsive polymer bearing alkoxysilane moiety, which can show LCST over a silicon surface. This can act as solid-supported thermosensitive system which has potential applications in immobilization of biomolecules, chromatography, biosensing and separation techniques.

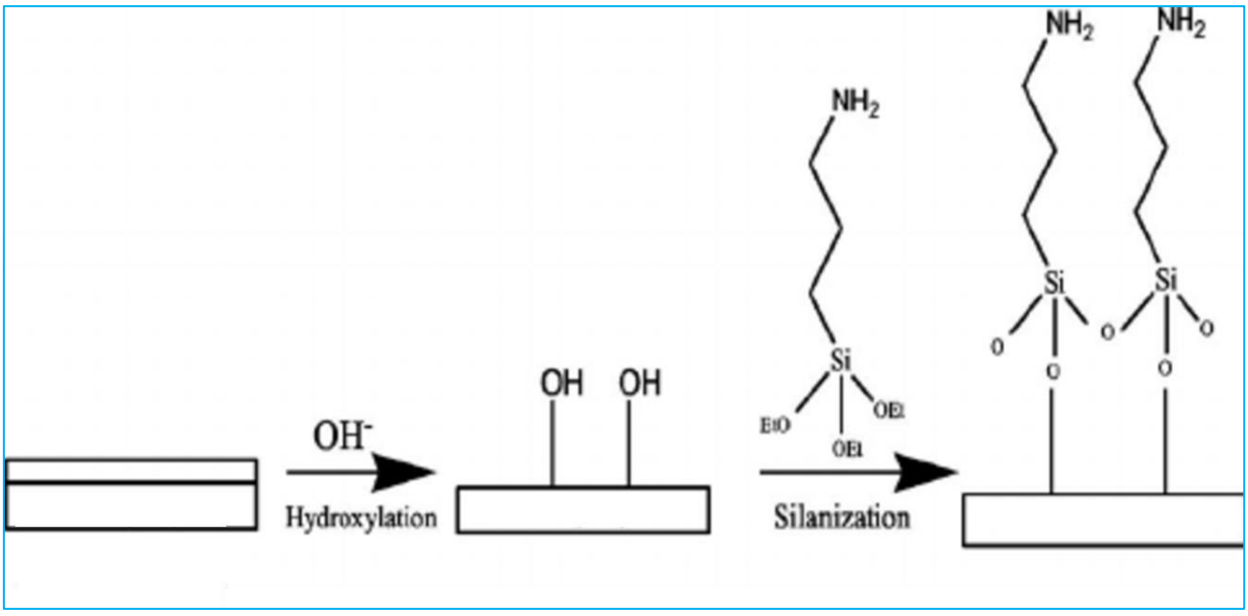

Fig. 11. Illustration of chemical bond formation between APTES and silicon wafer.

1.2.4.1 Motivation for Chapter 3

Ishida et al., [112] have already studied the phase transition of PNIPAM grafted onto silicon wafers. Li et al., [113] have used PNIPAM based silicon wafer systems for cell adhesion and detachment. Thus, our thought is to prepare silicon wafer modified using polyoxazolines and study their characteristics for predominant and desired properties. So, the termination of polymer chains of 2-ethyl-2-oxazoline was in-situ modified using (3-aminopropyl)triethoxysilane according to the literature to prepare a thermoresponsive polymer system. The polymer acts as the thermoresponsive moiety which show phase transition on increasing temperature and the aminosilane modification empower it to covalently bond with the exposed –OH groups on the silicon wafer, providing a solid-supported LCST showing polymer system.

Why poly (2-ethyl-2-oxazoline)?

This monomer species has ethyl as the alkyl side chain capable of hydrogen bonding and is tunable in nature, thus making the covalent bonding with silicon wafer possible.

Why polymer is terminally modified with APTES?

APTES molecule has 3 hydrolysable ethoxy groups, which are entitled to provide multiple points of surface attachments with other polymer molecules in both vertical and horizontal directions.

Why is silicon wafer used?

Formation of SAMs will be favorable with silicon wafer substrates, widely used for the formation of thin films and study their significant characteristics.

Novelty of the work?

Polyoxazolines have not been grafted onto silicon wafers before, allowing LCST to happen over 70 ^{o}C over a solid surface.

1.3 Plasmonic nanoparticles as tuning agents

1.3.1 Hydrogels and their properties

Hydrogels [114,115] are the three-dimensional network matrixes (Fig. 12) composed of hydrophilic homopolymers or copolymers that possess ability to swell and withhold a large amount in water. The physical and chemical crosslinking between the polymeric chains prevents the structure from breaking within. Hydrogels are capable of absorbing water atleast 10-20% of the total weight, where the upper limit of absorption can go up to several thousand times [116]. Hydrogels possess high thermodynamical affinity towards solvents (water) providing them with swelling properties.

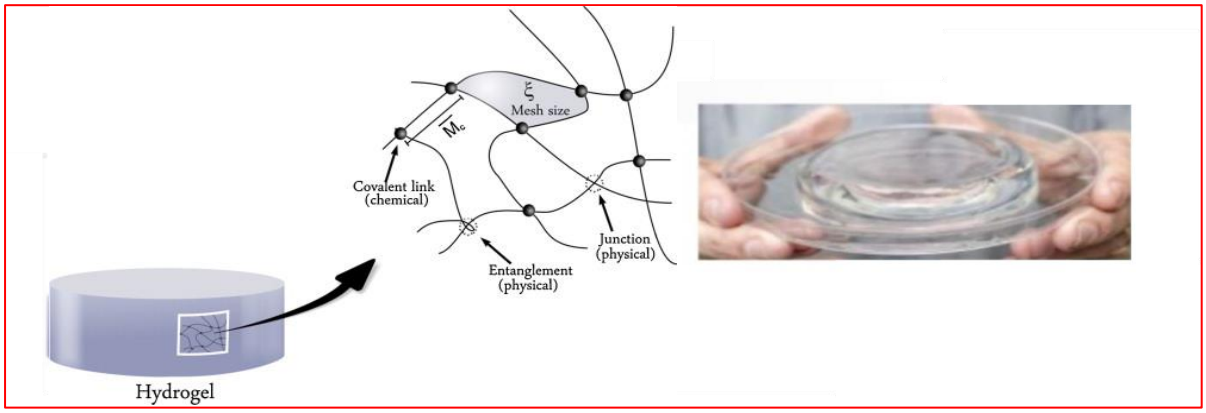

Fig. 12. Structural representation of hydrogels**.**

Smart polymer hydrogels can change their volume and structural phase transitions in response to a variety of physical (temperature, light, electric and/or magnetic fields, pressure etc.), chemical (ions, pH) and biochemical (enzymes, proteins, amino-acids) stimuli. The response and magnitude of these hydrogels may vary depending on the intensity of applied stimuli, degree of cross-linking, nature of monomer and its compositions. Many macromolecular structures can be synthesized like crosslinked or 3D networks of homolpolymers, linear or block copolymers or physical blends [116. These materials can be designed for their high tunability and versatility, making them fine

materials for study and their applications. Thus, many innovative hydrogels are being manufactured with the aim to be exploited in the fields of biomedical engineering [117], biotechnology [118], electronics [119] and some house-hold applications [120].

Hydrogels can be classified into various categories depending on factors being seen:

- On the basis of preparation method: The constituents can be homopolymers, copolymers or interpenetrating networks.
- On the basis of stimuli-responsive: Smart hydrogels can respond to physical, chemical or biochemical stimuli.
- On the basis of structure: They can be crystalline, semi-crystalline or amorphous in nature.
- On the basis of charges they possess: Hydrogels can be cationic, anionic or non-ionic.
- On the basis of source: Hydrogels can be formed from natural, synthetic or hybrid materials.

Thermoresponsive hydrogels can swell and shrink with the change in temperature. The volume phase transition of these gels results from the change in the interactions between the polymer pendent/ chain groups and the solvent molecules at the swollen and shrunken states. Interactions playing vital roles at the phase transitions of these gels have already been found out to be van der Waals, ionic interactions, hydrogen bonding and hydrophilic-hydrophobic interactions [121].

The thermosensitive gels can show either LCST type- phase transition (or thermoswelling type) where the hydrogel expands and swell after their critical temperature is reached or UCST-type phase behaviour (or thermoshrinking type) where hydrogels collapse and shrink once the critical temperature is reached.

Fig. 13. represents two phases to visualise the phase behaviour at the swelling and shrinking states [122]. At the swelling state, a mixed phase is created by the interactions of the polymer chains and solvent, creating an environment of maximum hydrophilicity. Extent of the swelling depends on factors like nature of pendent groups of the polymer, type of counterions in the solution and ionic strength. In response to change in stimuli (temperature, pH or other), the state of the gel is changed to separated shrunk phase. This state is majorly dominated by polymer-polymer and solvent-solvent interactions leading to maximum hydrophobicity possible in the system.

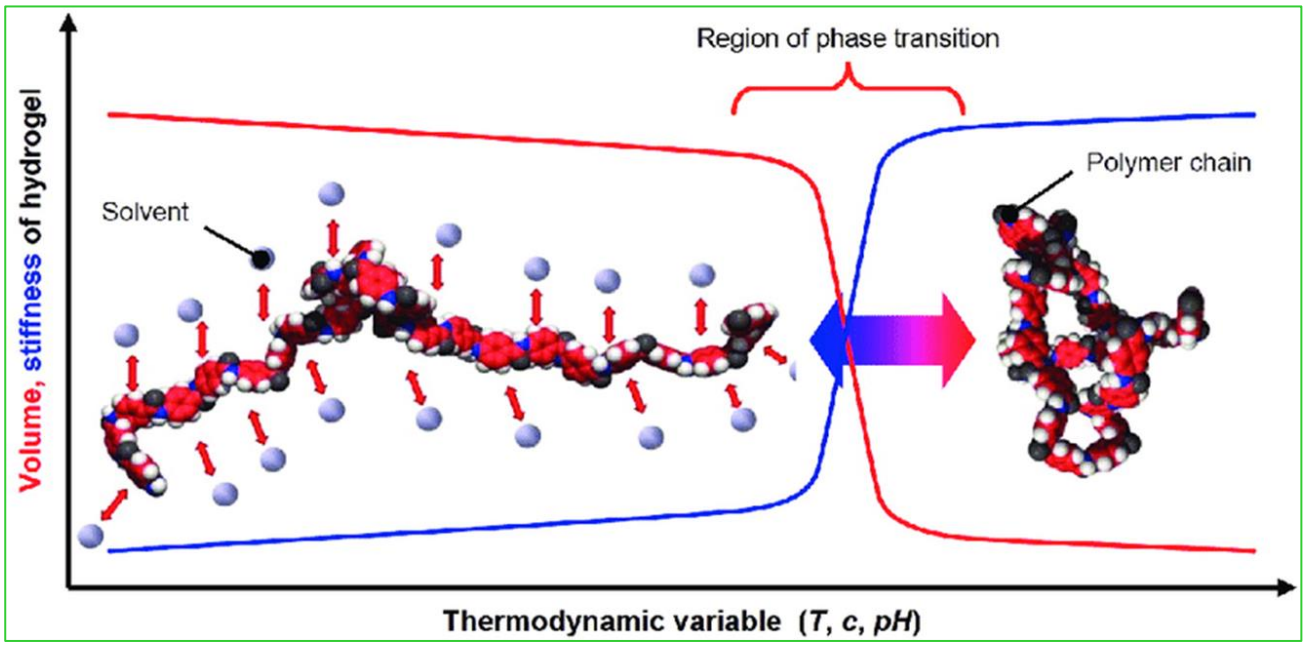

Fig. 13. Smart hydrogels showing volume and structural phase transition behaviour on the application of external stimuli (Reference: Sensors 2008, 8, 561-581.)

Some commonly used LCST-type polymers capable of forming thermoresponsive hydrogels are poly(N-isopropylacrylamide) (PNIPAM), poly(N,N-diethylacrylamide) (PDEAm) and copolymer of N-isopropylacrylamide and butyl methacrylate [P(NIPAM-co-BMA)] [123].

1.3.2 Applications of hydrogels

Owing to their flexibility of water uptake, tunability and compatibility within various environments, hydrogels have found use in extensive fields (Fig. 14.) ranging from household utilities like water-absorbent diapers and cosmetics to industrial use in separation filters in electrophoresis and chromatography to biomedical applications for drug deliveries and as scaffold in tissue engineering. Some of them have been mentioned below.

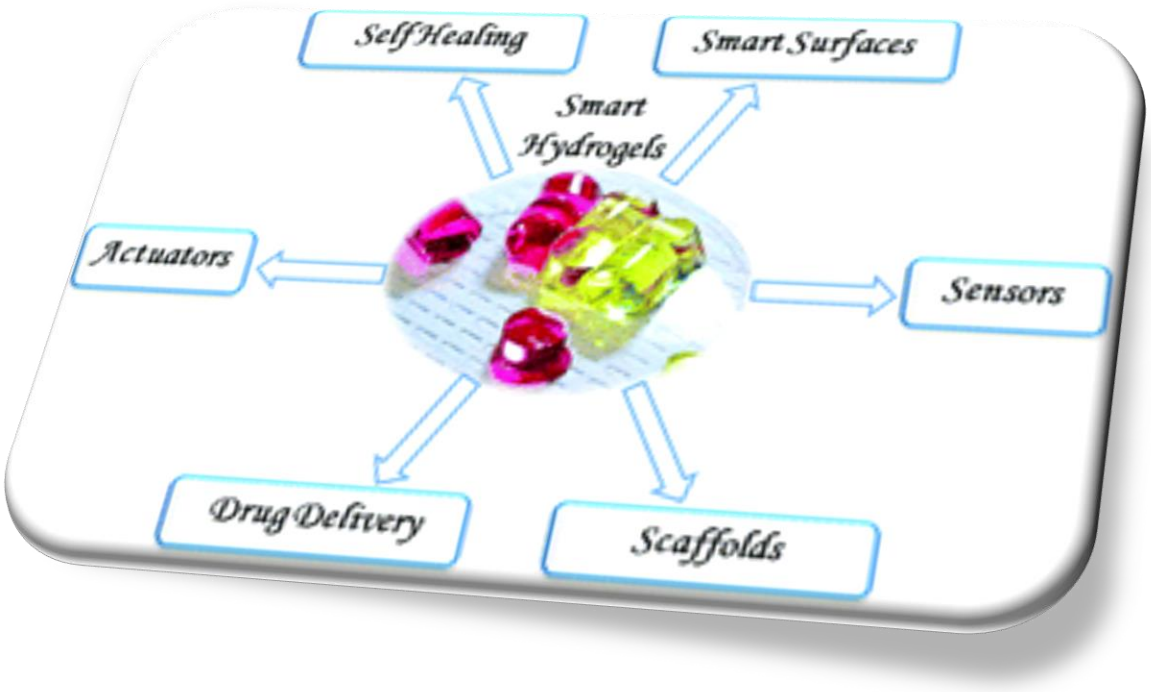

Fig. 14. Smart hydrogels finding applications in widespread fields. (Reference: *Biomater. Sci.*, 2014, **2**, 603-618)

- Diapers: Unlike sponges, which unstable trap water, super-water absorbent hydrogels are used to retain water in high amounts, creating wet-less environments. As in-use diapers takes years for their disposal, sodium polyacrylate based hydrogels are non-toxic and bio-degradable, forming an environmentally superior designs [124].

- Perfume deliveries: Car or air fresheners are made up of hydrogels utilizing the very same concept of swelling properties. When the hydrogel is wetted, release of aroma is triggered by the dynamic swelling force, due to osmotic diffusion of the species from the swollen polymer material. Thus, classic sodium dodecylbenzenesulfonate based perfumes and aroma diffusers are being replaced with smart hydrogels, which are environment friendly and have enhanced swelling and diffusion abilities [125].
- Watering beads for plants: Polyacrylate based hydrogels are employed to release water (thermoswelling type phase behaviour) to plants for stipulated amount of time. This technique can be used from small-scale use in houses as gardening to big-scale horticulture to genetic engineering [126].
- Electrophoresis: Polyacrylamide/ acrylamide-agarose based copolymers are promising systems for gel electrophoresis to be used in protein separation. These smart gels can be designed on the basis of high resolution for both low and high molecular weight biomolecules by focussing on the optimization of size and nature of the hydrogel pores [127].
- Tissue engineering: Hydrogels are considerably being used in biomedical applications as they possess flexibility very similar to animal tissues owing to their significant water update. They solve purposes in tissue engineering as they act as agents for filling vacant spaces, can provide support system for cells, aid in tissue formation and transport bioactive 3D structures inside. Synthetic hydrogel like poly(ethylene oxide) or poly(vinyl alcohol) are interesting as their physical and chemical properties can be tuned for properties. Natural polymers-based hydrogels like from alginate or chitosan opt to become excellent candidates for favourable tissue engineering scaffolds. They can also act as biological adhesives during surgical operations [128].

- Drug delivery: Hydrogels can attain fascinating properties once the biopolymers are used in the synthesis of smart materials. In addition to tissue engineering, they are able to release drugs systematically and controllably in a supreme fashion, causing a decrease in the side-effects. Silk Fibroin is a protein-based biomaterials composed of fibroin and sericine. Chinmoy et al, in 2011 created 3D silk fibroin based hydrogels for efficient attachment and detachment of heart cells [129].
- Contact lenses: Contact lenses are optical devices used to alter the corneal power of eyes by directly placing them over cornea. Soft hydrogels find use in this ophthalmology field by achieving an enhanced swelling properties to retain water over a large amount of time. Silicone –based hydrogels are majorly used for this application due to high permeability towards water, superior mechanical properties, stability towards hydrolysis and its non-toxic nature [130].

1.3.3 Nanoparticles (NPs)

Nanoparticles are quantum dots whose diameter lies from 1 to 100 nm [131]. They are extremely insightful as they bridge the gap between the bulk materials and subatomic-level materials. At nano-scale, significant changes in the physical properties takes place due to their large surface area keeping the same chemical properties [132]. For instance, bulk gold has a melting point of 1064 ^{o}C, however when Au NPs have diameter of 20 nm, the melting point become 1010 ^{o}C which further can be reduced to 500 ^{o}C if the particle diameter is 2 nm, giving us immense opportunity to tune the required physical properties [133]. Nanoparticles can be modified in various shapes like star, sphere, rod or cube (Fig. 15). They can be inorganic (metal based like Au, Fe) or organic (polymer based) in nature.

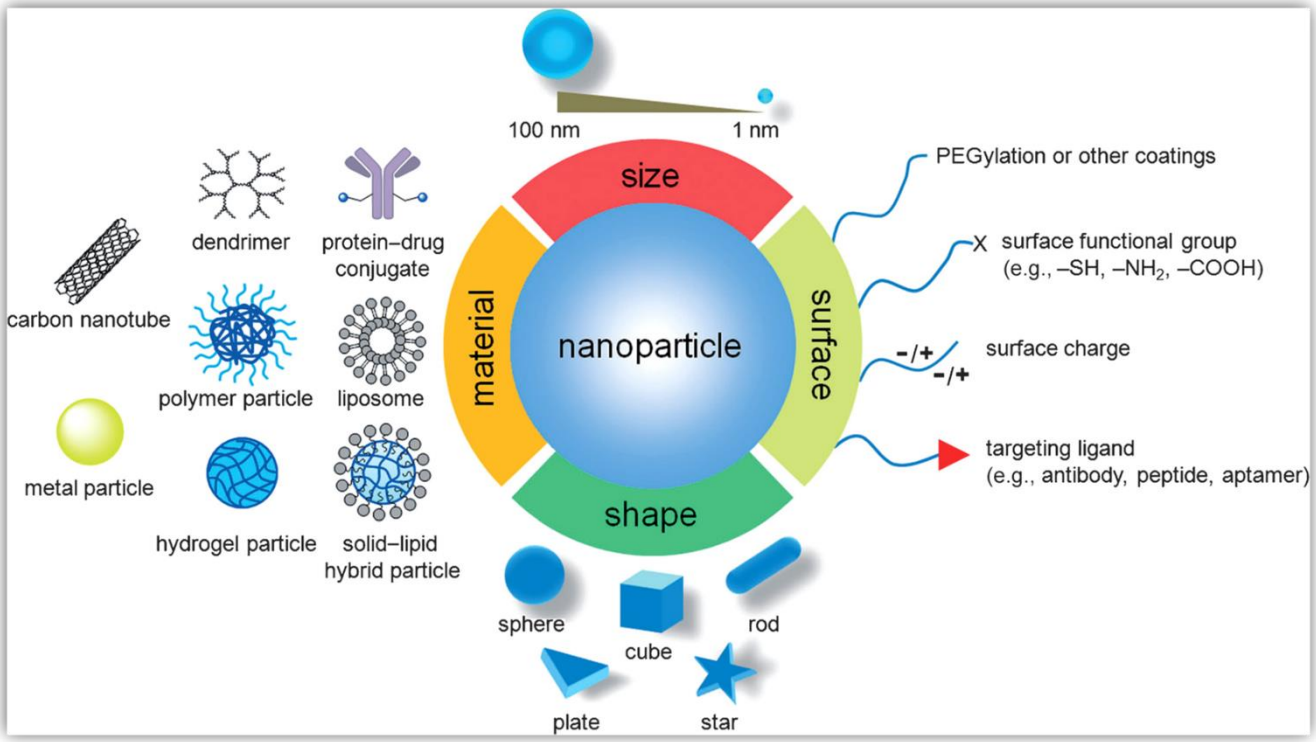

Fig. 15. Nanoparticle and its properties. (Reference: Surface Science Reports, 72, (2017) 1–58)

Metal nanoparticles like gold and silver NPs are extraordinary as they have beneficial physical and chemical properties [134,135]. Both Au and Ag are inert at room temperature, making them less susceptible for oxidation, making them stable enough at ordinary environments. Their electrochemical properties largely depend on particle size. Smaller sized particle are efficient for charging purposes because of their high surface area and chemical inertness. Ag NP can be used to catalytic oxidation of organic compounds such as carbon monoxide (CO) and nitrogen monoxide (NO). Au NPs can actively oxidize carbon monoxide and hydrogen gas. These nanoparticles also procure engaging optical properties because they can produce quantum effects [136]. For instance, Au NPs appear blue to red in solution, depending upon the size of the particles. Similarly, silicon NPs can be seen as yellow to grey. Ag NPs take the colour range of black-brown-yellow. This happens because of the plasmonic nature of these metal nanoparticles. According to the

Mie theory [137,138], a resonant oscillation of valence electrons is induced on the application of an electromagnetic frequency in the form of light. This phenomenon is called localized surface plasmon resonance (LSPR) (Fig. 16). Occurrence of these coherent oscillations is the reason we can observe variant colours from the nanoparticles solutions. Due to this resonance, the particles can either radiate light (plasmonic nature, Mie scattering) or it converts to heat energy (absorption). The LSPR band shows a surface plasmon absorption and thus, has a characteristic extinction band in the UV-Vis-near IR region [139]. The intensity, width and position of these bands rely on the size, shape and nature of surrounding medium [140,141]. Spherical gold nanoparticles absorbs at about 520 nm whereas spherical silver NPs absorbs at about 400 nm when the size ranges from 2-50 nm.

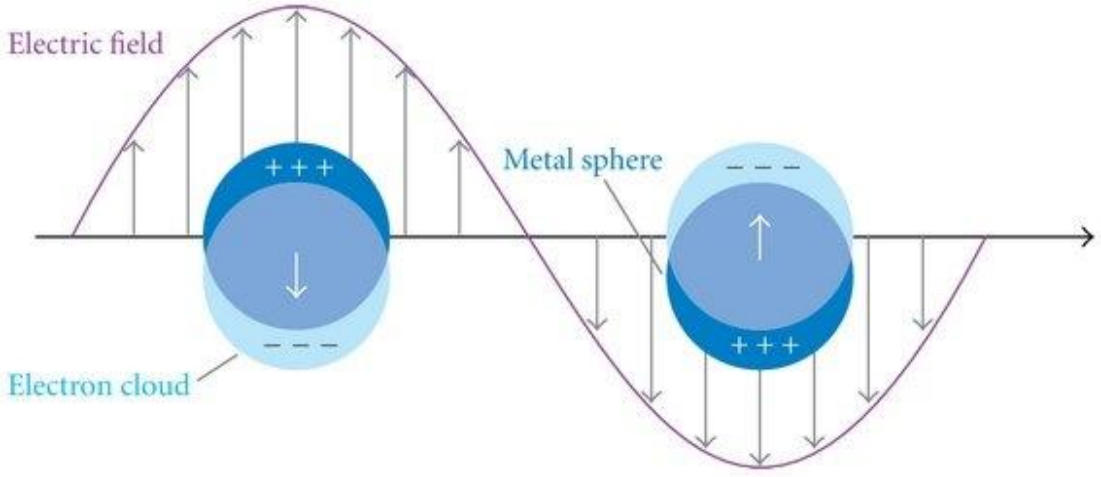

Fig. 16. LSPR resonance in metal nanoparticles. (Reference: Journal of Nanomaterials, 2012, Article ID 759830)

These unique and interesting properties have allowed the gold and silver nanoparticles to be tuned for their shape, diameter of particles, inter-particle distance, and ability to show surface plasmon resonance allowing them to be exploited in various chemical and biological fields [142,143]. Today, it can be said that there is no such field

where nanoparticles cannot be employed. (Fig. 17). Overview of some applications are presented below:

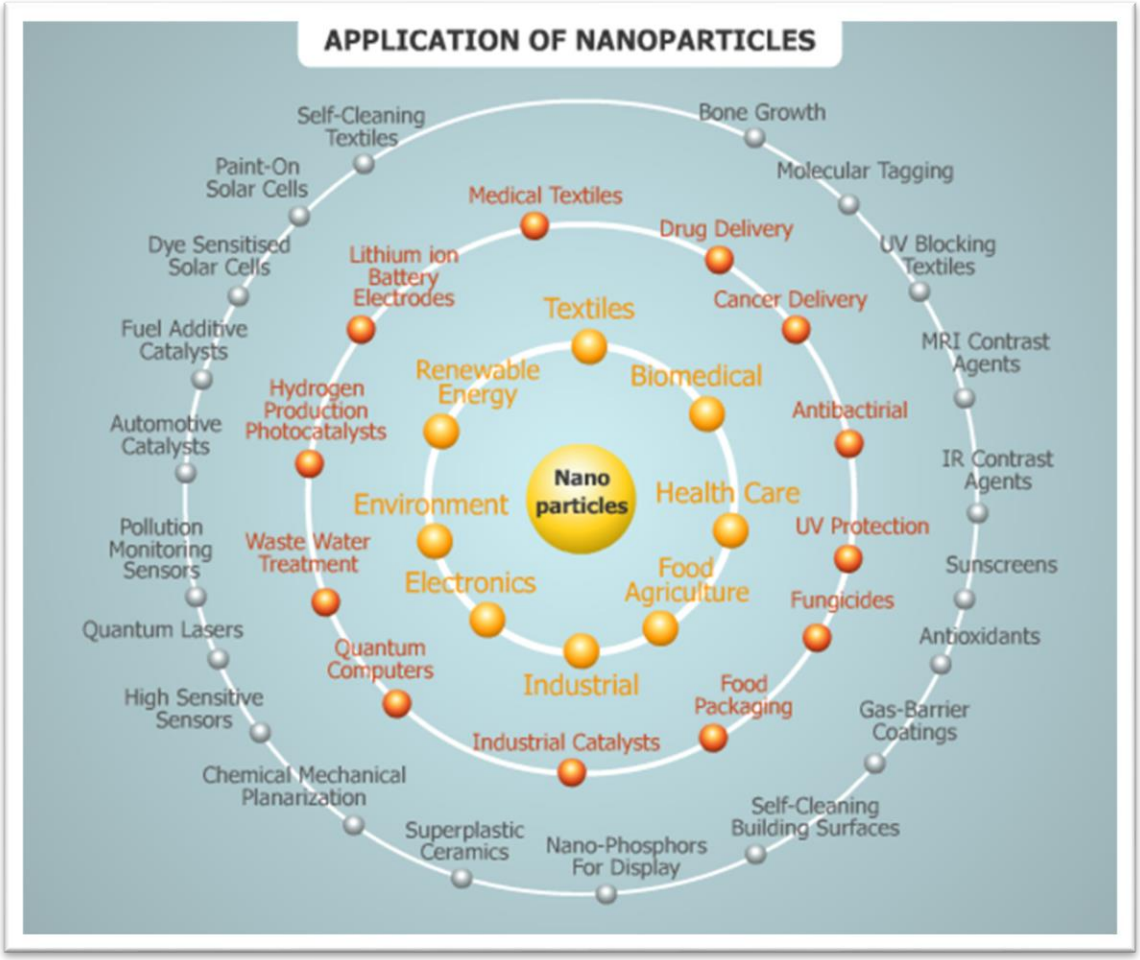

Fig. 17. Applications of nanoparticles used in widespread area. (Reference: prochimia.com)

Nanoparticles in Electronic & Energy

Cho et al, [144] have prepared nanotetrapods embedded with carbon nanoparticles for the development of low cost and highly efficient electrodes for fuel cells. They are able to completely replace the need of expensive platinum. Another collaborative study [145] by the researchers from U.S.A, U.K and Japan have already shown how silver nanoparticles can form conductive lines which leads to the evolution of a printing prototype on circuit boards with the help of standard inkjet printers. Yet another

study done by Abruna et al., [146] showed that 12 times more activity can be achieved than pure platinum if platinum-cobalt core-shell nanoparticles are synthesized to act as fuel cell electrocatalysts. Chen et al, [147] demonstrated that standalone graphene foam based nanoparticles can actively be used for efficient solar thermal capture and conversion device.

Nanoparticles in Environment

Fukumoto et al, [148] prepared composites of mesoporous manganese oxide and gold nanoparticles which allowed the catalysis of volatile organic pollutants in air, and thus can act as extensive air purifiers. Findings by Driessen et al., [149] conveyed the iron nanoparticles to be used as cleansing agents for carbon tetrachloride pollution in ocean and ground water. Yet another study from Roy et al, [150] suggested the use of iron-oxide based nanoparticles to clean arsenic pollutants from water wells.

Nanoparticles in Material Manufacturing

Silicon carbide based nanoparticles dispersed in molten magnesium were prepared by Xiao et al, [151] which showed to have enhanced strength, plasticity, superior flexibility and high thermal stability. Thus, they work as strong yet ultra-high performing lightweight material. Lester et al., [152] performed the dispersion of zinc oxide nanoparticle for the production of various industrial self-cleaning coatings to protect materials like plastic, wood, textiles from harmful UV rays. Another achievement was made by Zhu et al., [153] in 2012 where they found out that crystalline SiO_2 nanoparticles can be used to provide durability and strength to tennis racquets as NPs can fill in the gaps between carbon fibres. Company called Wilson Sporting Goods has already been preparing tennis balls, racquets and other sport equipments using SiO_2 NPs since 2004.

- Nanoparticles in Medicine

MIT researchers Hammond et al., [154] prepared functionalized nanoparticles to transport through the blood brain barriers and target tumours for brain cancer known as gliblastoma. It can deliver two chemotherapy drugs at the same time. Iron oxide nanoparticles coated by polymer were prepared by Barraud et al, [155] which can be used for breakage of bacteria clusters for enhanced treatment of chronic bacterial infections. Protein based nanoparticles were studied for their charges by DeSimone et al, [156] which could stimulate pulmonary immunization responses. Colvin et al, [157] displayed antioxidant properties of cerium oxide based NPs for the removal of free radicals present in the bloodstream when patient is caused with a traumatic injury.

1.3.4 Thermoresponsive polymers-plasmonic systems

Besides utilizing the nanoparticles alone, modification or functionalization of these via smart polymers can increase their applicability to hundredth fold. Surface functionalities and thermoresponsive nature of polymers coupled with tunable morphology, biocompatibility and unique plasmonic nature of nanoparticles make the thermoresponsive- plasmonic nanoparticle system apt for novel smart applications [158].

Researchers have already successfully synthesized thermoresponsive polymer- Au NP composites where polymers used are PNIPAM, polystyrene, poly(vinyl alcohol) or their copolymers, providing synergistic effect for the utilization in catalysis, drug delivery and other smart optical devices. Chilkoti et al., [159] prepared a thermosensitive biopolymer (elastin-like polypeptide) which can stabilize the reversible aggregation of Au NPs due to hydrophobic interactions. Heo et al., [160] reported that strong hydrogen bonds are the key parameters to provide excellent dispersion and reduce the

aggregations of Au NPs in a poly (styrene-co-4-vinylphenol) network. In addition, Lin et al., [161] were successful to utilize silk elastin-like polypeptide based thermoresponsive-plasmonic nanostructures in genetic engineering. PNIPAM-co-PAAm based thermoresponsive copolymer was prepared by Hamner et al, [162] in gold assemblies, which can be used to regulate DNA interactions. Zhao et al, [163] reported a synthesis procedure of thermoresponsive nanogels via click chemistry and RAFT polymerization.

Lately, few reports came up with the idea to use plasmonic nanoparticles as LCST tuning agents for thermosensitive polymers. Klok et al., [164] reported the synthesis of PPEGMA-coated gold nanoparticles and their size-dependent LCST properties. They were able to tune the LCST of polymer matrix by controlling the weight of the constituent NPs. Hu et al, [165] prepared PNIPAM-co-MAA based hydrogels and induced plasmonic nanoparticles like gold and silver to mimic colour changing ability of chameleons. They found out that NPs are able to tune the LCST of the copolymer hydrogels as they act as anchors to restrict the hydrophobic chains of the polymers from rotating at an early stage, thereby inducing a greater demand of thermal energy to collapse.

1.3.5 Ionic liquids and nanoparticles

On problem of metal nanoparticles is their instability over time even after using various stabilizing agents, thereby causing aggregation of nanoparticles [166], which reduces the effect of quantum dots. Hence, one of the ways to stabilise the nanoparticles is by chelating them with ionic liquids [167-168]. Ionic liquids are molten salts which have melting point of below 100 ^{o}C. These non-volatile green solvents are highly polar, have high chemical and thermal stability and most importantly, they can be tuned for their

cationic and anionic counterparts, providing apt opportunities to control the desired structure and properties.

Quite recently, researchers have found out the importance of stability of nanoparticles caused by the presence of ionic liquids in the system. Ionic liquids can be used as synthesizing medium and a source of surface functionalization, as well [169]. Interactions such as van der Waals, solvophobic and electrostatic, and hydrogen-bonding play vital roles in these ionic liquid-nanoparticles hybrids to avoid any agglomerations. Wagner et al, [170] have reported the stability of silica nanoparticles when prepared using colloidal 1-butyl-3-methylimidazolium tetrafluoroborate. They induced a solvation layer of functionalized fluorinated alcohol over N which interact with anion of the ionic liquid, thus stabilizing the particles. Turminee et al, [171] demonstrated the stable nature of ruthenium nanoparticles once synthesized in the 1-butyl-3-methylimidazolium bis(trifluoromethylsulfonyl)imide medium. Dupont et al, [172] prepared transition metal nanoparticles and checked their stability and catalytic activity in imidazolium-based ionic liquids for mutli-phase catalysis. They found out that the nanoparticle/ionic liquid/stabilizer combination provides a fascinating synergistic effect to enhance the durability of the catalyst.

Polymer-IL Copolymers:

Our group has already reported the tuning of LCST of PNIPAM by copolymerizing with imidazolium based ionic liquids [173]. It was observed the tuning of random co-polymers of PNIPAM-IL which showed clear dependency on hydrophobicity of cation and nature of anions. Thus, it was thought to combine the properties of thermoresponsive PNIPAM copolymerized with polymerizable imidazolium-based ionic liquid and further tune the network's LCST by addition of metal nanoparticles to form a LCST-showing hydrogels.

1.3.6 Motivation for Chapter 4

After taking inspiration from above literatures, it can be believed that the polymerized ionic liquid can stabilize the Au NPs and in turn, NPs could enhance the light to thermal efficiency of the thermo-sensitive polymer. This would double the opportunity of its use in different applications. Thus, for the first time, I incorporate distinct sizes of Au and Ag NP in (N-isopropylacrylamide-polymerizable N,N'-di-substituted imidazolium-based ionic liquids) hydrogels and study how the size of plasmonic nanoparticles and structure of polymerizable ionic liquids effect the fine-tuning of phase behaviour of these hydrogels. Citrate-coated gold and silver NPs ranging from 10 to 50 nm in size, were prepared, and further added to in-situ copolymerization of NIPAM with different polymerizable ionic liquids to form a plasmonic nanoparticles induced thermoresponsive hydrogels which showed tunable reversible LCST swelling/shrinking in water.

Why N-isopropylacrylamide as thermoresponsive monomer?

NIPAM structure (LCST: 32 ^{o}C) has hydrophilic (N-H, C=O) and hydrophobic (isopropyl) groups which can play important hydrophilic-hydrophobic interactions with ionic liquids.

Why ionic liquids as comonomers?

Ionic liquid can provide stability to nanoparticle and tunability towards structure and LCST behaviour of polymer hydrogel.

Why plasmonic nanoparticles needed?

They can act as anchors to restrict the motion of hydrophobic chains, thereby act as tuners which can be tuned on the basis of their size.

Novelty of the work?

Metal nanoparticles (Au and Ag) are incorporated into thermosensitive PNIPAM-co-IL hydrogels, whose LCST can be tuned by size of NP and hydrophilic nature of IL.

1.4 CST in ionic liquids (ILs)

As seen, thermoresponsive polymers, classified under "smart" materials are being researched intensively due to their widspread applications that include sensors, drug delivery, gene delivery and tissue engineering as these can respond to stimuli such as pH, temperature, ionic strength, electric or magnetic field, light and/or chemical and biological stimuli. These polymers can be classified based on the temperature of phase separation as LCST and UCST depending upon their miscibility behavior. However, many of these polymers are non-biodegradable.They may swell in water when not required, have high toxicity and flammability and are sensitive towards solvent and UV- light. Also, their production process may require extra health and environmental safeguards. Therefore, tailoring of these polymers is needed suiting the user's need. Consequently, ionic liquids [174,175] have been identified as the alternative material of choice due to easy designability and systematic evaluation of the desired properties

1.4.1 Introduction and characteristics of ionic liquids

Classified under environmentally benign solvents, ionic liquid are molten salts which by definition, melts below 100 ^{o}C. Some of them are liquid at room temperature and are called room temperature ionic liquids (RTILs). They can be constituted by diverse selection of organic or inorganic cationic and anionic parts, providing the user enough designability. First RTIL identified was ethylammonium nitrate (melting point 12 ^{o}C) which was synthesized and characterized by Paul Walden in 1914. Since then, versatile categories of cations and anions have been identified. Types and structures of some commonly used cations (like imidazolium, pyridinium, pyrrolidium, quaternary ammonium) and anions (water soluble like halides or water insoluble like hexafluorophosphate and $TFSI^{-}$) have been mentioned in the Fig. 18.

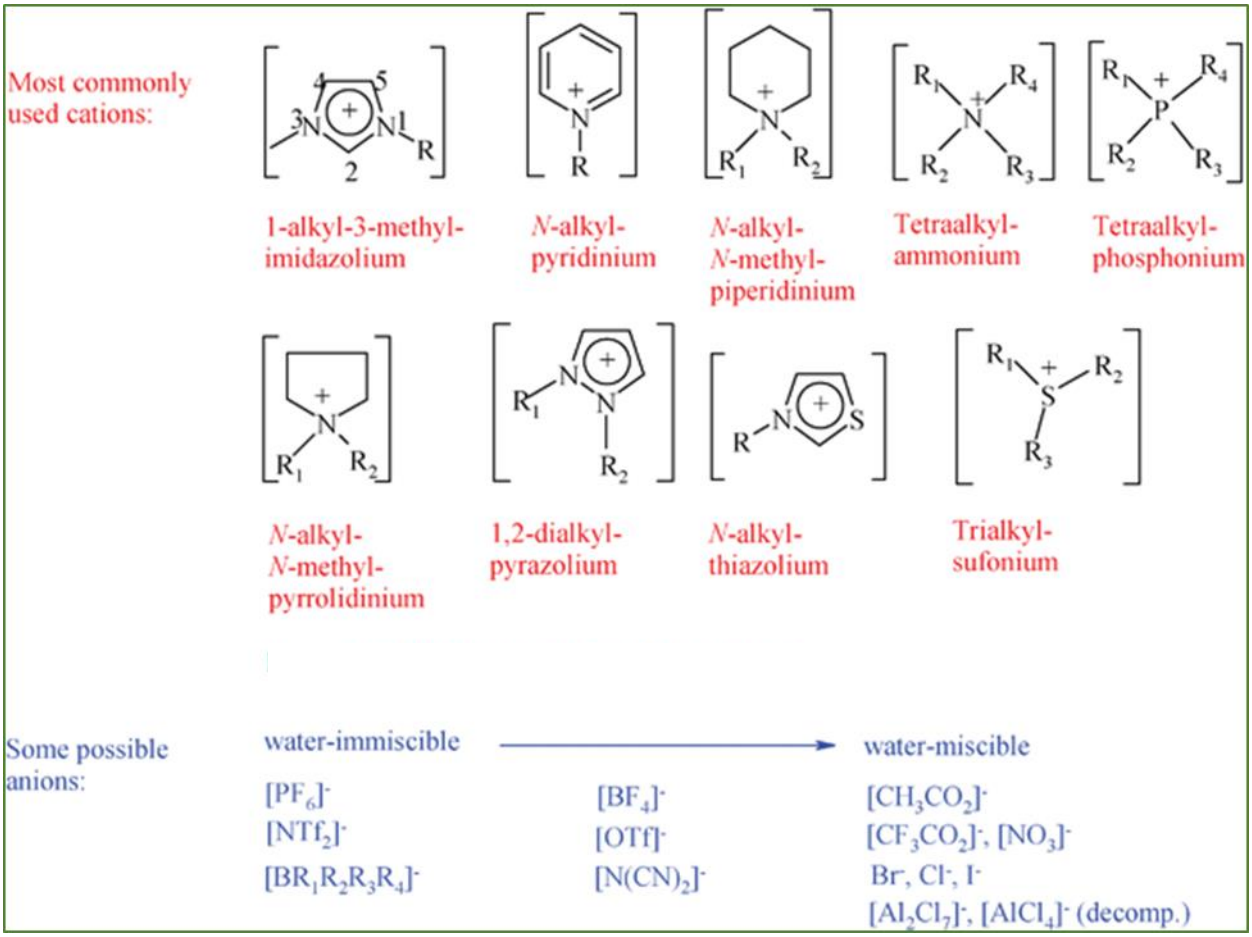

Fig. 18. Commonly used cations and anions in the synthesis of ionic liquids. (Reference: Chem. Soc. Rev., 2008, 37, 123–150)

Ionic liquids generally are viscous liquid. They also attain non-flammable, non-volatile and electrical & thermal stability properties. Owing to their polar and ionic nature, they show high thermal and electrical conductivities. They have negligible vapour pressure. Most captivating properties of these greener solvents are their designability and tunability [176]. A vast number of cation-anion combinations are available making it possible to "engineer" the physicochemical properties of the ionic liquids, as necessary. Various diverse properties like viscosity, hydrophobicity and stability in a medium can be tuned according to the requirements. For example, 1-ethyl-3-methylimidazolim bromide is a hydrophilic ionic liquid, but if we replace the anion with $N(SO_2CF_3)_2^-$, the system becomes hydrophobic [177]. Quaternary phosphonium- based ionic liquids are

more thermally stable and have a larger electrochemical window as compared to nitrogen-containing ILs.

Recently, these liquids are tagged as "clean solvents". Many organic synthetic reactions like Diels Alders, Friedel-Crafts reactions and some bio-catalytic reactions can be performed when ionic liquids act as solvents. They have technological applications [178] as well such as metal surface finishing, capacitors, batteries, fuel cells, nuclear waste treatment and others. Ionic liquids are also gaining worldwide recognition in various fields including organic chemistry, pharmaceuticals, catalysis, engineering, physical chemistry, analytical chemistry, gas handling, fundamental research and many other industrial application. Also they have potential to be applied as catalysts. Fig 19. lists some of the many applications where ionic liquids are being used extensively.

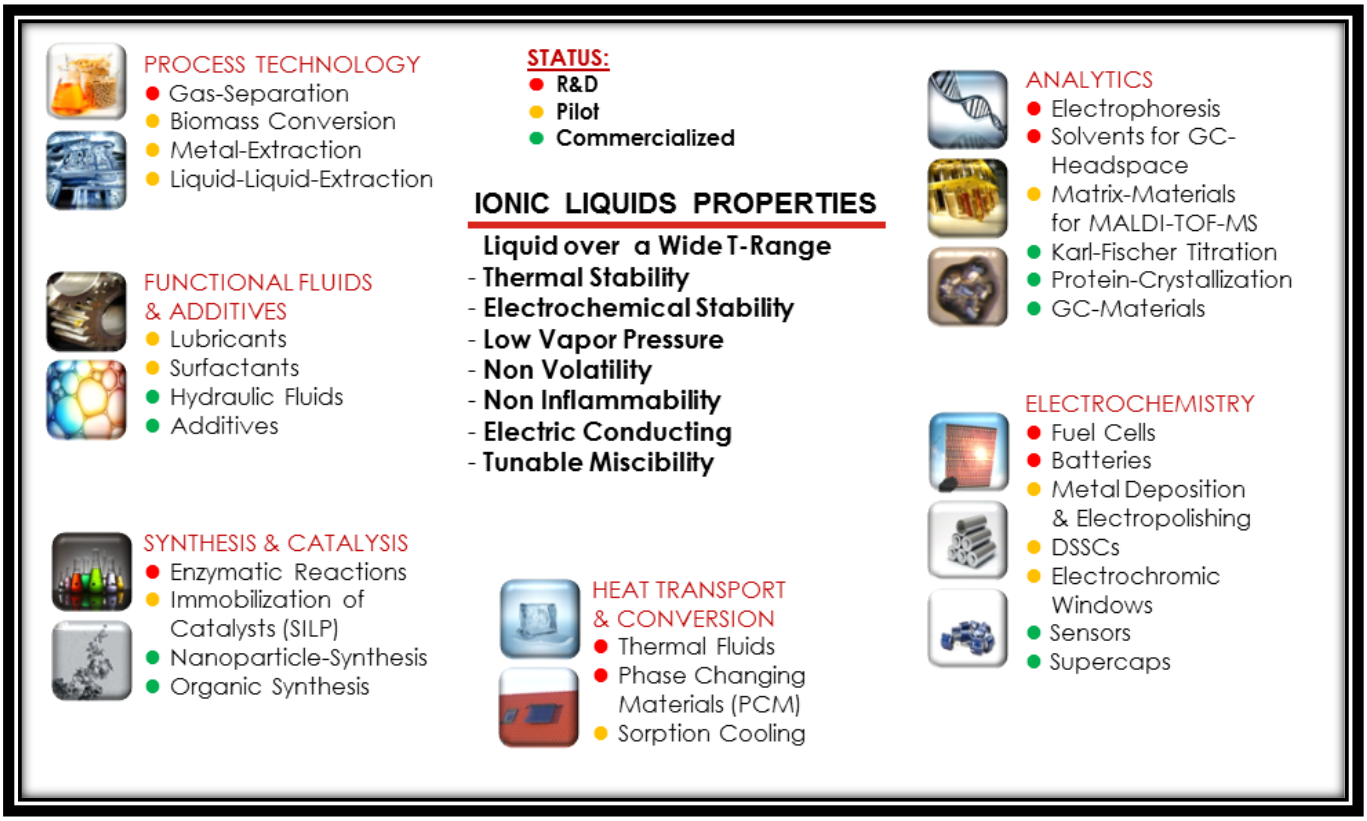

Fig. 19. Typical applications of ionic liquids.

1.4.2 Ionic liquid/water mixtures

Ionic liquids are very complex in nature. They can interact with other solvent like alcohol, water and other ionic liquids via dispersion, ionic, hydrogen bonding and dipole-dipole interactions. When polar molecules are present in the mixture, some ILs act as polar solvents and with non-polar solvents, as a non-polar solvent.

Huddleston et al, [179] reported the partition coefficients of several organic compounds between [1-ethyl-3methylimidazolium][PF_6] and water. Selvan et al, [180] recently reported liquid–liquid equilibrium data of ethyl-3-methylimidazolium triiodide ([emim][I_3]) with toluene and *n*-heptane. Friberg et al, [181] observed the coexistence of a lamellar liquid crystal phase with isotropic surfactant, ionic liquid and aqueous phase for Laureth (surfactant) + water system containing the ionic liquid 1-butyl-3-methylimidazolium hexafluorophosphate ([bmim][PF_6]). Liquid-liquid equilibria between alcohols and RTILs have been studied by Wu et al, [182].

Water is the universal solvent. Many biological activities and chemical systems work in aqueous systems. It has unique physicochemical properties due to hydrogen bonding. Therefore, choosing water as the other covalent partner in a mixture gives several advantages over other solvents owing to water's larger dipole moment and ability to form 3D hydrogen bond networks. These mixtures can act as functional fluids in bioscience. Much research on the importance of these mixtures, is being carried out today. ILs with hydrophobic fluorinated anions like [Tf_2N] and PF_6 are immiscible with water. These systems find use in liquid/liquid biphasic studies [183,184]. ILs with hydrophilic ions such as Cl^-, Br^-, PO_4^{3-} and $RCOO^-$ are generally soluble in water. Presence of water in various ionic liquids can control their physical properties by effecting their interionic interactions. Adjusting the water content gives the ability to significantly change viscosity, polarity,

surface tension and density as there occurs changes in intra- and inter-molecular hydrogen bonding between constituent ions. Also, the high electric constant of water is strong enough to be able to weaken the electrostatic interactions between the constituent cation and anion of the ionic liquid, thereby reducing the viscosity much more than any organic solvent like chloroform with lower electric constant. However, it is observed that addition of small amount of water not always leads to drastic changes in properties. Seddon et al, [184] showed that there is no density change at low water content when the same was investigated using 1-butyl-3-methylimidazolium tetrafluoroborate. Thus, complex nature of individual ions corresponds to unpredictable and unexpected nature of designed ionic liquids, thereby compelling us to study interactions for each type of ionic liquids separately.

By closely examining the phase separation of some of the IL/water systems, it was found out that like polymers, there are two temperature driven phase transitions in these liquid/liquid binary mixtures: Upper Critical Solution Temperature (UCST)-type and Lower Critical Solution Temperature (LCST)-type phase transitions as seen in Fig. 20 [185].

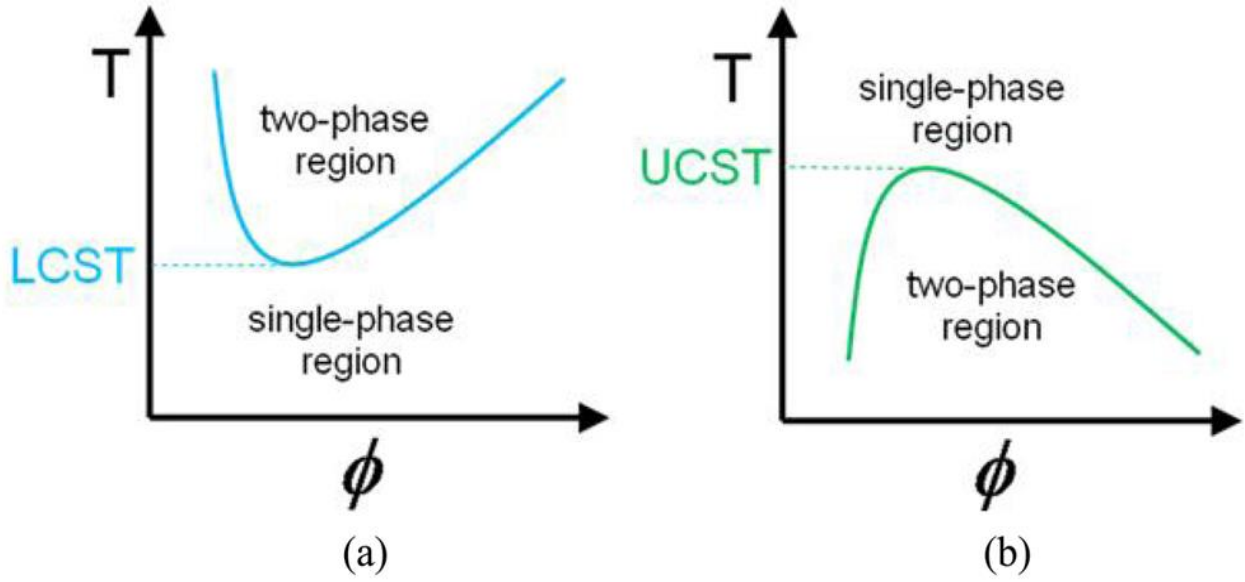

Fig. 20. Temperature vs concentration phase diagrams showing (a) LCST and (b) UCST of liquid/liquid biphasic mixtures.

LCST and UCST are critical temperatures below and above which the ionic liquid and solvent are completely miscible respectively. That is, an IL/water mixture is homogenously uniform below LCST and appears biphasic or cloudy above LCST. For UCST, it is the opposite phenomenon. Most IL/water mixture exhibit UCST. In this, solubility of two liquids increases upon heating. This transition is exhibited by sufficiently hydrophobic ionic liquids. In LCST-type phase transition, miscibility of two liquids increases upon cooling and these are generally observed in aqueous solutions of some non-ionic polymers.

Many examples of the thermosensitive phase transitions exhibited by ionic liquid/solvent are summarized in Fig. 21 [186]. Major cations examined are tetrabutylphosphonium (P_{4444}), tetrabutylammonium (N_{4444}) and 1-alkyl-3-methylimidazolium ($C_x$mim). Most of the entries were found to showcase UCST-type phase transition in water (entries 1-8). However, it was discovered by Weingartner et al [186], that tetrabutylammonium thiocyanate showed both LCST and UCST type phase transitions (entry 9). This is the first instance where IL/water showed LCST type transition. Since then, many researchers are trying to deduce LCST-type phase behvaior for various IL/solvent due to their potential applications in solution chemistry and biomedical applications. Various solvents like chloroform (entry 27, 32), benzene (28), toluene (29) and ethers (30) have been studied for ionic liquids to show CST. LCST is also displayed by ternary mixtures like in entry 12 and 32. Ohno et al, [186] revealed that LCST can be shown by amino-acid based anion which is N-trifluoromethanesulfonyl with tetrabutylammonium cation (entry 13). Most of the imidazolium-based ionic liquids tend to show UCST (entries 1, 2, 6, 8, 27, 28) owing to the coupled hydrophilic/hydrophobic nature of cation and anion. However, it was interesting to note by Rebelo et al, that ternary mixture of [C_4mim][PF_6], water and ethanol displayed LCST even though separate

Entry	IL	Solvent	Phase behaviour	T_c[b]/°C	Molar ratio[c] (solvent : IL)
1	$[C_4mim]BF_4$	Water	UCST	4.4	13 : 1
2	$[C_8mim]BF_4$	Water	UCST	—[d]	—[d]
3	$[Bet][Tf_2N]$	Water	UCST	56	20 : 1
4	$[N_{11N2OH}][Tf_2N]$	Water	UCST	72	19 : 1
5	$[P_{4444}][Fum]$	Water	UCST	62	50 : 1
6	$[C_6H_{13}OCH_2mim]X$ $X = [BF_4]^-, [Tf_2N]^-$	Aliphatic, aromatic hydrocarbons	UCST	Depending upon structure of hydrocarbons	—[d]
7	$[P_{66614}]X$ $X = Cl^-, Br^-$	Aliphatic hydrocarbons	UCST	33	37 : 1
8	$[C_4mim]X$ $X = PF_6^-, BF_4^-, Tf_2N^-, CF_3SO_3^-$	Alcohols	UCST	Depending upon structures of alcohols	—[d]
9	$[N_{4444}]SCN$[a]	Water	UCST and LCST	UCST; 150 LCST; −23	18 : 1
10	$[N_{444n}]Br$[a] $n = 12, 14, 16$	Water	LCST	Increasing upon increasing n values	—[d]
11	$[N_{4443}]I$[a]	Water	UCST and LCST	UCST; 73, LCST; 59	25 : 1
12	$[C_4mim]PF_6$	Water–ethanol	LCST	15	5.5 : 4.5 : 1 (ethanol–water–IL)
13	$[P_{4444}]$[Tf-AA]	Water	LCST	[Tf-Val]; —[c] [Tf-Leu]; 24 [Tf-Ile]; 25 [Tf-Phe]; 16	50 : 50[e] (by weight)
14	$[P_{4444}]$[Mal]	Water	LCST	22	20 : 1
15	$[C_4mim]FeCl_4$	Water	LCST	—[d]	—[d]
16	$[P_{4444}]CF_3COO$	Water	LCST	29	37 : 1
17	$[P_{4444}]$[2,4,6-alkyl-benzenesulfonate]	Water	LCST	[Tos]; 53 [DMBS]; 36 [TMBS]; 30	[Tos]; 44 : 1 [DMBS]; 33 : 1 [TMBS]; 39 : 1
18	$[N_{4444}]$[TMBS]	Water	LCST	53	47 : 1
19	$[P_{4448}]Br$	Water	LCST	24	14 : 1
20	$[P_{4448}]CH_3SO_3$ + $[P_{4448}]CF_3COO$	Water	LCST	Lowering upon increasing fraction of $[P_{4448}]CF_3COO$	—[d]
21	$[P_{444n}][BzIm]$ $n = 4, 8$	Water	LCST	$n = 4$; 28, $n = 8$; 18	$n = 4$; 63 : 1[e] $n = 8$, 72 : 1[e]
22	$[P_{4444}][Sal]$	Water	LCST	30	50 : 50[e] (by weight)
23	$[P_{666n}][(EtO)HPO_2]$ $n = 6, 8$	Water	LCST	$n = 6$; 33, $n = 8$; 15	50 : 1[e]
24	[P8C2P][a]	Water	LCST	11	35 : 1[e]
25	$[N_{555}C3S] + [N_{666}C3S]$	Water	UCST and LCST	UCST; 17 LCST; 41	35 : 0.67 : 0.33 (water–$[N_{555}C3S]$ $[N_{666}C3S]$)[e]
26	$[P_{4444}][SS]$	Water	LCST	33	49 : 1
27	$[P_{4446}][MC3S]$	Water	LCST	35	50 : 50[e] (by weight)
28	$[P_{6668}][Asp] + [P_{6668}][Lys]$	Water	LCST	6	31 : 1
29	$[C_4mim][Tf_2N]$ + $[C_5mim][Tf_2N]$	Chloroform	UCST and LCST	UCST; 32 ~ 97 LCST; −13 ~ 32, 97 ~	—[d]
30	$[C_{10}mim][Tf_2N]$	Benzene	UCST and LCST	UCST; 45 LCST > 100	55 : 1 (0.1 MPa)
31	$[N_{4444}]Br$	Toluene	LCST	25	36 : 1
32	$[C_4mim]PF_6$	Trifluoromethane	LCST	Depending upon both molar composition and pressure	—[d]
33	$[N_{11N2OH}][Tf_2N]$	Various ethers	LCST	Depending on both n values and structures of ethers	—[d]
34	$[C_1mim]I$ + 1,4-dipropoxypillar[5]-arene (DPP5)	Chloroform	LCST	50	IL–DPP5 = 5 : 1 (IL conc.; 0.27 M in chloroform)[e]

[a] Although these organic salts do not meet the definition of ILs, it is of significance to mention them here because of their structural analogy to ILs. [b] Phase transition temperature. [c] At critical composition. [d] Not available. [e] Critical composition was not observed, or not described.

Fig. 21. Examples of CST exhibiting ionic liquid/solvent mixtures. (Reference: Polym. Chem., 2015, 6, 2163)

mixtures of [C_4mim][PF_6]/ water and [C_4mim][PF_6]/ethanol showed UCST-type phase transitions. Hence, we are still at a stage where the LCST of imidazolium-based ionic liquid and their characteristics are evolving and much attention is needed to develop this class of greener solvents.

1.4.3 Techniques to find CST in IL/water mixtures

In literature, there are several techniques to study interactions, phase separation and transition properties of an IL/water mixture.

A. Use of a dye

Ohno et al, [175] in 2007 reported the use of a dye to find LCST-type phase transition of amino–acid based ionic liquid/water mixture. The dye used was Nile red which was soluble in organic phase. Fig. 22. shows image of temperature-dependent phase behaviour of tetrabutylphosphonium N-trifluoromethanesulfonyl-leucine ([P_{4444}]-[Tf-Leu])/water mixture.

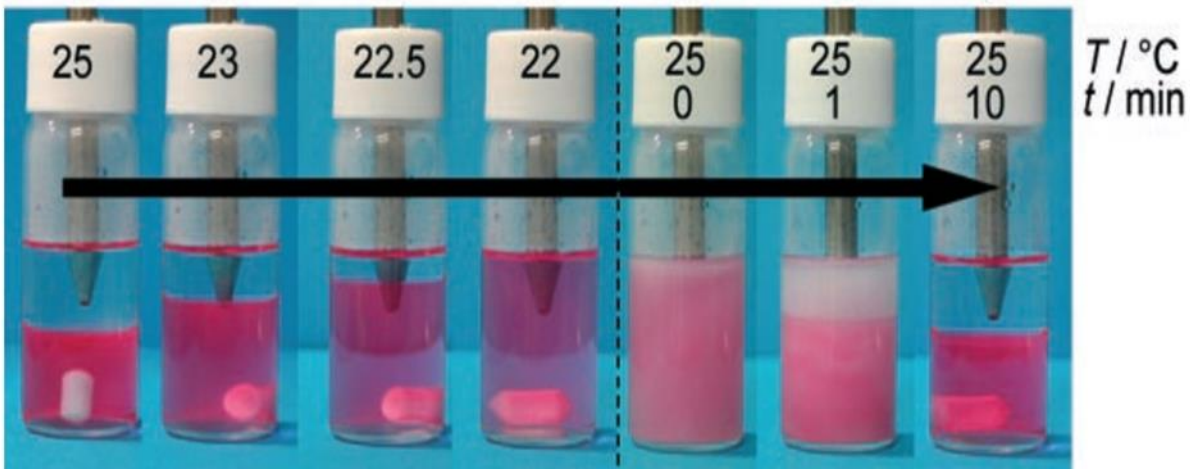

Fig. 22. Temperature dependent phase behavior of ([P_{4444}]-[Tf-Leu]/water mixture.

They found that [P_{4444}]-[Tf-Leu] is mixed with 50% water, phase separation occurs at 25 ^oC. On cooling, more ionic liquid separates out. But at 22 ^oC, the two liquids becomes soluble again.

B. UV-Visible Spectroscopy

Lee et al, [187] in 2010 used UV-Vis spectroscopy to evaluate cloud point for polyethylene oxide PEO-20 in 1-ethyl-3-methyl imidazolium tetra fluoroborate [emim][BF_4] as shown in Fig. 23.

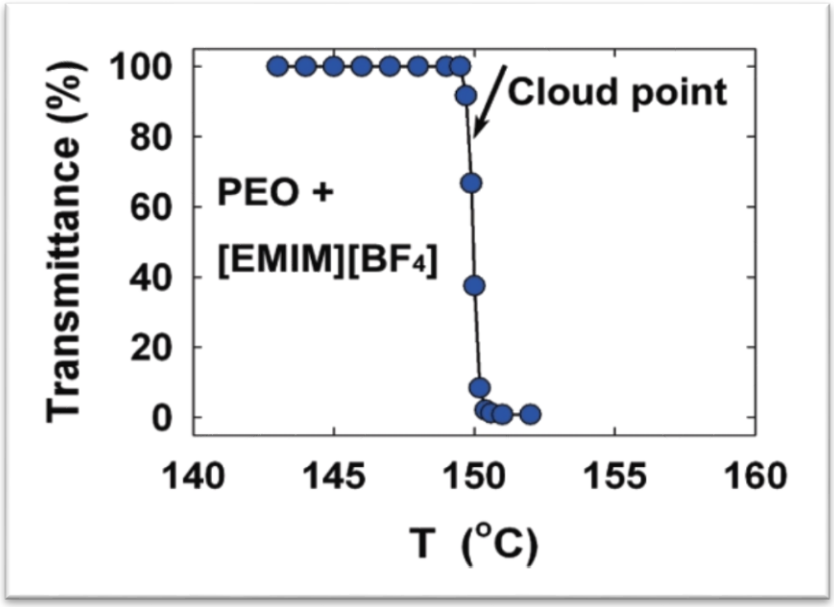

Fig. 23. Temperature dependence of transmittance at 632.8 nm for PEO-20 in [EMIM][BF_4] measured at a heating rate of ~1 °C/min.

C. Laser Light Scanning (LLS)

LLS was also used to study phase separation of ILs in water. LLS also helps in revealing the existence of mesoscopic phase, if present. One such case is shown in Fig. 24 [188].

D. Phase diagrams

Many of the examples show the use of phase diagrams to estimate phase separation behaviour of various IL mixtures. Fig. 25. shows liquid-liquid equilibria (LLE) phase diagram of 1-hexyl-3-methylimidazolium hexafluorophosphate in different alcohols [189].

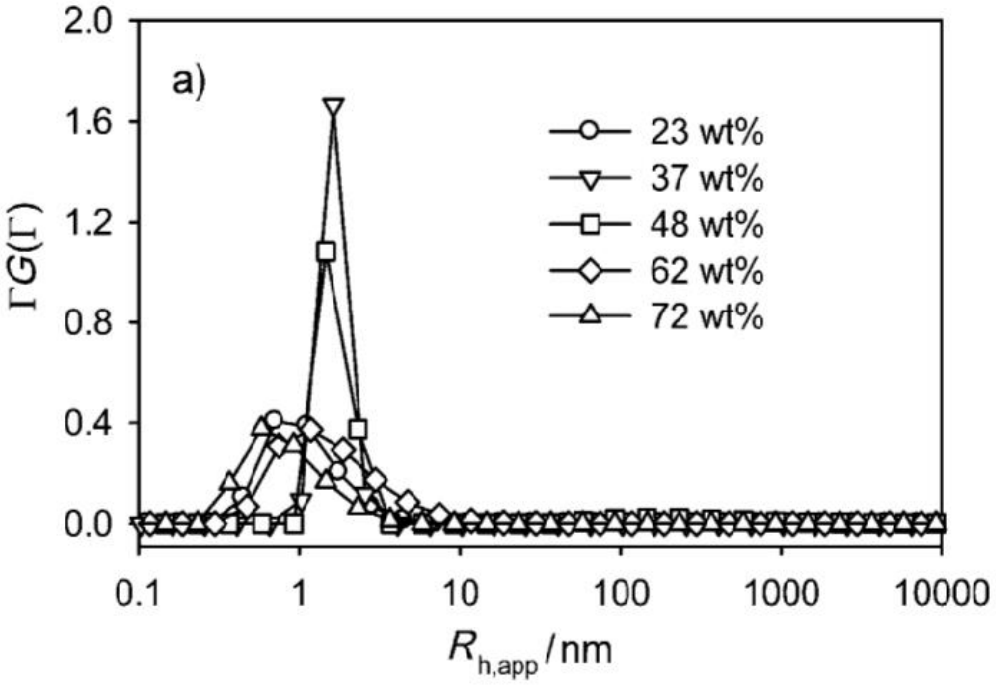

Fig. 24. Dynamic Light Scattering (DLS) results of $[C_4MIm]BF_4$/water.

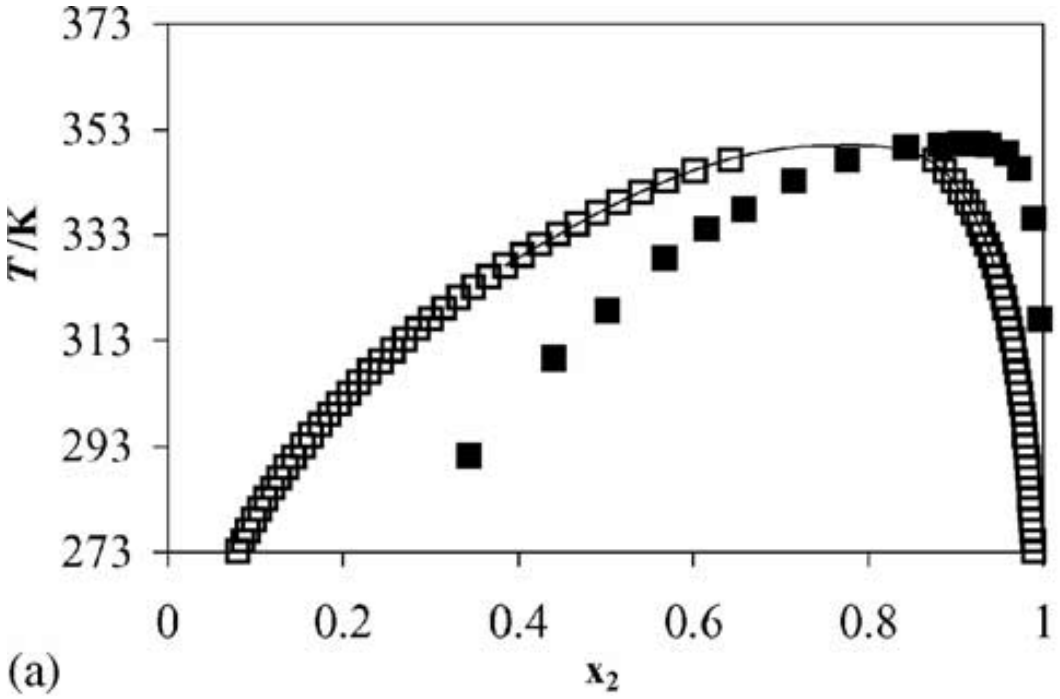

Fig. 25. Comparison of LLE phase diagram for the systems $[C_6MIm][PF_6]$ + butan-1-ol at 1 bar.

Several other techniques like composition diagrams and apparatus have been designed to study phase separation in ionic liquid-water mixtures. Researchers have also shown phase changes behavior by pulse-induced critical scattering (PICS) and Micro-calorimetry which are highly complex mechanisms and time-consuming.

All these physical techniques work when

- ILs are used which show turbidity near phase transition when mixed in water.
- ILs whose polarity is different than that of water are taken into account.

There are several other ionic liquid/ water systems which it is difficult to estimate phase separation properties by usual techniques. All the till date technique fails, when following situations arises:

- When phase separation of system is not very distinct and clear visually
- When the dye is almost equally soluble in both, water and ionic liquid.
- When visual, optical measurements and concentration measurements of the system fail to impact on the phase transition property of the system.

Therefore, there is a lack of diagnostic tool which could electrochemically determine phase changes in ionic liquids accurately and precisely.

1.4.4 Electrochemical Impedance Spectroscopy (EIS)

Electrochemical Impedance Spectroscopy or EIS [190,191] has gained much popularity in recent studies. It is a powerful and a well-known standard technique when it comes to investigating electrode processes and complex interfaces in electrochemical systems Main advantage of EIS is that with a single experiment in which a broad range of

frequencies are applied, many physical and electrochemical parameters can be studied at an applied potential.

Initially used to determine double layer capacitance and in ac-polarography, EIS is nowadays used in various applications in the field of characterization of materials such as in coatings, batteries, fuel cells and corrosion phenomena. It is being also applied to investigate diffusion across membranes and mechanisms in electro dissolution, passivity and at semiconductor interfaces [192].

EIS marks its impact for research and development, for product confirmation and quality assurance in manufacturing operations.

Principle of the technique

The technique involves the application of a small sinusoidal excitation signal which can be voltage or current perturbation to the system under observation. Then, the resultant response of current or voltage is measured along with the phase angle. These measurements are carried out at different AC frequencies and hence, EIS is also known as AC Impedance spectroscopy [193].

The response is then, plotted in terms of graphical plots to analyse the impedance data. At higher frequencies, electrolytes resonate and thus, electrolytic properties are observed at high frequencies. As frequencies are decreased, partial electrolyte and partial electrode properties are studied as resonance occurs due to partial electrolytic and double layer characteristic. Further, as the experiment is carried out at lower frequencies, one can observe more of electrode properties.

Advantages of EIS

EIS offers several advantages and is established as the one of the superior and sophisticated model technique over other physical an electrochemical techniques.

- Is a high-precision technique
- Real world measurements can be made using real operating conditions. *e.g.*, open circuit voltage or under load (DC voltage or current).
- A single experiment can aid in determining multiple parameters
- Simple setups are easy to operate ad handle
- Can characterize interfacial as well as bulk properties of the system
- Can verify reaction models

Other advantages are grouped in Fig. 26.

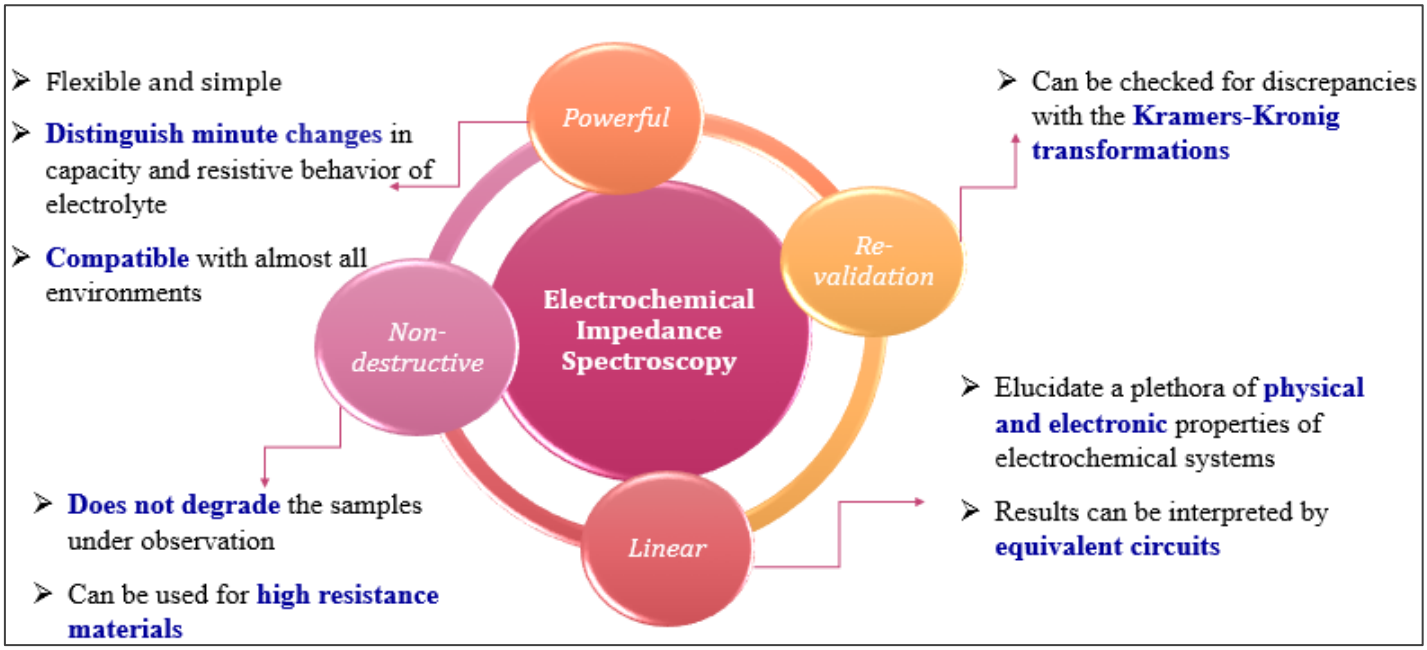

Fig. 26. Advantages of EIS

1.4.5 Kamlet-Taft parameter studies

The phase transition properties of various IL/water systems can be controlled reversibly by small thermal change, thereby increasing the potential applications of the system to purification, extractions and biopolymer separation. Many researchers over the globe are trying to analyse the parameters and factor effecting the critical phase temperature of these ionic liquids. Ohno et al, [194] have explored this field and been rigorously working on mechanistic and fundamental approaches of amino acid-based ionic liquids and their phase separation. Recently, Wang et al, [195]. have found out the mechanism of amino-acid based ionic liquids using molecular dynamics (MD) simulation. Still, there is a need for a comprehensive study to examine the factors effecting phase transitions in imidazolium-based ILs from their structural and design point of view. This will make the tunability and designability of these binary mixtures a lot more facile for their targeted features. Therefore, on the same path to understand transition mechanisms, hereupon imidazolium based ionic liquids will be analysed with respect to their physical and structural properties using Kamlet-Taft parameters studies [196-198].

Kamlet-Taft solvatochromic parameters provide details of the measure of hydrogen bond donor (α) and acceptor (β), dipolarity/polarizability (π*) and overall solvent polarity (E_T). For the calculation of these parameters, UV-Visible spectroscopy is performed with three dyes namely, zwitterionic Reichardt's dye, 4-nitroaniline and *N, N*-diethyl-4-nitroaniline. Charge transfer absorption between Reichardt's dye and ionic liquid is given in the form of $E_T(30)$ [Eq. (1)] and E_T^N [Eq. (2)] scales which discuss about the overall polarity and normalized polarity with respect to water respectively. These parameters in kcalmol^{-1}, were calculated using the maximum absorption wavelength with the dye λ_{max} [26].

$$E_T(30) = \frac{28591}{\lambda_{max}} \qquad (1)$$

$$E_T{}^N = \frac{E_T(30) - 30.7}{32.4} \qquad (2)$$

One of the Kamlet Taft parameter is $\pi*$ [Eq. (3)] which infers about the dipolarity/polarizability ratio of the solvent [25]. This depends on the maximum absorption wavelength of *N,N*-diethyl-4-nitroaniline dye in kilokeyser (kK) units.

$$\pi* = \frac{\nu_{max} - \nu_0}{s} \qquad (3)$$

Here, ν_0 denotes the regression value for a reference solvent system and has a value of 27.52 kK. s measures the susceptibility of intensity of absorption with a value of -3.182.

Kamlet Taft parameters α [Eq. (4)] and β [Eq. (5)] correspond to hydrogen bond donating ability and accepting ability, respectively [25]. They were calculated using $\pi*$ parameter and maximum absorption wavelength for dissolved 4-nitroaniline ν_1, and *N, N*-diethyl-4-nitroaniline ν_2.

$$\alpha = \frac{E_T(30) - 14.6(\pi* - 0.23) - 30.31}{16.5} \qquad (4)$$

$$\beta = \frac{1.035\nu_2 - \nu_1 + 2.64}{2.8} \qquad (5)$$

1.4.6 COMSO-RS Simulations

In the present scenario, 3 possible simulation techniques are possible, including force field type calculations, Group contribution and DFT calculations. Although these techniques are precise, these are time-consuming and highly approximated. So, introduction of a newer and easier technique will be better option as it will encourage more precise results in less time.

Thus, instead of incorporating Schrödinger wave model for getting atomistic details for these type of complicated systems, a continuum model is chosen which is known as COSMO-RS or conductor like screening model for realistic solvents [199,200]. It was introduced by Andreas Klamt in 1995 [201] and it is an automated algorithm to calculate electrostatic interactions between the solute and solvent particles. It acts as a database of unique combination of quantum chemical treatments of solute and solvents under same parameters. Herein, solvent surrounds the solute which is considered as a continuous conductor rather than discrete molecules. This will therefore, calculate the chemical potentials of water-cation-anion ternary mixture and identify the chemical equilibrium point. Evaluation and identification of liquid-liquid equilibrium using COSMO-RS is proven to be the most reliable and fastest type of calculation available till now. *COSMOtherm* is computational tool to calculate the statistical thermodynamics calculations like chemical potential using COSMO-RS [202]. Chemical potential will provide systematic and efficient qualitative prediction of both solvation event and thermodynamic parameters.

1.4.7 Motivation for Chapter 5

There is a need to study mechanistics, characteristics and features of phase behaviour of room temperature low molecular weight imidazolium-based ionic liquids owing to their versatility, tunability and stable nature. As the techniques like UV-Visible Spectroscopy and DLS fail to detect CST of ILs, electrochemical impedance spectroscopy is employed to study the critical temperature of these water-like polar ionic liquids. The mechanistic aspects and structural relationships were investigated using Kamlet-Taft parameter studies and the same were incorporated into COSMOTherm, a simulation software based on COSMO-RS theory, whereupon a prediction theory could be suggested to acknowledge the CST behaviour of ILs.

Why EIS?

It can detect minute changes in electrolyte, thereby enabling the detection of phase separation in water-like polar ILs.

Why Kamlet-Taft parameter studies?

It is able to measure polarity and hydrogen bonding, factors known to affect CSTs in ILs.

Why COSMO-RS Simulations?

These simulations take care of electrostatic interactions between solvent and solute particles, and solution can be studied as a whole in various molecular/weight/mass ratios.

Novelty of the work?

For the first time, phase transitions of imidazolium-based ILs were confirmed using a superior and more informative EIS. Fundamental aspects were found out due to which phase separation takes place and most interestingly, a prediction mechanism is built to foresee the phase behaviour of these kinds of ILs.

1.5 Research Outlook

1.5.1 Objective of this research work

The primary aim of this thesis work is to focus on the thermosensitivity and tunability of various polymer and ionic liquid systems. Literatures have shown the importance of temperature driven phase transitions and their utilization to widespread applications in science via fabrication of thermal devices (Fig. 27).

Thus, in the present thesis, thermoresponsive property is examined on three kinds of states:

1) Solid-supported LCST showing materials- An attempt will be made with thermoresponsive polyoxazolines to transform them into solid-state materials. Two approaches are chosen for this task. First, the polymer will be converted to organic-inorganic hybrids materials using silicate which could also tune the phase transitions of these hybrid materials. Second, the polyoxazolines will be covalently bonded to silicon substrate for enhanced solid-support.
2) LCST showing hydrogels- Further, dimensionally controlled plasmonic nanoparticles will be embedded into thermoresponsive PNIPAM copolymerized with polymerizable ionic liquids. Au and Ag both acts as tuning agents for phase transitions of these hydrogels.
3) LCST in liquid-liquid equilibria-Phase transitions of imidazolium based ionic liquids in water will be studied using EIS. Further, their structural-activity relationships will be determined using Kamlet-Taft parameters and a prediction theory will be devised using COSMO-RS simulations.

Successful completion of this research would open several strategies and aspects to prepare innovative thermoresponsive smart materials with enhanced properties. It will also provide with the ability to tune phase transitions of these materials for the fabrication of smart and intelligent thermal devices.

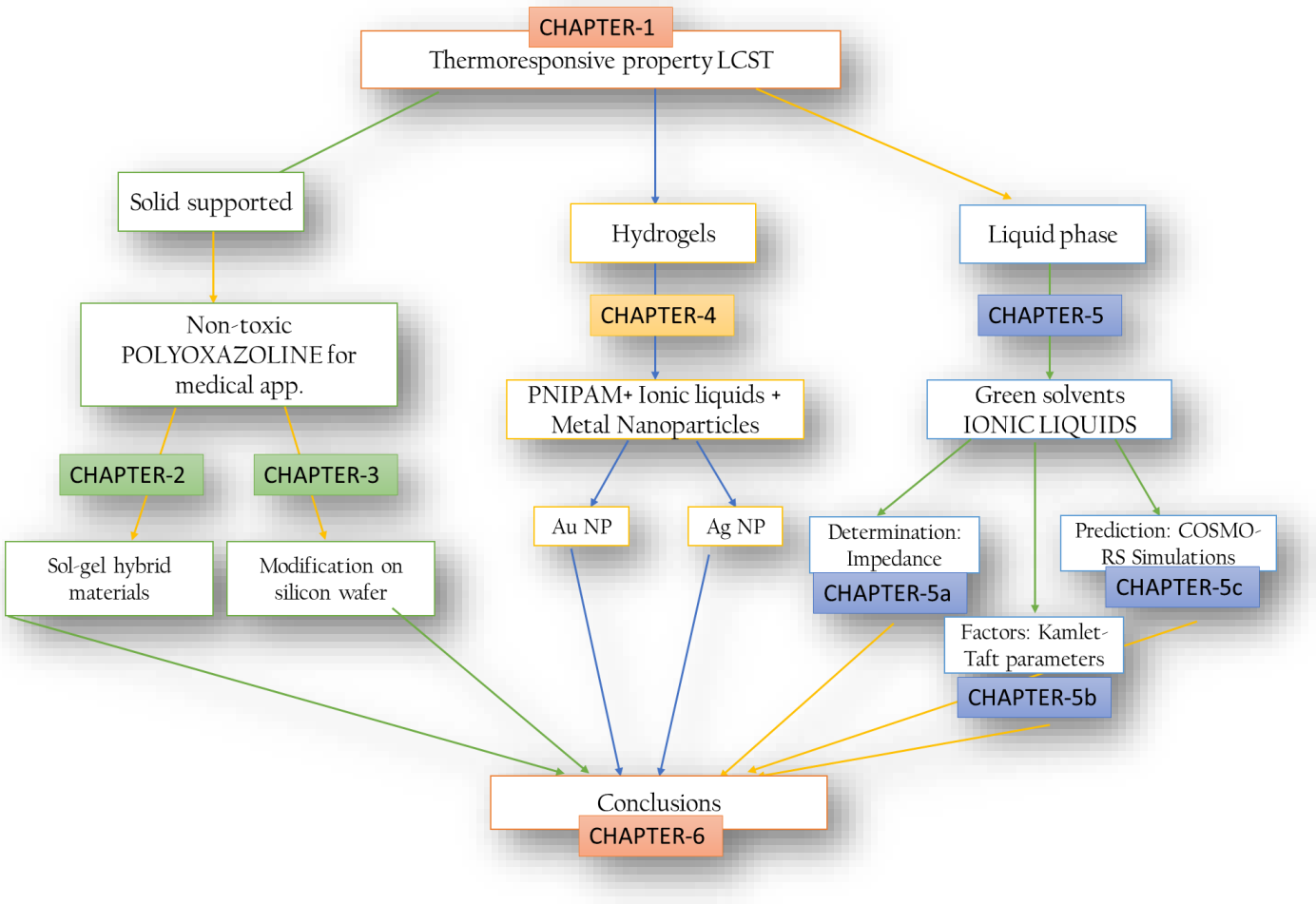

Fig. 27. Flowchart representing outline and topics of the thesis.

1.5.2 Chapter Outlines

Chapter-2: Fine-tuning of LCST behaviour of oxazoline copolymer based organic-inorganic hybrids as solid-supported sol-gel materials.

This chapter describes the synthesis of novel sol-gel hybrids using thermoresponsive copolymer of 2-ethyl-2-oxaoline and 2-isoporopyl-2-oxazoline with tetramethylorthosilicate as the silicate compound. It also reports the method to fine-tune the thermoresponsive property of these hybrids.

Chapter-3: Silicon wafer modification with thermoresponsive oxazoline based copolymer as solid-supported phase gradients.

In this work, silicon wafers are exposed to extreme acidic conditions to covalently bind with the thermosensitive polymer of 2-ethyl-2-oxazoline. The system works as a solid-supported phase gradient.

Chapter-4: Controlled phase behaviour of thermally sensitive poly(N-isopropylacrylamide/ionic liquid) with embedded nanoparticles.

Next, focus was made to target the applications shown by the formation of hydrogels and nanoparticles along with the thermosensitivity due to polymers. Hence, PNIPAM was copolymerized with different imidazolium based ionic liquids such as 1-allyl-3-octylimidazolium bromide and 1-hexyl-3-methyl imidazolium acrylate with tunable properties and the corresponding in-situ polymerization was done using Ag and Au nanoparticles. How the size of nanoparticles and structure of IL play a major role in LCST tunability was investigated.

Chapter-5: Can we predict the Critical Solution Temperature (CST) for imidazolium-based ionic liquids?

Further, focus was made to study liquid-liquid phase systems. Hence, room temperature imidazolium-based ionic liquids was found to exhibit LCST and UCST properties. A more advance, superior and informative technique which is electrochemical impedance spectroscopy was used as the diagnostic tool to evaluate the phase transition temperature as clear visualization of the separation cannot be observed optically. Factors affecting the CST in ionic liquids and its mechanism was scrutinized using Kamlet-Taft parameter studies. Also, COSMO-RS simulations were carried out which suggested a procedure to predict the occurrence of phase transitions, and if so, what type in ILs.

Chapter-6: Conclusions and Future work

Lastly, this chapter summarised the findings of each chapter above. It also gave an outlook towards future for the utilization of these materials.

1.6 References

[1] Y. Zhang, S. Furyk, D. E. Bergbreiter, and P. S. Cremer, *J. Am. Chem. Soc*, 2005, 127, 14505–14510.

[2] Q. Yan, Y. Xin, R. Zhou, Y. Yin, and J. Yuan, *Chem. Commun*., 2011, 47, 9594–9596.

[3] H. G. Schild, *Prog. Polym. Sci.*, 1992, 17, 163–249.

[4] L. F. Boesel, C. Greiner, E. Arzt, and A. del Campo, *Adv. Mater.*, 2010, 22, 2125–2137.

[5] Y. Zhao, *Macromolecules*, 2012, 45, 3647–3657.

[6] Y. Osada and J.-P. Gong, *Adv. Mater.*, 1998, 10, 827–837.

[7] M. Schwartz, Ed. *Smart Materials*, CRC Press Boca Raton 2008

[8] E. N Ashammakhi, R. Reis, E. Chiellini, M. Rosa and S. Roman, *Topics in Tissue Engineering*, 2007, 3, 1-27.

[9] H. Kirsebom, I.Yu and G. Mattiasson, *Polym Sci Part B: Polym. Phys.*, 2011, 49(3), 173-178.

[10] M. Wei, Y. Gao, X. Li and M. J. Serpe, *Polym. Chem.*, 2017, 8, 127-143.

[11] A. S. Hoffman, *Artificial Organs*, 1995, 19, 458–467.

[12] H. G. Schild, *Prog. Polym. Sci.*, 1992, 17, 163–249.

[13] J. Seuring and S. Agarwal, *Macromol. Rapid Commun.*, 2012, 33, 1898–1920.

[14] C. Chevillard and L. D. P. Chimie, *Colloid Polym. Sci.*, 1997, 275, 537–545.

[15] M. Heskins and J. E. Guillet, *J. Macromol. Sci. Chem,* 1968, 2, 1441–1455.

[16] M. A. Ward and T. K. Georgiou, *Polymers,* 2011, 3 (3), 1215–1242.

[17] K. Shimizu, H. Fujita and E. Nagamori, *Biotechnol Bioeng,* 2010, 106(2), 303-310.

[18] F. Liu and M. W. Urban, *Prog. Polym. Sci.*, 2010, 35, 3–23.

[19] M. C. Hacker, L. Klouda, B. B. Ma et al., *Biomacromolecules*, 2008, 9, 1558-1570.

[20] Y. Kumashiro, M. Yamato, and T. Okano, *Ann. Biomed. Eng.*, 2010, 38, 1977–1988.

[21] H. Feil, Y. H. Bae, J. Feijen et al. *Macromolecules,* 1993, 26, 2496-2500.

[22] G. Pasparakis and M. Vamvakaki, *Polym Chem,* 2011, 2, 1234-1248.

[23] R. Koningsveld, W. H. Stockmayer, E. Nies, Oxford University Press, Oxford, 2001, ISBN 978-0198556350.

[24] F. Liu, M. W. Urban, *Prog Polym Sci,* 2010, 35, 3-23.

[25] C. Wohlfarth, Polymer Handbook, 87th ed., CRC press, 2006, chapter 13, pp 19-34, ISBN 978-0849304873.

[26] A. Nakajima, F. Hamada, S. Hayashi, *J. Polym. Sci. Part C: Polym. Symp.,* 1966, 15, 285-294.

[27] C. Wohlfarth, *Upper Critical (UCST) and Lower Critical (LCST) Solution Temperatures of Binary Polymer Solutions*, Polymer Handbook, 87th ed., CRC press, 2006, chapter 13, pp 19-34, ISBN 978-0849304873.

[28] J. M. G. Cowie, I. J. McEwen, *J. Polym. Sci. Polym. Phys. Ed.*, 1974, Volume 12, pp 441-443.

[29] O. Pfohl, T. Hino, J. M. Prausnitz, *Polymer*, 1995, 36, 2065-2073.

[30] H. G. Schild, *Prog Polym Sci*, 1992, 17, 163-249.

[31] S. Fujishige, K. Kubota, I. Ando, *J. Phys. Chem.*, 1989, 93, 3311–3313.

[32] M. Shibayama, T. Norisuye, S. Nomura, *Macromolecules,* 1996, 29, 8746-8750.

[33] C. Wu, X. Wang, *Physical Review Letters*, 1998, 80, 4092–4094.

[34] Y. Maeda, T. Higuchi, and I. Ikeda, *Langmuir,* 2010, 16, 7503–7509.

[35] S. Vshivkov, A. P. Safronov, *Macromolecular Chemistry and Physics*, 1997, 198, 3015-3023.

[36] H. Kojima and F. Tanaka, *Macromolecules*, 2010, 43, 5103–5113.

[37] Y. Okada and F. Tanaka, *Macromolecules*, 2005, 38, 4465–4471.

[38] R. Koningsveld, W. H. Stockmayer, E. Nies, *Polymer Phase Diagrams*, Oxford University Press, Oxford, 2001, ISBN 978-0198556350.

[39] P. J. Flory, *Journal of Chemical Physics,* 1941, 9 (8), 660- 661.

[40] M. L. Huggins, *Journal of Chemical Physics,* 1941, 9 (5), 440-440.

[41] A. Hatefi, B. Amsden, *J. Control Release*, 2002, 80, 9-28.

[42] J. P. Chen, A. S. Hoffman, *Biomaterials*, 1990, 11, 631-634.

[43] M. D. Lavigne, S. S. Pennadam, J. Ellis et al., *J. Gene Med,* 2007, 9, 44-54.

[44] R. Langer, J. P. Vacanti, *Science,* 1993, 260, 920-926.

[45] I. Tan, F. Roohi, M. Magdalena, *Analytical Methods,* 2012, 4, 34–43.

[46] D. S. Jones, C. P. Lorimer, C. P. McCoyet al., *Chem Eng Sci,* 2007, 62, 990-999.

[47] D. C Coughlan, O. I Corrigan, *Int J Pharm,* 2006, 313, 163-174.

[48] Y. Okuyama, R. Yoshida, K. Sakai et al. *J. Biomater. Sci. Polym. Ed.,* 1993, 4, 545- 556.

[49] D. Q Wu, F. Qiu, T Wang *ACS Appl Mater Interfaces*, 2009, 1, 319-327.

[50] Z. W. Ma, D. M. Nelson, Y. Hong, *Biomacromolecules, 2010*, 11, 1873-1881.

[51] S. E. Stabenfeldt, A. J. Garcia, M. C. LaPlaca, *J Biomed Mater Res Part A*, 2006, 77, 718-725.

[52] H. S. Shin, S. Y. Kim, Y. M. Lee, *J Appl Polym Sci*, 1997, 65, 685-693.

[53] Q. F. Wang, S. M. Li, Z. Y. Wang, *J Appl Polym Sci,* 2009, 111, 1417-1425.

[54] S. Kim, E. H. Chung, M. Gilbert, *J Biomed Mater Res Part A*, 2005, 75, 73-88.

[55] J. Akimoto, M. Nakayama, *Mol Pharmacol*, 2010, 7, 926-935.

[56] H. Wei, X. Z. Zhang, W. Q. Chen, *J Biomed Mater Res Part A*, 2007, 83, 980-989.

[57] S. J Wilson, A. V. Gorelov, Y. A. Rochev, *J Biomed Mater Res Part A*, 2003, 67, 667-673.

[58] Y. Ito, G. P. Chen, Y. Q. Guan, *Langmuir*, 1997, 13, 2756-2759.

[59] L. H. Li, X. L. Jiang, R. X. Zhuo, *J Polym Sci Part A*, 2009, 47, 5989-5997.

[60] S. M. Zhang, L. N. Zhang, B. F. He, *Nanotechnology*, 2008, 19, 325608-325611.

[61] G. Fundueanu, M. Constantin, P. Ascenzi, *Int J Pharm,* 2009, 379, 9-17.

[62] Y. C. Wang, Y. Li, X. Z. Yang, *Macromolecules*, 2009, 42, 3026-3032.

[63] M. A. Ward and T. K. Georgiou, Polymers 2011, 3(3), 1215-1242.

[64] J. Ulbricht, R. Jordan, R. Luxenhofer, Biomaterials, 2014, 35, 4848-4861.

[65] N. A. Alcantar, E. S. Aydil, J. N. Israelachvili, *J Biomed Mater Res.*, 2000,51(3), 343-51.

[66] T. Tagami, K. Nakamura, T. Shimizu, N. Yamazaki, H. Kiwada, J.Control. Release, 2010, 142, 160-166.

[67] T. X. Viegas, M. D. Bentley, J. M. Harris, Z. Fang, K. Yoon, F. M. Veronese, et al., *Bioconjugate Chem.*, 2011, 22, 976–986.

[68] V. R. Rosa, A. V. D. Bulckle and R. Hoogenboom, Material Matters, 2016., 11.3.

[69] V. R. Rosa, Z. Zhang, B. G. Geest and R. Hoogenboom, Adv. Funct. Mater, 2015, 25, 2511-2519.

[70] F. C. Gaertner, R. Luxenhofer, B. Blechert, R. Jordon, M. Essler, *J. Control Release*, 2007, 119, 291- 300.

[71] B. Claeys, A. Vervaeck, C. Vervaet, J. P. Remon, R. Hoogenboom,B. G. Geest, *Macromol. Rapid Commun*. 2012, 33. 1701-1707.

[72] L. Y. Qiu, L. Yan, L. Zhang, Y. M. Jin, Q. H. Zhao, *Int. J. Pharm*, 2013, 456, 315- 324.

[73] R. Luxenhofer, A. Schulz, C. Roques, S. Li, T. K. Bronich, E. V. Batrakova, R. Jordan, A.V. Kabanov, *Biomaterials*, 2010, 31, 4972- 4979.

[74] C. Legros, M. C. G. D. Paux,K. C. Tam, S. Lecommandoux, D. Taton, *Polym. Chem.,* 2013, 4, 4801-4808.

[75] P. J. M. Bouten, D. Hertsen, M. Vergaelen, B. D. Monnery, M. A. Boerman, H. Goossens, S. Catak, J. C. M. van Hest, V. Van Speybroeck and R. Hoogenboom, *Polym. Chem.*, 2015, 6, 514-518.

[76] O. Koshkina, T. Lang, R. Thiermann, D. Docter, R. H. Stauber, C. Secker, H. Schlaad, S. Weidner, B. Mohr, M. Maskos, and A. Bertin, *Langmuir*, 2015, *31* (32), 8873–8881.

[77] E. Calo, V. V. Khutoryanskiy, *Eur. Polym J.,* 2015, 65, 252-267.

[78] G. J.Owens, R. K. Singh, F. Foroutan, M. Alqaysi, C. M. Han, C. Mahapatra, H .W. Kim, J. C. Knowles, *Progress in Materials Science,* 2016, 77, 1-79.

[79] S. H. Mir, L. A. Nagahara, T. Thundat, P. Mokarian, H. Furukawa and A. Khosla, *Journal of The Electrochemical Society*, 2018, 165 (8), 3137-3156.

[80] K. Tsuda, *J. Jpn. Petrol. Inst*., 2007, 50, 240-248.

[81] K. Ramam, M. Lopez, *J. Alloys Compd.*, 2008, 466, 398-403.

[82] S. H. Kim, J. H. Koh, *J. Eur. Ceram. Soc.*, 2008, 28, 2969-2973.

[83] J. M. Saad, P. T. Williams, *Energy Fuels*, 2016, 30(4), 3198-3204.

[84] K. MatsuzakiD, A. N.Taneda, T. Mukaiyama, M.Ikemura, *Journal of Non-Crystalline Solids*, 1989, 112, 437-441.

[85] M. S. Yen, M. C. Kuo, *Dyes and Pigments,* 2012, 94(2), 349-354.

[86] Vivek Babu Kandimalla, Vijay Shyam Tripathi, and Huangxian Ju, Critical Reviews in Analytical Chemistry, 36:73–106, 2006

[87] B. C. Dave, X. Hu and Y. Devaraj, *Journal of Sol-Gel Science and Technology*, 32, 143–147, 2004.

[88] A. Comite, "Current Trends and Future Developments on (Bio-) Membranes", *Silica Membranes: Preparation, Modelling, Application, and Commercialization,* 2017, 3-23.

[89] M. Rowena, N. Monton, E. M. Forsberg and John D. Brennan, *Chem. Mater.*, 2012, *24* (5), 796–811.

[90] D. A. Ward and E. I. Ko, *Ind. Eng. Chem. Res.*, 1995, *34* (2), 421–433.

[91] Y. Chujo, S. Kure, H. Matsuki and T. Saegusa, *Proc. Japan Acad.*, 1994, 70, 138-142.

[92] K. M. Kim, D.K. Keum and Y. Chujo, *Macromolecules,* 2003, 36, 867-875.

[93] L. Venema, *Nature*, 2011, 479, 309–309.

[94] Y. Sun, C. Chen, H. Xu, K. Lei, G. Xu, L. Zhao and M. Lang, *Appl. Surf. Sci.*, 2017, 419, 642–649.

[95] Q. Weiping, X. Bin, W. Lei, W. Chunxiao, S. Zengdong, Y. Danfeng, L. Zuhong and W. Yu, *J. Inclusion Phenom. Macrocyclic Chem.*, 1999, 35, 419–429.

[96] N. S. K. Gunda, M. Singh, L. Norman, K. Kaur and S. K. Mitra, *Appl. Surf. Sci.*, 2014, 305, 522–530.

[97] K. Zhang, J. Ma, B. Zhang, S. Zhao, Y. Li, Y. Xu, W. Yu and J. Wang, *Mater. Lett.*, 2007, 61, 949–952.

[98] R. P. Weis, J.-L. Montchamp, J. L. Coffer, D. G. Attiah and T. A. Desai, *Dis. Markers*, 2002, 18, 159–165.

[99] R. J. Hamers, J. S. Hovis, S. Lee, H. Liu and J. Shan, *J. Phys. Chem. B*, 1997, 101, 1489–1492.

[100] J. Sagiv, *J. Am. Chem. Soc*., 1980, 399, 92–98.

[101] S. Kobayashi, T. Nishikawa, T. Takenobu, S. Mori, T. Shimoda, T. Mitani, H. Shimotani, N. Yoshimoto, S. Ogawa, Y. Iwasa, *Nat. Mater.* 2004, 3, 317-322.

[102] G. Ashkenasy, D. Cahen, R. Cohen, A. Shanzer, A. Vilan, *ACC. Chem. Res.*, 2002, 35, 121-128.

[103] J. C. Love, L. A. Estroff, J. K. Kriebel, R. G. Nuzzo, G. M. Whitesides, *Chem. Rev*., 2005,

[104] N. Glass, R. Tjeung, P. Chan, L. Yeo, J. Friend, Biomicrofluidics, 2012, 5 , 1-7.

[105] F. Schreiber, *Prog. Surf. Sci*., 2000, 65, 151–257.

[106] B. Arkles, P. Dispersants**,** *Paint Coat. Ind. Mag.*, 2006, 1-10.

[107] A. R. Yadav, R. Sriram, J. A. Carter, B. L. Miller, *Mater Sci Eng C Mater Biol Appl.*, 2014, 35, 283-90.

[108] L. A. Chrisely, G. U. Lee, C. E. O Ferrall, *Nucleic Acids Res.*, 1996, 24, 3031–3039.

[109] E. F. Vansant, P. V. D. Voort, K. C. Vrancken, *Elsevier*, 1995.

[110] T. H. Tran, J. W. Lee, K. Lee, Y. D. Lee, B. K. Ju, *Sens.Actuators B: Chem.*, 2008, 129, 67–71.

[111] M. Zhu, M. Z. Lerum, W. Chen, *Langmuir*, 2012, 28(1), 416–423.

[112] N. Ishida and S. Biggs, *Langmuir*, 2007, 23, 11083–11088.

[113] L. Li, Y. Zhu, B. Li and C. Gao, *Langmuir*, 2008, 24, 13632–13639.

[114] J. Kopecek, *Nature*, 2002, 417, 388-389, 391.

[115] L. H. Nazihia, N. Chirani, L. Gritsch L, et al., *J Biomedical Sci.*, 2015, 4:2, 1-23.

[116] O. Wichterle, D. Lím, *Nature,* 1960, 185, 117-118.

[117] A. S.Hoffman, Advanced Drug Delivery Reviews, 2012, 64, 18-23.

[118] G. Milcovich, S. Lettieri, F. E. Antunes, B. Medronho, A. C. Fonseca, J. F. J. Coelho, P. Marizza, et al., *Adv Colloid Interface Sci.*, 2017, 249, 163-180.

[119] S. Lin, H. Yuk, T. Zhang, G. A. Parada, H. Koo, C. Yu, and X. Zhao, *Adv Mater.*, 2016, 28(22), 4497–4505.

[120] P. P. Pande, International Journal of Materials Science ISSN 0973-4589 Volume 12, Number 1 (2017), 11-14.

[121] T. Tanaka. et al., Phase Transitions of Gels; Mechanics of Swelling. NATO ASI Series (Series H: Cell Biology), vol 64. Springer, Berlin, Heidelberg, 1992.

[122] A. Richter, G. Paschew, S. Klatt, J. Lienig, K.F. Arndt, H.J.P. Adler, Sensors. 2008; 8(1): 561-581.

[123] A. Gandhi, A. P. Suma, O. S. Kalyan, K. Sen, *Asian Journal of Pharmaceutical Sciences,* 2015, 10 (2), 99-107.

[124] T. Tanaka, In: *Encylopedia of Polymer Science and Engineering*. 2nd ed. Vol 6, 1986, 514-536. Wiley.

[125] T. Subkowski, C. Bollschweiler, J. Wittenberg, W. Siegel, R. Pelzer, International Patent WO 1999004830 A1. Low molecular weight modulators of the cold-menthol receptor trpm8 and use thereof, 2013.

[126] G. Umachitra, Bhaarathidhurai, *J. Environ. Sci. Eng.*, 2012, 54, 447-452.

[127] A. Rogowska-Wrzesinska, M. C. Le Bihan, M. Thaysen-Andersen, P. Roepstorff, *J. Proteomics,* 2013, 88, 4-13.

[128] K. Y. Lee, D. J. Mooney, *Chem Rev*, 2001, 101, 1869-1879.

[129] C. Patra, S. Talukdar, T. Novoyatleva, S. R. Velagala, C. Mühlfeld, B. Kundu, S. C. Kundu, F. B. Engel, *Biomaterials, 2012,* 33 (9), 2673-2680

[130] R. Michalek, M. Hobzova, M. Pradny, M. Duskova, Hydrogels Contact Lenses in: Bio-medical Applications of Hydrogels Handbook, Springer (2010). 303-315.

[131] J. Alemán, A. V. Chadwick, J. He,M. Hess, K. Horie, R. G. Jones, P. Kratochvíl, R. F. T. Stepto, R. F. T. et al, *Pure and Applied Chemistry*, 2007, 79(10), 1801-1829.

[132] C. Buzea, I. I. Pacheco, K. Robbie, *Biointerphases*, 2007, 2 (4), 17-71.

[133] P. *Buffat, J. P. Borel, Physical Review A.,* 1976*, 13 (6), 2287–2298.*

[134] P. R. West, S. Ishii, G. V. Naik, N. K. Emani, V. M. Shalaev and A. Boltasseva, *Laser Photonics Rev*., 2010, 4, 795-808.

[135] N. N. Greenwood, A. Earnshaw, *Chemistry of the Elements. Elsevier Science: Oxford*, 1997.

[136] Y. L. Hewakuruppu, L. A. Dombrovsky, C. Chen, V. Timchenko, X. Jiang, S. Baek, R. A. Taylor, *Applied Optics, 2013,* 52 (24), 6041–6050.

[137] E. C. Dreaden, A. M. Alkilany, X. Huang, C. J. Murphy and M. A. El-Sayed, *Chem. Soc. Rev.*, 2012, 41, 2740-2779.

[138] Y. C. Yeh, B. Creran and V. M. Rotello, *Nanoscale*, 2012, 4, 1871-1880.

[139] I. Tokarev and S. Minko, *Soft Matter*, 2012, 8, 5980-5987.

[140] Y. Sun and Y. Xia, *Science*, 2002, 298, 2176-2179.

[141] S. K. Ghosh and T. Pal, *Chem. Rev*., 2007, 107, 4797-4862.

[142] Y. Kim, R. C. Johnson and J. T. Hupp, *Nano Lett.,* 2001, 1, 165-167.

[143] W. Lu, A. K. Singh, S. A. Khan, D. Senapati, H. Yu and P. C. Ray, *J. Am. Chem. Soc.,* 2010, 132, 18103-18114.

[144] J. S. Lee, G. S. Park, S. T. Kim, M. Liu,* and J. Cho, *Angew. Chem. Int. Ed.* 2013, 52, 1026–1030.

[145] Y. Kawahara, S. Hodges, B. S. Cook, C. Zhang, *UbiComp'13,* September 8–12, 2013, Zurich, Switzerland.

[146] D. Wang, H. L. Xin, R. Hovden, H. Wang, Y. Yu, D. A. Muller, F. J. DiSalvo and H. D. Abruña, *Nature materials*, 2013, 12, 81-87.

[147] Y. Yang, R. Zhao, T. Zhang, K. Zhao, P. Xiao, Y. Ma, P. M. Ajayan, G. Shi, and Y. Chen, *ACS Nano,* 2018, 12, 829–835.

[148] A. K. Sinha, K. Suzuki, M. Takahara, H. Azuma, T. Nonaka, and K. Fukumoto, *Angew. Chem,.* 2007, 119, 2949–2952.

[149] J. T. Nurmi, P. G. Tratnyek, V. Sarathy, D. R. Baer, J. E. Amonette, K. Pecher, C. Wang, J. C. Linehan, D. W. Matson, R. L. Penn, and M. D. Driessen, *Environ Sci. Technol,* 2005, 39, 1221-1230.

[150] D. De , S. M. Mandal , J. Bhattacharya , S. Ram & S. K. Roy, *Journal of Environmental Science and Health Part A,* 2009, 44, 155–162.

[151] L. Y. Chen, J. Q. Xu, H. Choi, M. Pozuelo, X. Ma, S. Bhowmick, J. M. Yang, S. Mathaudhu and X. C. Li, *Nature*, 2015, 528, 539-543.

[152] B. Stieberova, M. Zilka, M. Ticha, F. Freiberg, P. Caramazana-González, J. McKechnie, and E. Lester, *ACS Sustainable Chem. Eng.*, 2017, 5, 2493−2500.

[153] Z. Zhu, *Advanced Materials Research Online,* 04-25 ISSN: 1662-8985, 2012, 507, 75-78.

[154] F. C. Lam, S. W. Morton, J. Wyckoff, T. L. V. Han, M. K. Hwang, A. Maffa, E. Balkanska-Sinclair, M. B. Yaffe, S. R. Floyd & P. T. Hammond, *Nature commun.*, 2018, 9, 1991, 1-11.

[155] T. K. Nguyen, H. T. T. Duong, R. Selvanayaga, C. Boyer & N. Barraud, *Environ. Sci. Technol.,* 2005, 39, 5, 1221-1230.

[156] C. A. Fromena, G. R. Robbinsb, T. W. Shend, M. P. Kaia, J. P. Y. Ting and J. M. DeSimonea, *PNAS,* 2015, 112 (2) 488-493.

[157] S. S. Lee, W. Song, M. Cho, H. L. Puppala, P. Nguyen, H. Zhu, L. Segatori and V. L. Colvin, *ACS Nano*, 2013, 7 (11), 9693–9703.

[158] M. Grzelczak, J. Vermant, E. M. Furst and L. M. Liz-Marzan, *ACS Nano*, 2010, 4, 3591-3605.

[159] N. Nath and A. Chilkoti, *J. Am. Chem. Soc*., 2001, 123, 8197-8202.

[160] K. Heo, C. Miesch, T. Emrick and R. C. Hayward, *Nano Lett.,* 2013, 13, 5297-5302.

[161] Y. Lin, X. Xia, M. Wang, Q. Wang, B. An, H. Tao, Q. Xu, F. Omenetto and D. L. Kaplan, *Langmuir*, 2014, 30, 4406-4414.

[162] K. L. Hamner and M. M. Maye, *Langmuir*, 2013, 29, 15217-15223.

[163] X. Lian, J. Jin, J. Tian and H. Zhao, *ACS Appl. Mater. Interfaces*, 2010, 2, 2261-2268.

[164] M. I. Gibson, D. Paripovic, H. A. Klok, *Adv.Mater*.,2010, 22, 4721–4725.

[165] Y. Yan, L. Liu, Z. Cai, J. Xu, Z. Xu, D. Zhang and X. Hu, *Scientific Reports,* 2016, 6, 31328.

[166] W. Zhang, *Adv Exp Med Biol.*, 2014, 811, 19-43.

[167] P. D. Sarah, M. M. Robert, W. J. Scott, *Journal of Molecular Catalysis A: Chemical,* 2010, 329, 86-95.

[168] K. Manojkumar, A. Sivaramakrishna, K. Vijayakrishna, *J Nanopart Res,* 2016, 18, 103, 1-22.

[169] Z. He and P. Alexandridis, *Phys. Chem. Chem. Phys.*, 2015, 17, 18238-18261.

[170] J. Gao, R. S. Ndong, M. B. Shiflett and N. J. Wagner, *ACS Nano*, 2015, 9 (3), 3243-3253.

[171] G. Salas, A. Podgorsˇek, M. Turminee et al, *Phys. Chem. Chem. Phys* ., 2011, 13, 13527–13536.

[172] P. Migowski and J. Dupont, *Chem. Eur. J.*, 2007, 13, 32–39.

[173] K. Jain, R. Vedarajan, M, Watanabe, M. Ishikiriyama and N. Matsumi, *Polym. Chem.*, 2015, 6, 6819-6825 .

[174] P. Wasserscheid, W. Keim, *Angew. Chem. Int. Ed. Engl.* 2000, 39, 3772-3789.

[175] Y. Kohno and H. Ohno, *Chem Commun.,* 2012, 48, 7119-7130.

[176] K. N. Marsh, J. A. Boxall, R. Lichtenthaler, *Fluid Phase Equilibria,* 2004, 219, 93-98.

[177] D. R. MacFarlane, N. Tachikawa, M. Forsyth, J. M. Pringle, P. C. Howlett, G. D. Elliott, J. H. Davis, Jr., M. Watanabe, P. Simon and C. A. Angell, *Energy & Environmental Science,* 2014, 7, 232-250.

[178] Z. Q. Tan, J. F. Liu, L. Pang, *Trends in Analytical Chemistry* 2012, 39, 218-227.

[179] J. Huddleston, J. C. Abelaira, R. Wang, A. Lyddiatt., *J Chromatogr B Biomed Appl.,* 1996, 17, 680, 31-41.

[180] M. Selvan, M. D. McKinley, R. H. Dubois, and J. L. Atwood, *J. Chem. Eng. Data*, 2000, 45, 841-845.

[181] S. Friberg, *J. Soc. Cosmet. Chem.*, 1990, 41, 155-171.

[182] C.T. Wu, K. N. Marsh, A. V. Deev, and J. A. Boxall, *J. Chem. Eng. Data*, 2003, *48* (3), 486–491.

[183] K. E. Gutowski, G. A. Broker, H. D. Willauer, J. G. Huddleston, R. P. Swatloski, J. D. Holbrey, and R. D. Rogers *J. Am. Chem. Soc*. 2003, 125, 6632-6633.

[184] K. R. Seddon, A. Stark, M. J. Torres, *Pure and Applied Chemistry*, 2000, 72, 2275-2287.

[185] M. G. Freire, L. M. N. B. F. Santos, A. M. Fernandes, J. A. P. Coutinho, I. M. Marrucho *Fluid Phase Equilibria,* 2007, 261, 449–454.

[186] Y. Kohno, S. Saita, Y. Men, J. Yuan and H. Ohno, *Polym. Chem.*, 2015, 6, 2163-2178.

[187] H. N. Lee and T. P. Lodge *J. Phys. Chem. Lett.* 2010, 1, 13, 1962–1966.

[188] Y. Chen, F. Ke, H. Wang, Y. Zhang, and D. Liang, *ChemPhysChem* 2012, 13, 160 – 167.

[189] D. S. H. Wong, J. P. Chen, J. M. Chang, C. H. Chou, *Fluid Phase Equilibria,* 2002, 194–197, 1089–1095.

[190] J. Bard, L.R. Faulkner, *Electrochemical Methods; Fundamentals and Applications, A,* Wiley Interscience Publications 2000.

[191] E. Barsoukov, J. R. Macdonald, eds., *Impedance Spectroscopy; Theory, Experiment, and Applications, 2nd edn,* Wiley Interscience Publications, 2005.

[192] J. R. Scully, D. C. Silverman, and M. W. Kendig, editors, *Electrochemical Impedance: Analysis and Interpretation,* ASTM, 1993.

[193] E. Yeager, J. O'M. Bockris, B. E. Conway, S. Sarangapani, M. Sluyters-Rehbach, J. H. Sluyters, chapter 4 "AC Techniques", Comprehensive Treatise of Electrochemistry; Volume 9 Electrodics: Experimental Techniques;, Plenum Press 1984.

[194] K. Fukumoto, M. Yoshizawa, H. Ohno, *J. Am. Chem. Soc.* 2005, *127*, 2398–2399.

[195] Y. Zhao, H. Wang, Y. Pei, Z. Liu, J. Wang, *Phys. Chem. Chem. Phys.*,2016, *18*, 23238–23245.

[196] M. A. Ab Rani, A. Brant, L. Crowhurst, A. Dolan, M. Lui, N. H. Hassan, J. P. Hallett, P. A. Hunt, H. Niedermeyer, J. M. Perez-Arlandis, et al., *Phys. Chem. Chem. Phys.* 2011, *13*, 16831-168490.

[197] J. M. Lee, S. Ruckes, J. M. Prausnitz, *J. Phys. Chem. B* 2008, *112,* 1473–1476.

[198] D. J. Eyckens, B. Demir, T. R. Walsh, T. Welton, L. C. Henderson, *Phys. Chem. Chem. Phys.* 2016, *18*, 13153–13157.

[199] A. Klamt, F. Eckert, W. Arlt, *Annu. Rev. Chem. Biomol. Eng.* 2010, *1*, 101–122.

[200] R. Anantharaj, T. Banerjee, *Ind. & Eng. Chem. Res.* 2010, *49*, 8705-8725.

[201] A. Klamt, *J. Phys. Chem.* 1995, *99*, 2224–2235.

[202] D. S. Boucher, *Colloids Surfaces A: Physicochem. Eng. Asp.* 2015, *487*, 207–213.

****

Chapter 2

Fine-Tuning of LCST of oxazoline copolymer based organic-inorganic hybrids as solid-supported sol-gel materials

Abstract

Silica-supported organic-inorganic polymer hybrids were synthesized via in-situ sol-gel condensation of silicate monomer in the presence of oxazoline copolymer. A stable copolymer of 2-ethyl-2-oxaoline and 2-isopropyl-2-oxazoline was prepared using methyl p-tosylate as the living polymerization initiator with molecular mass of 4200g/mol. Lower critical solution temperature (LCST) of this copolymer was thermally found to be at 77 ^{o}C. The copolymer was mixed with tetramethoxysilane (TMOS) in different amounts (1:0.0014 to 1: 0.006 molar ratio) via in-situ sol-gel condensation to produce organic-inorganic hybrids including thermosensitive copolymer. Tuning of these solid-supported materials showed sharp phase changes in a temperature range from 42 ^{o}C to 58 ^{o}C, which was confirmed using Differential Scanning Calorimetry. Enthalpy of the phase transition were also calculated using the area above the endothermic peak. A typical concave curve was obtained for LCST-type phase diagram suggesting the dependence of phase transition temperature on the concentration of the copolymer in the hybrid.

2.1 Introduction

Stimuli-responsive "smart" polymers are being researched intensively since many years ago as these are capable of showing distinct changes in acknowledgement to external stimuli like light, heat, pH, electric or magnetic fields [1–3]. Of which, thermo-sensitive polymers are of great significant due to ease to control transition temperature manually and naturally as well. These polymers tend to undergo coil-to-globule phase change under the influence of temperature [4]. And thus, are known to showcase phase change phenomenon like as Lower Critical Solution Temperature (LCST) and Upper Critical Solution Temperature (UCST) depending upon their miscibility, optical and other physiochemical properties [5]. LCST (/UCST) is exhibited by polymers which show a decrease(/increase) in miscibility with solvent after applying enough heat to display phase change as the hydrophobic interactions between hydrophobic groups of the polymer becomes dominant (coil to globule) [6]. Applications of these smart materials range from bio-engineering which include sensors, drug delivery, gene delivery and tissue engineering to chemistry in catalysis, separation, batteries and chromatographic analysis [7,8]. Therefore, prudent structure design of these polymers is needed to meet the user's need to achieve a sharp and fine-tune phase behavior. One such crucial and conventional class of thermos-sensitive polymers is poly(*N*-isopropylacrylamide) (or PNIPAM) [9]. The structure has both hydrophilic and hydrophobic moieties capable of undergoing coil to globule transition at the transition temperature. It specialty lies in the sharpness of the transition point (31-33 ^{o}C) and that it is closer to human body temperature, making it a suitable candidate to be studied in biomedical applications [10,11]. However, recently reports have been encountered for the toxic levels [12] of the polymer implying the need of a non-toxic polymer whose LCST lies at optimum

temperatures. As an alternative, one such class of thermo-responsive polymer is poly-(2-oxazolines) (POx) [13–16], some of which are non-toxic in nature, as approved by Food and Drug Administration (FDA) [17,18]. Selecting this polymer, will enhance the utility of the resulting hybrid materials as ring opening cationic polymerization enables diversity on the end-group structure providing the reversible coil-to globule transition in a wide range of temperature. The structure of generally used 2-alkyl-2-oxaoline derivatives for polymerization is depicted in Fig. 1. It is well reported that the phase behavior of this generally depends on its molecular weight [19,20]. Typically, poly(2-ethyl-2-oxazoline) has LCST beyond 90 °C, if the molar mass of the polymer increases to 6700 g/mol [15]. Synthesis of organic-inorganic hybrid materials using thermosensitive copolymers are being done due to handling ease, opening a wide spectrum of applications [1,21–28].

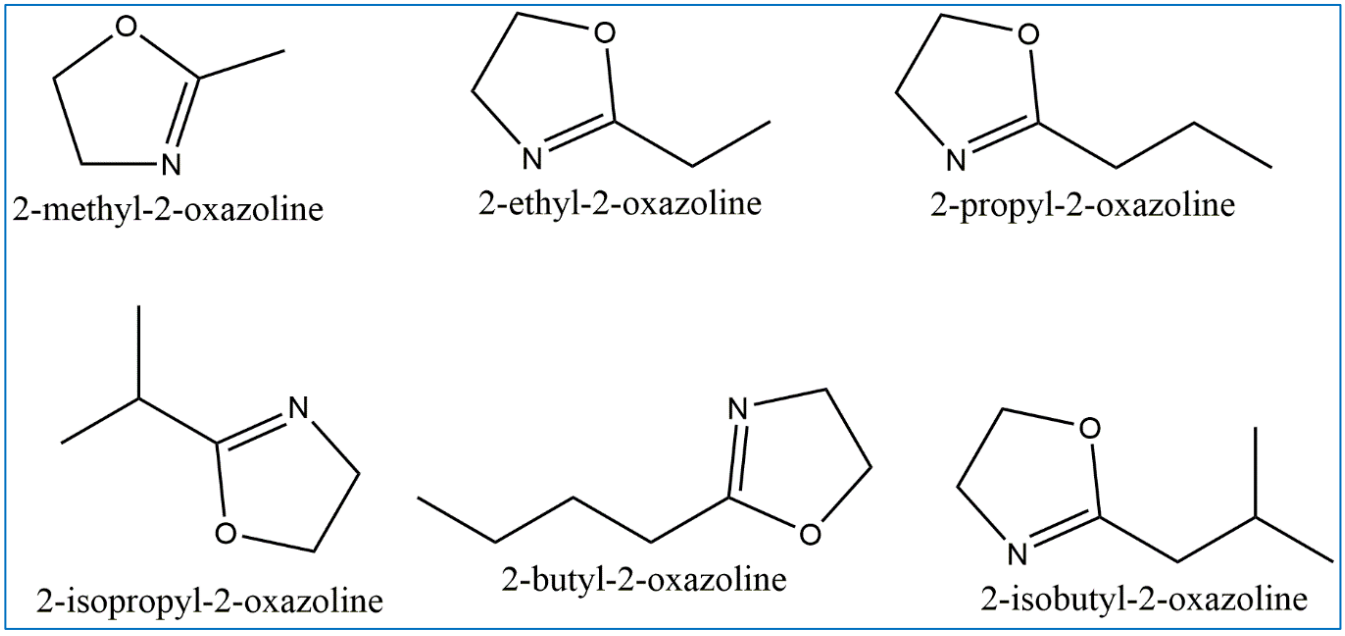

Fig. 1. Structures of 2-alkyl-2-oxazolines used for polymerization.

Objective of the work:

In the present study, thermoresponsive behavior of organic-inorganic hybrid materials including copolymer of 2-ethyl-2-oxazoline and 2-isopropyl-2-oxazoline was investigated. Oxazoline based copolymer was prepared and characterized as reported in literatures [1,19,21,29]. Phase transition behavior was monitored using optical and thermal analysis. Furthermore, in-situ sol-gel condensation was performed using tetramethoxysilane (TMOS) as the silane monomer to prepare solid-supported organic-inorganic hybrid systems. Fine-tuning of the phase behaviour of these hybrids was examined by varying the copolymer content keeping the TMOS concentration constant. Lastly, a phase diagram was constructed to study the fine-tuning of transition temperature for the poly(oxazoline)-based organic-inorganic hybrid materials. So, the objective of the work is to fine-tune the phase behavior of oxazoline based thermoresponsive copolymers by preparing their organic-inorganic hybrids.

2.2 Experimental

2-Ethyl-2-oxazoline (Tokyo Chemical Industry Co. Ltd.), 2-isopropyl-2-oxazoline (Tokyo Chemical Industry Co. Ltd.) and acetonitrile (Kanto Chemical Co., Inc.) were purified by calcium hydride overnight (Wako Pure Chemical Industries) and distilled. Methyl p-toluenesulfonate (Tokyo Chemical Industry Co. Ltd.), dichloromethane (DCM, Wako Pure Chemical Industries), diethyl ether (Wako Pure Chemical Industries), sodium hydroxide (Wako Pure Chemical Industries), methanol (Kanto Chemical Co., Inc.) and hydrochloric acid (HCl, Kanto Chemical Co., Inc) were used without any further purification.

Measurements

Proton-Nuclear Magnetic Resonance Spectroscopy (^{1}H-NMR) was executed on an Ultrashield™ Plus Bruker spectrometer, Z101355 which had the operating frequency of 400 MHz. Chemical shifts were recorded in parts per million (ppm) downfield from the reference tetramethylsilane (TMS). Molecular weight distributions were studied utilizing Gel Permeation Chromatography (GPC, Shimadzu). The instrument was equipped with a DGV-20A Degasser, RID-10A Refractive Index Detector, LC-20AD Liquid Chromatograph and a CTO-20A column oven. The solvent used as an eluent was stabilizer-free tetrahydrofuran. The flow rate for the elution was kept as 0.5mL/min at a temperature of 30 ^{o}C. Polystyrene (PSt) standards were used for the calibration. JASCO FT-IR420 (JASCO) was used to measure the Fourier-transformed Infrared spectroscopy. Thermal analysis was carried out on a Differential Scanning Calorimeter (DSC, Shimadzu- DSC-60Plus C309353) under nitrogen atmosphere. Infrared absorption spectra for the organic-inorganic hybrids were analyzed by Fourier transform infrared spectroscopy (FTIR) (Bruker Tensor 27).

Synthesis of the copolymer of 2-ethyl-2-oxazoline and 2-isopropyl-2-oxazoline with a hydroxyl end group:

A modified literature scheme was used for the synthesis [19,29] **(Scheme 1)**. In a 2-neck round bottom flask, 2-ethyl-2-oxazoline (1.75 mL, 17.4mmol) and 2-isporopyl-2-oxazoline (0.6mL, 5.04mmol) were added in inert atmosphere. To that, purified acetonitrile (9mL) was put in to prepare a 25 wt% solution. 2 mol% (0.08g, 0.44mmol) methyl p-toluenesulphonate was added to the reaction mixture and was heated at 70 ^{o}C

for 3 days in the presence of nitrogen surroundings. Once the polymerization was over, the reaction mixture was cooled to room temperature. The reaction was quenched with appropriate amount of 1.0 M methanolic sodium hydroxide (till white precipitation occurs) to incorporate the –OH group at the terminal group of the polymer chains. Then, the polymer was washed using dichloromethane. And the polymer was extracted in diethyl ether in a separation funnel. The solvent was removed under reduced pressure. It was further purified by overnight by drying at 40 ^{o}C under vacuum.

^{1}H-NMR (Fig. 2) (400MHz, $CDCl_3$): δ = 3.36 (s, CH_2-CH_2), 2.97 (s, CH_3-N), 2.84 (m, -CH-), 2.51 (d, -CH_2-CH_3), 0.963 (m, CH_3-C).

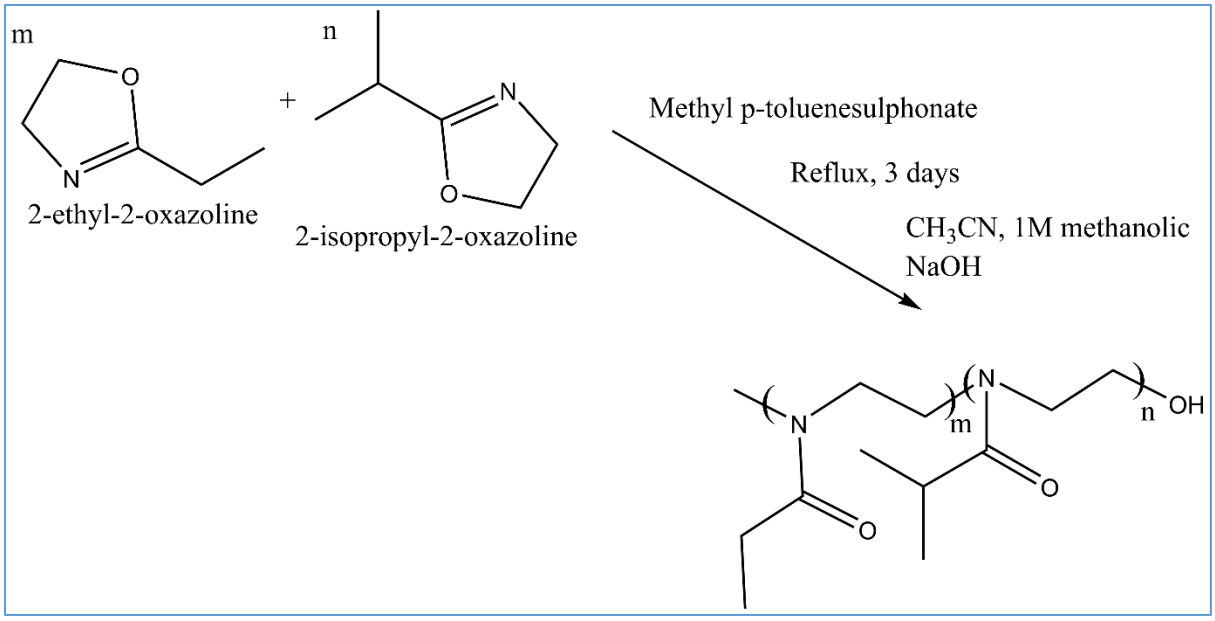

Scheme 1: Schematic diagram for the synthesis of copolymer of 2-ethyl-2-oxazoline and 2-isopropyl-2-oxazoline using methyl p-tosylate as the initiator.

Synthesis of organic-inorganic hybrids materials:

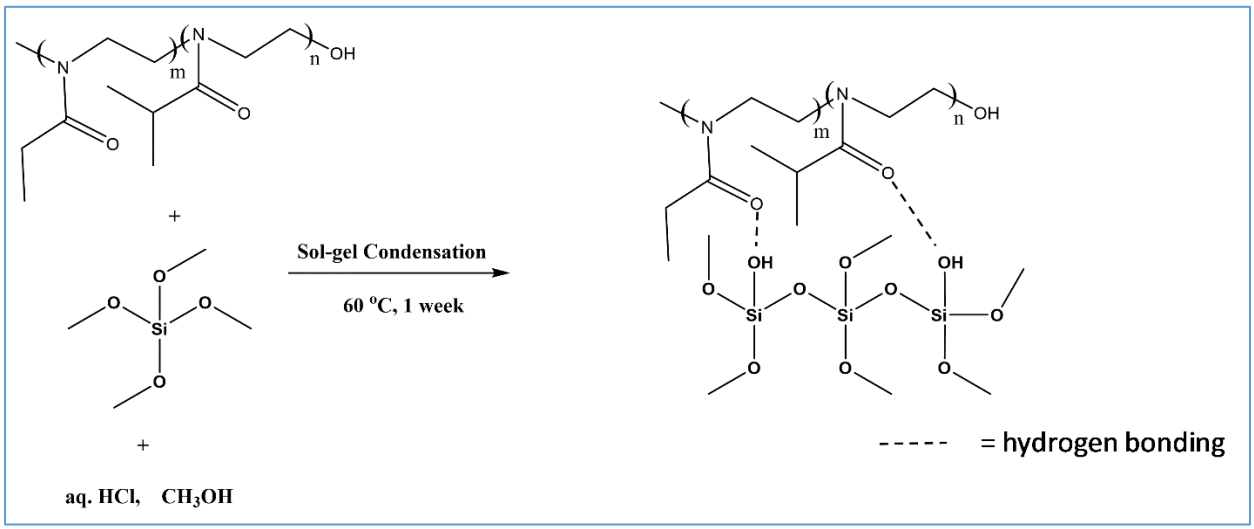

Scheme 2: Schematic diagram represesnting the synthesis via in-situ sol-gel condensation incorporating TMOS as the inorganic silicate and oxazoline copolymer as the organic thermoresponsive substrate in acidic catalyst medium.

A typical in-situ sol-gel condensation procedure [23,30] was pursued for the synthesis of hybrids materials **(Scheme 2)**. To different amounts of oxazoline copolymer ranging from 3.5e-6moles to 1.5e-5moles (A – 0.015 g, 3.5e-3 mmol; B – 0.030 g, 7.1e-3 mmol, C – 0.033 g, 7.8e-3 mmol; D – 0.035 g, 8.3e-3 mmol; E- 0.040 g, 9.5e-3 mmol; F – 0.042 g, 1.0e-2 mmol; G – 0.045 g, 1.1e-2mmol and H – 0.060 g, 1.4e-2mmol), a constant amount of tetramethyoxysilane (TMOS, 0.38 g, 2.5 mmol) was added (Table 2). Condensation was catalysed by 1.0 N HCl aq. (0.06g) which acted along with methanol (0.16 g, 5 mmol). Solvent used was acetonitrile (2.5mL). Once all the requisite details were added in a round bottom flask, the solution was stirred vigorously at room temperature for 4 hours. Afterwards, the resulting mixture was poured in a plastic container. The solution was dried and rested undisturbed at 60 °C for 7 days till all the solvent evaporated leaving behind the dried hybrid film material.

Measurement of Phase Transition Temperature

The solid-liquid equilibrium [31] of the copolymer was detected using (1) optical analysis (determination of turbidity by naked eye) using a digital thermometer (NETSUKEN SN3000-01 range: -50 to 280 ^{o}C). The analysis was done in aqueous medium (polymer/water= 10 mg/ mL). (2) Differential Scanning Calorimetry, was performed in inert atmosphere at heating rate of 1 ^{o}C/min from 20 ^{o}C to 90 ^{o}C.

For the films, a small amount of the material was taken and dispersed in water via sonication. It was then subjected to Differential Scanning Calorimetry under nitrogen atmosphere at a heating rate of 1^{o}C/min from 20 ^{o}C to 90 ^{o}C. Endothermic enthalpy was calculated from the system software.

2.3 Characterization

Ring-opening cationic copolymerization of 2-ethyl-2-oxaozline and 2-isopropyl-2-oxazoline was carried out using methyl tosylate as the cationic initiator. The copolymer was terminated using methanolic NaOH. The synthesized polymer was characterized by ^{1}H-NMR (400 MHz) in $CDCl_3$ (Fig. 2). It was seen that the monomer peaks were absent, and that the broad polymeric peaks were observed in the region 0-4ppm. The structure was characterized as on the Fig. 2. From the integration ratios, composition of the copolymerization [29] was found to be 2-ethyl-2-oxazoline: 2-isopropyl-2-oxazoline = 72.4%: 27.6%. Gel Permeation Chromatography (GPC traces) of the copolymer solution in stabilizer-free THF solution was performed for the molecular weight determination.

The number-average molecular weight (M_n) of the copolymer was found to be 4200 g/mol. The degree of polymerization (PDI) was found to be 1.02 confirming the living-type polymerization behavior.

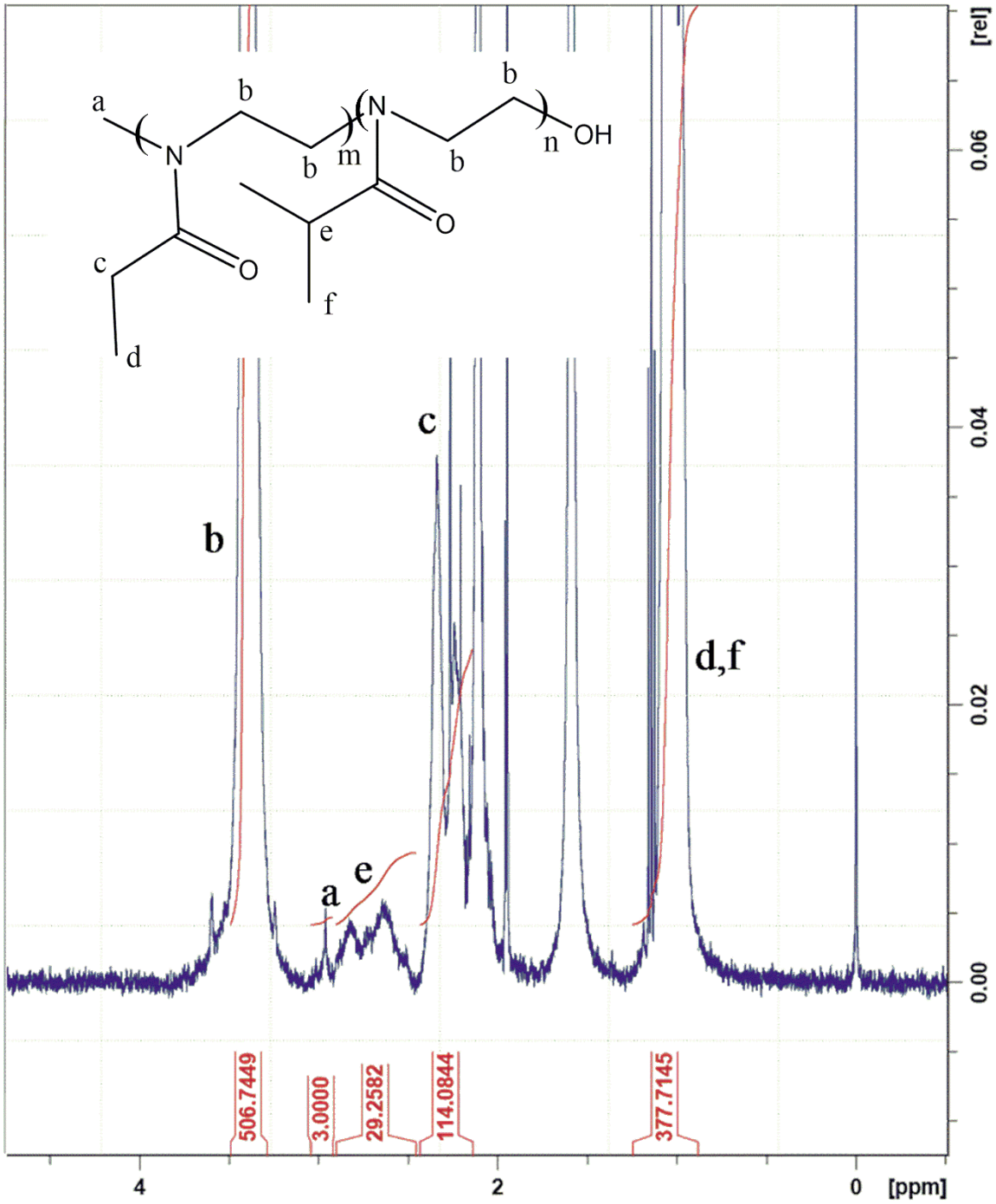

Fig. 2. ^{1}H-NMR spectrum of the copolymer prepared from (2-ethyl-2-oxazoline and 2-isopropyl-2-oxazoline)

2.4 Results and Discussion

With the copolymer being soluble in non-protic solvents like acetonitrile, THF, dimethylsulfoxide (DMSO), acetone and chloroform, it was interesting to investigate solubility in protic solvents like water and methanol (Table 1). The terminal hydrophilic hydroxyl group makes it a viable polymer to be used in various solvents, thereby expanding the horizon of its applications.

Table 1: Solubility table for copolymer

	water	methanol	acetone	acetonitrile	THF	DMSO	chloroform
copolymer	+	+	+	+	+	+	+

To further demonstrate its stability, a DSC (Fig. 3) measurement was performed from 20 °C to 550 °C at a scan rate of 10 °C/min. It was noted that the polymer was stable up to 360 °C, which upon further heating degraded/decomposed. No evident glass transition temperature was found for this copolymer.

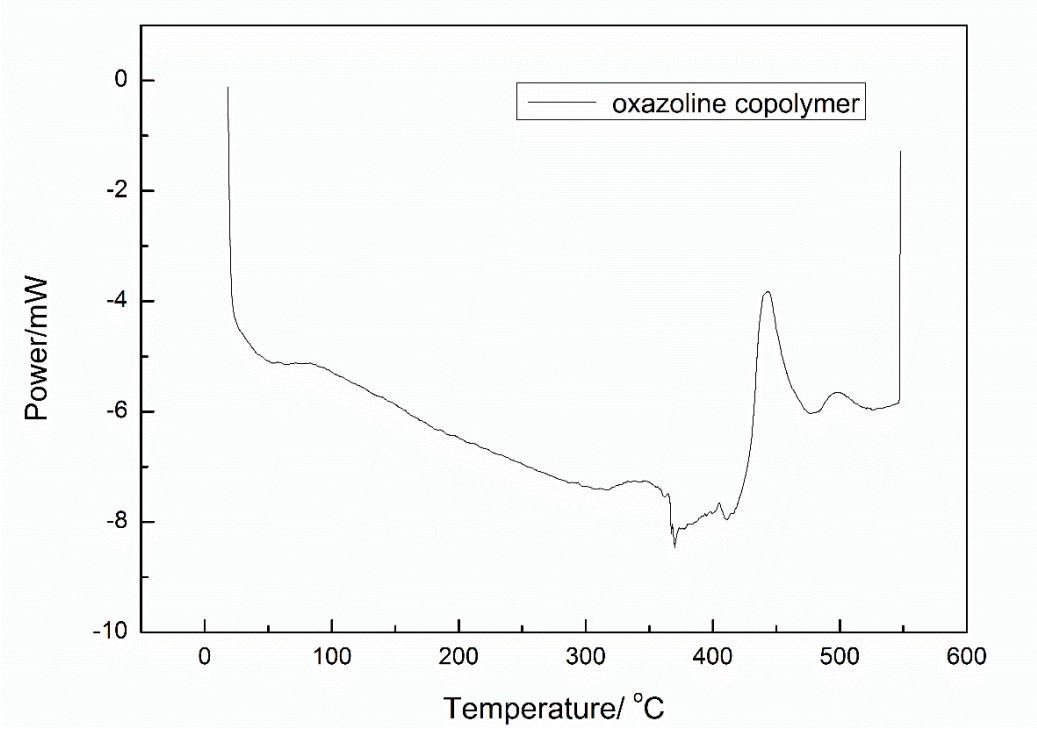

Fig. 3. DSC profile of the copolymer (2-ethyl-2-oxazoline and 2-isopropyl-2-oxazoline). The rate of heating was kept as 10 °C/ min from 20 °C to 550 °C.

Further, a series of organic-inorganic materials was designed by sol-gel condensation reaction. The concentration of the copolymer was chosen to be the vacillating component in the compositional matrix in each set to be able to requisitely tune the transition temperature. Tetramethoxysilane (TMOS) was selected to act as the inorganic silane monomer due to its ease to handle and predominance. Its amount was taken as the constant parameter to control the phase transition due to presence of thermoresponsive oxazoline copolymer. The appearance of the hybrids was as listed in Table 2. It was observed to be translucent (A-D) or white turbid (E-H), flaky (A-H) and brittle (A-H). The affirmation of the synthesis was done by obtaining the IR spectra. IR measurements were performed in both functional (4000 cm^{-1} -1450 cm^{-1}) and fingerprint region (1450 cm^{-1} – 500 cm^{-1}). As seen in the representative IR spectra [Fig. 4. (a) (A-D) and (b) (E-H)], the spectra are broadly similar. The strongest absorption peak of the spectra was found between 1100-1000 cm^{-1}, which can be assigned to the Si-O-Si siloxane bond, forming the structural framework of the hybrids. The peak at ~950 cm^{-1} was observed due to Si-OH stretch. A small absorption at ~760 cm^{-1}, is attributable to the incomplete hydrolysis of TMOS backbone of $Si\text{-}OCH_3$ [26,32], leading to a development of both 3D network of the hybrid with some terminal OH (Scheme 2). A weak broad band was observed from 3600-3000 cm^{-1} which is ascribed to the Si-O-H stretch formed during the hydrolysis of the methoxy groups of TMOS. Further, presence of C=O carbonyl band was observed at ~ 1650 cm^{-1}, reaffirming the indulgence of the organic copolymer functionalities. As no peak was observed around 2850 cm^{-1}, it was certain that no unreacted methoxysilane element was present in the hybrid matrix [32].

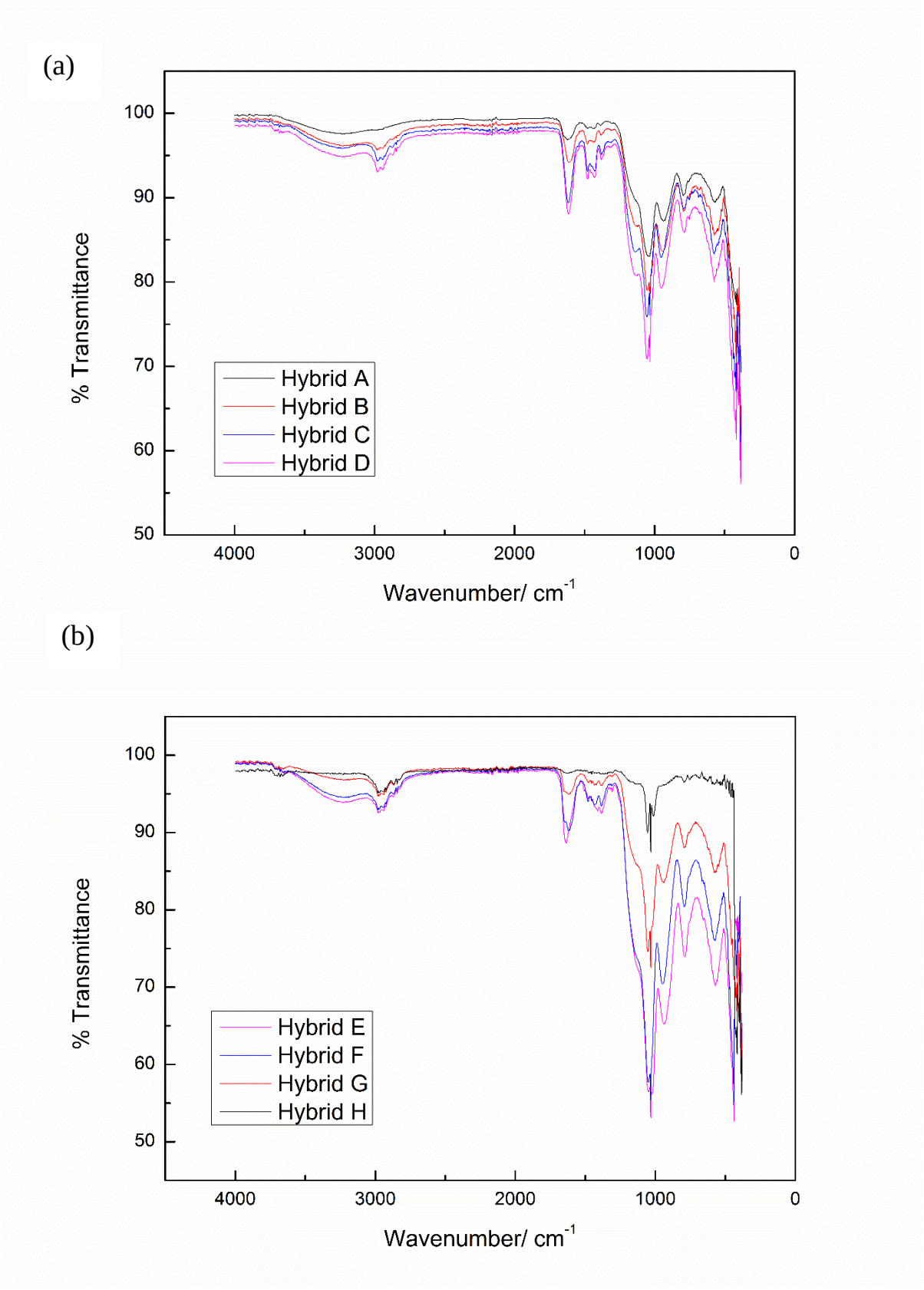

Fig. 4. FT-IR spectra for organic-inorganic polymer hybrids A-D (a) and E-H (b)

Phase Transition Property:

Cloud point (transition temperature) for the polyoxazoline in aqueous medium, depends on the hydrogen bonding with water [33]. Before LCST, the polymer is a coiled chain, whose hydrophilic group (here, carbonyl and nitrogen of the chain) subsequently interacts with the hydrogens of water. After LCST, system acquired enough enthalpy to overcome the polar dipole-dipole interactions, thereby increasing the growth of hydrophobic interactions (methyl, isopropyl groups of the side chains) of the system. This happens once the polymer forms a globule state as seen with the emergence of a turbidity in the appearance [34]. For the oxazoline copolymer, it thus becomes evident to examine the visual changes at LCST. For that, 10 mg/mL copolymer solution in water was prepared and heated. It was observed that the solution turns from transparent to opaque as heated from room temperature to 80 ^{o}C (Fig. 5). Once the solution was cooled, turbidity disappears signifying the solubility of the copolymer in water again increased, also portraying the reversible nature of the LCST transition of polymer.

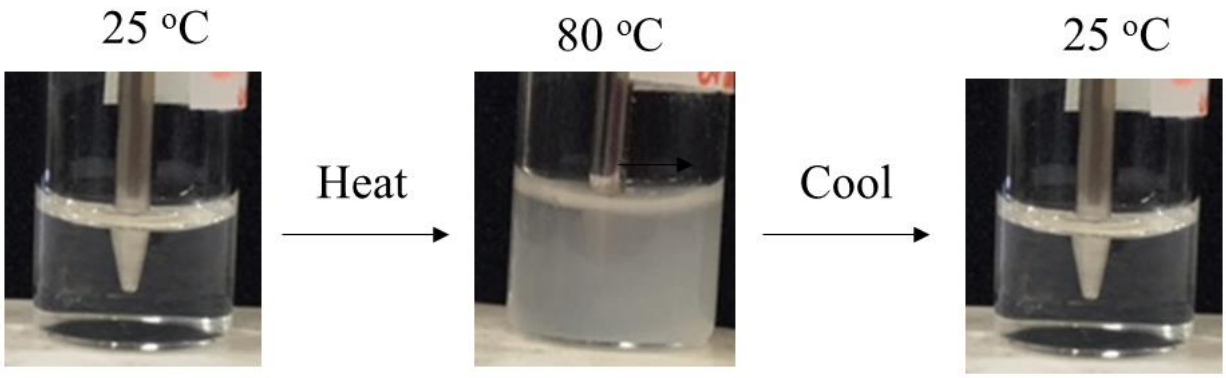

Fig. 5. Optical images demonstrating the reverisble nature of LCST of oxazoline copolymer.

A DSC was performed from 20 °C to 100 °C. An endothermic peak was detected with peak position at 78 °C owing to the phase transition. The heat of the transition after calibration, was calculated as 83.46 J/g (Fig. 6).

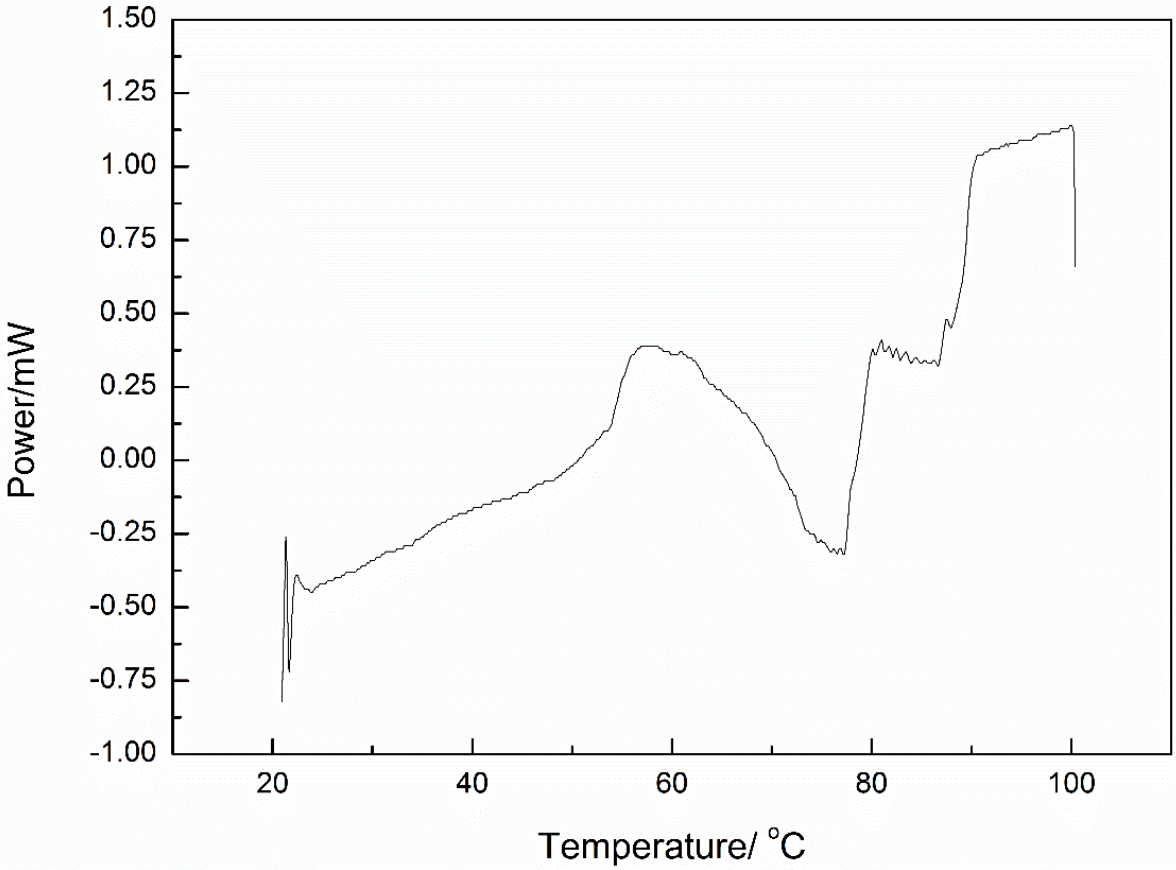

Fig. 6. DSC profile indicating the LCST behaviour of copolymer of 2-ethyl-2-oxazoline and 2-isoporopyl-2-oxaoline.

Table 2: Composition, appearance, phase transition temperature and corresponding enthalpies for the solid-supported organic-inorganic hybrids.

Hybrid Name	Oxazoline amount	TMOS amount	Appearance at RT	Transition temperature	Enthalpy of the transition
A	0.015 g	0.038 g	Translucent	No LCST	-
B	0.030 g	0.038 g	Translucent	58 °C	449.81 J/g
C	0.033 g	0.038 g	Translucent	49 °C	332.39 J/g
D	0.035 g	0.038 g	Translucent	44 °C	168.67 J/g
E	0.040 g	0.038 g	Turbid	42 °C	115.28 J/g
F	0.042 g	0.038 g	Turbid	50 °C	260.69 J/g
G	0.045 g	0.038 g	Turbid	56 °C	561.33 J/g
H	0.060 g	0.038 g	Turbid	58 °C	622.28 J/g

Afterwards, the hybrids A to H were examined (Table 2) for the fine-tuning of the phase transition temperature of copolymers. All the hybrids were dispersed/dissolved in water (10 mg/ mL). Furthermore, phase diagrams were prepared to depict the relation of copolymer concentration with respect to phase transition temperature peak positions and their corresponding enthalpies. For the material symbolized as A, the hybrid showed no transition peak. This implied that the copolymer concentration was not enough for the phenomenon to take place. It thus, tends to remain completely soluble in the water at temperature range of 20-80 °C. Neither poly-oxazoline nor silicate moiety was able to show phase transition. However, with an increase in copolymer concentration from 2.85 mM to 5.6 mM, all showcased a wide-endothermal peak attributed to the phase transition temperature (Fig. 7). In most cases, the onset starts at room temperature, probably because the hybrid is dispersed in water. The peak expands till the copolymer in the hybrid gains sufficient energy to exhibit globule formation in the solution. And, afterwards a sharp baseline appears. Hence, the transition temperature was monitored as the bottommost point of the endothermic peak.

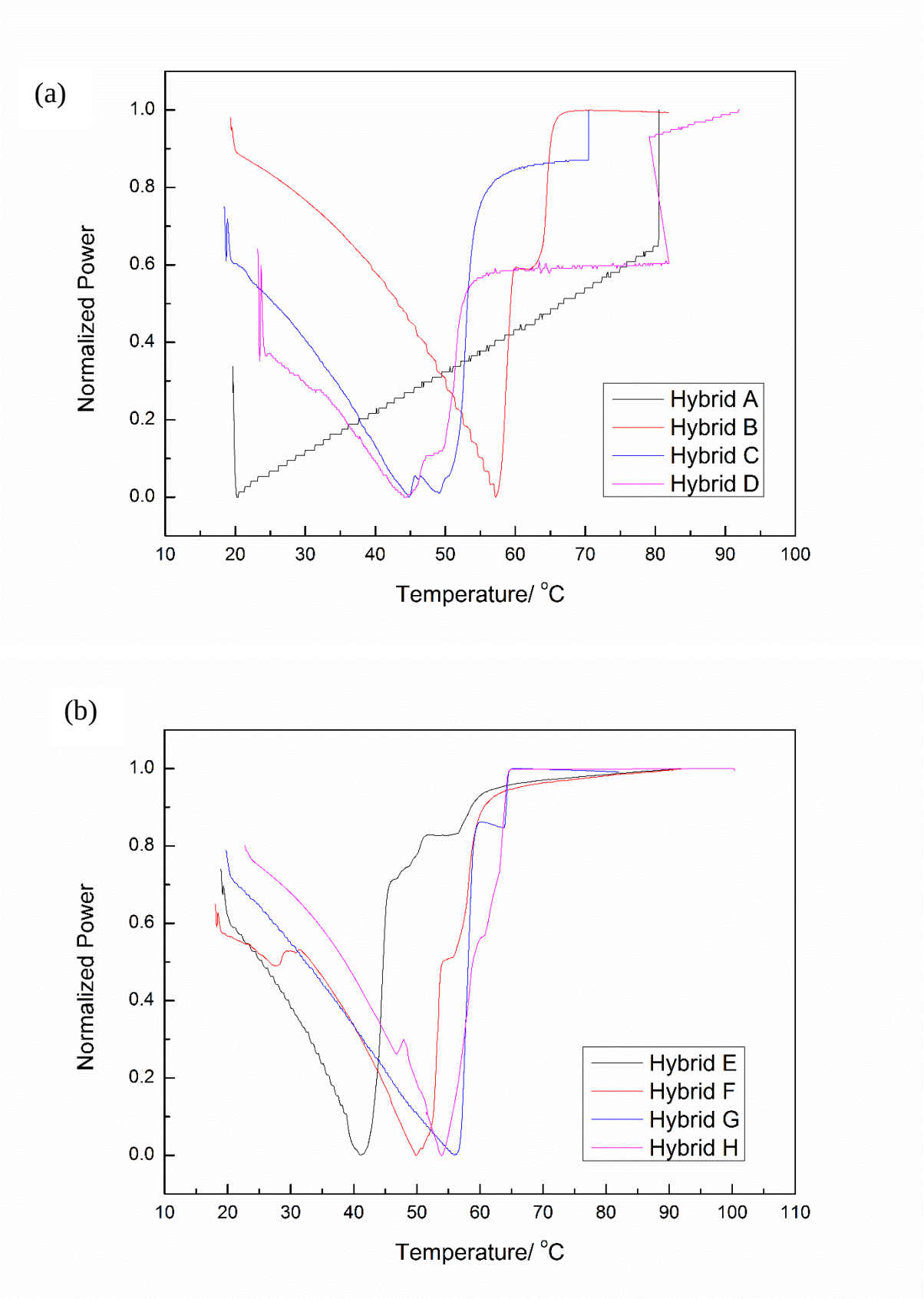

Fig. 7 DSC profiles demonstrating the phase behavior for organic-inorganic polymer hybrids A-D (a) and E-H (b)

Consequently, a typical concave up binodal curve [35] is perceived (Fig. 8). As can be scrutinized from the temperatures graphs in the range of 20-100 °C, fine-tuning of phase behvaiour of the copolymer hybrids can be appreciated. The temperature range can be varied from 42 °C to 58 °C with the change in concentration of copolymer. The temperatures decreased initially from 58 °C to 42 °C with the increase in the amount of copolymer. The temperature of 42 °C, lowest in our case was achieved with the polymer concentration being 3.80 mM. Again increasing the amount to 5.6 mM, led to an increase in the phase transition temperature upto 58 °C. It can also be easily perceived that due to the incorporation of the inorganic silicate substance, the hybrids showed a decreased phase transition temperature when compared with that of the original copolymer, probably as the silicate acts as a hydrophobic moiety thereby weakening the hydrogen bonds with water [36,37]. As reported, this entropy-driven phenomenon depends on the enthalpic factors like specific interactions between polymer and silicate molecules, solubility of product and other entropic losses from any possible interactions [38–40]. Thus, increasing the copolymer ratio with respect to silicate matrix, decreases the phase separation behaviour till the concentration reaches a molar ratio of 3.8e-3 : 1, suggesting the dominant role of silicate moiety. Besides, increasing the copolymer content further, led to an increase in the transition temperature apparently due to increase in the hydrophilic content in the form of copolymer. Therefore, it was well-comprehended that the phase behavour for this copolymer is concentration dependent with respect to the silicate matrix. Furthermore, for the calculation of enthalpy change of the transition, above the curve was calculated by extrapolating the stipulated baseline above the endothermic peak. Area above the significant endotherms in the DSC thermograms was calculated and calibrated by the amount of the hybrid taken for the analysis in the DSC pan. Interpretation of the enthalpies revealed the similar trend as per the concave up

phase curve (Fig. 9). Enthalpy changes correspond to the energy of conformational change and the hydrophobic interaction of the copolymer/silicate hybrid in aqueous medium [39,41]. It showed a linear dependence with transition temperature (as phase transition temperature increases, enthalpy increases) as silicate acts as a hydrophobic component [42–44], thereby increasing the enthalpy of transition when compared with the copolymer solution.

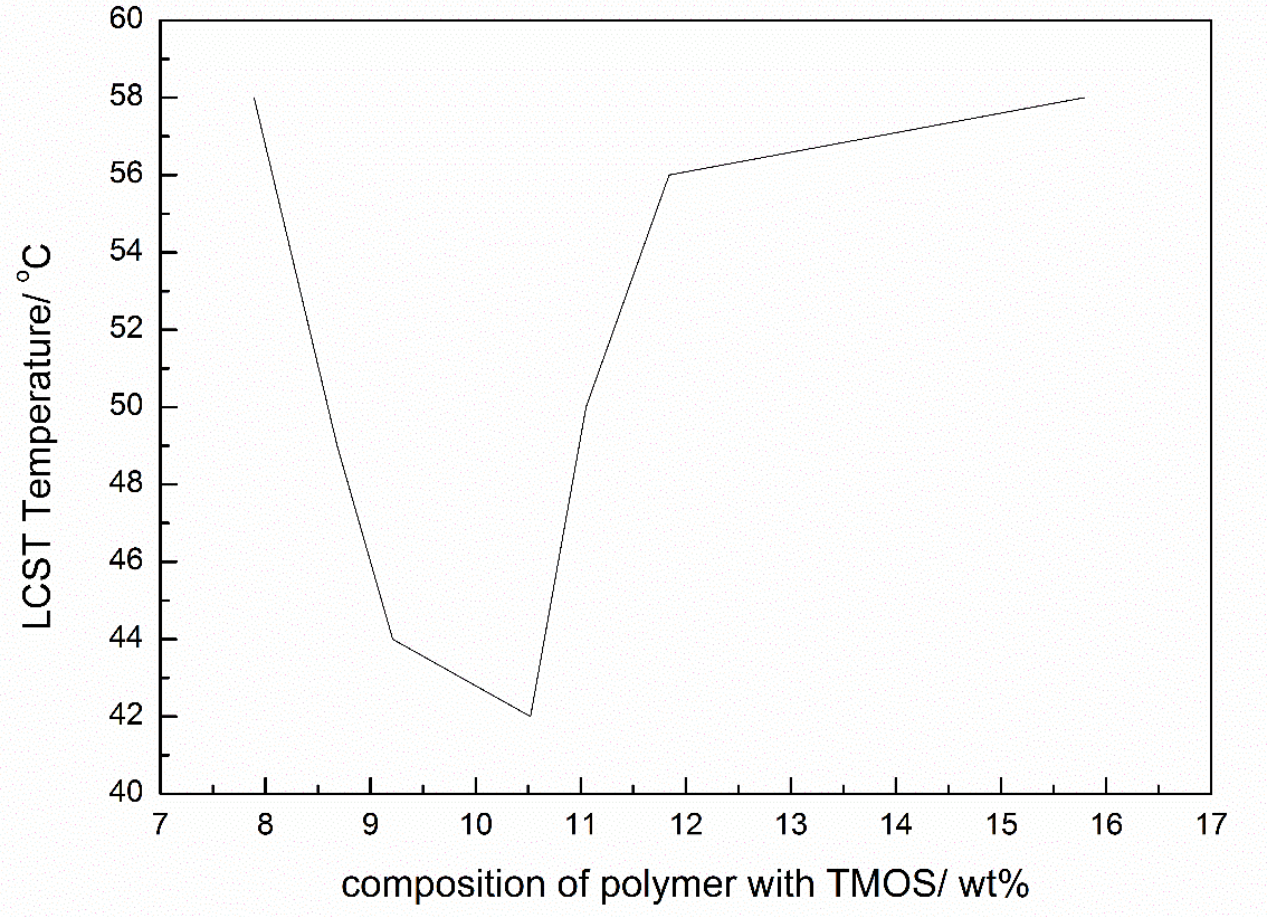

Fig. 8. Phase diagram corresponding to the change in oxazoline copolymer composition with respect to temperature.

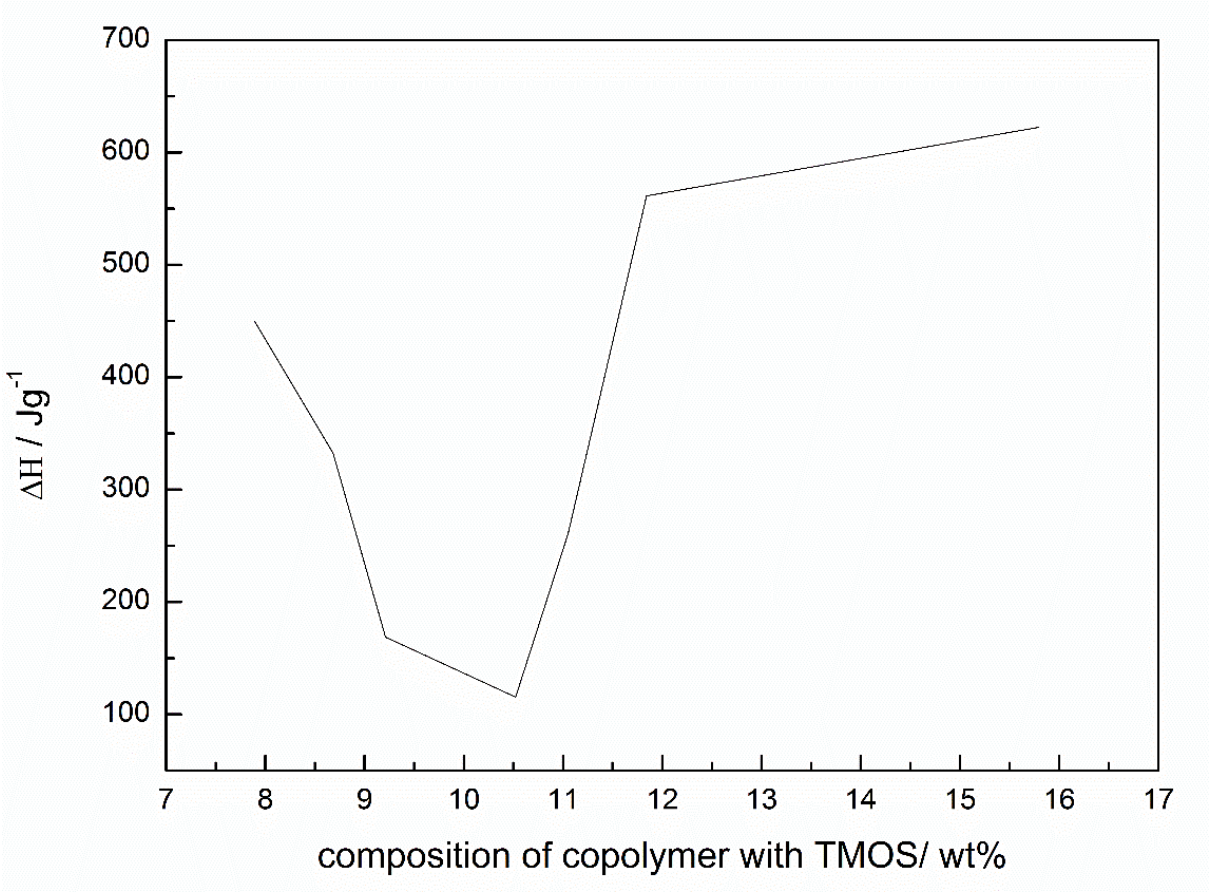

Fig. 9. Phase diagram corresponding to the change in oxazoline copolymer grams with respect to the heat of transition.

2.5 Conclusion

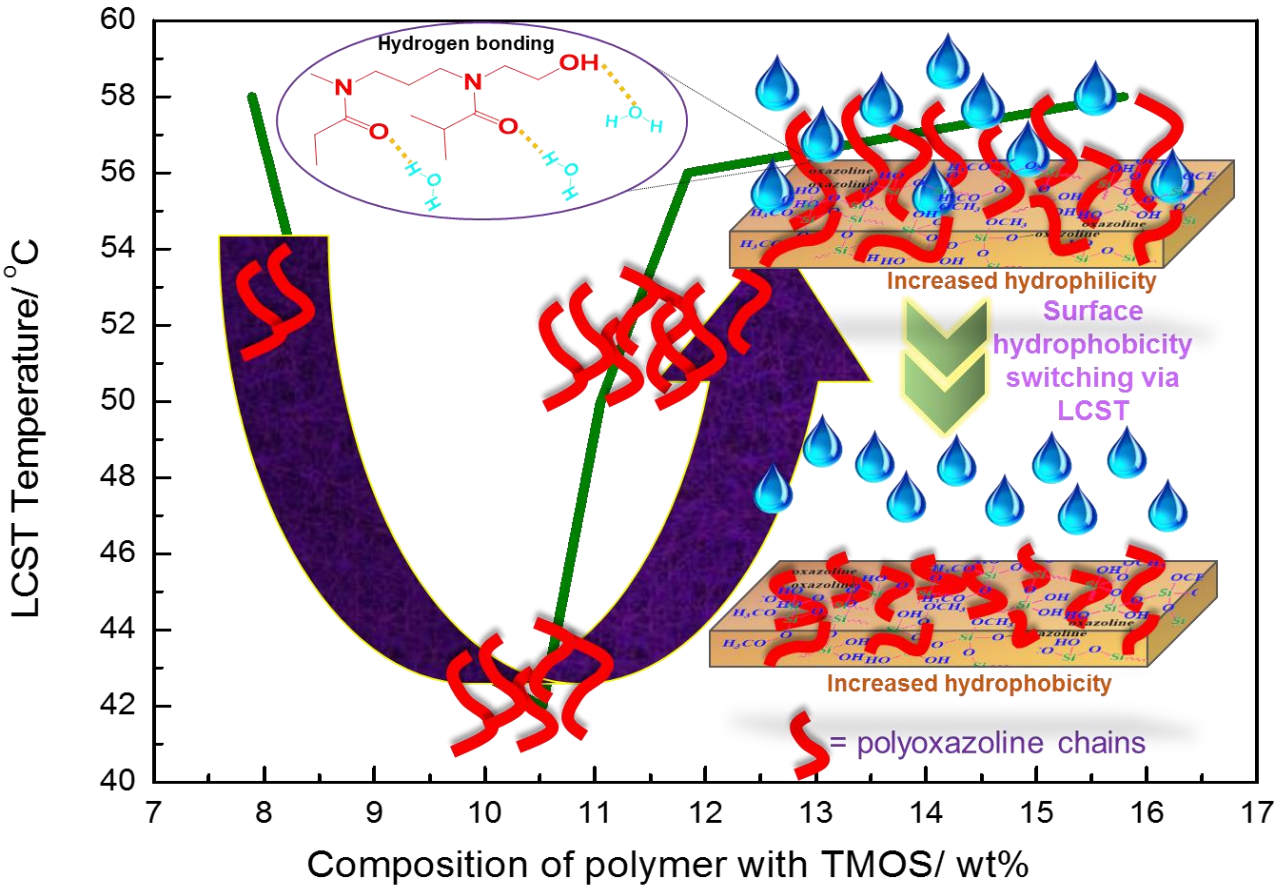

Fig. 10. Graphical illustration of fine-tuning of phase behaviour of polyoxazoline based copolymer using inorganic silicate material.

Thermosensitive organic-inorganic polymer hybrids were prepared utilizing 2-ethyl-2-oxazoline and 2-isopropyl-2-oxazaoline via living cationic polymerization using methyl tosylate as an initiator. LCST of the copolymer in water was at 77 °C. The materials contained constant moles of inorganic TMOS and were characterized using FT-IR spectroscopy. With the variation in the amount of copolymer, the solid-supported hybrids synthesized by in-situ sol-gel condensation, can be modulated for their phase behaviour in a wide range of 42 °C to 58 °C. This observation unveiled the composition dependency of phase transitions in thermosensitive polymer/silicate hybrids, along with

their enthalpy changes. Enthalpy change of the transition was found to be maximum (622.26 Jg^{-1}) for hybrids showing phase behaviour at 58 ^{o}C, and lowest (115.28 J g^{-1}) for hybrid showing lowest phase transition at 42 ^{o}C. Thus, fine-tuning of the solid-supported organic-inorganic hybrid materials is possible on the basis of control of the concentration of the copolymer used in the silicate matrix. This can provide a strategy for custom designing of the thermos-responsive materials for feasible applications for smart materials [24]. (Fig. 10).

2.6 References

[1] C. Tsitsilianis, *Soft Matter*, 2010, 6, 2372-2388.

[2] Y. Kohno, S. Saita, Y. Men, J. Yuan and H. Ohno, *Polym. Chem.*, 2015, 6, 2163–2178.

[3] M. Taylor, P. Tomlins and T. Sahota, *Gels*, 2017, 3, 4, 1-31.

[4] R. Liu, M. Fraylich and B. R. Saunders, *Colloid Polym. Sci.*, 2009, 287, 627–643.

[5] M. Sahn, L. M. Stafast, M. Dirauf, D. Bandelli, C. Weber and U. S. Schubert, *Eur. Polym. J.*, 2018, 100, 57–66.

[6] A. Halperin, M. Kröger and F. M. Winnik, *Angew. Chem. Int. Ed.*, 2015, 54, 15342–15367.

[7] A. Gandhi, A. Paul, S. O. Sen and K. K. Sen, *Asian J. Pharm. Sci.*, 2015, 10, 99–107.

[8] M. A. Haq, Y. Su and D. Wang, *Mater. Sci. Eng.*, 2017, 70, 842–855.

[9] H. G. Schild, *Prog. Polym. Sci.*, 1992, 17, 163–249.

[10] K. Jain, R. Vedarajan, M. Watanabe, M. Ishikiriyama and N. Matsumi, *Polym. Chem.*, 2015, 6, 6819–6825.

[11] S. Ashraf, H.-K. Park, H. Park and S.-H. Lee, *Macromol. Res.*, 2016, 24, 297–304.

[12] L. H. Lima, Y. Morales and T. Cabral, *Int. J. Retin. Vitr.*, 2016, 2, 23, 1-7.

[13] A. Dworak, B. Trzebicka, A. Kowalczuk, C. Tsvetanov and S. Rangelov, *Polimery*, 2014, 59, 88–94.

[14] M. Einzmann and W. H. Binder, *J. Polym. Sci. Part A: Polym. Chem.*, 2001, 39, 2821–2831.

[15] R. Hoogenboom, H. M. L. Thijs, M. J. H. C. Jochems, B. M. van Lankvelt, M. W. M. Fijten and U. S. Schubert, *Chem. Commun.*, 2008, 5758–5760.

[16] N. Adams and U. S. Schubert, *Adv. drug Deliv. Rev.*, 2007, 59, 1504–20.

[17] T. X. Viegas, M. D. Bentley, J. M. Harris, Z. Fang, K. Yoon, B. Dizman, R. Weimer, A. Mero, G. Pasut and F. M. Veronese, *Bioconjugate Chem.*, 2011, 22, 976–986.

[18] R. Hoogenboom and U. S. Schubert, *Green Chem.*, 2006, 8, 895-899.

[19] C. Diehl and H. Schlaad, *Macromol. Biosci.*, 2009, 9, 157–161.

[20] C. Diab, Y. Akiyama, K. Kataoka and F. M. Winnik, *Macromolecules*, 2004, 37, 2556–2562.

[21] J. Livage, *Bull. Mater. Sci.*, 1999, 22, 201–205.

[22] G. Schottner, *Chem. Mater.*, 2001, 13, 3422–3435.

[23] M. Catauro, M. C. Mozzati and F. Bollino, *Acta Astronaut.*, 2015, 117, 153–162.

[24] C. Sanchez, P. Belleville, M. Popall and L. Nicole, *Chem. Soc. Rev.*, 2011, 40, 696–753.

[25] Y.-H. Han, A. Taylor, M. D. Mantle and K. M. Knowles, *J. Non-Crystalline Solids*, 2007, 353, 313–320.

[26] K. S. Smaran, R. Vedarajan and N. Matsumi, *Int. J. Hydrog. Energy*, 2014, 39, 2936-2942.

[27] I. Zaręba-Grodź, W. Miśta, W. Stręk, E. Bukowska, K. Hermanowicz and K. Maruszewski, *Opt. Mater.*, 2004, 26, 207–211.

[28] S. J. Lue, C.-H. Chen and C.-M. Shih, *J. Macromol. Sci. Part B*, 2011, 50, 563–579.

[29] J.-S. Park and K. Kataoka, *Macromolecules*, 2006, 39, 6622–6630.

[30] P. Banet, P. Griesmar, S. Serfaty, F. Vidal, V. Jaouen and J.-Y. Le Huerou, *J. Phys. Chem. B*, 2009, 113, 14914–14919.

[31] M. Tamaki, T. Taguchi, Y. Kitajyo, K. Takahashi, R. Sakai, T. Kakuchi and T. Satoh, *J. Polym. Sci. Part A: Polym. Chem.*, 2009, 47, 7032–7042.

[32] A. M. Ullman, J. W. Brown, M. E. Foster, F. Léonard, K. Leong, V. Stavila and M. D. Allendorf, *Inorg. Chem.*, 2016, 55, 7233–7249.

[33] M. Rackaitis, K. Strawhecker and E. Manias, *J. Polym. Sci. Part B: Polym. Phys.*, 2002, 40, 2339–2342.

[34] M. M. Contreras, C. Mattea, J. C. Rueda, S. Stapf and F. Bajd, *Des. Monomers Polym.*, 2014, 18, 170–179.

[35] J. S. Higgins, J. E. G. Lipson and R. P. White, *Philos. Trans. R. Soc. A: Math. Phys. Eng. Sci.*, 2010, 368, 1009–1025.

[36] Y. Ma, A. S. Foster and R. M. Nieminen, *J. Chem. Phys.*, 2005, 122, 144709.

[37] J. J. Yang, S. Meng, L. F. Xu and E. G. Wang, *Phys. Rev. B*, 2005, 71, 035413.

[38] Heyda, S. Soll, J. Yuan and J. Dzubiella, *Macromolecules*, 2014, 47, 2096–2102.

[39] S. Bharadwaj, P. B. Sunil Kumar, S. Komura and A. P. Deshpande, *J. Chem. Phys.*, 2018, 148, 084903.

[40] I. Bischofberger, D. C. E. Calzolari, P. De Los Rios, I. Jelezarov and V. Trappe, *Sci. Reports*, 2014, 4, 4377, 1-7.

[41] A. L. Tasca, F. Ghajeri and A. J. Fletcher, *Adsorpt. Sci. & Technol.*, 2017, 36, 327–342.

[42] A. P. Rao, A. V. Rao and G. M. Pajonk, *Appl. Surf. Sci.*, 2007, 253, 6032–6040.

[43] G. D. Smith and D. Bedrov, *J. Phys. Chem. B*, 2003, 107, 3095–3097.

[44] K. Klier, J. H. Shen and A. C. Zettlemoyer, *J. Phys. Chem.*, 1973, 77, 1458–1465.

****

Chapter 3

Silicon wafer modification with thermoresponsive oxazoline based copolymer as solid-supported phase gradients

Abstract

Solid-supported LCST showing materials find tremendous use in distinguished fields like separation, drug delivery and tissue engineering. Hence, in order to prepare solid state phase gradients, a polymer of (3-aminopropyl)triethoxysilane terminated 2-ethyl-2-oxazoline had been prepared which exhibited thermoresponsive properties. Self-assembled monolayers of this polymer was coated over a silicon wafer substrate via covalent binding. The formation of polymer thin films over silicon substrate was confirmed by various techniques including XPS and FTIR. Surface conversion rate of Si wafer with polymer was detected to be 21% by XPS analysis. Polymer showed the LCST of 75 ^{o}C while silane modified polymer showed LCST at 68 ^{o}C. Contact angle measurements showed the presence in the hydrophobic nature on the film. Thus, a solid-state material was developed which has the ability to show phase transition at a temperature of 68 ^{o}C.

3.1 Introduction

Silicon [1] provides broad range applications in the field of semiconductor industry and integrated technologies due to its semiconductor properties and its ease of packaging. Hence, silicon surface texturing via wafer modification [2,3] is considerably the foremost and significant technology for the fabrication of electronic, photonics and optical devices, for example sensors [4] and solar cells [5]. Reactive silicon wafers have already been modified using various hydrophilic silanol terminated moieties or hydrophobic hydrogen-terminated compounds. In general, wafer bonding involves formation of thin films in the form of uniform self-assembled monolayers (SAMs) [6] in the form of large 2D ordered molecular domains. The compound being coated over the wafer interacts with the chemically opposing terminal groups deposited onto the silicon substrate. SAMs are established to serve as a versatile and robust surface modification technology to fine-tune the surface properties by the combination of surface coupling agents and organic molecules. Formation of SAMs makes it possible to optimize the film growth over thickness from few nanometers to several micrometres. Another interesting feature of SAMs is that their own structural diversity and inexpensively high flexibility due to their smaller weight and volume. This makes them perfect candidates for device miniaturizations [7]. Hence, functional films and materials are realized to be used in battery research, optics, organic electronics and process technology [8–11].

Modification of the targeted physical or chemical properties can be easily done by the deposition of the polymeric materials on the silicon substrate. This widen the potential of the modified semiconductor material and allows the polymeric thin films to be employed in biological applications such as cell cultivation, synthesis of filter membranes and highly efficient antibacterial surfaces and immobilisation of bioactive

species on the surface [12–16]. Thin films of polymers are modified and coated over with silicon wafers via majorly used coupling agents, i.e., aminosilanes [17]. Aminosilanes are bifunctional in nature. They have the ability to form strong covalent bond in the form of Si-O-Si linkages through their expandable long alkyl chains allowing the formation of superior close-packed monolayers. The amine group possess a distinctive surface reaction chemistry as it catalyses the formation and hydrolysis of siloxane bonds at the ambient temperatures. It can bind to silicon atoms of self and neighbouring aminosilane molecule via inter- and intra-molecular interactions to form a cyclic intermediates. This increases the potential of these systems to be exploited in chromatography[18], medicine [19], detection of desired gases [20] and biosensors [21].

Thermoresponsive polymers are of great interest in today's era as they display phase changes at a critical behaviour in the form of phase-in behaviour (upper critical solution temperature, UCST) and phase-out behaviour (lower critical solution temperature, LCST) [22]. Phase separation phenomenon at LCST is known to be widely exploited in biomedical and some physical applications such as separation [23], drug delivery [24] , tissue engineering [25] and gene therapy [26]. This requires the production of extensively intelligent and smart materials whose LCST can be tailored according to the user's need. Researchers have already coated PEO-based polymer chains onto the silicon wafer and created materials with dominant metal-oxo surfaces and physical adhesion. Recently, Matyjaszewki et al., [27] prepared thermally responsive, stable star polymer chains onto the silicon wafers. The thermoresponsive polymer was PEO-based oligomer functionalized with methyl ether methacrylate. Ishida et al., [28] have already studied the phase transition of PNIPAM grafted onto silicon wafers. Li et al. [29], have used PNIPAM based silicon wafer systems for cell adhesion and detachment. Lately, polyoxazolines [30]

have found to be a class of non-toxic, highly efficient thermosensitive polymers which exhibit a wide tunable LCST range of 0 - 100 ^{o}C. They mimic biological proteins due to the presence of the polyamide backbone, thus making them excellent biocompatible materials [31]. Because they are synthesized via ring opening living polymerization, this provides us with the ability to incorporate highly tunable and desired functionalities on termination. Hence, these materials serves as the eminent and facile choice to be terminated with aminosilane based coupling agents and further, to be modified on silicon wafers. Based on this thought, silicon wafer modified using novel thin films of alkoxysilyl terminated polyoxazolines were prepared for the first time and studied their characteristics for predominant and desired LCST properties.

Objective of the work:

In this work, the termination of polymer chains of poly(2-ethyl-2-oxazoline) was carried out using (3-aminopropyl)triethoxysilane (APTES) to prepare a thermoresponsive polymer system. The polymer acts as the thermoresponsive moiety which show phase transition at a temperature of 75 ^{o}C and the aminosilane modification empower it for covalently bonding with the exposed –OH groups on the silicon wafer. It has been known that factors like reaction temperature, solvent, time, concentration and nature of coupling agent deeply affect the thickness, durability and uniformity of the SAMs. Hence, it becomes vital not to overlook these parameters and study and characterize the thin films in detail. Hence, the thin films made over the silicon wafers were optimized and scrutinized for their effective work-up and excess polymer was removed to avoid any ambiguity. The system was characterized by FT-IR and XPS measurements. DSC analysis performed on modified silicon wafer showed occurrence of phase transition over silicon wafer at 68 ^{o}C. Further, modified silicon wafer was checked

for its thermosensitivity which showed that the substrate is capable to separate water at 80 ^{o}C even from the moisture, creating a superior solid-supported LCST showing phase gradient system.

3.2 Experimental

3.2.1 Materials: 2-ethyl-2-oxaozline was purchased from Tokyo Chemical Industry Co. Ltd and acetonitrile from Wako Co. Ltd and these chemicals were purified further over Calcium hydride (Sigma Aldrich) followed by distillation. Silicon wafer was purchased from Azone. Co. Ltd. Methyl-p-toluenesulphonate, (3-aminopropyl)triethoxysilane (Tokyo Chemical Industry Co. Ltd) and chloroform, hexane, hydrogen peroxide, sulfuric acid, ethanol (Wako Co. Ltd) were used as received. Amberlyst A-21 was bought from Sigma Aldrich.

3.2.2 Instrumentation: Perkin Elmer Spectrum 100 was used as the FT-IR spectrometer to record the Fourier-transformed infra-red spectra. MALDI-TOF was carried out on a Perseptive Biosystems (now Applied Biosystems Inc.) Voyager DE PR. Ultrashield™ Plus Bruker, Z101355 was utilized for the 400MHz Nuclear Magnetic Spectroscopy. Contact angle measurements were conducted on a DropMaster DM-501 by Kyowa Interface Science Co., Ltd.

3.2.3 Synthesis of silyl terminated polymer: Similar procedure was used as already reported in literature [32]. Purified 2-ethyl-2-oxazoline (1.57 g, 15.8 mmol) and methane-p-toluenesulphonate (0.26 g, 1.4 mmol) were refluxed and stirred in acetonitrile (10 mL) under nitrogen atmosphere at 80 ^{o}C for 10 hours. Then, (3-aminopropyl)triethoxysilane (APTES) (0.47 g, 2.13 mmol) was added at 0 ^{o}C to the reaction mixture and it was allowed

to stir at room temperature for 2 days for complete termination. Next, the solution was treated with ion-exchange Amberlyst A-21. The pure polymer was isolated via reprecipitation from chloroform to n-hexane, then dried in vacuum. (Scheme 1).

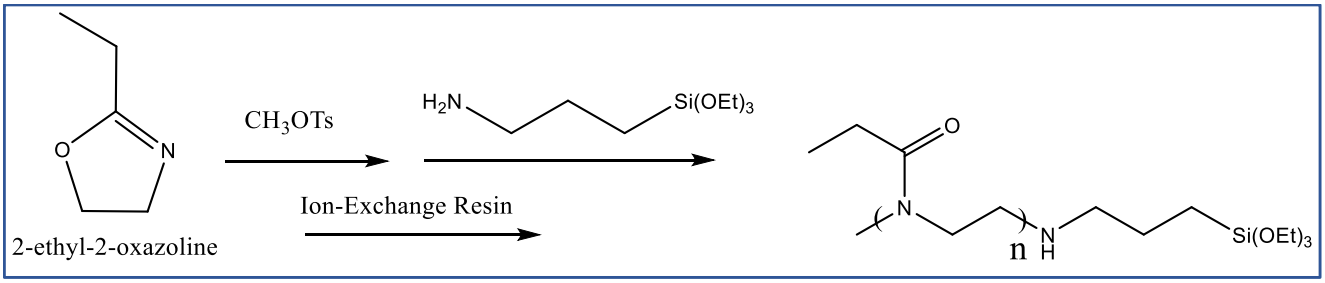

Scheme 1: Reaction scheme for the synthesis of thermoresponsive polyoxazoline terminated by APTES.

3.2.4 Synthesis of polymer modified silicon wafer: Taken a square piece of silicon wafer and immersed it in a 30:70 H_2O_2:H_2SO_4 Piranha solution (10 mL) at 120 ^oC for 3 hours. The wafer was washed with first water, then ethanol and again water 2 mL each via sonication for 2 minutes each. Then, a 25 mg polymer solution was dissolved in 0.25 mL ethanol and this was added via syringe to the silicon wafer which was kept for incubation period of 12 hours at 60 ^oC to evaporate ethanol and for the covalent bonding to happen. As it is very important to take special care on the work-up on silicon wafers, these were sonicated for the optimized time of 10 minutes in ethanol to remove any unassociated polymer chains. Further, the silicon wafer was dried in vacuum and purged the surface with nitrogen for few seconds to complete drying, which was used for further analysis.

3.3 Characterizations

The synthesized thermoresponsive polymer was characterized using 400MHz nuclear magnetic resonance (NMR) spectrometer by ^{1}H NMR in DMSO as shown in Fig. 1. The MALDI-TOF analysis was performed and the molecular weight of the polymer was found out to be m/z= 1563 g/mol. This confirmed the synthesis of alkoxysilane-terminated polymer ready to be coated onto the silicon wafer by covalent bonding.

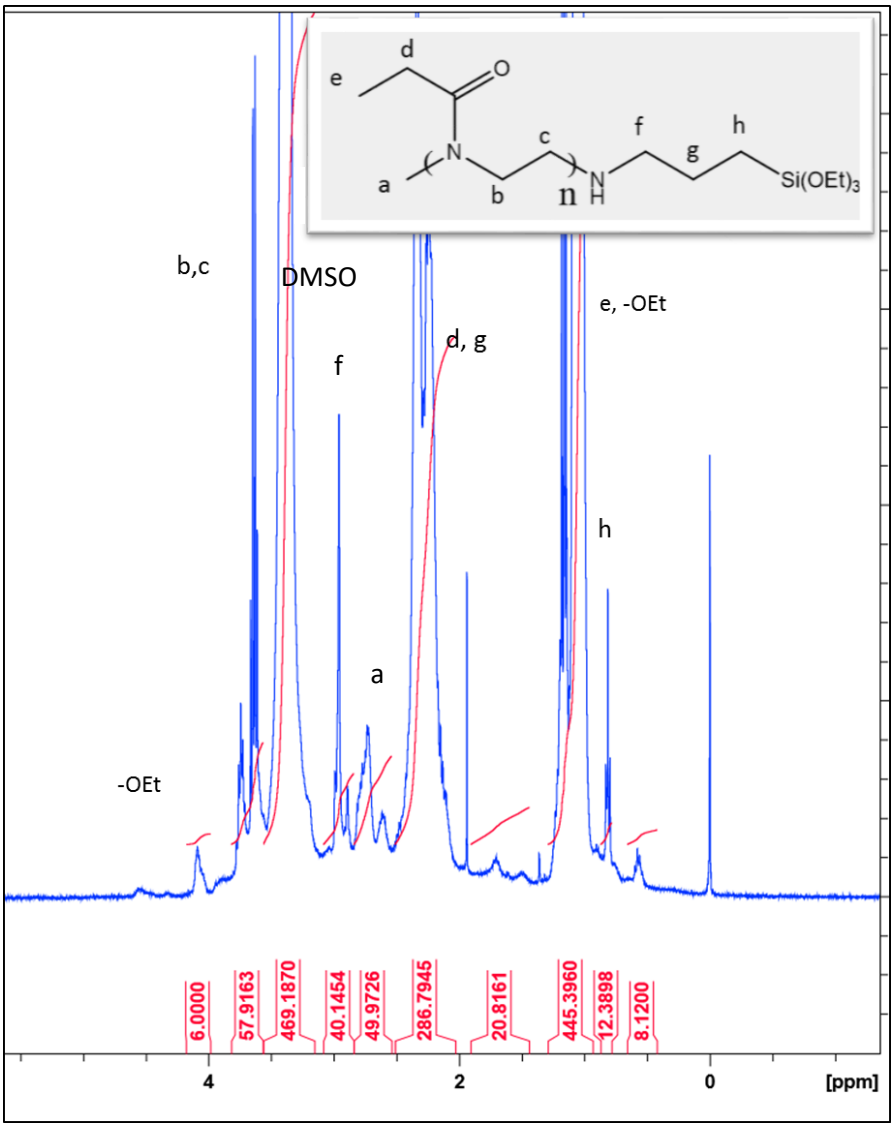

Fig. 1. ^{1}H-NMR spectrum of trialkoxysilyl-terminated polyoxazoline.

3.4 Results and Discussion

A homopolymer of 2-ethyl-2-oxazoline was synthesized by ring opening methyl-p-toluenesulphonate initiator. The termination was done by coupling aminosilane APTES which empower the polymer to covalently bond with the silicon wafers. Once the synthesis polymer is characterized, it needed to form thin films in the form of self-assembled monolayers on the silicon wafer. To further enhance the chances of covalent bonding between the wafer and polymer, the silicon substrate is exposed to vigorous oxidative environment (Piranha solution) to form Si–OH (silanol groups) at the surface for effective coupling.

Once the coating was done via incubation for 12 hours, it was necessary to remove any unreacted or physisorbed polymer remains to form a stable uniform chemisorbed layers of the polymer. Hence, studies were done to optimise the work-up time after the incubation was performed. Solvent taken was ethanol, which was then added to silicon wafer kept in a 50 mL beaker and sonicated for different time of 2, 5, 10 and 20 minutes. It was optimized that sonicating the silicon wafer for 10 minutes removed the physisorbed polymer. Hence, after sonicating for this time, the wafer was subjected to further analysis.

3.4.1. Characterizations of Synthesis of Self-assembled Monolayers of Polymer on Wafer

After the optimizations, it is evident to investigate about the nature and aspects of thin films formed. Fig. 2. shows a schematic illustration about the Si-O-Si linkage formation between the polymer and silicon wafer supposed to happen. The process involved silicon substrate treatment with piranha solution, and then generation of polymer modified silicon wafer.

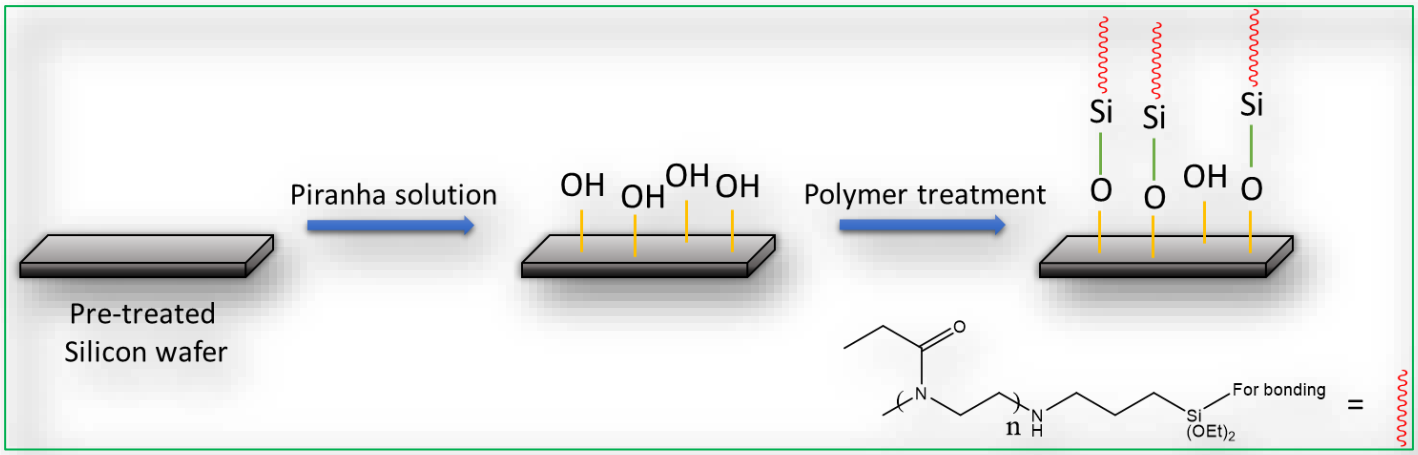

Fig. 2. Schematic representation of the formation of modified silicon wafers.

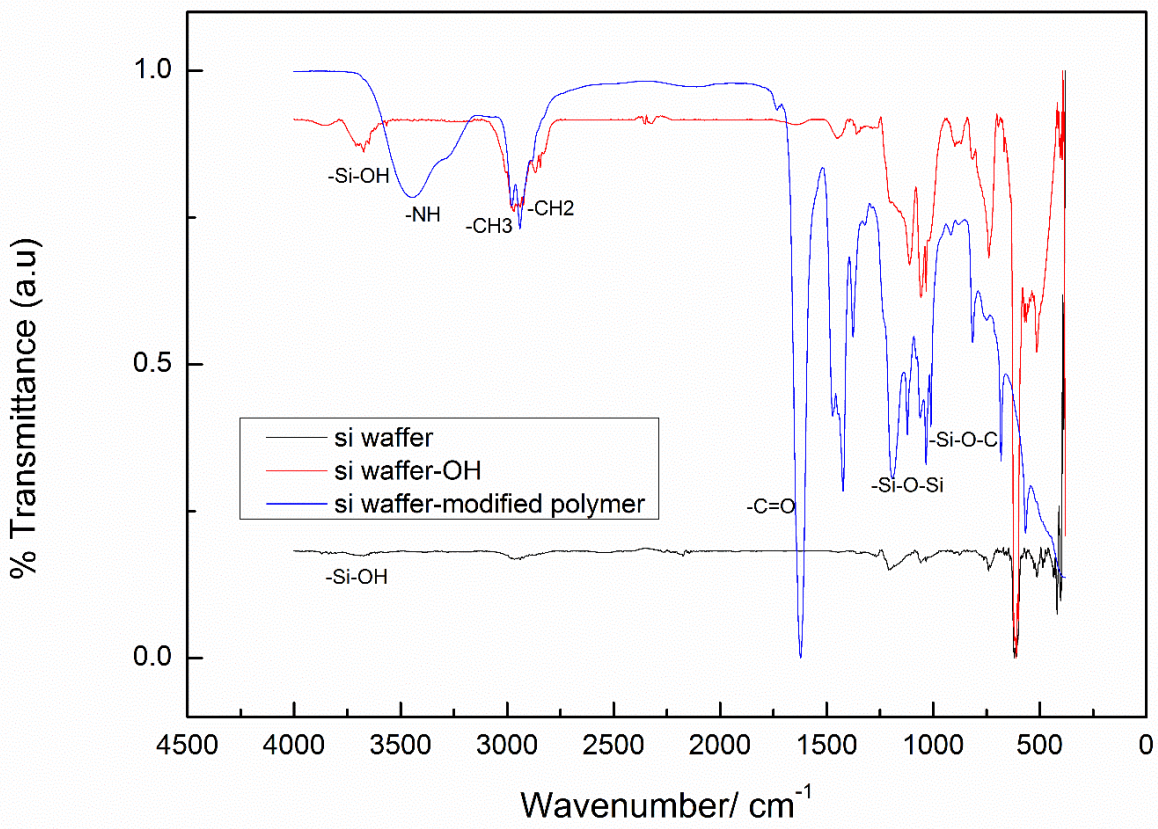

Fig. 3. FT-IR spectra for bare Si (black), Si wafer exposed to Piranha solution (red) and polymer modified silicon wafer (blue).

At first, the polymer layer characterization was done by FT-IR spectra as shown in Fig. 3. The spectra for untreated Si showed major peaks of Si-OH at ~3650 cm^{-1} which can be due to free –OH or –hydrogen bonded OH and a little peak at ~2150 cm^{-1} owing to extremely low presence of Si-H bonds. When the silicon wafer was exposed for acidic treatment, the spectra more or less remained similar to the bare Si. Now, when the polymer is bonded over the wafer, clear changes in the spectra in both the functional and fingerprint regions can be seen. There appeared a strong broad peak at ~3450 cm^{-1}, suggesting the presence of N-H bond from the polymer's terminal group. Asymmetric

aliphatic stretching of –C-H bonds from the polymer backbone was also observed at ~3050-2950 cm^{-1}. The polymer also showed strong carbonyl peak at ~1650 cm^{-1}. The most important peaks which characterise the bond formation between the polymer and the silicon wafer are found at ~1150 cm^{-1} and ~1020 cm^{-1} which are corresponding to the Si-O-Si longitudinal and transverse stretching modes, respectively. Appearance of a doublet peak at ~1080 cm^{-1} and a peak at ~950 cm^{-1} corresponds to Si-OCH_2CH_3. Further, Si-O-C bonding mode can be identified at ~1100 cm^{-1}. Region of 1300-1200 cm^{-1} is assigned to the C-N, C-C and NH_2 bending modes of the polymer. The characterization confirmed the covalent bonding the polymer and silicon substrate [33].

Further, another surface-sensitive technique was implemented on the silicon modified surfaces in the form of X-ray photoelectron spectroscopy (XPS) to analyse the electronic states of the elements present, and thus the surface chemistry of the material. The XPS spectra of bare Si showed peaks of silicon, oxygen and carbon (due to impurity of carbon tape), as expected. The spectra for polymer modified silicon wafer contained the signals of silicon, oxygen, carbon (due to polymer and carbon tape) and nitrogen.

Because nitrogen is not present in untreated silicon, its peak due to secondary amine group present in the polymer served as the point of analysis for the bonding between the species. The deconvoluted XPS spectra of polymer coated substrate is represented in Fig. 4. When the Si 2p high resolution spectra (Fig. 4a) was analysed, it was observed signal at a binding energy of 97.4 eV owing to formation of aminosilane on the SiO_2 layer of wafer (Si-O-Si). Other binding energies at 98.9 and 101.8 eV corresponds to the SiO_2 and bulk Si, as shown. The N 1s fine-scale spectra (Fig. 4b) was also examined which portrayed two distinct components at the binding energies of 399.4 eV and 400.7 eV corresponding to non-bonded –N-H (to wafer), and H-bonded –NH, respectively. Both

represented and further confirmed the growth of polymer layers on the silicon wafer. Polymer deposited onto the silicon wafer was found out to be 21%. (using area of –H-bonded N-H and total N-H of polymer) One of the probable reasons of low density bonding is the presence of long-alkyl chain and polymer backbones.

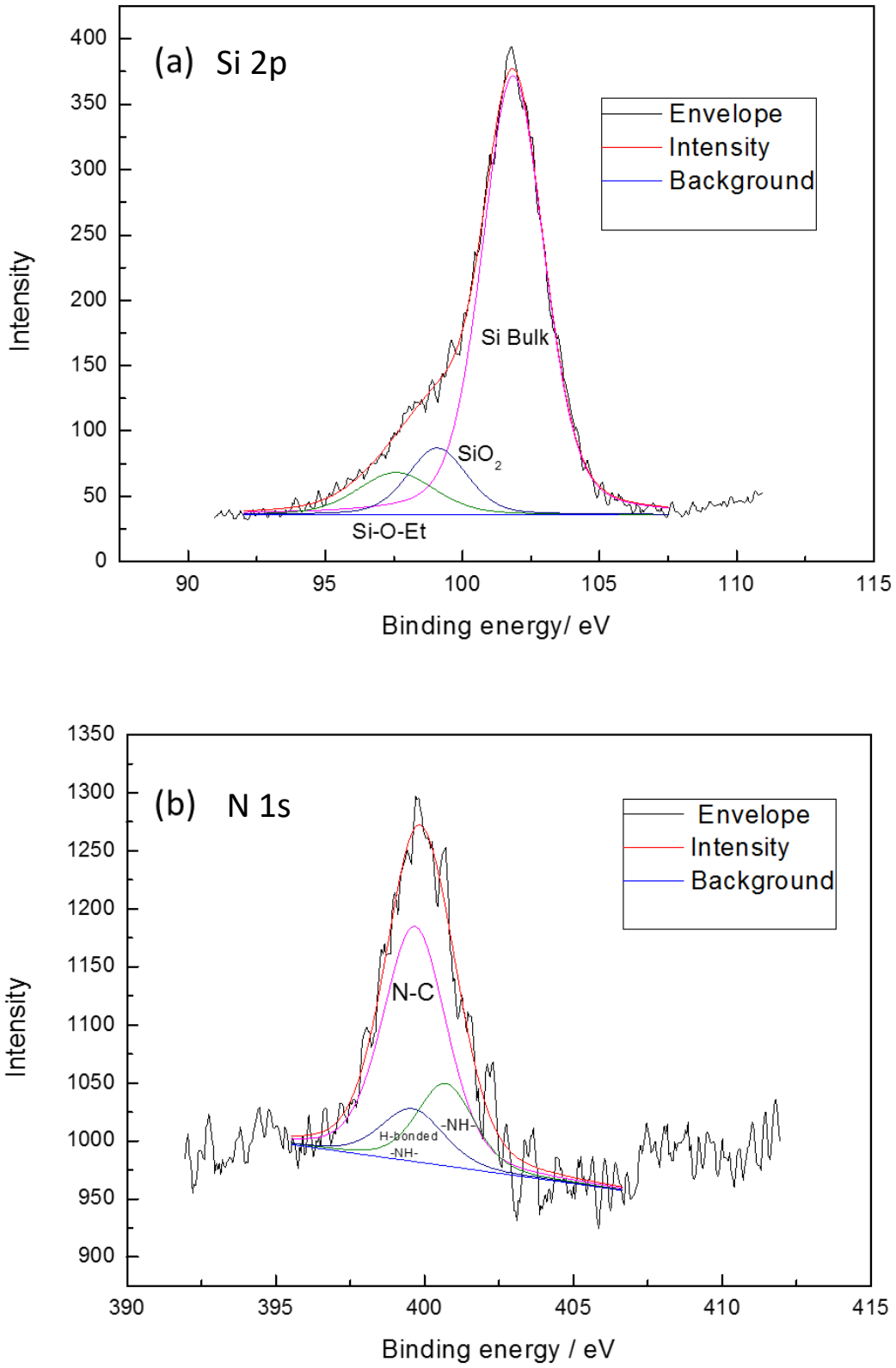

Fig. 4. Deconvoluted XPS spectra for (a) Si 2p and (b) N 1s for the polymer modified silicon wafer.

3.4.2. LCST determination on the silicon wafer for solid-supported phase gradients

Afterwards, the thermoresponsive behaviour of the silane terminated polyoxazoline was checked via differential scanning calorimetry as seen in Fig. 5. The measurement was done at a temperature range of 25-90 ^{o}C at a heating rate of 1 ^{o}C/min. The polymer concentration was taken as 0.5 mg/mL in water. A small broad yet clearly distinguishable endothermic peak was observed at a critical temperature of 74.4 ^{o}C, showcasing the occurrence of LCST in the polymer. As expected, presence of hydrophilic ethyl group in oxazoline moiety and polar groups like -Si(OEt)$_3$ and –NH increases the

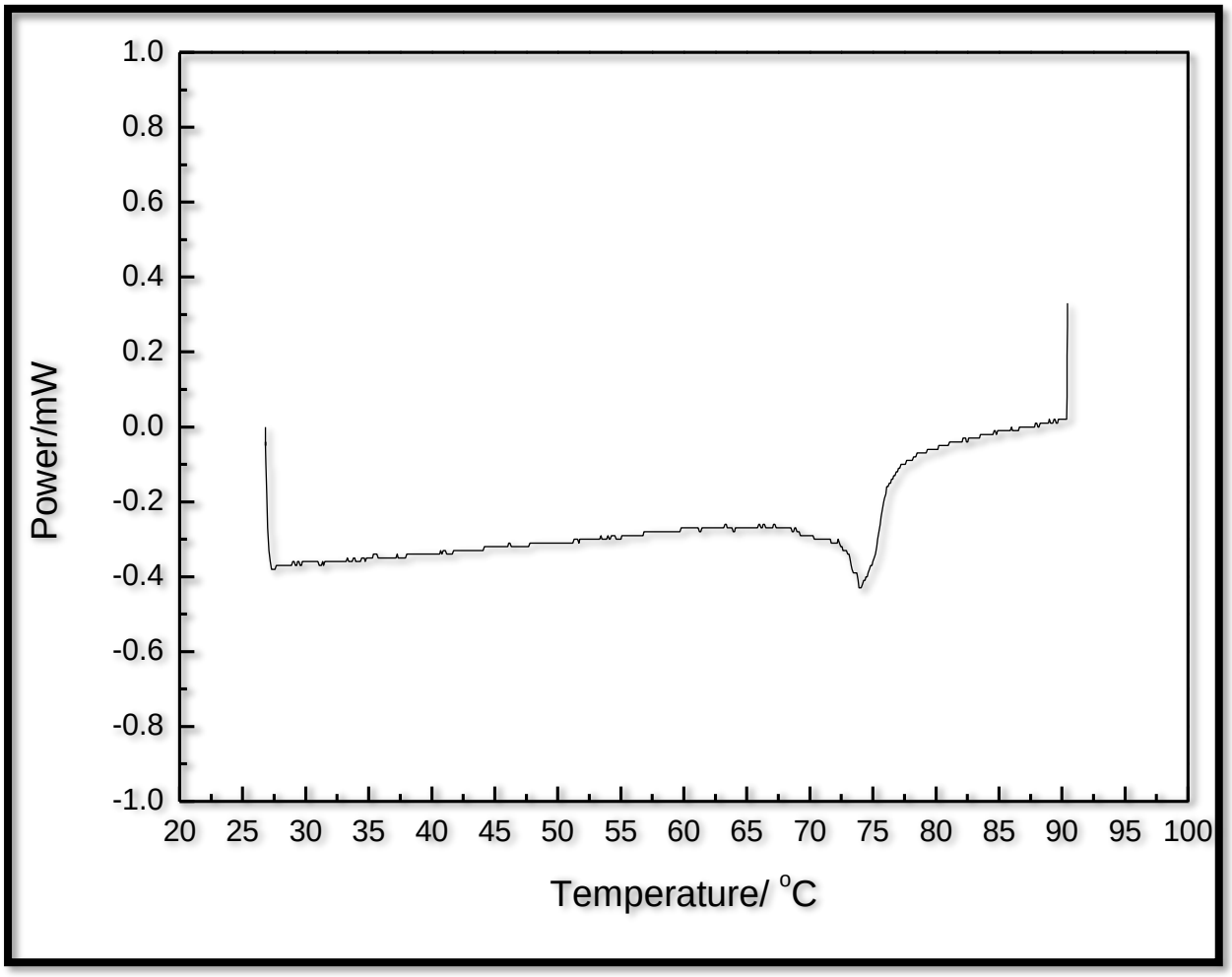

Fig. 5. DSC profile of the silyl-terminated polyoxazoline.

hydrophilicity in the molecule, thereby delaying the collapse of hydrophobic globule, causing the LCST to occur at this temperature.

Next, silicon wafer modified by this thermoresponsive polymer was evaluated for its phase transition behaviour using differential scanning calorimetry as seen in Fig. 6 in water. The measurement was done at a temperature range of 35-80 ^{o}C at a heating rate of 1 ^{o}C/min. A broad endothermic peak was observed at a critical temperature of 68 ^{o}C, showcasing the occurrence of phase transition over the silicon wafer polymer, thus enabling formation of a solid-supported LCST showing material. It is seen that silicon wafer act as a hydrophobic entity and incorporation of this inorganic component decreases the LCST of the polymer. This trend is similar to what we observed in the case of polyoxazoline –based organic-inorganic hybrids.

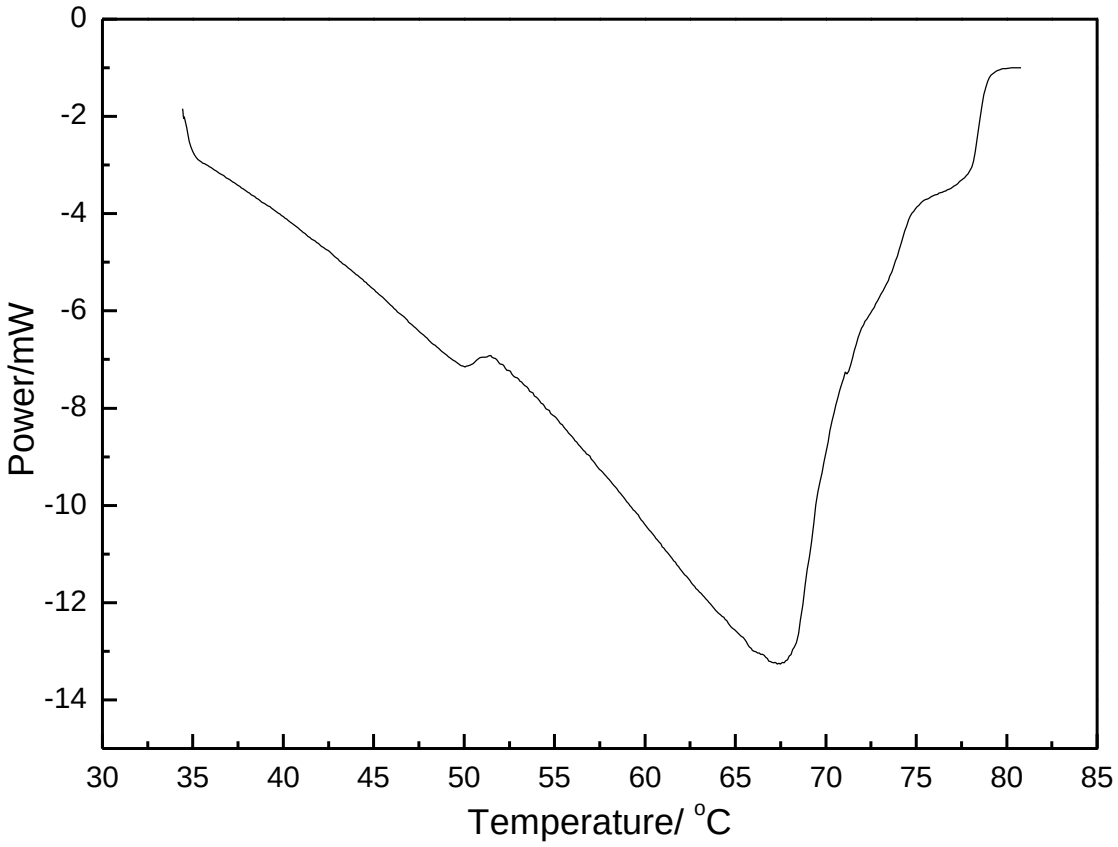

Fig. 6. DSC profile of the silicon wafer modified by silyl-terminated polyoxazoline.

Next, wetting properties of the thin film formed was checked by contact angle measurements (Fig. 7.). It was performed for 6 times to get an average on these silicon wafer sonicated for different times and the results are portrayed in the Table 1. It was observed that bare silicon (with no exposed –OH groups) are more hydrophilic as it conveyed the contact angle of 20 ^{o} at room temperature. This suggested that the surface has good wettability and higher solid surface free energy. When the measurements were done for modified silicon wafer (TEST-10) sample for at room temperature, it was observed that the surface becomes more hydrophobic than bare Si wafer. The angle increases due to the presence of hydrophobic polymer chains and APTES molecules, thereby decreasing the wettability and adhesive strength. This clearly indicated that the surface becomes hydrophobic after coating.

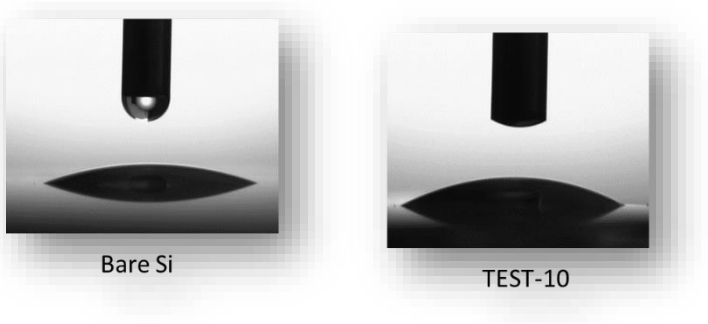

Fig. 7. Contact angle measurements of uncoated silicon wafer (Bare Si), and polymer modified Si surface after film formation.

Table 1: Contact angles measured for Bare Si and modified wafers sonicated for 10 minutes done for 6 times for optimizations.

Sample name	Exp 1	Exp 2	Exp 3	Exp 4	Exp 5	Exp 6	Avg.	Std. dev
Bare Si	22.9	20.2	17.9	20.3	17.8	21.1	**20.0**	1.9
TEST-10	28.5	31.5	28.7	30.2	23.6	27.9	**28.4**	2.4

For further affirmation of LCST on solid support, another experimental series was carried out where the samples of polymer on wafer kept at temperatures above and below LCST of polymer for 24 hours were washed with in $CDCl_3$ and then recovered $CDCl_3$ was used to measure the integration of water due to moisture by conducting ^{1}H-NMR experiments. The experiment was done in two different environments of air (room temperature) and vacuum. The integration due to water was normalized with the control sample of pure $CDCl_3$ + known constant amount of TMS. Results obtained are tabulated in Table 2. It is noteworthy that no water is added for this experiment, and all the integral values are corresponding to moisture. It was observed that the polymer on silicon wafer absorbed much amount of moisture (integral) at room temperature, however more in air than vacuum as expected because the polymer is able to retain water from moisture more in air. And when the sample were kept at 90 ^{o}C for 24 hours, similar water integral was detected for different environment. It is as expected that the integration values are less for 90 ^{o}C as the water separation from polymer should takes place above LCST and it was found accordingly. The study thereby, confirmed the production of LCST exhibiting solid-support in the form of silicon wafer covalently bonded to silane terminated thermosensitive polyoxazoline whose LCST is at 68 ^{o}C. This work, henceforth opens up new opportunities for the design of solid-supported thermoresponsive smart materials.

Table 2: Integration of water presence in the sample due to presence of polymer at the temperature of 25 °C (below LCST) and 90 °C (above LCST).

Sample Name	Water integration	Normalized integration of water due to moisture only
Pure $CDCl_3$ + TMS	2.1289	-
RT Vacuum	23.5595	11.0665
RT Air	35.9796	16.9006
90 °C Vacuum	8.3552	3.9247
90 °C Air	9.5152	4.4695

3.5 Conclusion

2-Ethyl-2-oxazoline was polymerized using ring opening methyl-p-toluenesulphonate initiator and terminated by silane coupling agent (3-aminopropyl)triethoxysilane for effective coupling with silicon substrate. The polymer was characterized by proton NMR and its molecular weight of the polymer was found to be 1600 g/mol by MALDI-TOF analysis.

Silicon wafer was treated with Piranha solution to expose the surface with extreme acidic conditions to form silanol groups which is readily available for covalent bonding formation. Synthesis of self-assembled monolayers of the polymer was characterized by FT-IR and XPS measurements. The FT-IR analysed confirmed the characterization of Si-O-Si linkages between the polymer and Si substrate. The surface conversion rate of Si wafer with polymer was estimated to be 21% by XPS deconvoluted data.

The polymer in water was able to show an endothermic peak at 75 °C in the DSC profile owing to its phase transition temperature. Silicon wafer coated polymer showed an endothermic peak at 68 °C. The polymer modified silicon wafer was studied for its LCST characteristics by performing NMR analysis for amount of moisture present above/below the phase transition temperatures.

Hence, it is concluded that the silane terminated polyoxazoline modified silicon wafer revealed thermoresponsive properties at a critical temperature of 68 °C. This solid-supported system formed over silicon based substrate affirmed itself to act as solid supported phase transition showing materials for thermal devices (Fig. 8.).

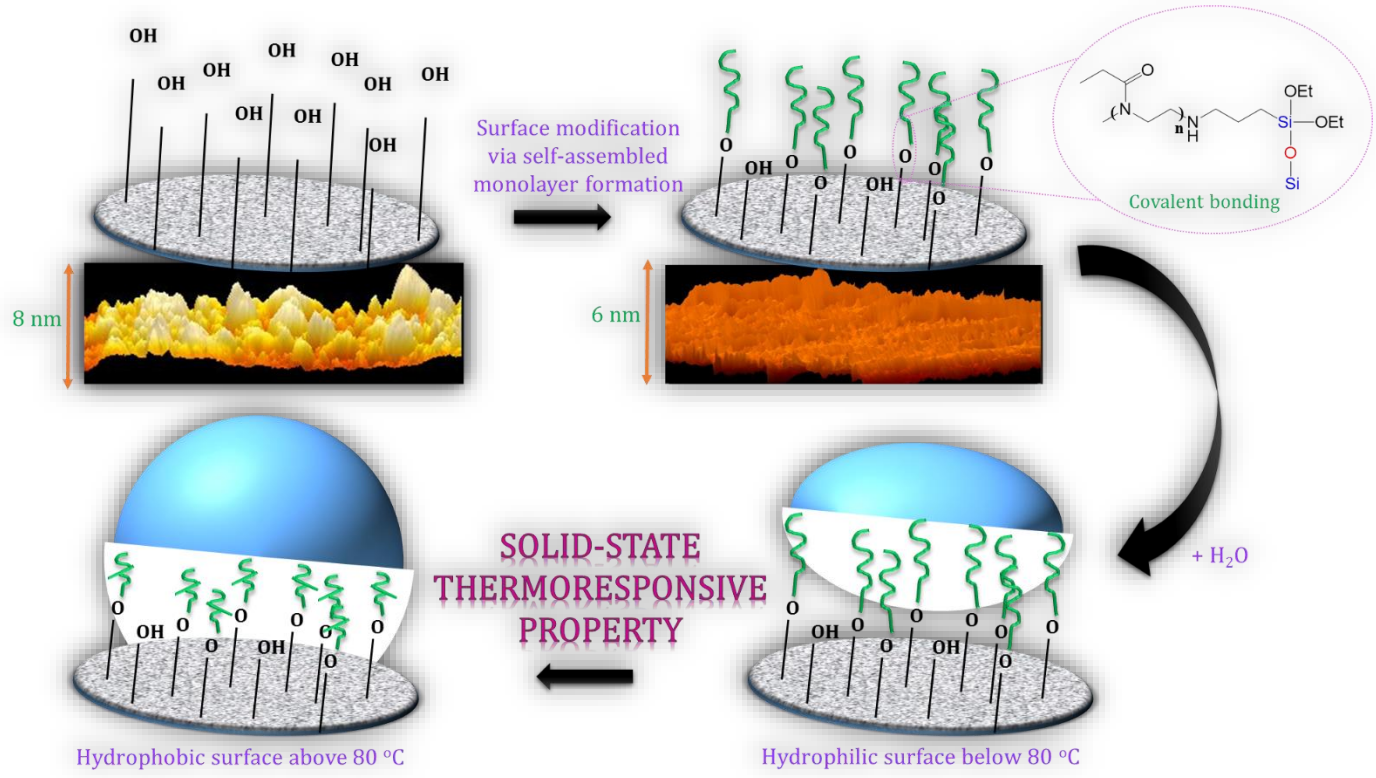

Fig. 8. Graphical illustration showing solid-supported thermoresponsive polymer modified silicon wafer for thermal devices.

Acknowledgement: The author would like to thank Mr. Kazuki Tsuchiya for his help with the XPS measurements and Assist. Prof. Rajashekhar Badam for assist in XPS analysis. The authors are also grateful to Assos. Prof. Kazuaki Matsumura, JAIST for teaching and allowing to perform contact angle measurements.

3.6 References

[1] L. Venema, *Nature*, 2011, 479, 309–309.

[2] K. Dasgupta, S. Ray, A. Mondal and U. Gangopadhyay, *Mater. Today: Proc.*, 2017, 4, 12698–12707.

[3] M. Mozetič, *Materials*, 2019, 12, 441-449

[4] T. He, H. Ding, N. Peor, M. Lu, D. A. Corley, B. Chen, Y. Ofir, Y. Gao, S. Yitzchaik and J. M. Tour, *J. Am. Chem. Soc.*, 2008, 130, 1699–1710.

[5] A. Druzhinin, V. Yerokhov, S. Nichkalo and Y. Berezhanskyi, in *2015 IEEE 35th International Conference on Electronics and Nanotechnology (ELNANO)*, 2015, 249–251.

[6] S. Flink, F. C. J. Veggel and D. N. Reinhoudt, *J. Phys. Org. Chem*., 2001,14, 407–415.

[7] D. Liu and Q. Miao, *Mater. Chem. Front.*, 2018, 2, 11–21.

[8] T. Suga, F. Mu, M. Fujino, Y. Takahashi, H. Nakazawa and K. Iguchi, *Jpn. J. Appl. Phys.*, 2015, 54, 030214, 1-5.

[9] N. Liu, *J. Laser Micro/Nanoengineering*, 2016, 11, 232–238.

[10] Y. Jiang, X. Zhang, F. Wang and Y. Zhao, *RSC Adv.*, 2015, 5, 69629-69635.

[11] C.-W. Hsu, W.-Y. Wang, K.-T. Wang, H.-A. Chen and T.-C. Wei, *Sci. Reports*, 2017, 7, 9656, 1-11.

[12] Y. Sun, C. Chen, H. Xu, K. Lei, G. Xu, L. Zhao and M. Lang, *Appl. Surf. Sci.*, 2017, 419, 642–649.

[13] Q. Weiping, X. Bin, W. Lei, W. Chunxiao, S. Zengdong, Y. Danfeng, L. Zuhong and W. Yu, *J. Inclusion Phenom. Macrocyclic Chem.*, 1999, 35, 419–429.

[14] N. S. K. Gunda, M. Singh, L. Norman, K. Kaur and S. K. Mitra, *Appl. Surf. Sci.*, 2014,

305, 522–530.

[15] K. Zhang, J. Ma, B. Zhang, S. Zhao, Y. Li, Y. Xu, W. Yu and J. Wang, *Mater. Lett.*, 2007, 61, 949–952.

[16] R. P. Weis, J.-L. Montchamp, J. L. Coffer, D. G. Attiah and T. A. Desai, *Dis. Markers*, 2002, 18, 159–165.

[17] M. Tanaka, T. Sawaguchi, M. Kuwahara and O. Niwa, *Langmuir*, 2013, 29, 6361–6368.

[18] S. C. Terry, J. H. Jerman and J. B. Angell, *IEEE Trans. Electron Devices*, 1979, 26, 1880–1886.

[19] S. P. Low, N. H. Voelcker, L. T. Canham and K. A. Williams, *Biomaterials*, 2009, 30, 2873–2880.

[20] T. H. Tran, J.-W. Lee, K. Lee, Y. D. Lee and B.-K. Ju, *Sensors Actuators B: Chem.*, 2008, 129, 67–71.

[21] N. Majoul, S. Aouida and B. Bessaïs, *Appl. Surf. Sci.*, 2015, 331, 388–391.

[22] M. Heskins and J. E. Guillet, *J. Macromol. Sci. Part - Chem.*, 1968, 2, 1441-1455.

[23] A. Kondo, T. Kaneko and K. Higashitani, *Biotechnol. Bioeng.*, 1994, 44, 1–6.

[24] G. Fundueanu, M. Constantin and P. Ascenzi, *Int. J. Pharm.*, 2009, 379, 9–17.

[25] P. S. Stayton, T. Shimoboji, C. Long, A. Chilkoti, G. Ghen, J. M. Harris and A. S. Hoffman, *Nature*, 1995, 378, 472–474.

[26] E. Piskin, *Expert Rev. Med. Devices*, 2014, 2, 501–509.

[27] S. Park, M. Zhong, T. Lee, H. Paik and K. Matyjaszewski, *ACS Appl. Mater. & Interfaces*, 2012, 4, 5949–5955.

[28] N. Ishida and S. Biggs, *Langmuir*, 2007, 23, 11083–11088.

[29] L. Li, Y. Zhu, B. Li and C. Gao, *Langmuir*, 2008, 24, 13632–13639.

[30] R. Hoogenboom, H. M. L. Thijs, M. J. H. C. Jochems, B. M. van Lankvelt, M. W. M. Fijten and U. S. Schubert, *Chem. Commun.*, 2008, 5758–5760.

[31] T. X. Viegas, M. D. Bentley, J. M. Harris, Z. Fang, K. Yoon, B. Dizman, R. Weimer, A. Mero, G. Pasut and F. M. Veronese, *Bioconjugate Chem.*, 2011, 22, 976–986.

[32] Y. Chujo, E. Ihara, K. Suzuki and T. Saegusa, *Polym. Bull.*, 1993, 31, 317–322.

[33] J. Kim, P. Seidler, L. S. Wan and C. Fill, *J. Colloid Interface Sci.*, 2009, 329, 114–119.

****

Chapter 4

Controlled phase behaviour of thermally sensitive poly(N-isopropylacrylamide/ionic liquid) hydrogels with embedded Au and Ag nanoparticles

Abstract

Poly(N-isopropylacrylamide/ionic liquid) with deposited metal nanoparticles like gold and silver was prepared. The size of nanoparticles range was varied from 10 - 45 nm and these were characterized by TEM analysis. Ionic liquids were chosen by varying the polymerizable unit to be both in cationic (allyl) and anionic (acrylate) moiety. One-pot polymerization was done with NIPAM and ionic liquids (ILs) using ammonium persulphate as the initiator, to which were added already prepared Au or Ag NPs. These thermal sensitive composites formed, possessed reversible swelling/deswelling abilities in water and demonstrated a reversible visible phase transition, which was detected by Differential Scanning Calorimetric measurements. The LCST showed dependency on the size of nanoparticles and the ionic liquid independently. It was seen that the LCST of

PNIPAM based composite films can be tuned from 32 °C to a range of 23 - 67 °C by choosing the desired Au NP size (10-35 nm) and kind of ionic liquid. Controlling the size of silver nanoparticles from 31 nm to 45 nm can tune the LCST from 34 – 56 °C.

4.1 Introduction

Extremely productive and versatile classes of environmentally responsive materials [1,2] have been studied since ages which can change their physical, chemical or electronic conformations on stimuli like light, temperature, pH, ions, electric/magnetic fields or biological agents. Temperature is one such stimuli present naturally and artificially, making thermo-responsive polymers a fascinating category for examination. These tend to show phase transitions like Lower Critical Solution Temperature (LCST) [3] where the polymer shows decreased solubility at elevated temperatures. A simple, intensively effective and rigorously investigated temperature sensitive polymers include poly(N-isopropylacrylamide) (PNIPAM) [4]. It exhibits a sharp LCST at exactly 31-33 °C in aqueous media, near to physiological body temperature which makes it of tremendous use in biological applications [5]. It undergoes coil-to-globule transition in presence of water due to changes in conformation around its hydrophobic part. As the temperature of the system is increased, hydrophobic interactions of non-polar backbone and isopropyl groups becomes dominant [6] causing the polymer structure to collapse in a globule separated from water. This is visually seen as a turbid occasion. As PNIPAM's LCST do not depends on the polymer concentration or its molecular weight [3,7] tuning of this class of polymer is done widely by adding different salts or entities [8], by changing the functionalities [9] or via co-polymerization [10,11]. These tuned LCST of

composites/hybrids gives potential for utilization in drug deliveries [12], sensors [13,14], catalysis, bio-engineering [15], separation [16] etc.

One such method to tune the LCST of polymers can be the use of green solvents, ionic liquids as co-monomers [17, 18]. Its general properties include low vapour pressure, high electrical and chemical stability, high conductivity and most importantly, their designability on the basis of hydrophilic/hydrophobic parts, providing tunability [19]. Other versatile properties of these environmentally benign solvents depend on the class of ionic liquids being utilized. For example, pyrrolidinium-based ionic liquids [20] have high energy storage capacity making them suitable for heat transfer media while phosphonium-based ionic liquids [21] lack of acidic protons and less dense than water, which makes them apt for separation. Meanwhile, imidazolium-based ionic liquids [22] are the best candidates when polarity or hydrophobicity/hydrophilicity needs to be tailored for a chosen application. Ohno et al., [23] have already reported the important role of hydrophobicity making it the key factor to show LCST/UCST of amino-acid based ionic liquids in aqueous media. Thus, ionic liquids become an important class of materials studying on the phase transitions. Our group has previously reported the tuning of LCST of PNIPAM by copolymerizing with imidazolium based ionic liquids. We have observed the tuning of random co-polymers of PNIPAM-IL which showed clear dependency on hydrophobicity of cation and structure of anions.

Plasmonic nanoparticles as tuning agents

Nowadays, nanoparticle chemistry is a hot topic and is currently under intense research. Gold nanoparticles (Au NPs) display distinctive physiochemical properties [24] based on different shape [25], size [26], solubility [27] and pH [28]. They show localized surface plasmon resonance (LSPR) and a strong absorption in UV-Vis-NIR range [24]. Hence, they

become very effective in the utility of electronics [29], catalysis [30], optics [31], diagnosis [32], biomedicine [33] and sensing [34]. It was already known that citrate-protected nanoparticles are susceptible to easy aggregation [35]. To overcome this problem, very recently, modification on PNIPAM is under way with the use of metal nanoparticles like gold and silver [13, 36–38]. Different methods like grafting-to and grafting-from have been developed to create PNIPAM brushes [39]/shells [40]/nanocomposite [41] coated over Au NPs. Hoongenboom et al. [42], reported the use of PNIPAM coated Au NPs in salt and its colorimetric sensing. Yuan et al. [43], has used the PNIPAM modified Au NP for bioactivity modulation. Many other groups are studying the mechanistic and kinetics of the variety of growth method, shell responses and phase transitions over NPs [44–47]. It was also reported by Hu et al. [48], that plasmonic NPs like Au and Ag improve the thermal and light sensitivity of thermo-sensitive polymers because they act as anchors to restrict the hydrophobic chains of the polymers from rotating at an early stage, thereby inducing a greater demand of thermal energy to collapse.

Objective of the work:

Taking inspiration from the above research perspectives, it seems quite interesting to incorporate distinct sizes of Au and Ag NPs in PNIPAM-IL copolymers and study its effect. It is believable that the polymerized ionic liquid can stabilize these metal NPs and in turn, NPs could enhance the light to thermal efficiency of the thermo-sensitive polymer. This would double the opportunity of its use in different applications [49, 50]. Thus, in this study, hydrophilic citrate-coated gold nanoparticles ranging from 10 to 35 nm and silver nanoparticles ranging from 30 to 45 nm in size have been prepared. Further, in the presence of these NPs, copolymerization of N-isopropylacrylamide with polymerizable N,N'-di-substituted imidazolium-based ionic liquids was done using ammonium

persulphate to form a polymer film which showed tunable reversible LCST behaviour in water, by swelling below LCST and shrinking above LCST. How the size of NPs and structure of IL affect the LCST and how they can be further tuned, were studied as the key points of understanding.

4.2 Experimental

Materials

1-methylimidazole, acetonitrile, diethylether, bromooctane, allylchloride, trisodium citrate, bis-acrylamide (BIS) and silver nitrate (Wako Co. Ltd.); acrylic acid, N-isopropylacrylamide (NIPAM), 1-allylimidazole, lithium bis(trifluoromethanesulfonyl)imide (Li TFSI) and N,N,N',N'-tetramethylenethylenediamine (TEMED) (Tokyo Chemical Industry Co. Ltd.); bromohexane, ammonium persulfate, L(+)-ascorbic acid, and gold chloride (Sigma Aldrich); all were used as received.

Instrumentation

400 MHz Nuclear Magnetic Spectroscopy was performed on Ultrashield TM Plus Bruker, Z101355, used to characterise ionic liquids. JASCO V-630 UV-Visible spectrometer was employed for NPs absorbance measurements. Transmission electron microscopy was done on a Hitachi H-7100 model at 100 kV to characterise the NP size and composite formation. LCST determination was done on a Differential Scanning Calorimeter Shimadzu DSC-60 Plus. MALDI-TOF was carried out on a PerSeptive Biosystems (now Applied Biosystems Inc.) Voyager DE RP.

Synthesis of ionic liquids:

The ionic liquids synthesized were namely, 1-allyl-3-methylimidazolium chloride (AMImCl), 1-hexyl-3-methylimidazolium acrylate (HMImAcr), 1-allyl-3-octylimidazolium bromide (AOImBr) and 1-allyl-3-octylimidazolium bis(trifluoromethanesulfonyl)imide (AOImTFSI). The synthesis was done as already reported in literature [51] (Scheme 1). All the ionic liquids were characterized by ^{1}H – NMR spectroscopy.

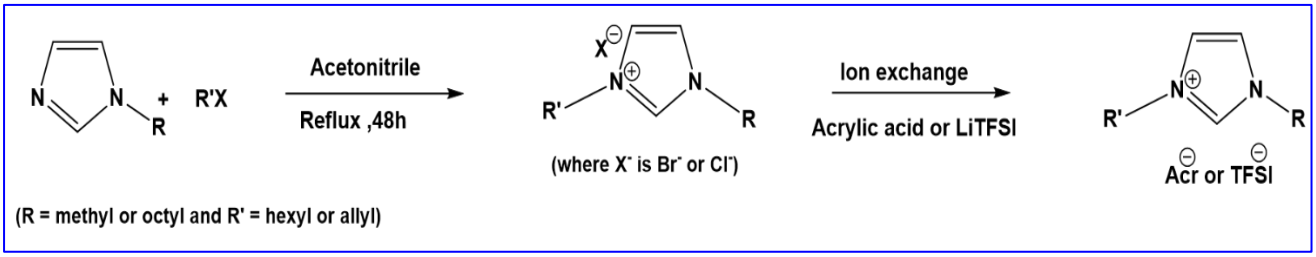

Scheme 1: Synthetic schemes for imidazolium-based polymerizable ionic liquids.

Synthesis of Gold nanoparticles:

Different methods were used to prepare different sizes of gold and silver nanoparticles [26, 52–54]. Trisodium citrate was used as the main reducing and capping agent. But to prepare smaller particles, a second reducing agent i.e., ascorbic acid was used. The concentration was measured using the absorbance values from UV-Visible spectroscopy and size distribution was analysed by TEM. The spherical diameters were obtained via size distribution curves (Fig 1.) and are mentioned in Table 1.

Preparation of samples 2-5: Taken 0.2 mL of 0.066 mM gold chloride (III) solution in 50 mL water in a 100 mL round bottom flask. It was then heated to boiling for 15 minutes with a constant stirring at 600 rpm. Respective volume (Table 1) of 0.040 mM

trisodium citrate solution was added and the reaction was stirred at same rpm for 1 hour at 80 ^{o}C. The solution was cooled to room temperature and further subjected to characterizations.

Preparation of samples 1 and 6: 2.2 mM trisodium citrate solution was prepared in 150 mL water. (0.1 mL 2.5 mM ascorbic acid was added to Sample 1 to reduce the size of NPs formed). The solution was heated to 70 ^{o}C (sample 1) and 150 ^{o}C (sample 6) for 15 minutes under vigorous stirring. Then, 1 mL 25 mM gold chloride solution was added and the resulting mixture was stirred at 90 ^{o}C for an hour. The solution was cooled to room temperature and further subjected to characterizations.

Synthesis of Silver nanoparticles:

Preparation of samples 7-9 (Table 2): 5 mM 100mL trisodium citrate was prepared and boiled for 15 minutes under vigorous stirring. Then, ascorbic acid (sample 7 – 0.01mL 0.05 mM, sample 8: 0.1 mL 0.01 mM and sample 9: no acid added) was added to reduce the size of nanoparticles. Then, 1 mL 25 mM silver nitrate was added in all solution which were then stirred at 100 ^{o}C for an hour. The solution was cooled to room temperature and further subjected to characterizations.

Synthesis of Gold/Silver NPs embedded copolymers of NIPAM and ILs [Au@PNIPAM-co-IL and Ag@PNIPAM-co-IL] (Scheme 2) as thermosensitive porous hydrogels:

A modified synthetic scheme has been employed [48, 55]. 1.5 mmol of NIPAM, 0.15 mmol of ionic liquid (AMImCl/AOImBr/AOImTFSI/HMImAcr) were mixed in 1 mL water. 10 mol% bisacrylamide (25 mg, 1.65 mmol) and 5 mol% (10 mg, 0.086 mmol) TEMED was added to the solution and was sonicated for 5 minutes to completely solubilize. 7.8 x 10^{-12} mmol Au NP solution [6, 56] (of required size) in water was added. The resulting mixture was put to a plastic vial. 80 µL of 5 wt% APS as polymerization catalyst was added. The mixture was heated in a vacuum oven at 60 ^{o}C till the solvent evaporates. After 3 days, a coloured polymer film (blue to red for Au NPs, blue to red to white for Ag NPs) was obtained, which was rigid in nature.

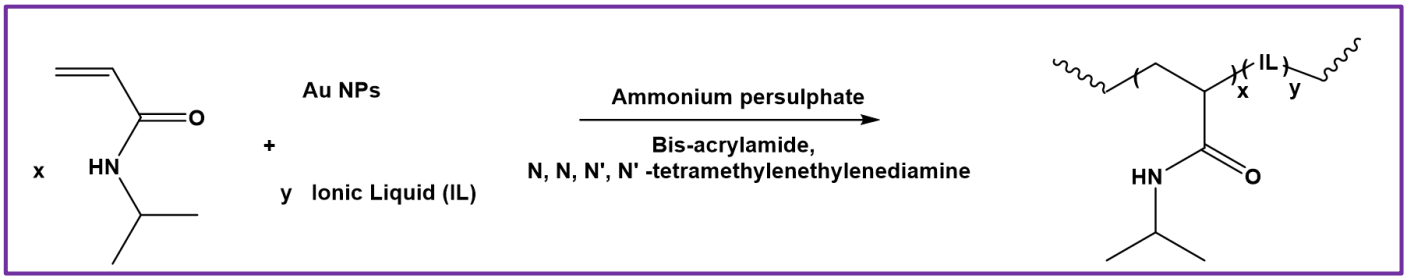

Scheme 2: Synthetic schemes for NP@PNIPAM-co-IL

4.3 Characterization

For the synthesis of gold nanoparticles, different reaction conditions were employed to create particles in the range 10-35 nm (Table 1). TEM images (Fig. 1) showed that monodispersed nanoparticles were formed with the polydispersity lying between 1.5-7.3%. Many factors including temperature were varied in the reaction procedure to obtain the desired diameter of the particles.

Similar procedure (Table 2) was used to form silver nanoparticles in the range 30-45 nm (Fig 2.). The polydispersity of silver nanoparticles lied between 5.9-9.5%. It is already observed that it is difficult to control the uniformity of silver nanoparticles in the range 20-65 nm. [61].

Table 1. Reaction concentrations, size and wavelength measurements for gold nanoparticles

Sample Name	$AuCl_3$ conc.	Sodium citrate conc.	Additive	Size of NP	Absorbance/ nm
Au-2	0.2 mL 0.066 mM	0.2 mL 0.040 mM	50 mL water	17.45 ± 0.50	520.5
Au-3	0.2 mL 0.066 mM	0.4 mL 0.040 mM	50 mL water	20.00 ± 0.30	523.0
Au-4	0.2 mL 0.066 mM	0.8 mL 0.040 mM	50 mL water	23.66 ± 1.55	526.5
Au-5	0.2 mL 0.066 mM	1.6 mL 0.040 mM	50 mL water	24.33 ± 1.15	529.5
Au-1	1.0 mL 25 mM	150mL 2.2 mM	0.1 mL 2.5 mM Ascorbic acid	10.89 ± 0.80	536.0
Au-6	1.0 mL 25 mM	150 mL 2.2 mM	water	32.93 ± 2.01	525.5

Table 2. Reaction concentrations, size and wavelength measurements for silver nanoparticles

Sample Name	$AgNO_3$ conc.	Sodium citrate conc.	Additive	Size of NP	Absorbance / nm
Ag-7	1.0 mL 25 mM	100 mL 5.0 mM	0.1 mL 0.05 mM Ascorbic acid	31.36 ± 3.90	409.0
Ag-8	1.0 mL 25 mM	100 mL 5.0 mM	0.1 mL 0.01 mM Ascorbic acid	41.00 ± 2.44	408.0
Ag-9	1.0 mL 25 mM	100 mL 5.0 mM	water	45.76 ± 4.33	420.0

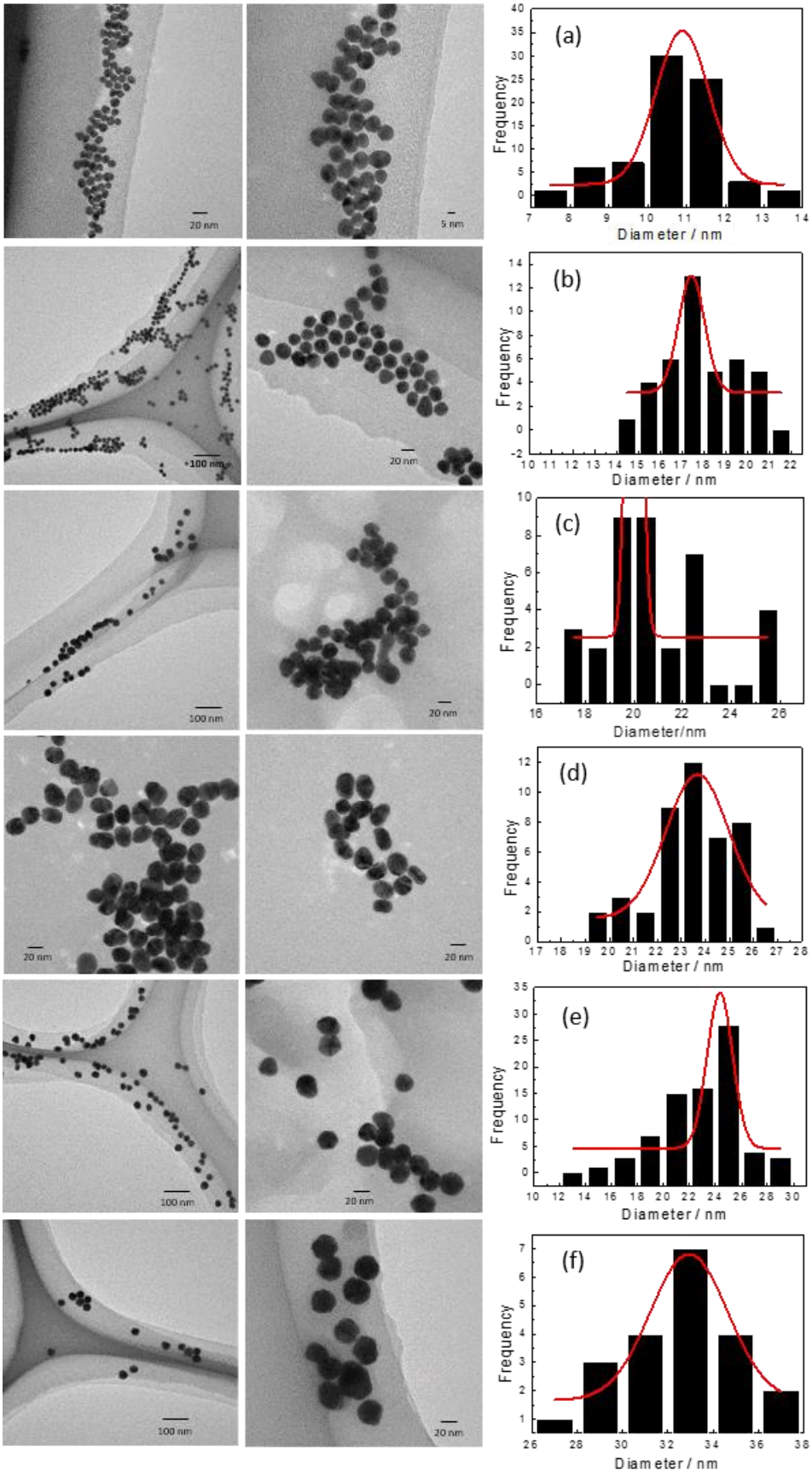

Fig 1. TEM analysis and size distributions for gold nanoparticles (a-f: sample 1-6)

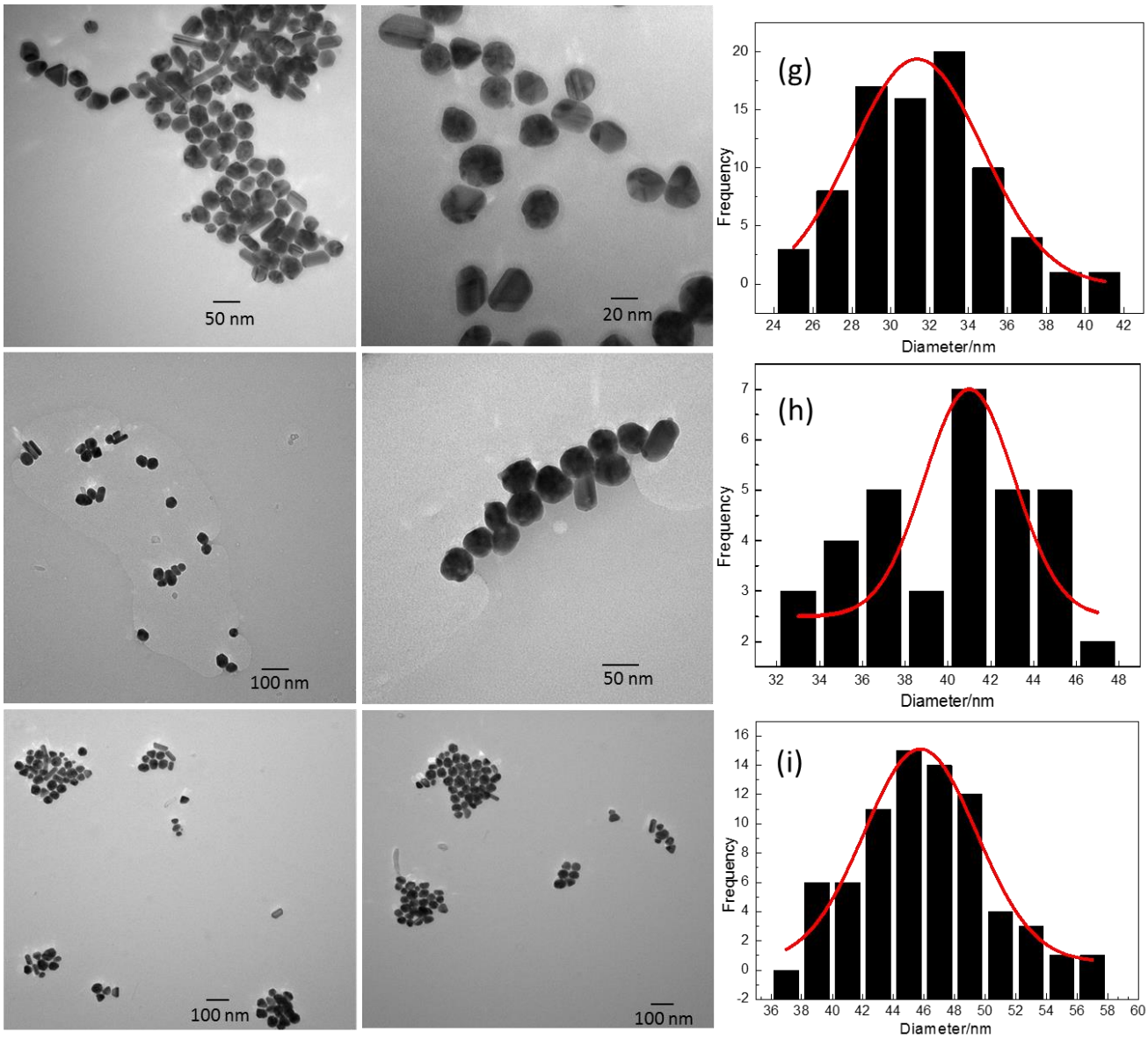

Fig 2. TEM analysis and size distributions for silver nanoparticles (g-i: sample 7-9)

The in-situ copolymerization of Au@PNIPAM-co-IL and Ag@PNIPAM-co-IL was done using ammonium persulfate as the initiator for the free-radical polymerization. A small amount of bisacrylamide was added while the reaction proceeded to ensure the formation of a 3D polymer network. The synthesis were confirmed by ^{1}H-NMR in DMSO-d^{6} (Fig 3, 4). MALDI-TOF measurements showed the molecular weight of the matrix to be

in the order of ~1050g/mol for Au@PNIPAM-co-IL and ~1300 g/mol for Ag@PNIPAM-co-IL. Hence, a low molecular weight oligomer framework was synthesized for PNIPAM-co-IL. TEM analysis was also carried out which showed the Au NPs being distinctively embedded and dispersed into the copolymer matrix of NIPAM and IL (Fig 5b). The size of the Au and Ag NPs remained almost same after the polymerization, which suggested the absence of aggregation of particles once incorporated into the matrix. This emphasised the fact that IL containing copolymer chains acted as a stabilizing ligand for the particles [57].

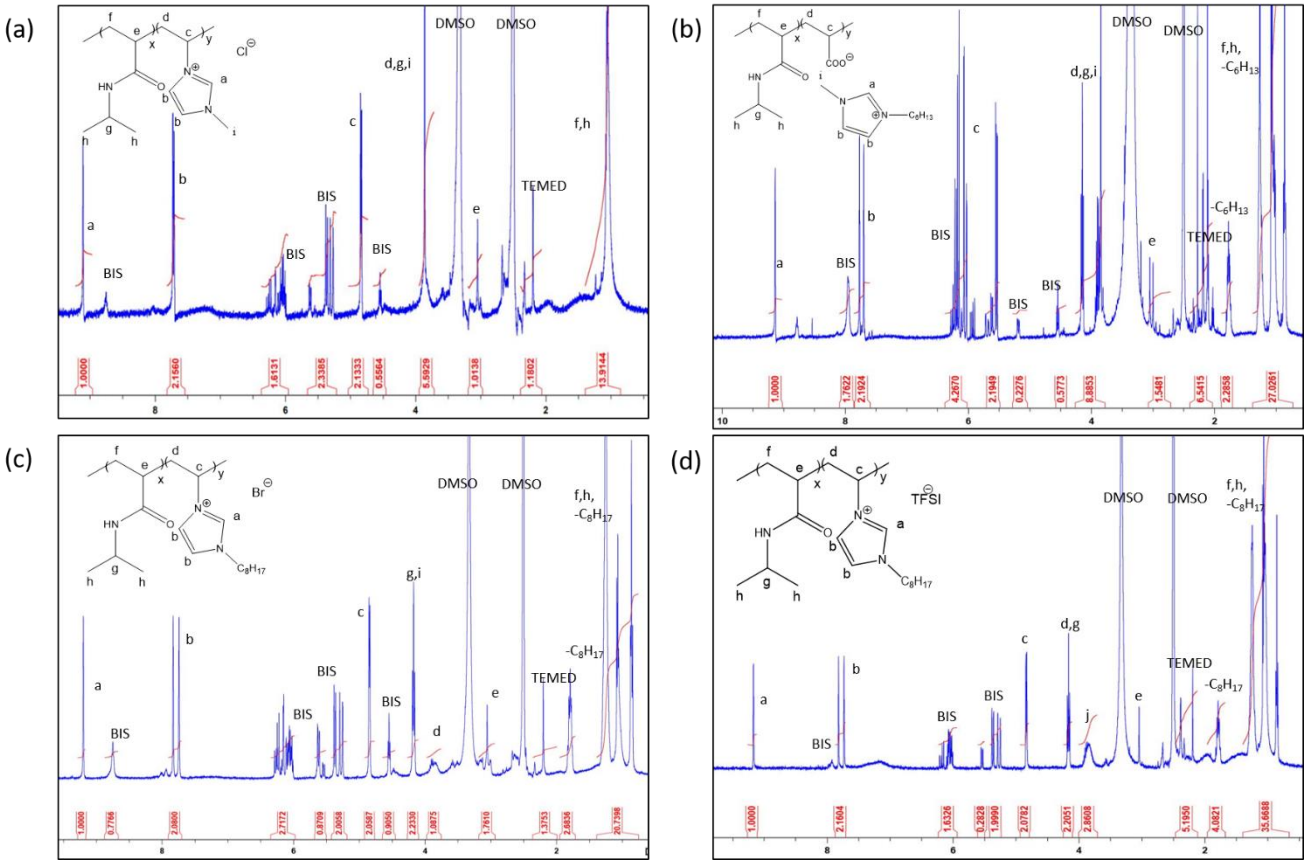

Fig 3. ^{1}H-NMR spectrum of (a) Au@PNIPAM-co-AMImCl, (b) Au@PNIPAM-co-HMImAcr, (c) Au@PNIPAM-co-AOImBr and (d) Au@PNIPAM-co-AOImTFSI. (BIS- bis-acrylamide, TEMED- N,N,N',N'-tetramethylenethylenediamine)

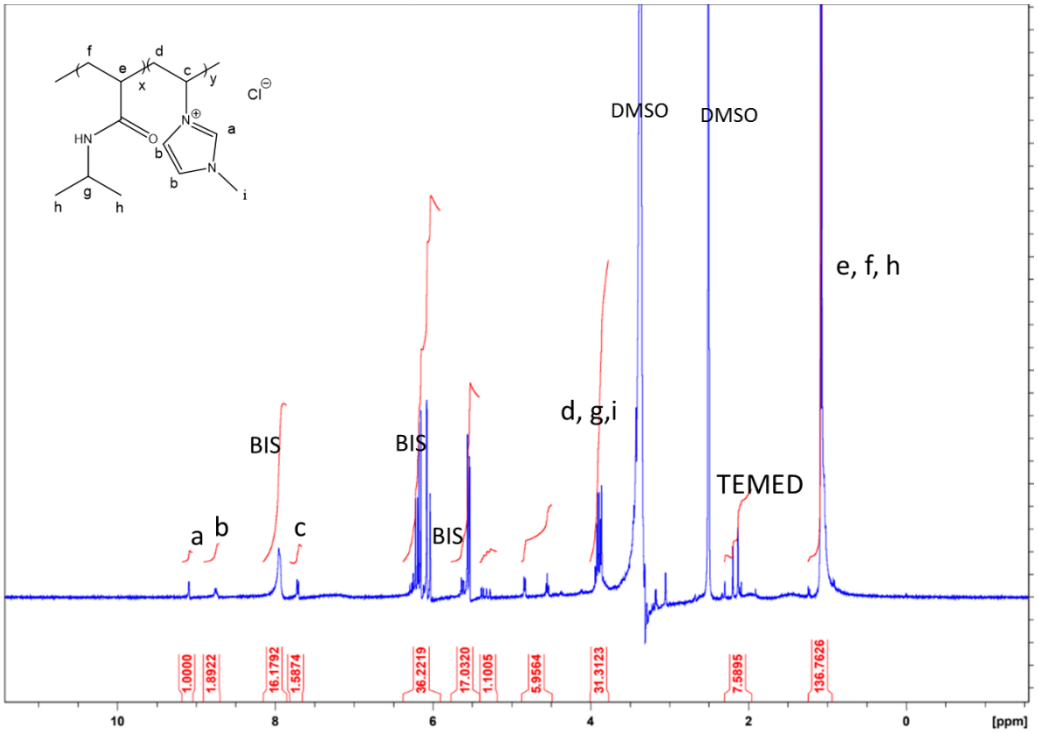

Fig 4. ^{1}H-NMR spectrum of (a) Ag@PNIPAM-co-AMImCl

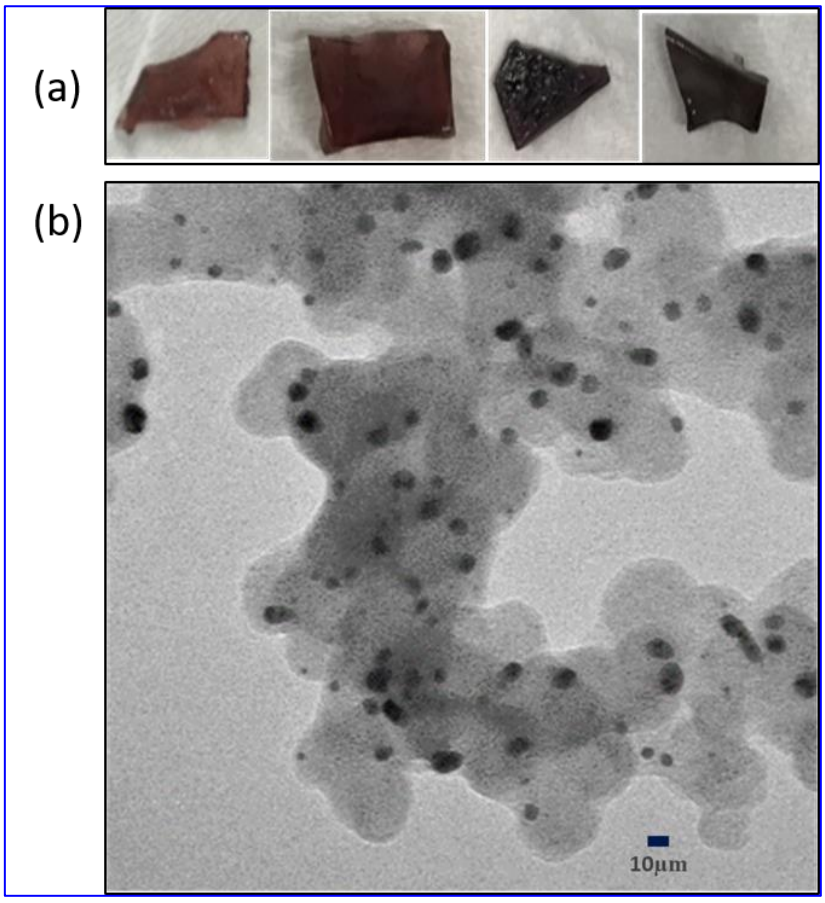

Fig 5. (a) Images of the Au@PNIPAM-co-AMImCl when the Au NP size is 17.45 nm, 20.00 nm, 23.44 nm, 24.33 nm. (b) TEM analysis of Au-17.45@PNIPAM-co-AMImCl.

4.4 Results and Discussion

At first, visual analysis was performed on the gold nanoparticles embedded copolymer system in water (Fig 6). 3 mg of Au-4@PNIPAM-co-AMImCl (where 4 is the sample number where the nanoparticle size was 24.33 nm) taken in a 2 mL glass vial containing 0.6 mL water and sonicated till the polymer matrix was dissolved and the solution was transparent. It was then, heated to a high temperature of 75 ^{o}C to observe a change in state and colour of the solution. It was seen that the solution separates a shrunken hydrophobic entity which was actually seen as a globule whose colour was changed to white. After cooling the system to room temperature, the globule was dissolved, re-swelled and the original solution with the copolymer was obtained.

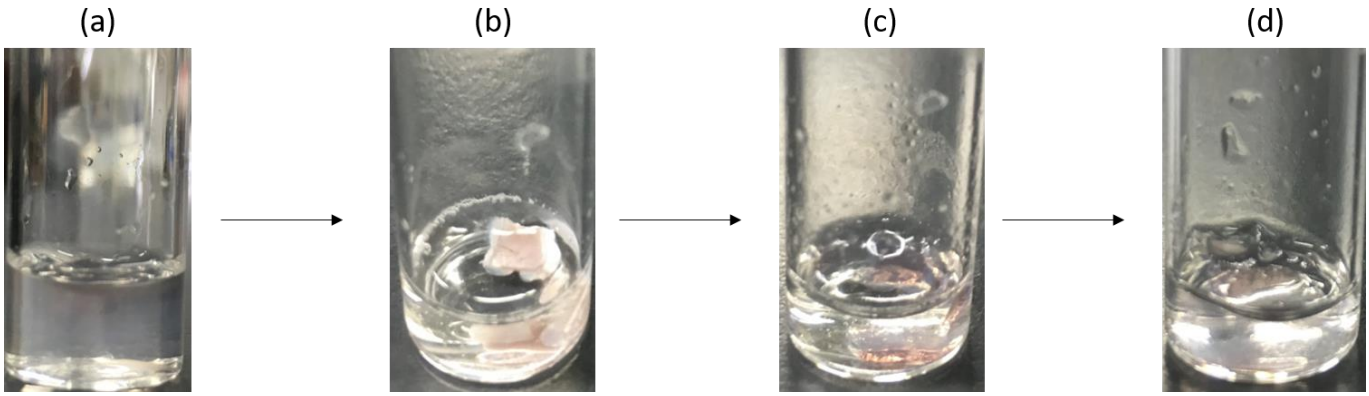

Fig 6. Visual images for LCST determination of Au@PNIPAM-co-AMImCl. (a) 50 w/v % aqueous solution after sonication at room temperature, (b) heated at 75 ^{o}C for 10 minutes, (c) decreased the temperature to 40 ^{o}C, (d) solution cooled completely to room temperature.

This experiment is important as it can establish a hypothesis about the mechanism of the LCST in the polymer matrix. At the room temperature, the copolymer is completely mixed with water (or gelled), giving a transparent colour to the solution (Fig. 5a). When the temperature is increased to 75 ^{o}C, it can be estimated that the hydrophobicity of PNIPAM isopropyl chains and ionic liquid's allyl moiety becomes dominant, thereby allowing the formation of a separate shrunken aggregate [58] enclosed in which are the nanoparticles (due to its colour) (Fig. 5b). This also suggests that PNIPAM chains are at the surface of the globule as the colour of the solution became white. After the enthalpy of the system is decreased, the hydrogen bonding increases between the molecules and the globule is dissolved again (Fig. 5d), giving the transparency to the viscous solution again confirming the occurrence of a reversible transition. Similar results were observed for other gold and silver nanoparticles embedded copolymer hydrogels.

If no sonication is done, the hydrogel is swelled when kept at room temperature. However, when the solution is heated above its LCST temperature, the hydrogel shrinks which is reversible in nature all for Au and Ag induced hydrogels.

For the LCST temperature determination, 1 mg of the hydrogel was dissolved in 2 mg water via sonication for 2 hours and solution made above after sonication was taken and subjected to differential scanning calorimetry at a rate 1 ^{o}C/min for 15-90 ^{o}C. Fig. 7. shows the normalized DSC profiles of Au@PNIPAM-co-ILs and Fig. 8. shows the normalized DSC profiles for Ag@PNIPAM-co-ILs carried in water. Henceforth, the effect of nature of polymerizable ionic liquids and size of Au and Ag NPs was studied on the LCST of this polymer matrix hydrogel.

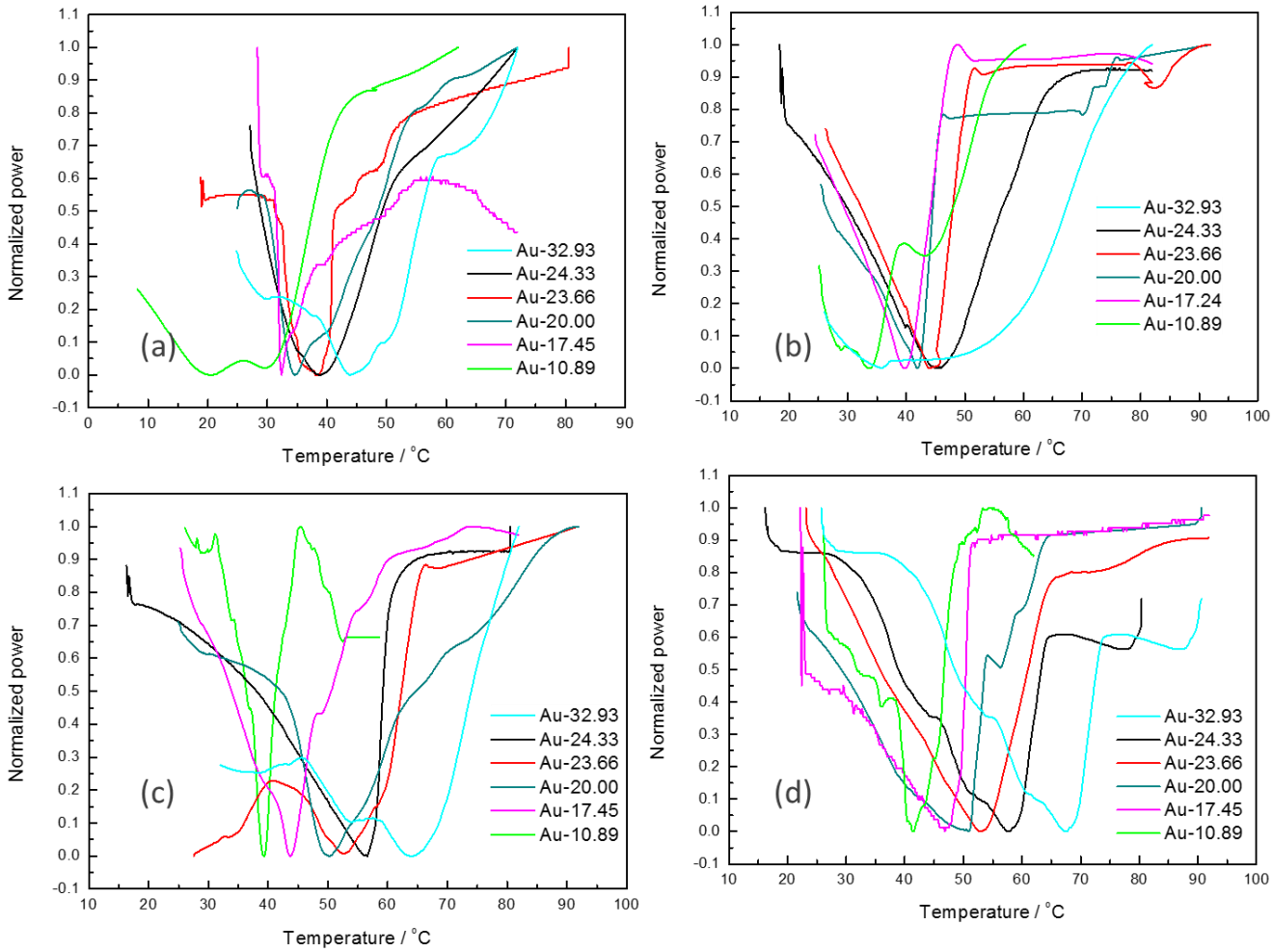

Fig 7. DSC profiles for LCST determination of (a) Au@PNIPAM-co-AOImTFSI, (b) Au@PNIPAM-co-AOImBr, (c) Au@PNIPAM-co-HMImAcr and (d) Au@PNIPAM-co-AMImCl. (in graph - Au is plotted by varying the size of nanoparticles)

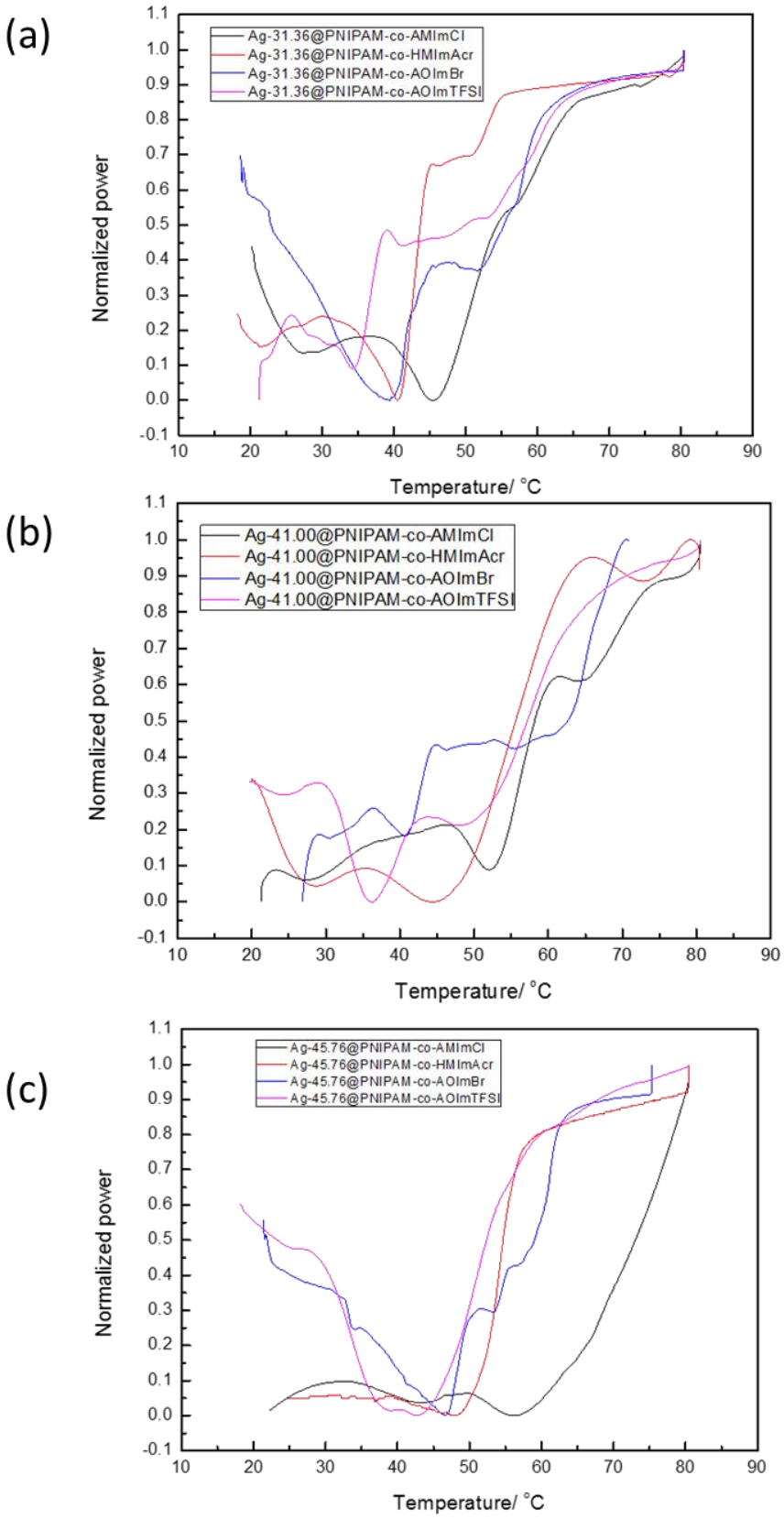

Fig 8. DSC profiles for LCST determination of Ag@PNIPAM-co-IL where Ag size is (a) 31.36 nm, (b) 41.00 nm and (c) 45.76 nm

4.4.1 Effect of polymerizable ionic liquid on LCST of Au/Ag@PNIPAM-co-IL composites

Gold nanoparticles:

Table 3. LCST of Au-10.89@PNIPAM-co-IL

Ionic liquid	LCST (°C)
AMImCl	41
HMImAcr	39
AOImBr	33
AOImTFSI	23

Under constant size of Au NP (sample 1: 10.89 + 0.80 nm), structures of ionic liquid were changed and the results of LCST measurements were as procured in Table 3. It is seen clearly that the phase transition temperature depends on the hydrophobicity/hydrophilicity of the ionic liquid as excepted. For example, Au-1@PNIPAM-co-AMImCl (where 1 stands for nanoparticle size 10.89 + 0.80 nm) has the LCST of 41 °C whereas Au-1@PNIPAM-co-AOImTFSI has it at 23 °C. AMImCl is the most hydrophilic moiety amongst the IL structures, where chloride ion and short alkyl chains (allyl and methyl) have strong ion-dipole forces to overcome the hydrogen bonds between water molecules. Hence, it takes enough energy to surpass this condition and for hydrophobicity of allyl group to become dominant, thereby delaying the phase transition temperature from 32 °C of pure PNIPAM to 41 °C. As we increase the hydrophobicity in the ionic liquid molecule by increasing the chain length from hexyl-methyl to allyl-octyl, the LCST temperature decreased.

Thus, Au-1@PNIPAM-co-HMImAcr has LCST of 39 °C while Au-1@PNIPAM-co-AOImBr has at 33 °C. As already known that TFSI is a bulky anion water-repellent in nature [59], thus it became interesting to note that the LCST when using this ionic liquid becomes lower even than the pure PNIPAM. As more of the hydrophobic moieties are introduced in water, the surface tension is maximized as they agglomerate (hydrophobic effect) [58], thereby maximizing the hydrogen bonding between the molecules under the operation of hydrophobic interaction. Thus, it takes less energy to disrupt the composite/water interface and hence, the LCST temperature is lowered. Hence, both cation and anion play a key role in the phenomenon of phase behaviour.

Silver nanoparticles:

Table 4: LCST of Ag-31.36@PNIPAM-co-IL

Ionic liquid	LCST (°C)
AMImCl	45
HMImAcr	40
AOImBr	39
AOImTFSI	34

Similar to gold nanoparticles, the ionic liquids were varied while embedding silver nanoparticles during the synthesis. Constant size of silver nanoparticles was kept as 31.36 nm (Table 4). The trend remained similar as the hydrophilic ionic

liquid AMImCl showed LCST at 45 ^{o}C and the presence of bulky hydrophobic TFSI group in AOImTFSI decreased the LCST to 34 ^{o}C. Thus, decreasing the hydrophilicity which means increasing the hydrophobicity requires a less demand for the thermal need for hydrophobic groups to dominate, thereby decreasing the critical phase temperature itself. The LCST of Au-10.89 nm induced hydrogels were comparatively lesser than that of Ag-31.36 nm simply because of the bigger size of the silver nanoparticles.

Thus, keeping the size of nanoparticles constant, hydrogen bonding between the polymer chains/ionic liquid's cation and anion with water plays significant role towards LCST. This suggests that changing the hydrophobic/hydrophilic nature of the ionic liquid can help in the fine-tuning of the LCST of these copolymers. Here, just by changing the structure of the ionic liquid, the LCST can be customised from 32 ^{o}C to 23 - 41 ^{o}C for gold nanoparticles (size – 10.89 nm) and to 34 – 45 ^{o}C for silver nanoparticles (size- 31.36 nm). This trend is systematic and was similarly observed in all the ionic liquids irrespective of any nanoparticle nature and size. Not to forget, different sized nanoparticles will yield different results, which can be used to further tune the phase behaviour of systems and will be discussed in the subsequent sections.

4.4.2 Effect of gold nanoparticle size on LCST of Au/Ag@PNIPAM-co-IL composites

Gold nanoparticles:

Table 5. LCST temperatures obtained by DSC for (a) Au@PNIPAM-co-AOImTFSI, (b) Au@PNIPAM-co-AOImBr, (c) Au@PNIPAM-co-HMImAcr and (d)Au@PNIPAM-co-AMImCl.

(a)

NP Name	Size (nm)	LCST (°C)
Au-1	10.89 ± 0.80	23
Au-2	17.45 ± 0.50	32
Au-3	20.00 ± 0.30	33
Au-4	23.66 ± 1.55	36
Au-5	24.33 ± 1.15	38
Au-6	32.93 ± 2.01	43

(b)

NP Name	Size (nm)	LCST (°C)
Au-1	10.89 ± 0.80	33
Au-2	17.45 ± 0.50	40
Au-3	20.00 ± 0.30	42
Au-4	23.66 ± 1.55	44
Au-5	24.33 ± 1.15	46
Au-6	32.93 ± 2.01	51

(c)

NP Name	Size (nm)	LCST (°C)
Au-1	10.89 ± 0.80	39
Au-2	17.45 ± 0.50	45
Au-3	20.00 ± 0.30	50
Au-4	23.66 ± 1.55	54
Au-5	24.33 ± 1.15	56
Au-6	32.93 ± 2.01	64

(d)

NP Name	Size (nm)	LCST (°C)
Au-1	10.89 ± 0.80	41
Au-2	17.45 ± 0.50	47
Au-3	20.00 ± 0.30	51
Au-4	23.66 ± 1.55	53
Au-5	24.33 ± 1.15	58
Au-6	32.93 ± 2.01	67

In this research work, the diameter of the spherical gold nanoparticles were varied from 10.89 nm to 32.93 nm in 6 different sizes. (Table 5). The normalised DSC profiles showed distinguished endotherms due to the LCST temperature (Fig 6). LCST increased as the size of the nanoparticles increased irrespective of the ionic liquid structure. This can be clearly perceived upon discussing each case particularly. Starting with the results for Au@PNIPAM-co-AMImCl, with the enlarged sized induction of NPs from 10.89 + 0.80 nm to 17.45 + 0.50 nm in the matrix, LCST increased from 41 °C to 47 °C. With increasing NP size subsequently

to 32.93 + 2.01 nm, the attained maximum LCST was at 67 °C. This reason can be well deciphered if we understand the mechanism at the sub-atomic level. Because the nanoparticles are well distributed in the matrix, Au NPs can act like anchors and control the movement of the polymer chains. They reduce the rotation of polymer chains and ionic liquid moieties to restrict the formation of the hydrophobic globule [58]. This delays the conformational change of polymers and thus, a greater amount of energy is required to overcome this restriction, which foster as an increase in the LCST temperature. As we keep the concentration of the nanoparticles constant, it can also be presumed that as the size of the nanoparticle is increased, the onset energy for bond rotation increases.

When the ionic liquid is changed to hydrophilic one, i.e., HMImAcr, for the copolymers Au@PNIPAM-co-HMImAcr, the lowest LCST of 39 °C was achieved when the spherical diameter was smallest and it further increased to 64 °C as the size of nanoparticles increased. The trend is same as observed for Au@PNIPAM-co-AMImCl. But the LCST of Au@PNIPAM-co-HMImAcr was lower than Au@PNIPAM-co-AMImCl due to more hydrophobic nature of HMImAcr. Later, keeping the bromide ion as anion, the chain length of ionic liquid was increased from hexyl-methyl to allyl-octyl, which was apt enough to show the LCST similar to that of PNIPAM at 10.89 + 0.80 nm. And then, same dependency was observed on the nanoparticle size.

The results became more fascinating when we further decreased the hydrophilicity in the ionic liquid structure and changed it to AOIMTFSI. For Au@PNIPAM-co-AOImTFSI, the general trend remained same, but when the Au NP size was 10.89 + 0.80 nm, its LCST was even lowered compared to that of PNIPAM.

The reason attributing to this circumstance can be observed as AOImTSI has long alkyl chain (octyl) and bulky bis(trifluoromethanesulfonyl)imide anion, both of which are much hydrophobic in nature. Thus, hydrophobicity of both the cation and anion in the ionic liquid becomes so dominant that the LCST was lowered from 32 ^{o}C to 23 ^{o}C.

To picture the image of how captivating the dependency of size of nanoparticle and ionic liquid structure is on the LCST of these Au@PNIPAM-co-IL, a 3-dimensional plot was created as represented as in Fig. 9. The LCST is contingent upon the Au NP size and ionic liquids structure. Careful investigation of the 3D plot portrayed the increase in phase transition temperature of the film can be as a function of the size of nanoparticles. Thus, this conveys the fact that LCST is independently yet synergistically dependent on both the factors. Both can be individually or equally worked upon to tune the LCST of the coloured copolymer film. Hence, it is possible to widen the temperature range of PNIPAM from 32 ^{o}C to 23 ^{o}C ~ 67 ^{o}C. As four of the ionic liquids show similar trend, it becomes viable to assume the trend might be followed by another types of ionic liquids. This can aid in the customization of the phase behaviour of the materials tailored to the user's needs.

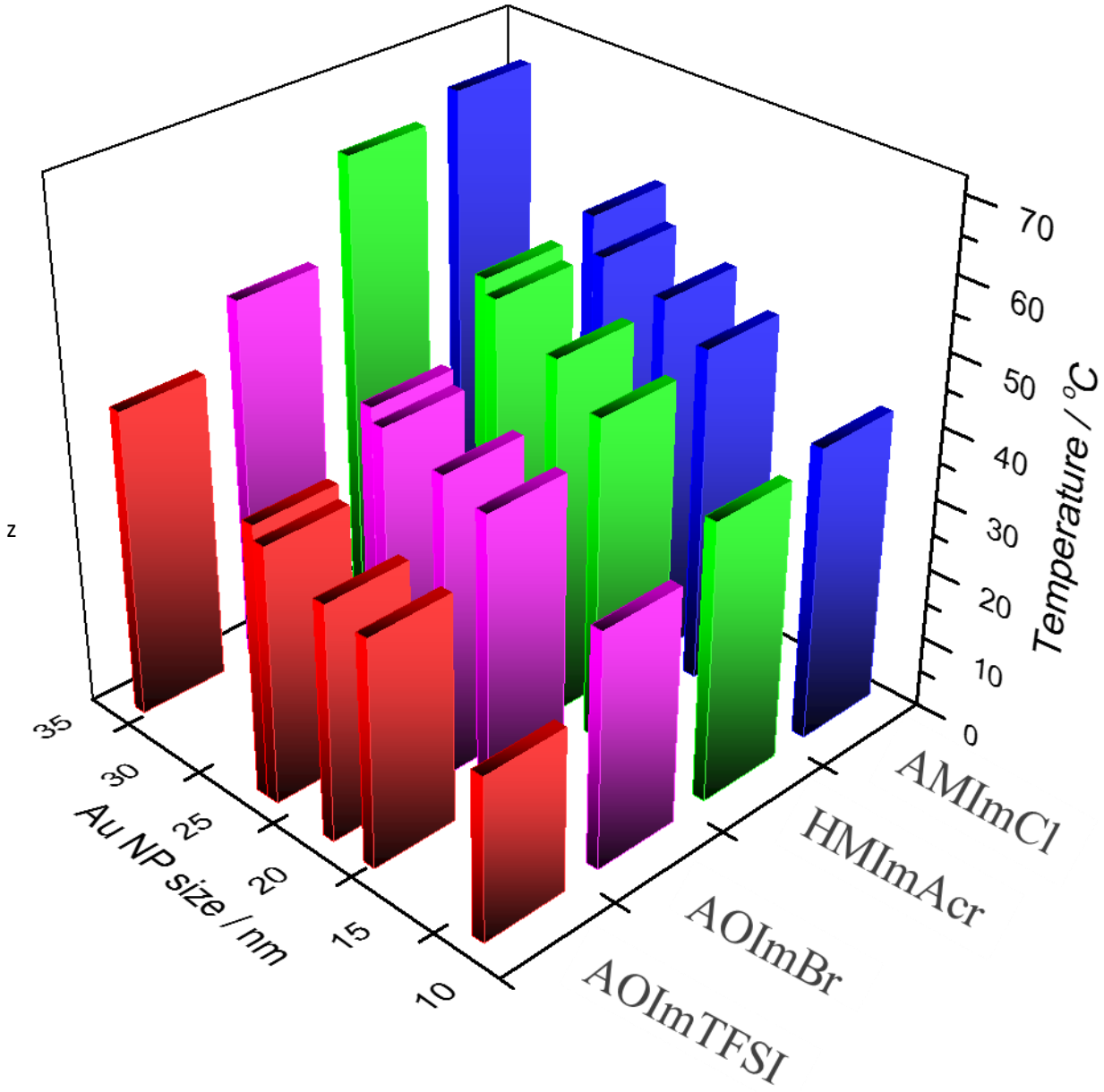

Fig 9. 3-D plot depicting the simultaneous dependence of type of IL in copolymers and size of Au on LCST of Au NP induced copolymers.

Silver nanoparticles:

For silver nanoparticles, LCST of hydrogels incorporating 3 different sized nanoparticles ranging diameter from 31 nm to 45 nm were studied (Table 6), covering and the expanding the total size distribution of plasmonic nanoparticles

from 10 nm to 45 nm combined. The normalized DSC profiles are showed in Fig. 7 which showed distinguished endotherms corresponding to the phase transitions, similar to hydrogels synthesized using gold nanoparticles. Similar results were found out which showed that LCST increased as the size of nanoparticles increased, irrespective of the ionic liquid nature.

Table 6. LCST temperatures obtained by DSC for (a) Ag@PNIPAM-co-AOImTFSI, (b) Ag@PNIPAM-co-AOImBr, (c) Ag@PNIPAM-co-HMImAcr and (d)Ag@PNIPAM-co-AMImCl.

(a)

NP Name	Size (nm)	LCST (°C)
Ag-7	31.36 ± 3.90	34
Ag-8	41.00 ± 2.44	36
Ag-9	45.76 ± 4.33	42

(b)

NP Name	Size (nm)	LCST (°C)
Ag-7	31.36 ± 3.90	39
Ag-8	41.00 ± 2.44	41
Ag-9	45.76 ± 4.33	46

(c)

NP Name	Size (nm)	LCST (°C)
Ag-7	31.36 ± 3.90	40
Ag-8	41.00 ± 2.44	45
Ag-9	45.76 ± 4.33	48

(d)

NP Name	Size (nm)	LCST (°C)
Ag-7	31.36 ± 3.90	45
Ag-8	41.00 ± 2.44	51
Ag-9	45.76 ± 4.33	56

For the ionic liquid AMImCl (Table 6d), as the size of nanoparticles increased from 31 nm to 41 nm, the LCST increased from 45 °C to 51 °C which increased to 56 °C when the silver NP are 46 nm large. The reason behind the increase can be similarly visualized as the larger nanoparticles acting as the more effective anchors to restrict the motion of the hydrophobic groups and chains in the polymer matrix, thus increasing the demand of heat energy, hence greater the LCST temperature. This overall increase in the LCST with increase in size of silver nanoparticles showed the same trend for other ionic liquids studies here (i.e., HMImAcr, AOImBr and AOImTFSI). Also, similar trend in the overall

decrease in the LCST was observed when the ionic liquids were changed from hydrophilic one (AMImCl, highest LCST = 56 ^{o}C) to hydrophobic one (AOImTFSI, highest LCST = 34 ^{o}C) when compared to the results of gold nanoparticles embedded hydrogels.

The dependence of both size of nanoparticles and ionic liquid structure was presented in a 3-D plot as shown in Fig. 10 for silver nanoparticles. Again, both the factors size of NPs and ionic liquid nature, plays important roles in the tuning the displayed LCST of these polymer hydrogels. For the sized range of 30 - 45 nm, the LCST can be tuned from 34 ^{o}C to 56 ^{o}C.

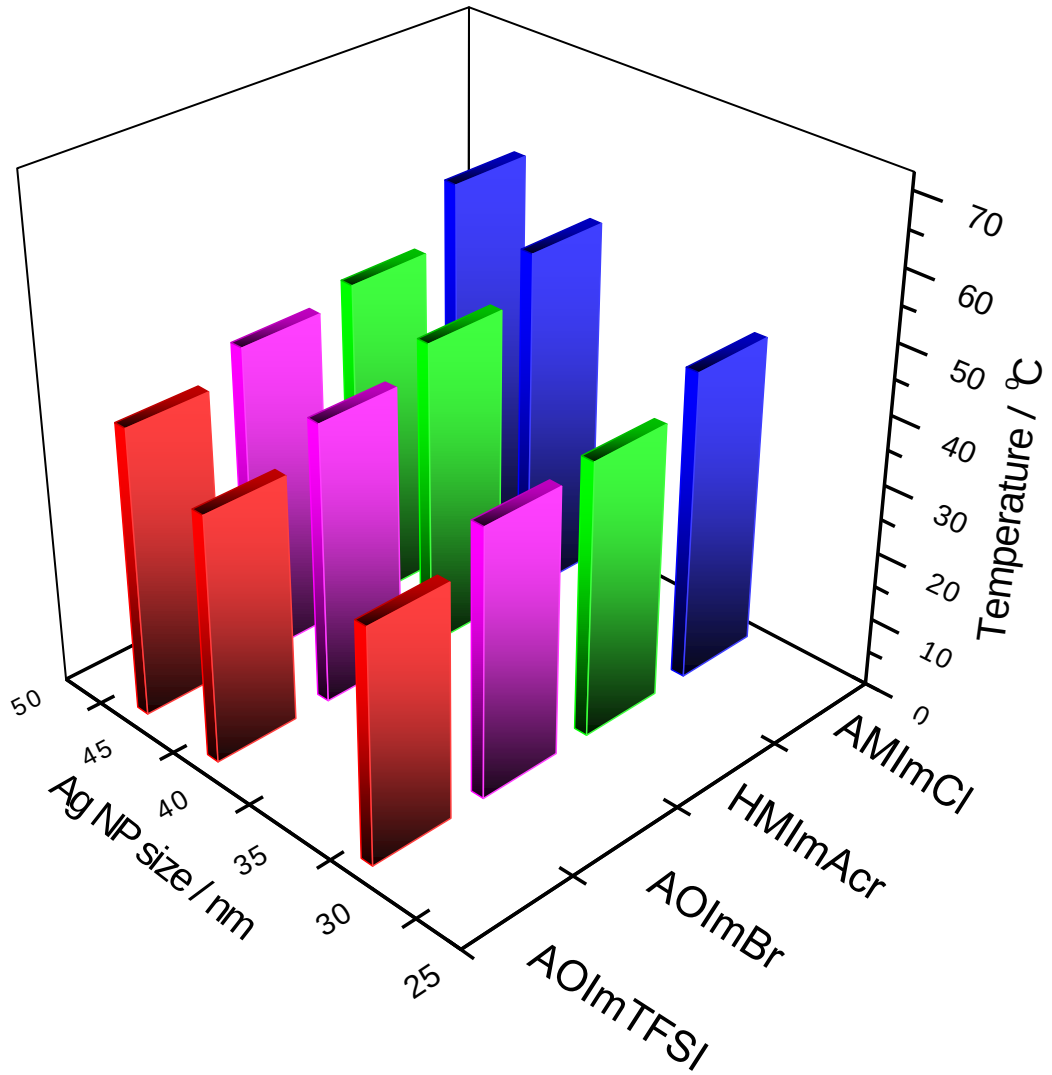

Fig 10. 3-D plot depicting the simultaneous dependence of type of IL in copolymers and size of Ag on LCST of Au NP induced copolymers.

Comparison between Au and Ag Np embedded thermoresponsive hydrogels:

Gold and silver nanoparticles were chosen as they are known to be less reactive and more stable in air [62], than other plasmonic nanoparticles like copper. Thus, it can be seen that both the nanoparticles are able to effectively tune the phase transition temperatures of the copolymer hydrogels. However, it is observed that gold NPs are a better tuning agent than silver NPs for this case of thermoresponsive PNIPAM-co-IL matrix. The reasons can be assumed as followed:

- It is already believed that silver NPs are more prone to oxidation in air, as compared to gold NPs, which are stable in air for a longer time.
- Silver NPs often do no portray a nice size distributions. This is also confirmed in our case where the poly dispersity was higher in the case of Ag NPs (1.5-7.3%), rather than Au NPs (5.9-9.5%). This might lead to ineffective restriction of rotation of hydrophobic chains during the phase transitions.

PNIPAM-co-IL

Table 7. LCST for PNIPAM-co-IL

Name	LCST (°C)
PNIPAM-co-AMImCl	56
PNIPAM-co-HMImAcr	53
PNIPAM-co-AOImBr	44
PNIPAM-co-AOImTFSI	34

To investigate the mechanism of NPs on the film further, control experiments were also carried out wherein, no nanoparticles were added while synthesizing the

films. So, the film obtained were PNIPAM-co-IL and their LCST were recorded in Table 7. As already observed by our group in previous reports [18], ionic liquid can also alter the LCST of PNIPAM (same ratio of PNIPAM and ionic liquid as studied in this work) up to a certain limit, which is observed in this case as well. This study reveals that gold and silver nanoparticles do play an important role in modifying the LCST of copolymer. It was very keen to discover that all PNIPAM-co-IL films show LCST as if they were induced with the gold nanoparticle of size 20.00-24.33 nm. This becomes interesting as this might be the threshold of rotation causes by the hydrophobic bonds. Irrespective of the ionic liquid used, the LCST lies as if size of diameter is in this range. The reason presumed can be similar as already discussed. Smaller sized nanoparticles might not be powerful enough to hinder the bond rotations. As the size decreases, hydrophobicity/hydrophilicity of the ionic liquid structure might play a dominant role. For silver nanoparticles, the LCST of PNIPAM-co-IL lies in the same range as if the silver nanoparticles were varied from 30 nm to 45 nm. This suggests that gold nanoparticles are comparatively less effective to restrict the motion of hydrophobic chains as compared to gold nanoparticles. This also suggests that the LCST of the hydrogels are easy to tune with gold nanoparticles rather than silver nanoparticles.

Researchers have already prepared PNIPAM-Au NPs based hydrogels via grafting to and grafting from approaches [60]. They showed that factors like molecular weight, size of nanoparticles and temperature play an important role for the swelling/shrinking/aggregation and cloud point (LCST) of the systems. Gibson et al. [13], have prepared PNIPAM coated nanoparticles with molecular weight being 2800 g/mol, 5700 g/mol and 11300 g/mol while varying the nanoparticle size

from 15 nm to 40 nm. They showed that there is no LCST when the molecular weight is 2800 g/mol while with 5700 g/mol, it was 74 ^{o}C. This showed that molecular weight is an important factor to determine the LCST of this system. Our results showed that Au and Ag@PNIPAM-co-IL show LCST even when the molecular weight is low enough due to strong plasma resonance. On the same path to combine plasmonic properties of silver nanoparticles and optical properties of thermoresponsive polymers, Frey et al., [63] have used silver nanoparticles synthesized with thermosensitive PNIPAM as nucleating and capping agents. Fan et al., [64] functionalized PNIPAM with C18 surfactant and hence, created silver nanoparticles based nanoparticles and superlattices. Very recently, Kim et al, [65] showed the antimicrobial activity of the silver NPs encapsulated in PNIPAM-based nanoparticles. Henceforth, this opens up the applications of these novel copolymer embedded NPs to wider biomedical fields.

4.4.3 Swelling/De-swelling abilities to act as hydrogels:

Water absorbing property of the hydrogel: The hydrogels were tested to act as hydrogels at room temperature. A red-brown rectangular piece of Au-23.66@PNIPAM-co-HMImAcr was taken whose original weight was 80.3 mg and its length was 0.85 cm. It was soaked in aqueous solution (10 mL) and its swelling images, weight and length were recorded at definite time intervals (Fig. 11). Only after 10 minutes, the water absorption was 73% and the length of the film rise up to 5.9%, showcasing a rapid absorption of water within surface layers. After an hour, water penetrated by 345% and stretchiness increased by 29.4%. After 3

hours, a maximum of 750% of water was absorbed and almost the length increased to 1.5 times the original. The film became extremely stretchy and fragile. On careful examination, it was noted that the colour due to nanoparticles was concentrated in the core of the hydrogel and the surface showed transparency. This suggests only the superficial layers are involved in the water absorption. This was also confirmed by SEM images (Fig. 13) wherein the swelled chunk exhibited extremely swelled layered structures on the surface. After 24 hours, the film de-swell and its original weight is acquired. Also, if the piece is left as desired, it will shrink to its modified shape. The cycle was repeated 3 times to test the repeatability.

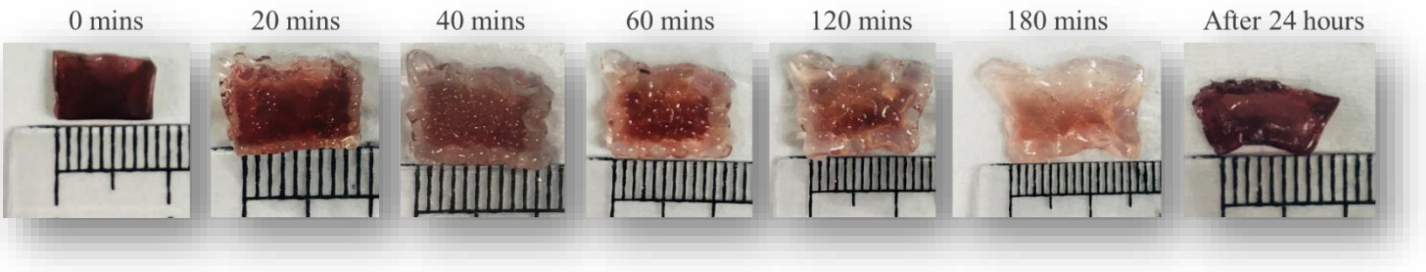

Fig. 11. Images of swelling/de-swelling of Au-20.00@PNIPAM-co-AMImCl at different time intervals.

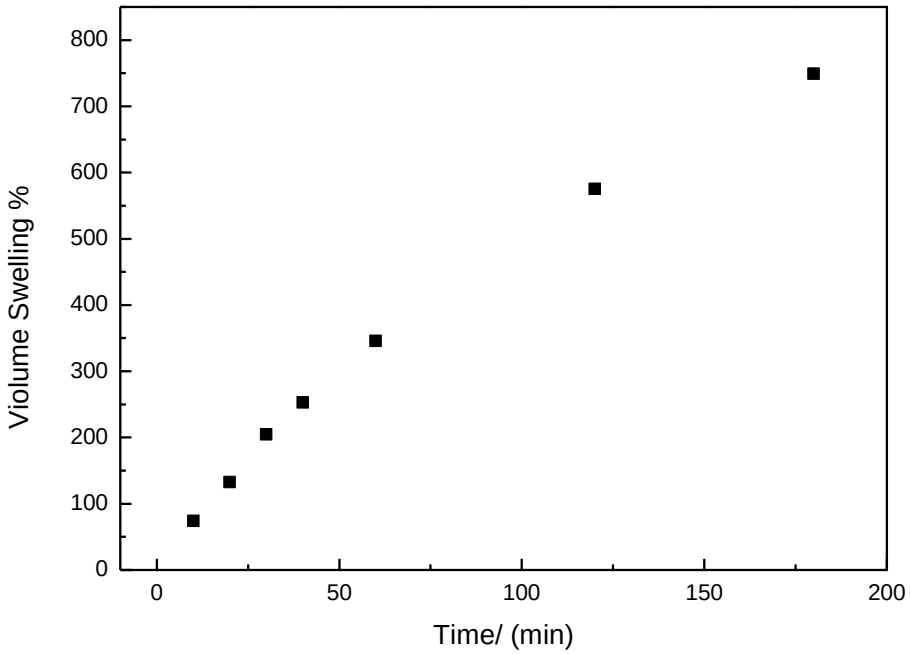

Fig. 12. Swelling/shrinking abilities of Au-23.66@PNIPAM-co-HMImAcr

Swelling rate for the same material was calculated using the following equation.

$$\%S = \frac{m_s - m_0}{m_0} \; x \; 100$$

where m_s is the weight of the swelled hydrogel at a particular time, and m_0 is the weight of the original material. A graph between swelling % and time (min) is represented in Fig. 12.

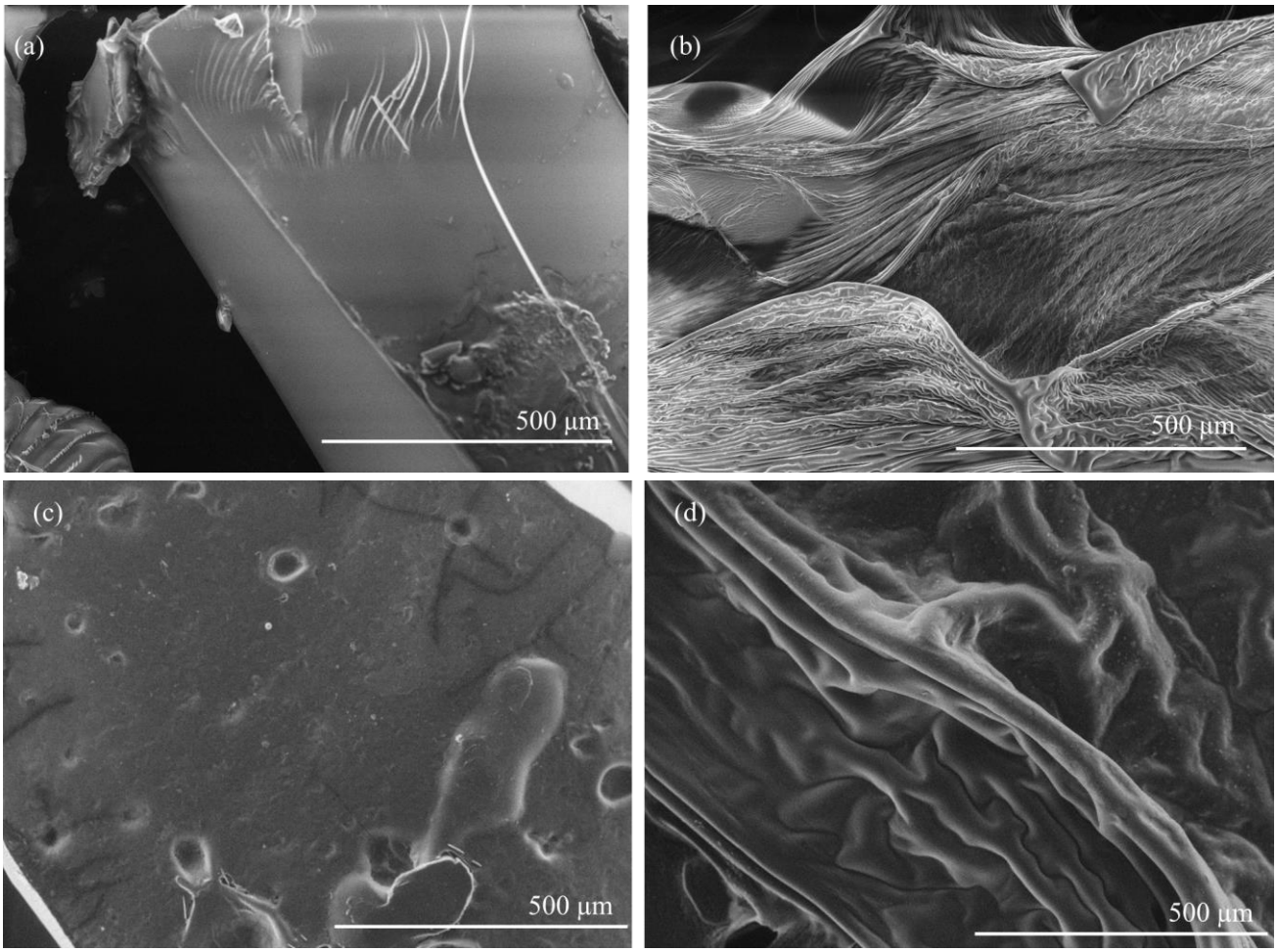

Fig. 13. SEM images of de-swelling (a-Au-24.33@PNIPAM-co-HMImAcr; c- Au-24.33@PNIPAM-co-AOImTFSI) and swelling (b-Au-24.33@PNIPAM-co-HMImAcr; d-Au-24.33@PNIPAM-co-AOImTFSI) after 24 hours.

The hydrogels possess the ability to swell below LCST in water. As seen in Fig. 14. (for Au@PNIPAM-co-AOImBr) and 15. (for Ag@PNIPAM-co-HMImAcr), the hydrogels

swell when kept in solvent for an hour if the length of a side is chosen as the point of reference. However, when the LCST is reached in water, the hydrogels shrink immediately, causing the re-lapse to the original state. This showed that these copolymer materials can successfully act as potential hydrogels which can absorb water up to 750 times of their weight. This property is extremely productive for them to be used as nanoparticles embedded thermoresponsive copolymers as hydrogels to be used in biomedical, optical and sensor applications.

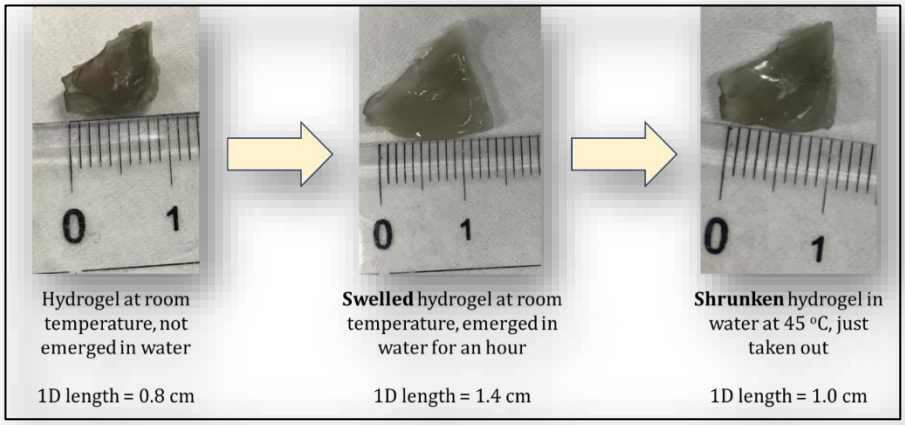

Fig. 14. Swelling/ shrinking images of Au-24.33@PNIPAM-co-AOImBr below/ above LCST.

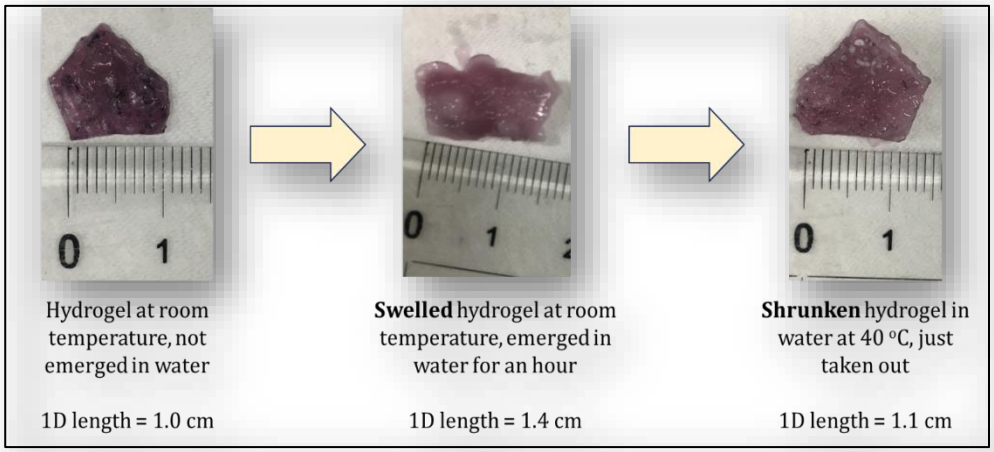

Fig. 15. Images of swelling and shrinking of Ag-31.36@PNIPAM-co-HMImAcr below and above its LCST.

4.5 Conclusions

Novel gold and silver nanoparticles embedded PNIPAM-co-IL polymers were systematically designed and were elucidated for their phase transition properties. Gold nanoparticle size was varied from 10 to 35 nm, while silver from 30 to 45 nm. Structures of polymerizable ionic liquid were varied by changing both the cation and anion specifically. LCST can be altered by varying the size of nanoparticles used or changing the hydrophobicity/hydrophilicity in the ionic liquid structure. Both the factors played an essential role in tuning the LCST and that can widen the range to 23 – 67 ^{o}C. The results can be utilized for the profound understanding of the LCST behaviour of PNIPAM-based materials, its mechanism and effect of nanoparticles. The present tuning provides a fruitful strategy for custom designed thermo-sensitive materials and their applications (graphical abstract Fig. 16).

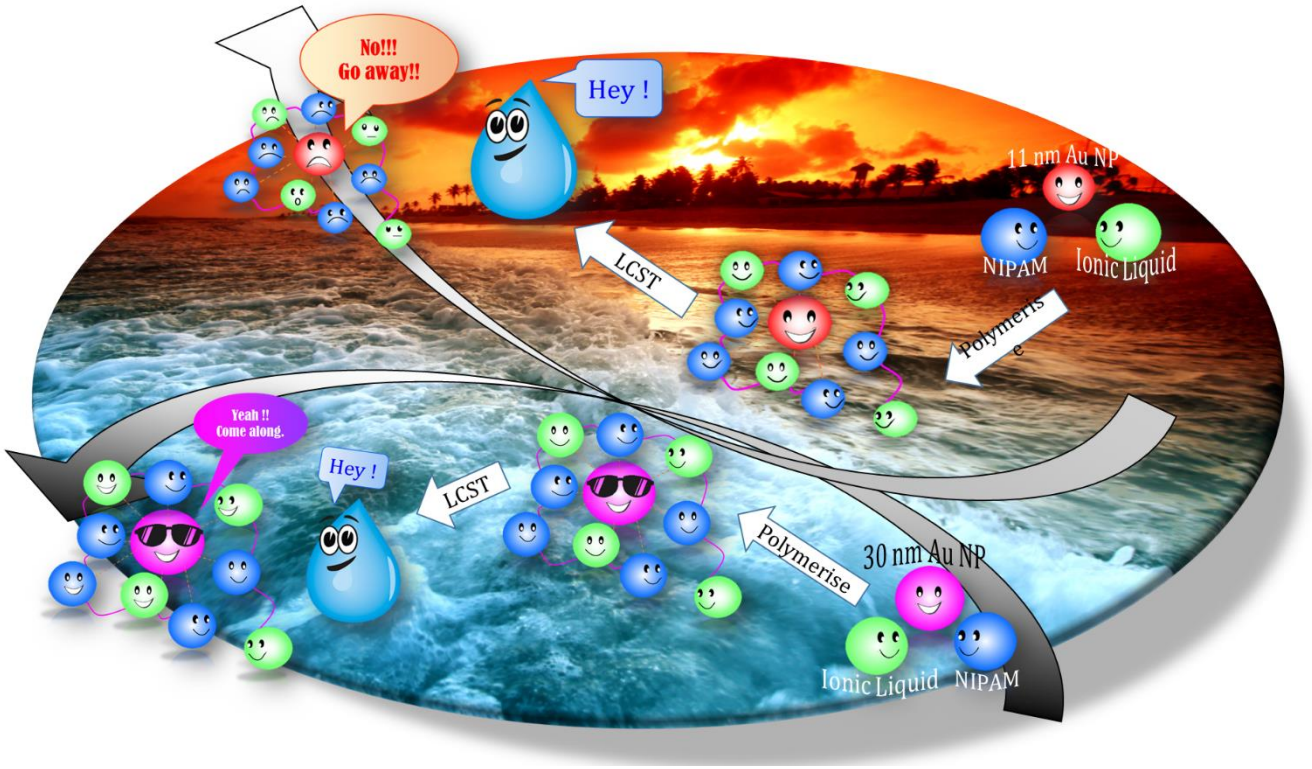

Fig. 16. Graphical abstract representing the role of nanoparticle size in the nanoparticles embedded PNIPAM based hydrogels using polymerized ionic liquids.

4.6 References

[1] R. Liu, M. Fraylich and B. R. Saunders, *Colloid Polym. Sci*., 2009, 287, 627–643.

[2] A. S. Hoffman, *Artif. Organs*, 1995, 19, 458–467.

[3] M. Heskins and J. E. Guillet, *J. Macromol. Sci. Part - Chem*., 1968, 2, 1441–1455.

[4] S. Fujishige, K. Kubota and I. Ando, *J. Phys. Chem*., 1989, 93, 3311–3313.

[5] A. Pelah and T. M. Jovin, *ChemPhysChem*, 2007, 8, 1757–1760.

[6] C. Wu and S. Zhou, *Macromolecules*, 1995, 28, 5388–5390.

[7] H. G. Schild and D. A. Tirrell, *J. Phys. Chem*., 1990, 94, 4352–4356.

[8] K. Van Durme, H. Rahier and B. Van Mele, *Macromolecules*, 2005, 38, 10155–10163.

[9] L. Valencia, F. J. Enríquez, M. Valencia and R. Díaz, Macromol. *Chem. Phys*., 2017, 218, 1600556.

[10] H. Feil, Y. H. Bae, J. Feijen and S. W. Kim, *Macromolecules*, 1992, 25, 5528–5530.

[11] C. S. Brazel and N. A. Peppas, *Macromolecules*, 1995, 28, 8016–8020.

[12] G. Fundueanu, M. Constantin and P. Ascenzi, *Int. J. Pharm*., 2009, 379, 9–17.

[13] S. Won, D. J. Phillips, M. Walker and M. I. Gibson, *J. Mater. Chem. B,* 2016, 4, 5673–5682.

[14] H. Akiyama and N. Tamaoki, *Macromolecules*, 2007, 40, 5129–5132.

[15] P. S. Stayton, T. Shimoboji, C. Long, A. Chilkoti, G. Ghen, J. M. Harris and A. S. Hoffman, *Nature*, 1995, 378, 472–474.

[16] A. Kondo, T. Kaneko and K. Higashitani, *Biotechnol. Bioeng*., 1994, 44, 1–6.

[17] E. Karjalainen, N. Chenna, P. Laurinmäki, S. J. Butcher and H. Tenhu, *Polym. Chem*., 2013, 4, 1014–1024.

[18] K. Jain, R. Vedarajan, M. Watanabe, M. Ishikiriyama and N. Matsumi, *Polym. Chem.*, 2015, 6, 6819–6825.

[19] T. L. Greaves and C. J. Drummond, *Chem. Rev*., 2008, 108, 206–237.

[20] M. Musiał, K. Malarz, A. Mrozek-Wilczkiewicz, R. Musiol, E. Zorębski and M. Dzida, *ACS Sustain. Chem. & Eng*., 2017, 5, 11024–11033.

[21] A. C. Barsanti, C. Chiappe, T. Ghilardi and C. S. Pomelli, *RSC Adv.,* 2014, 4, 38848–38854.

[22] C. P. Fredlake, J. M. Crosthwaite, D. G. Hert, S. N. V. K. Aki and J. F. Brennecke, *J. Chem. & Eng. Data*, 2004, 49, 954–964.

[23] Y. Kohno and H. Ohno, *Chem. Commun*., 2012, 48, 7119-7130.

[24] M. A. K. Abdelhalim and M. M. Mady, *J. Nanomedicine & Nanotechnol*., 2012, 3, 1-5.

[25] F. Tian, F. Bonnier, A. Casey, A. E. Shanahan and H. J. Byrne, *Anal. Methods*, 2014, 6, 9116–9123.

[26] N. R. Jana, L. Gearheart and C. J. Murphy, *Langmuir*, 2001, 17, 6782–6786.

[27] B. J. Henz, P. W. Chung, J. W. Andzelm, T. L. Chantawansri, J. L. Lenhart and F. L. Beyer, *Langmuir*, 2011, 27, 7836–7842.

[28] K. Wagers, T. Chui and S. Adem*, IOSR J. Appl. Chem*., 2014, 7, 15–20.

[29] G. Yang, J. Nanda, B. Wang, G. Chen and D. T. Hallinan, *ACS Appl. Mater. & Interfaces*, 2017, 9, 13457–13470.

[30] D. T. Thompson, *Nano Today*, 2007, 2, 40–43.

[31] M. O. Stetsenko, S. P. Rudenko, L. S. Maksimenko, B. K. Serdega, O. Pluchery and S. V. Snegir, *Nanoscale Res. Lett*., 2017, 12, 348-358.

[32] X. Huang and M. A. El-Sayed, *J. Adv. Res.*, 2010, 1, 13–28.

[33] V. Kumar, D. Bano, D. K. Singh, S. Mohan, V. K. Singh and S. H. Hasan, *ACS Sustain. Chem. & Eng.*, 2018, 6, 7662–7675.

[34] K. Saha, S. S. Agasti, C. Kim, X. Li and V. M. Rotello, *Chem. Rev*., 2012, 112, 2739–2779.

[35] R. Pamies, J. G. H. Cifre, V. F. Espín, M. Collado-González, F. G. D. Baños and J. G. de la Torre, *J. Nanoparticle Res*., 2014, 16, 2376-2387.

[36] N. Singh and L. A. Lyon, *Chem. Mater.*, 2007, 19, 719–726.

[37] G. Marcelo and M. Fernández-García, *RSC Adv.,* 2014, 4, 11740–11749.

[38] H. Han, J. Y. Lee and X. Lu, *Chem. Commun*., 2013, 49, 6122-6124.

[39] S. Christau, T. Möller, F. Brose, J. Genzer, O. Soltwedel and R. von Klitzing, *Polymer*, 2016, 98, 454–463.

[40] R. Contreras-Cáceres, J. Pacifico, I. Pastoriza-Santos, J. Pérez-Juste, A. Fernández-Barbero and L. M. Liz-Marzán, *Adv. Funct. Mater*., 2009, 19, 3070–3076.

[41] C.-L. Zhang, F.-H. Cao, J.-L. Wang, Z.-L. Yu, J. Ge, Y. Lu, Z.-H. Wang and S.-H. Yu, *ACS Appl. Mater. & Interfaces*, 2017, 9, 24857–24863.

[42] S. Maji, B. Cesur, Z. Zhang, B. G. De Geest and R. Hoogenboom, *Polym. Chem*., 2016, 7, 1705–1710.

[43] F. Liu, Y. Cui, L. Wang, H. Wang, Y. Yuan, J. Pan, H. Chen and L. Yuan, *ACS Appl. Mater. & Interfaces*, 2015, 7, 11547–11554.

[44] M. I. Gibson, D. Paripovic and H.-A. Klok, *Adv. Mater*., 2010, 22, 4721–4725.

[45] A. Housni and Y. Zhao, *Langmuir*, 2010, 26, 12933–12939.

[46] S. Murphy, S. Jaber, C. Ritchie, M. Karg and P. Mulvaney, *Langmuir*, 2016, 32, 12497–12503.

[47] N. Chen, X. Xiang and P. A. Heiden, *J. Colloid Interface Sci.,* 2013, 396, 39–46.

[48] Y. Yan, L. Liu, Z. Cai, J. Xu, Z. Xu, D. Zhang and X. Hu, *Sci. Reports*, 2016, 6, 31328.

[49] K. Kusolkamabot, P. Sae-ung, N. Niamnont, K. Wongravee, M. Sukwattanasinitt and V. P. Hoven, *Langmuir*, 2013, 29, 12317–12327.

[50] M. Rahimi, S. Kilaru, G. E. L. Hajj Sleiman, A. Saleh, D. Rudkevich and K. Nguyen, *J. Biomed. Nanotechnol.,* 2008, 4, 482–490.

[51] S. V. Dzyuba and R. A. Bartsch, *J. Heterocycl. Chem*., 2001, 38, 265–268.

[52] J. Piella, N. G. Bastús and V. Puntes, *Chem. Mater*., 2016, 28, 1066–1075.

[53] S. Kumar, K. S. Gandhi and R. Kumar, *Ind. & Eng. Chem. Res.,* 2007, 46, 3128–3136.

[54] N. G.Bastus, J.Comenge and V. Punter*, Langmuir*, 2011, 27, 11098-11105.

[55] T. Gotoh, Y. Nakatani and S. Sakohara*, J. Appl. Polym. Sci*., 1998, 69, 895–906.

[56] X. Liu, M. Atwater, J. Wang and Q. Huo, *Colloids Surfaces B: Biointerfaces*, 2007, 58, 3–7.

[57] R. B. Grubbs, *Polym. Rev*., 2007, 47, 197–215.

[58] N. T. Southall, K. A. Dill and A. D. J. Haymet, *J. Phys. Chem. B*, 2001, 106, 521–533.

[59] G. B. Appetecchi, S. Scaccia, C. Tizzani, F. Alessandrini and S. Passerini, *J. Electrochem. Soc.*, 2006, 153, 1685-1691.

[60] S. T. Jones, Z. Walsh-Korb, S. J. Barrow, S. L. Henderson, J. del Barrio and O. A. Scherman, *ACS Nano*, 2016, 10, 3158–3165.

[61] S. Agnihotri, S Mukherji and S. Mukherji, *RSC Adv.*, 2014, 4, 3974-3983.

[62] K. S. Lee and M. A. El-Sayed, *J. Phys. Chem. B*, 2006, 110, 19220-19225.

[63] J. R. Morones and W. Frey, *Langmuir*, 2007, 23, 8180-8186.

[64] B. Li, D.-M. Smilgies, A. D. Price, D. L. Huber, P. G. Clem, and H.Fan, *ACS Nano,* 2014, 8 (5), 4799-4804.

[65] M. Qasim, N. Udomluck, J. Chang, H. Park, and K. Kim*, Int. J. Nanomedicine*, 2018, 13, 235–249.

****

Chapter 5

Can we predict the Critical Solution Temperature (CST) for imidazolium-based ionic liquids?

Abstract

In this chapter, I suggest for the first time, a general rule for prediction of critical solution behavior of low molecular weight imidazolium-based Ionic Liquids (ILs) using COSMO-RS Simulations. Based on the values of chemical potential/H-bond energy (vs temperature), water-like aprotic ILs can be anticipated to show LCST (Lower Critical Solution Temperature) or UCST (Upper Critical Solution Temperature). Mechanistic and structural aspects of ILs exhibiting Critical Solution behavior (CST) were also studied using Kamlet-Taft parameters. It was seen that structural aspects like polarity, chemical potential and hydrogen-bonding play a crucial role for CST phenomenon. Impedance analysis was also carried out to confirm the LCST/UCST temperatures of imidazolium-based ILs. This also confirmed the fundamental theory of why/how ILs show CST.

5.1 Introduction

Room temperature low molecular weight ionic liquids (RTILs)[1], as a green solvent have gained great attention in the fields including biphasic reaction catalysis, electrochemical actuator membranes[2], diluents and separation membrane. These materials have diversified cation and anionic counterparts which can be aesthetically manipulated and tailored to the user's need. As their toxicity levels have not been proven till date, they are being used rapidly in biological applications like tissue engineering[3], drug delivery[4] and gene therapy[5].

Like thermoresponsive polymers[6,7], many ionic liquids (ILs) display critical phase separation behaviour[8,9] making them potential candidates for versatile use with sensors[10], micelles[11], fuel cells[12] and extraction processes[13]. Some ionic liquids exhibit Lower Critical Solution Temperature (LCST)[14] and/or Upper Critical Solution Temperature (UCST)[15]. It is already reported that optimum ratio of hydrophilic/hydrophobic nature of the constituting ions play a major role in deciding the occurrence of either phenomenon [16,17].

Why imidazolium-based Ionic liquids?

Due to facile synthetic route, imidazolium-based ionic liquids can act as potential substitute for polymers owing to their high stability, high viscosity and low flammability. These ionic liquids possess polarity [18] similar to that of water, thereby enhancing the utilization in biological systems. Imidazolium-based ionic liquids can show miscibility property from being completely soluble (hydrophilic) to being completely non-soluble (hydrophobic) in water. Solubility increases with decreasing temperature (for LCST

showing ILs) and decreasing chain length of alkyl substitution in the imidazolium ring. This gives quite a range to study these systems. 1, 3-dialkylimidazolium based ionic liquids were chosen as a part of research due to their ease of synthesis. These are RTILs with substituted imidazolium-based cations which consist of aromatic five membered ring containing two non-adjacent nitrogen atoms. Both alkyl substitutions and anions in the ionic liquid structure can be varied.

PART-A

5.2 Objective - I

There are several ionic liquid/ water systems where it is difficult to estimate phase separation properties by techniques like use of a dye, UV-Visible spectroscopy or Laser Light Scanning. All the till date technique fails, when following situations arises:

- When phase separation of system is not very distinct and clear visually
- When the dye is almost equally soluble in both, water and ionic liquid.
- When visual, optical measurements and concentration measurements of the system fail to impact on the phase transition property of the system.

Imidazolium-based ionic liquids, also belongs to the category above wherein, the phase behaviour is very difficult to find. Therefore, there is a lack of diagnostic tool which could electrochemically determine phase changes in imidazolium-based ionic liquids accurately and precisely. Therefore, the foremost objective of this chapter is to detect CST in imidazolium-based ionic liquids using Electrochemical Impedance Spectroscopy (EIS) as the diagnostic tool.

5.2.1 Electrochemical Impedance Spectroscopy

Electrochemical Impedance Spectroscopy [19,20] was chosen as it is powerful and a non-destructive tool to detect slight changes of capacitance. As impedance measurements are generally applicable to any kind of solvent systems, it can potentially show universal utility as diagnostic tool for thermosensitive behaviour of systems. Further, through the analysis of fitting parameters for equivalent circuits, wide variety of

electronic and physicochemical properties will be available. Such information can be a strong tool to investigate mechanism of thermosensitive behaviour of systems. Being motivated by the above-mentioned idea, in the present work, for the first time, evaluation of LCST behaviour of thermosensitive materials was investigated by electronic impedance measurements.

Proposed mechanism of CST determination using EIS

An electrolyte solution possesses inductive, capacitive and resistive behaviour [21] as sensed by a three-electrode cell system[22]. In the presence of ionic species, application of some potential to electrochemical cell leads to well-known electrochemical double-layer formation which significantly affects interfacial components of impedance spectra. It is expected that dissociation or association of water from (with) ionic liquid molecules and subsequent phase transitions triggered by such hydrophobicity changes will largely affect the behaviour of electrochemical double layer at electrode-electrolyte interface [23]. This distortion can be easily seen in bode plot where phase angle changes significantly (Scheme 1).

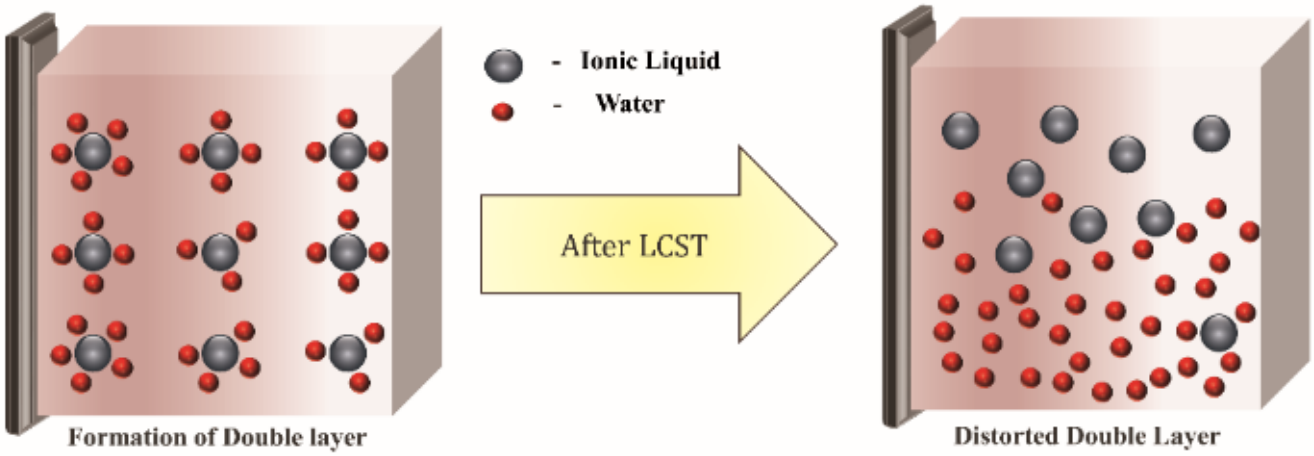

Scheme 1. Principal mechanism underlying the Impedance Spectroscopy for the implementation to identify CST behavior of ILs.

5.2.2 Experimental

All the chemicals were purchased from either WAKO Co. Ltd. or TCI chemicals Ltd. and were used as received. Proton NMR was done on Bruker Ultrashield plus 400-*NMR*. Electrochemical Impedance experiments were performed on Biologic VSP s/n 1190 with temperature being controlled on the thermostat (Eyela NCB-1200). UV-Visible Spectroscopy was done using JASCO V-630 Spectrometer. DSC was performed on SII X-DSC 7000 T EXSTAR. Fourier transformed infrared spectroscopy was performed on JASCO FT/IR-4100 spectrometer.

5.2.3 Synthesis of low molecular weight imidazolium-based ionic liquids

(General Procedure) [24]: 1 equivalent of 1-methylimidazole and 1.1 equivalent of 1-bromoalkane were mixed in a 500 mL round bottom (RB) flask. The solvent used was acetonitrile. Refluxed the contents of RB at 90 ^{o}C overnight using water condenser. Work up was done with diethyl ether to remove alkyl halide impurities. The obtained ionic liquid was dried under reduced pressure. Any present moisture in ionic liquid was removed by vacuum drying the ionic liquid overnight to get pure IL as shown in Scheme **2**. For 1-hexyl-3-methylimidaozlium bromide, 1-bromohexane was used. For 1-octyl-3-methylimidazlium bromide, 1-bromooctane was used. Reaction was done at atmospheric pressure.

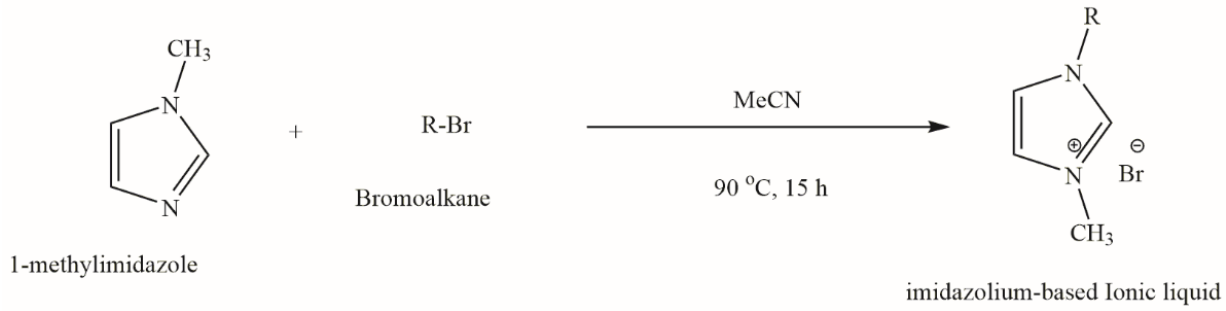

Scheme 2: General synthetic scheme for the synthesis of room-temperature imidazolium-based ionic liquids

Anion exchange was performed at room temperature by stirring equimolar amounts of the imidazolium based ionic liquid and ammonium hexafluorophosphate in water overnight in a round bottom flask. The desired ionic liquid was extracted in dichloromethane. The ionic liquid was then purified under reduced pressure and purified under vacuum overnight to get dried IL. (Scheme **3**)

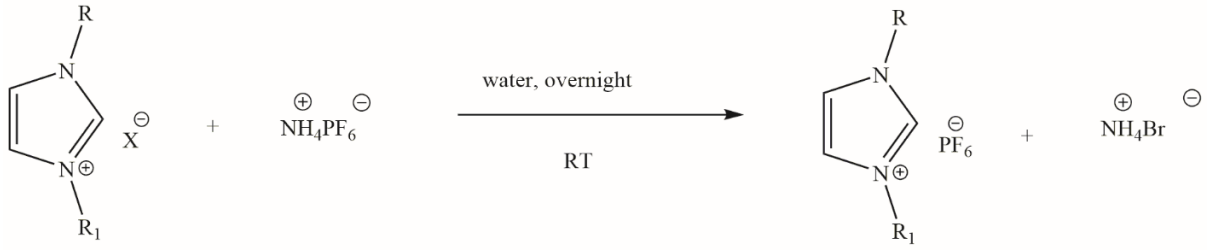

Scheme 3: General scheme for anion-exchange of bromide to hexafluorophosphate.

5.2.4 Characterizations of ionic liquids

The synthesized low molecular weight room temperature ionic liquids were characterized by ^{1}H-NMR and FT-IR spectroscopy. Examples of characterization for 1-hexyl-3-methylimidazolium bromide are shown below. The FT-IR spectra (Fig. 1.) showed the presence of peaks, all of which can be associated to imidazolium moiety. IR characterization was done for other ionic liquids and peaks were assigned similarly.

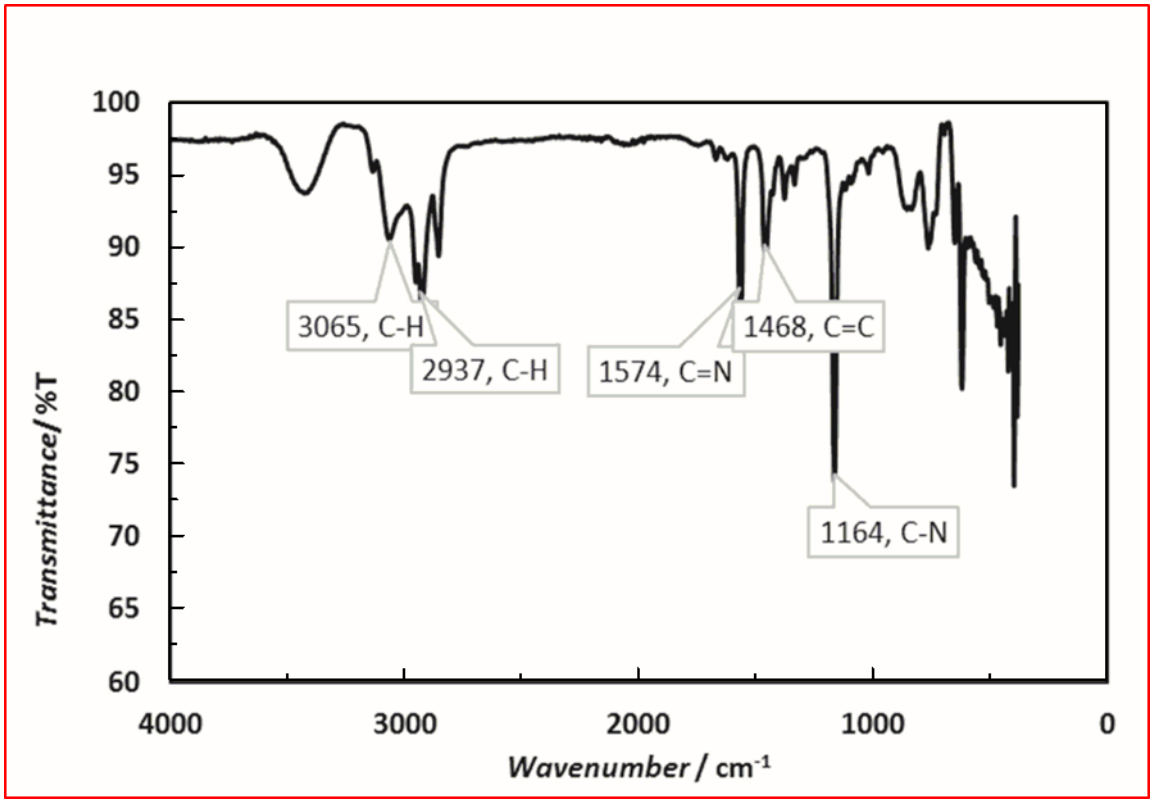

Fig. 1. FT-IR spectrum of HMImBr.

The ^{1}H-NMR (400MHz, DMSO-d_6) (Fig. 2 shown for HMImBr) data shows the presence of characteristic peak between 4.0 to 4.5 ppm confirming the bond formation between alkyl halide and nitrogen present in imidazolium ring.

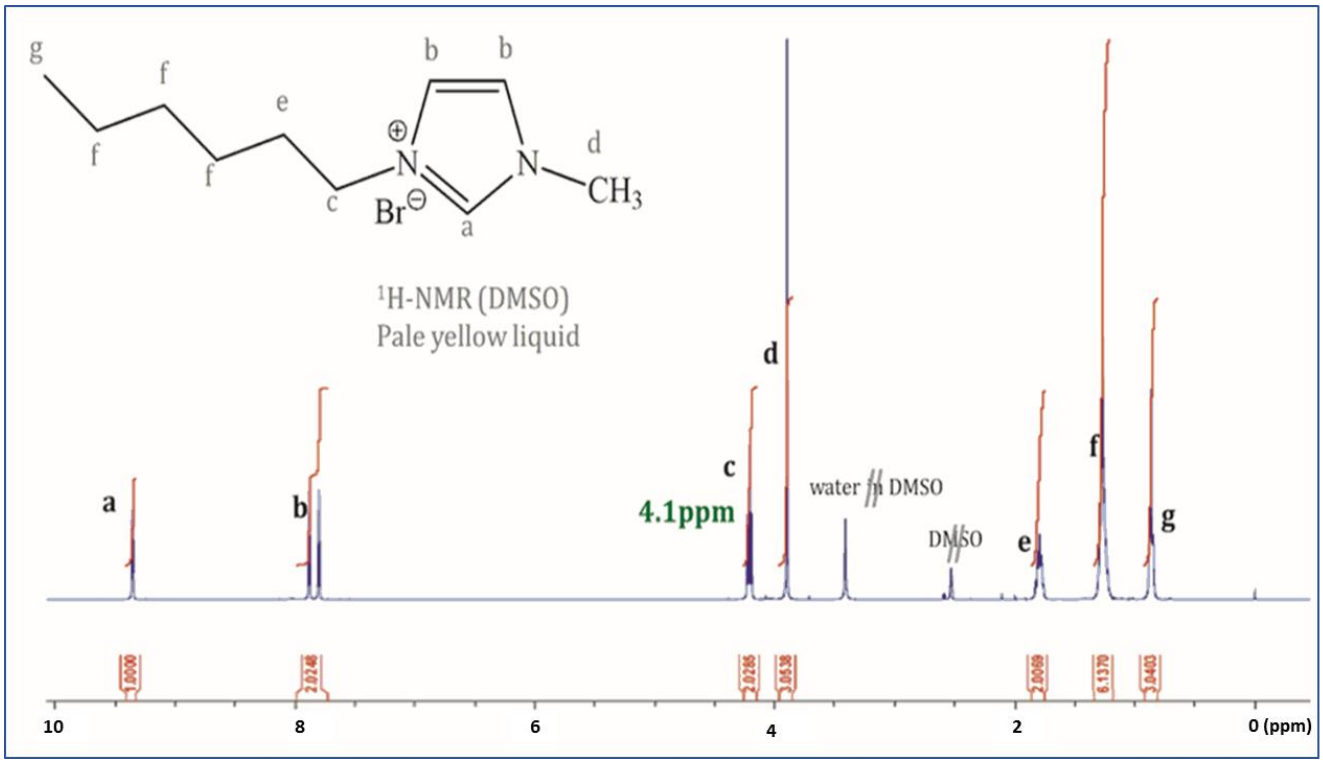

Fig. 2. ^{1}H-NMR of HMImBr.

5.2.5 Impedance set-up and experimental conditions

A three electrode cell was constructed with working and counter electrodes as Platinum (1 cm^2 and 4 cm^2 respectively) and reference electrode as saturated Ag/AgCl. Electrolyte taken was 1:1 wt % IL/water. In potentiostatic mode, the experiments were done at fixed DC voltage of 10 mV. A sinusoidal current perturbation was superimposed to the DC current and applied to the cell further in the frequency range of 1 MHz to 0.01 mHz. Between each temperature measurement, 60 minutes of stabilization time was given to the cell.

Set-up for measurement of potentio-static Impedance spectroscopy: To perform PEIS measurements for ionic liquids, a 3-elecetrode cell was constructed which was

jacketed into a thermostat (temperature controller). Working and counter electrodes were taken as a Platinum chips (surface area – 1 cm^2 and 4 cm^2). The ionic liquid solution (50 wt%) was working as the electrolyte. EIS was performed in the range of 1MHz to 0.01mHz with the amplitude being 10mV. Before each impedance measurement at various temperatures, ample amount of time (1 hour) was given to the system to stabilize at that temperature. Once the system attains equilibrium, impedance was run for 15 minutes.

A schematic representation of the cell set-up is showm below:

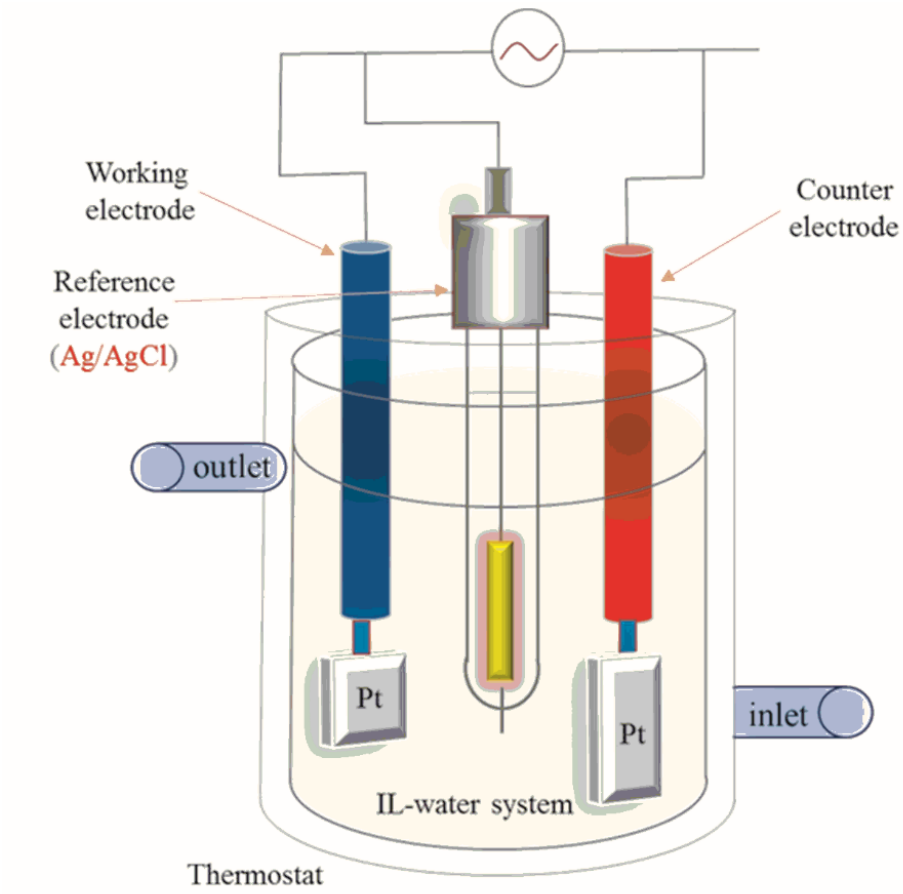

Fig. 3. Schematic representation of the cell-setup for the impedance spectroscopy

5.2.6 Results and Discussions

After the synthesis of ionic liquids, samples of ionic liquids were mixed in different amount of water and were further subjected to phase transition analysis. The ionic liquid 1-hexyl-3-methylimidazolium bromide (HMImBr) was chosen to study phase transitions in detail.

Why EIS is needed?

Usual techniques applied

A. Optical analysis

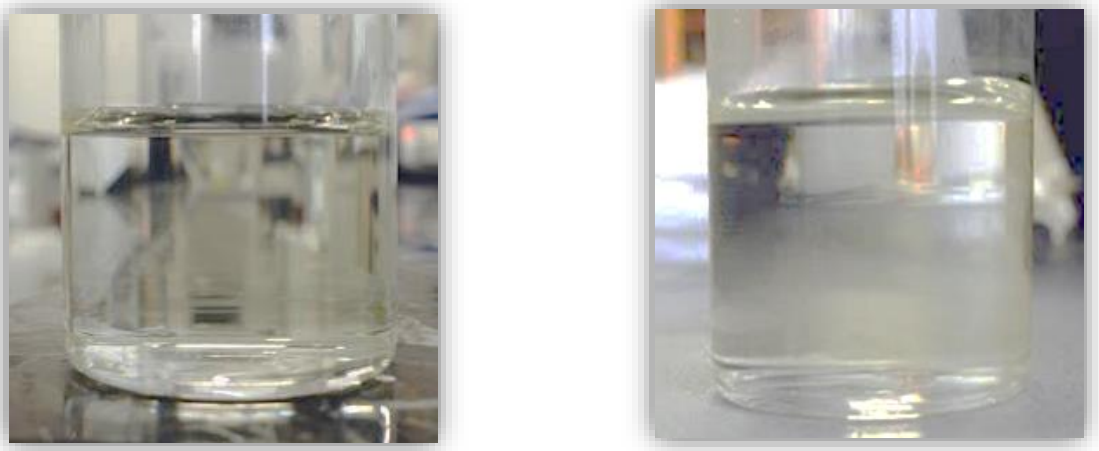

(a) (b)

Fig. 4 (a) Image of 50% w/w HMImBr/water at room temperature (b) image of 50% w/w HMImBr/water after 2 days at 4 ^{o}C.

When equal contents of HMImBr and water were mixed at room temperature, the liquids were miscible in one another in all compositions. It was observed that even on heating, no changes in phase occurred. But cooling the system for 2 days at 4-5 ^{o}C, it appeared that the system had undergone changes (Fig. 4). It could be estimated, however not in detail that system has separated in two phases as seen in (b), there was a formation of a turbid layer at the bottom of the system.

B. Optical analysis

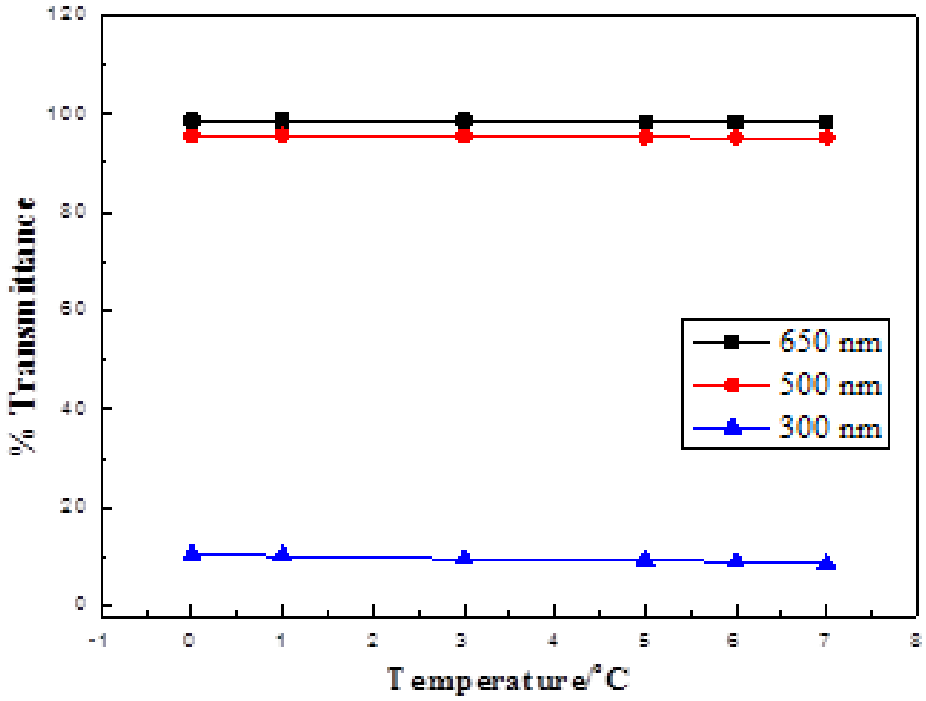

Fig. 5. UV-Visible spectroscopic analysis for 50% w/w HMImBr in water.

It was thought that like polymers, it could be possible for ionic liquid systems to investigate LCST or UCST via UV-Visible spectrometer. So the same system was tried to achieve a cloud point using optical technique and the spectrum was obtained in Fig. 5. UV-Visible spectra was recorded for HMImBr in water at temperatures of 0-7 ^{o}C. Transmittance graph was linear and showed no sudden change as expected to show for phase transitions. Because there were no significant changes in turbidity and absorption of light throughout the system (as not seen visually also), as expected UV-Vis studies fails to establish a cloud point. There occurred no sharp changes in the transmittance of the system at different wavelengths. Hence, optical analysis also failed.

Hence, the literature techniques did not help to estimate the critical temperature of water-like ionic liquids. Thus, creating a lookout for newer and advanced techniques.

Studies using EIS

Examining 50 wt% HMImBr-water system as the electrolyte, I carried out potentiostatic EIS experiment (Fig. 6) from 1 °C to 7 °C to carefully observe the phenomenon in the frequency range of 1 MHz to 0.01 mHz.

Bode phase plots for the same were obtained and plotted. A change in phase angle had started at 3 °C. This is due to change in double layer capacitance due to dissociation of ionic liquid molecules with water, which is detected by this impedance spectroscopy and marked the trigger point of the event. Thus, phase separation starts at 3 °C and system stabilizes after 7 °C. This led us to the inference that LCST for HMImBr-water system is a wide-ranged phenomenon with peak temperature being 5 °C. These results confirm the occurrence of LCST in HMImBr.

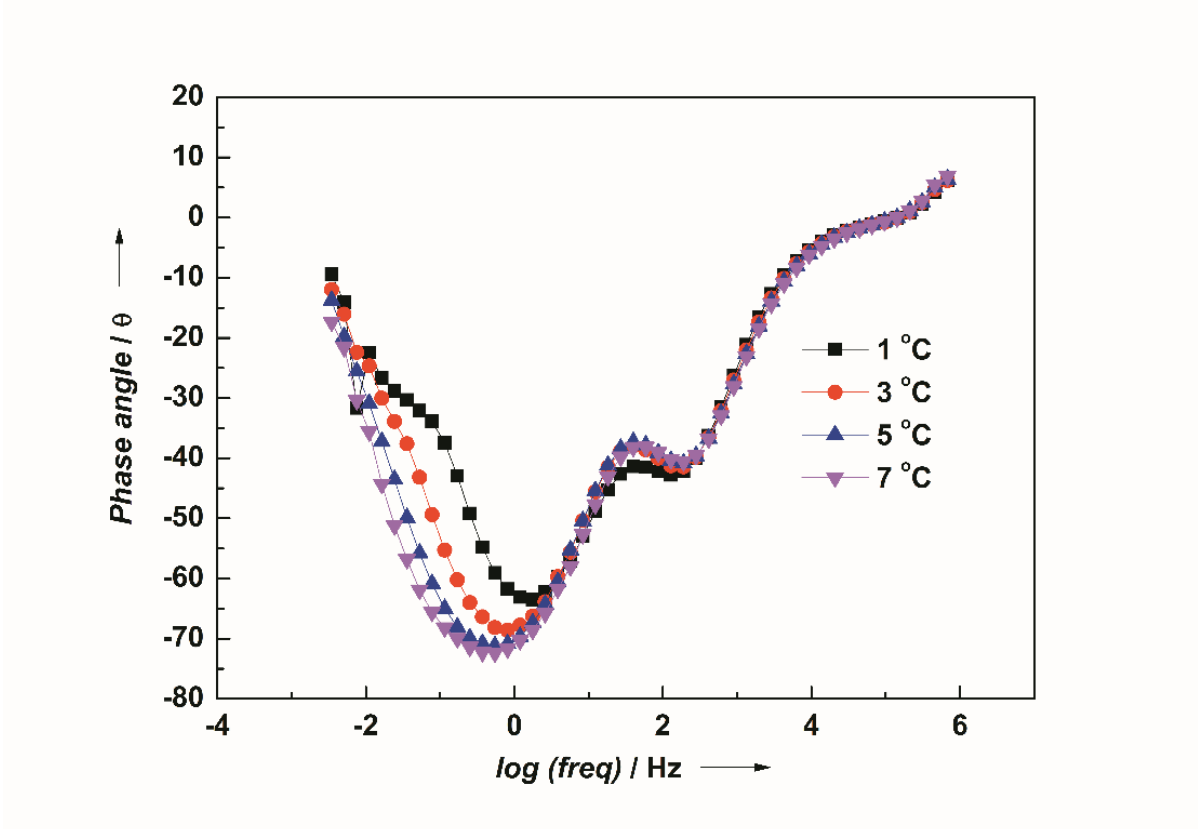

Fig 6. Bode phase for PEIS experiment for 50 wt% HMImBr-water electrolyte system.

Curve-fitting values for 50wt% HMImBr-water system:

As an added advantage of this dominant technique, one can give physical meaning to this impedance. Therefore, impedance values were fitted to obtain an equivalent circuit. ZSim was used as the software for curve-fitting. The PEIS data was used for the fitting. The best fit equivalent circuit obtained was R(Q(R(CR)))(CR) for which the chi-square value reached to a very low of 10^{-5}, providing a well-fit circuit interpretation shown in Table 1.

Table 1: Fitting values of the HMImBr-water system.

Temperature/ ^{o}C	R1	CPE or Q	R2	C3	R3
1	15.25	8.17e-5	125.00	6.00e-4	5162
3	14.24	8.23e-5	108.00	2.08e-4	11600
5	13.33	3.04e-4	60.00	1.00e-4	18400
7	12.51	2.96e-4	54.38	1.00e-4	19500

It was scrutinized that four components in the system are playing vital role towards transition (Fig. 7.). The first and essential component was the bulk resistance or the total solution resistance R1, which is present by virtue of the electrolytic composition between the counter and reference electrodes of the electrolytic cell. The second component was the IL phase represented by CPE2 and R2. This phase showcased the presence of a smaller third layer which is composed of both ionic liquid and water

molecule in close proximity. This phase is represented by C3 and R3. This is present due to strong affinity of bromide in water.

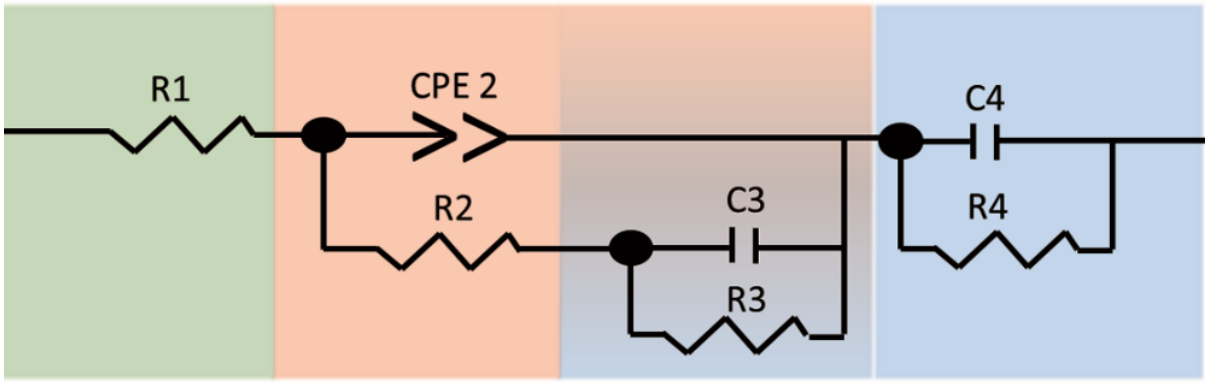

Fig. 7. Circuit obtained by curve fitting for PEIS experiment for 50 wt% HMImBr-water electrolyte system. The green color represents the total solution resistance, red stands for ionic liquid and blue portrays water layer.

Lastly, because water is separated, it is the last component depicted by C4 and R4. It was deduced that not two, but a smaller third layer is existent in the solution at the critical transition temperature. One good reason why water has strong affinity towards HMImBr and the system is not able to completely separate into distinguished layers is because HMImBr has very similar polarity as that of water. This is also complemented by E_T^N results obtained for HMImBr. Normalized polarity of water was taken to be 1.000, while for HMImBr, it was in the similar range of 1.199-1.237. This mixed layer was found to be of high importance and can act as a transferring medium, suggesting the use of this ionic liquid in other vital applications. As double layer capacitance CPE2 is the crucial parameter to evaluate the phenomenon occurring in the electrolytic system, it would be more favorable to examine the change with temperature. For the temperatures 1-7 ^oC, CPE2 values were plotted to procure a graph as in Fig. 8. As expected, there observed an

increase in capacitance at the critical point because the ionic liquid molecules are free from water of hydration and thus, ionically more conducting. Capacitance reached a maximum at 5 ^{o}C after which, the system tries to attain stability.

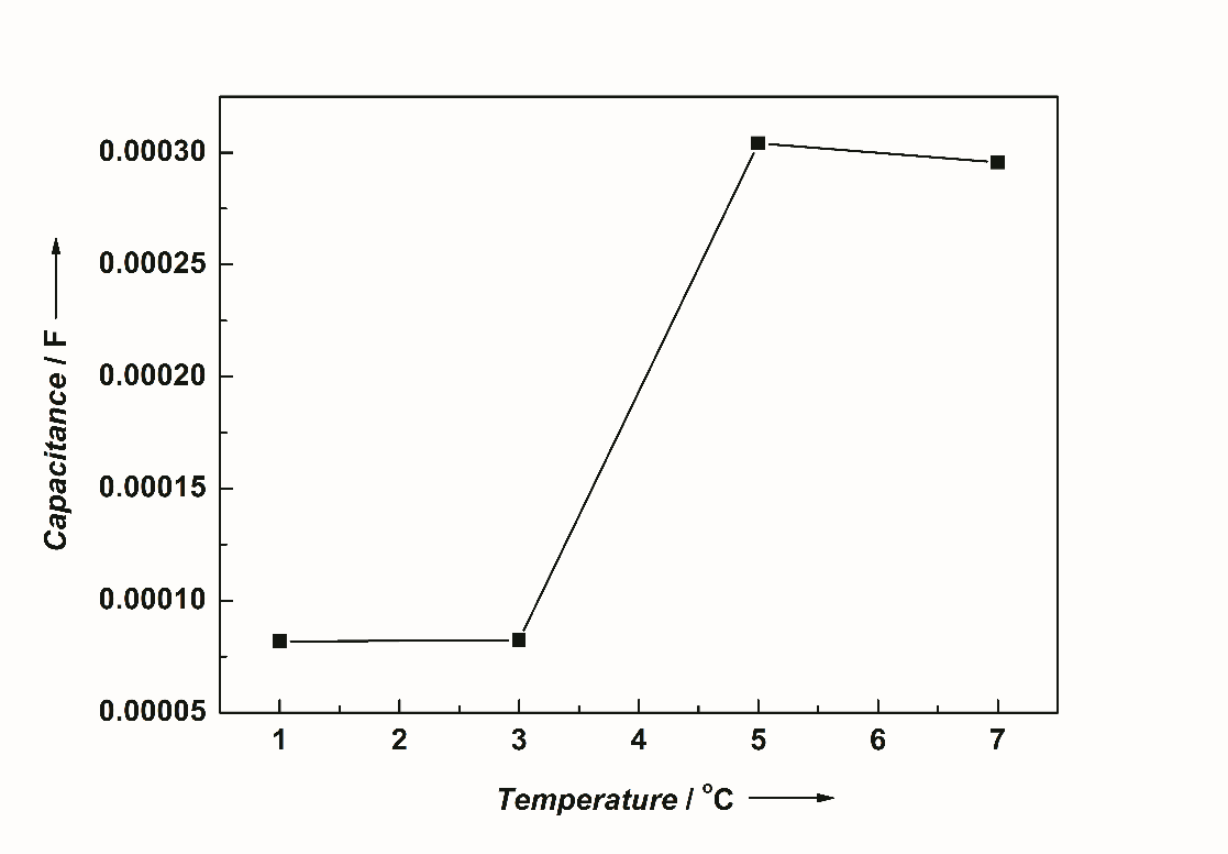

Fig. 8. Change in Double layer capacitance with Temperature for 50wt% HMImBr-water electrolyte system.

It was evident that impedance spectroscopy not only recognized the transition phenomenon, but also gave a physical significance to the transition taking place at the molecular level.

PEIS and curve-fitting data for AMImBr (1-allyl-3-methylimidazolium bromide) [Comparison for non-CST showing ionic liquid]:

The ionic liquid AMImBr was studied for comparison with HMImBr as AMImBr showed no CST. Hence, the Bode plot (Fig. 9.) for AMImBr showed no change from the temperatures of 5 °C to 45 °C, suggesting that LCST did not occur in AMImBr in this range.

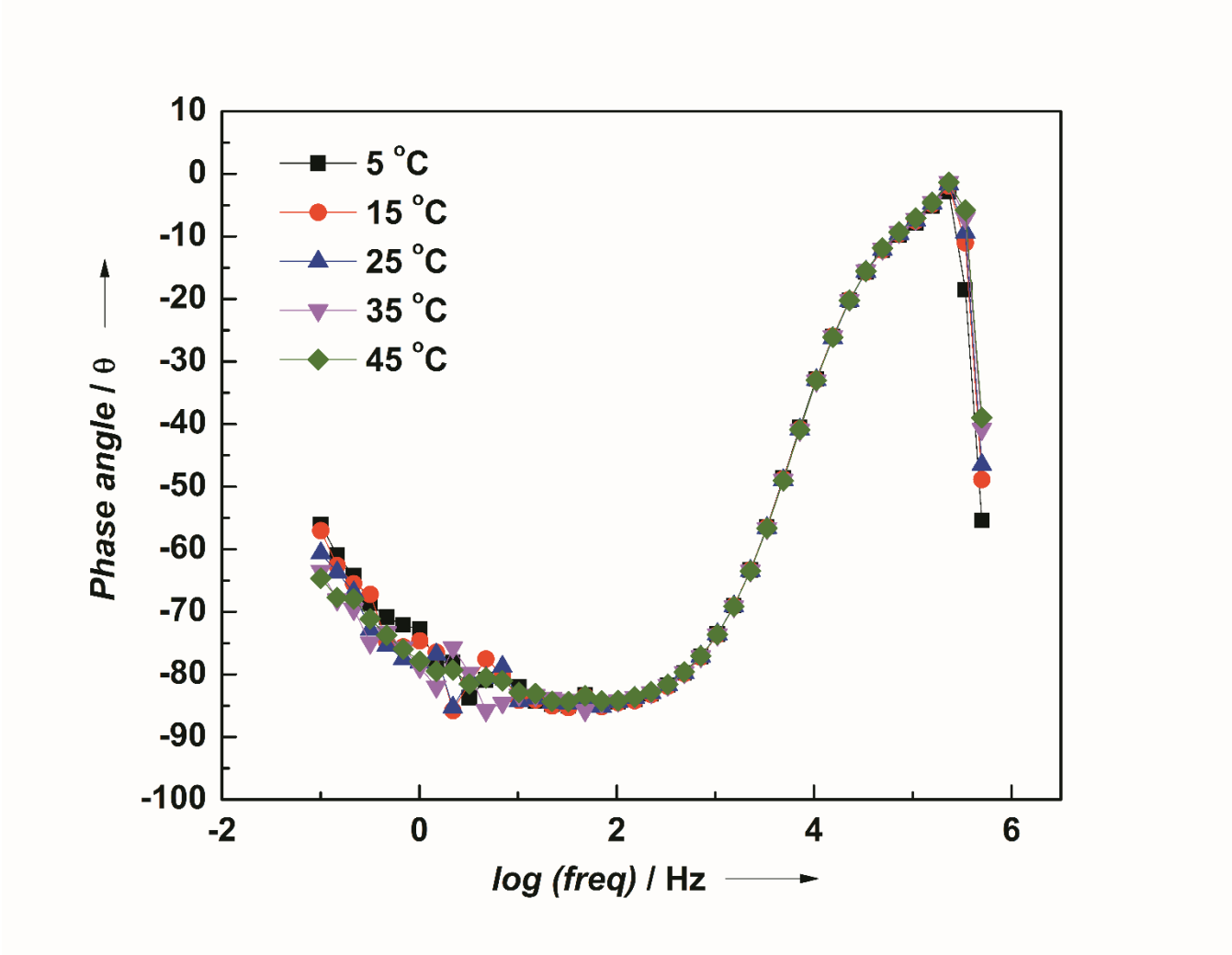

Fig 9. PEIS Spectroscopic analysis for 50 wt% AMImBr in water. The experiment was carried out in the range 5 °C to 45 °C. There appeared no change in the phase angle in this range. Hence, AMImBr showed no CST in the range of 5-45 °C

Also, the capacitance (Fig. 10.) was plotted on similar lines using the same circuit as HMImBr. But there is no change in this graph either. Hence, the ionic liquid do not show any CST.

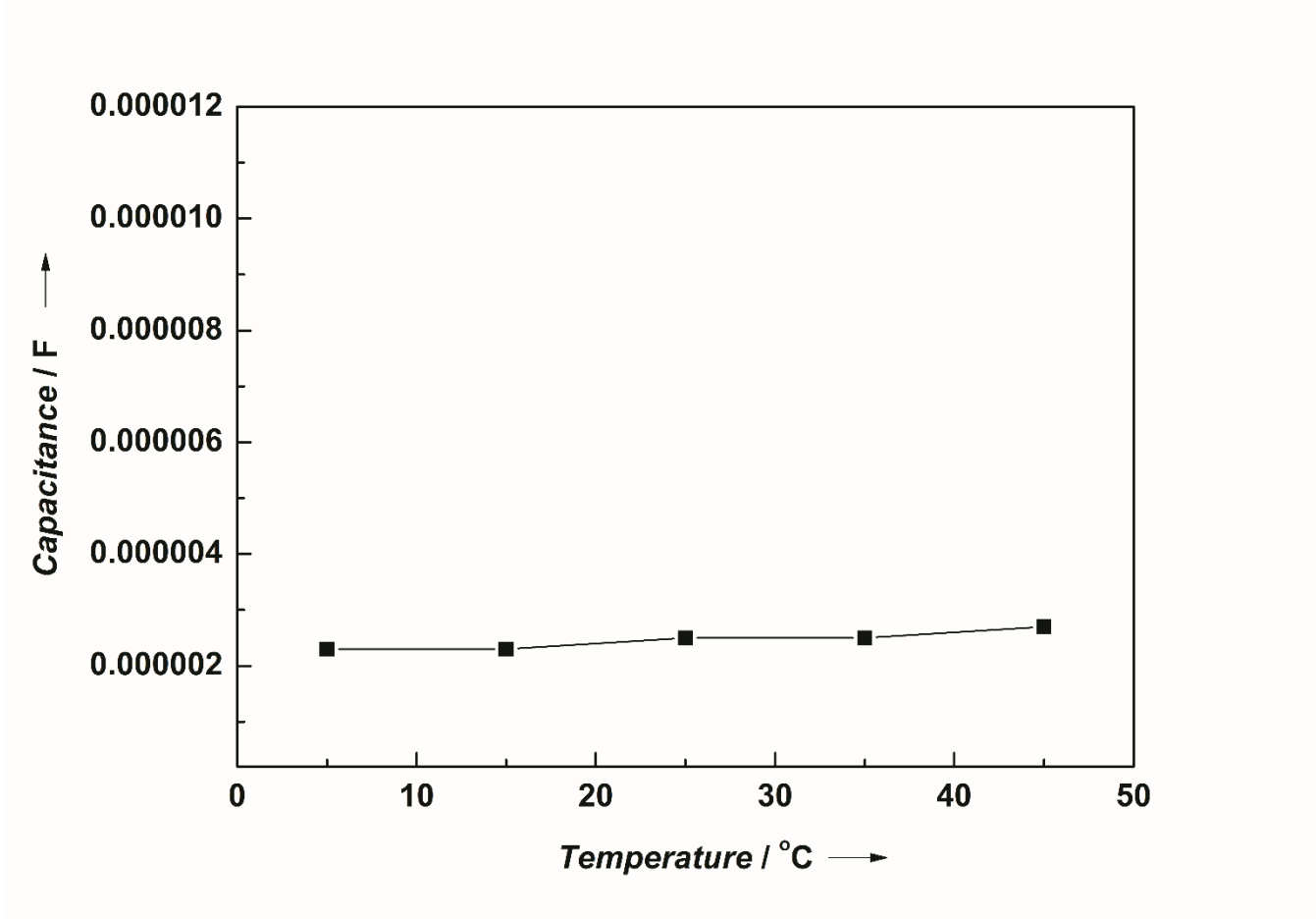

Fig. 10. Change in Double layer capacitance with temperature for 50 wt% AMImBr-water system. The circuit used for curve-fitting was R(Q(R(CR)))(CR).

Other ionic liquids/water systems were able to show change in phase angle in response to change in phase behvaiour. Some of the plots are showcased below:

1. 1-Octyl-3-methylimidazolium bromide (OMImBr)

OMImBr-water acted as the electrolyte for the cell-setup. The results showed the change in phase angle at 54 °C (Fig. 11).

Potentio-static Impedance Spectroscopy (PEIS) for OMImBr:

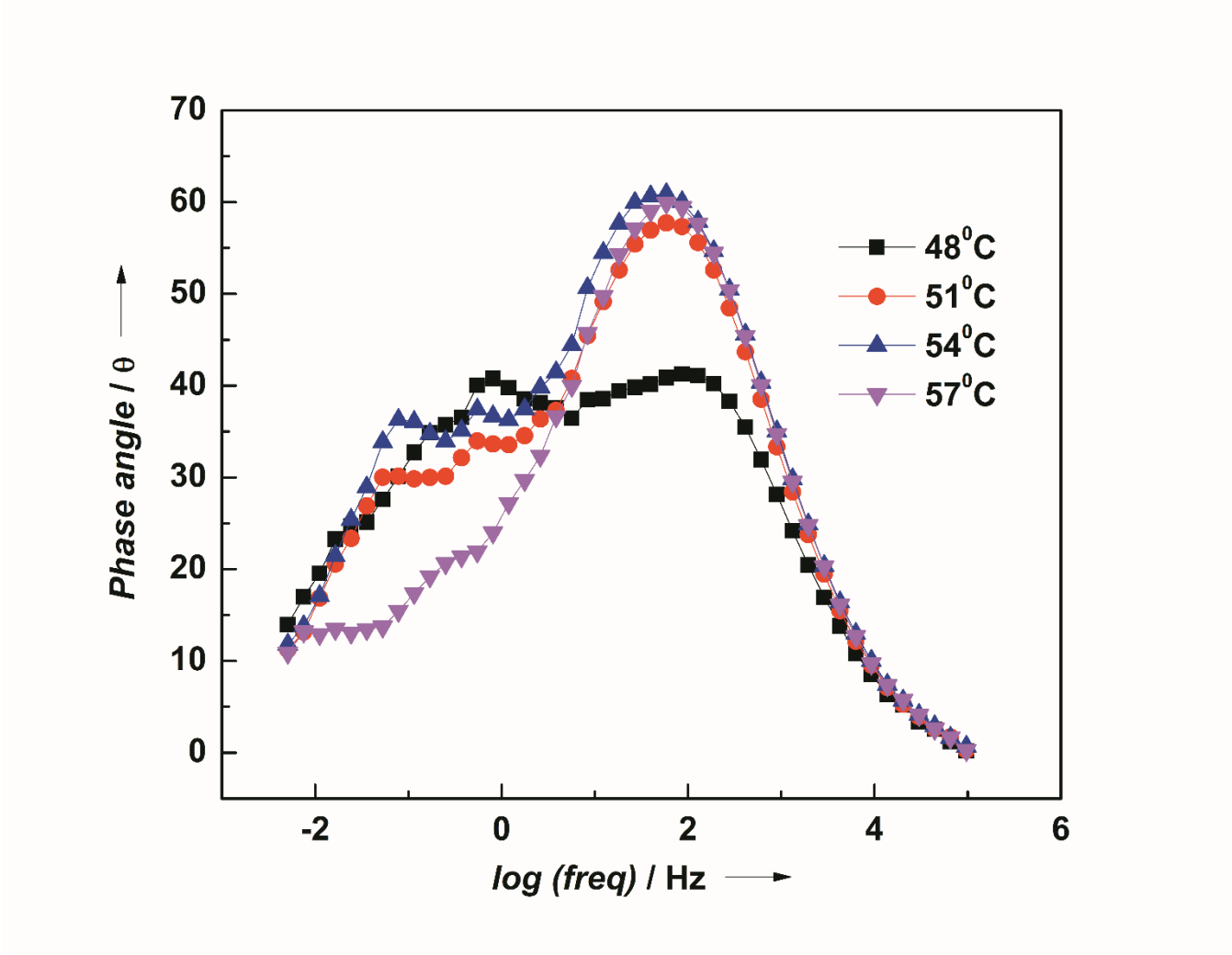

Fig 11. PEIS Spectroscopic analysis for 50% w/w OMImBr in water.

2. 1-Hexyl-2, 3-dimethylimidazolium bromide (HDMImBr)

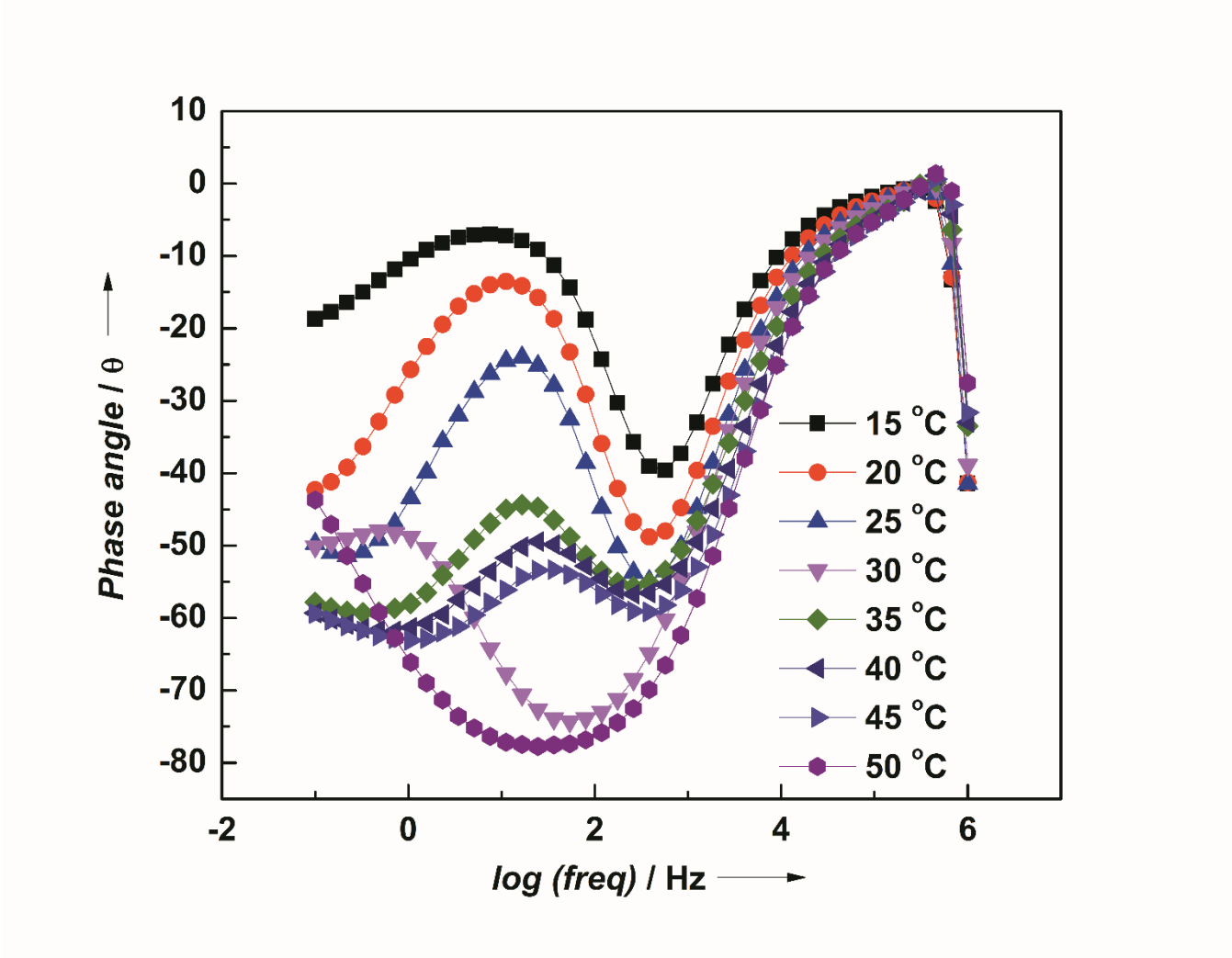

Fig. 12. PEIS Spectroscopic analysis for 50 wt% HDMImBr in water.

The experiment was carried out in the range 15 °C to 50 °C. There appeared a change in the phase angle in 30 °C (Fig. 12). Hence, HDMImBr showed LCST at 30 °C.

3. 1-octyl-3-methylimidazolium hexafluorophosphate ($OMImPF_6$)

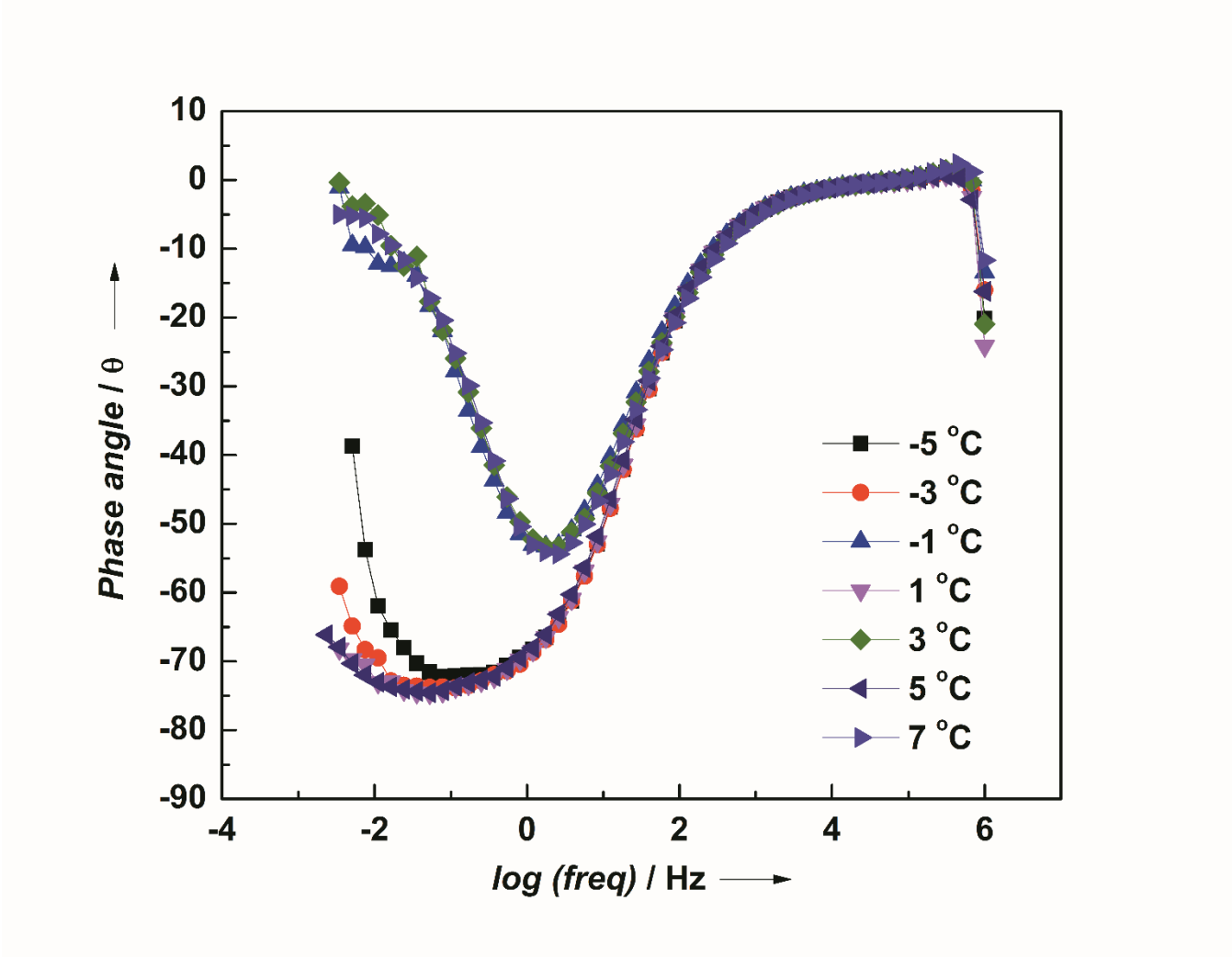

Fig. 13. PEIS Spectroscopic analysis for 50 wt% $OMImPF_6$ in water.

The experiment was carried out in the range -5 °C to 7 °C. There appeared a change in the phase angle in 1 °C (Fig. 13). Hence, this ionic liquid shows LCST at 1 °C.

4. 1-hexyl-3-methylimidazolium hexafluorophosphate ($HMImPF_6$)

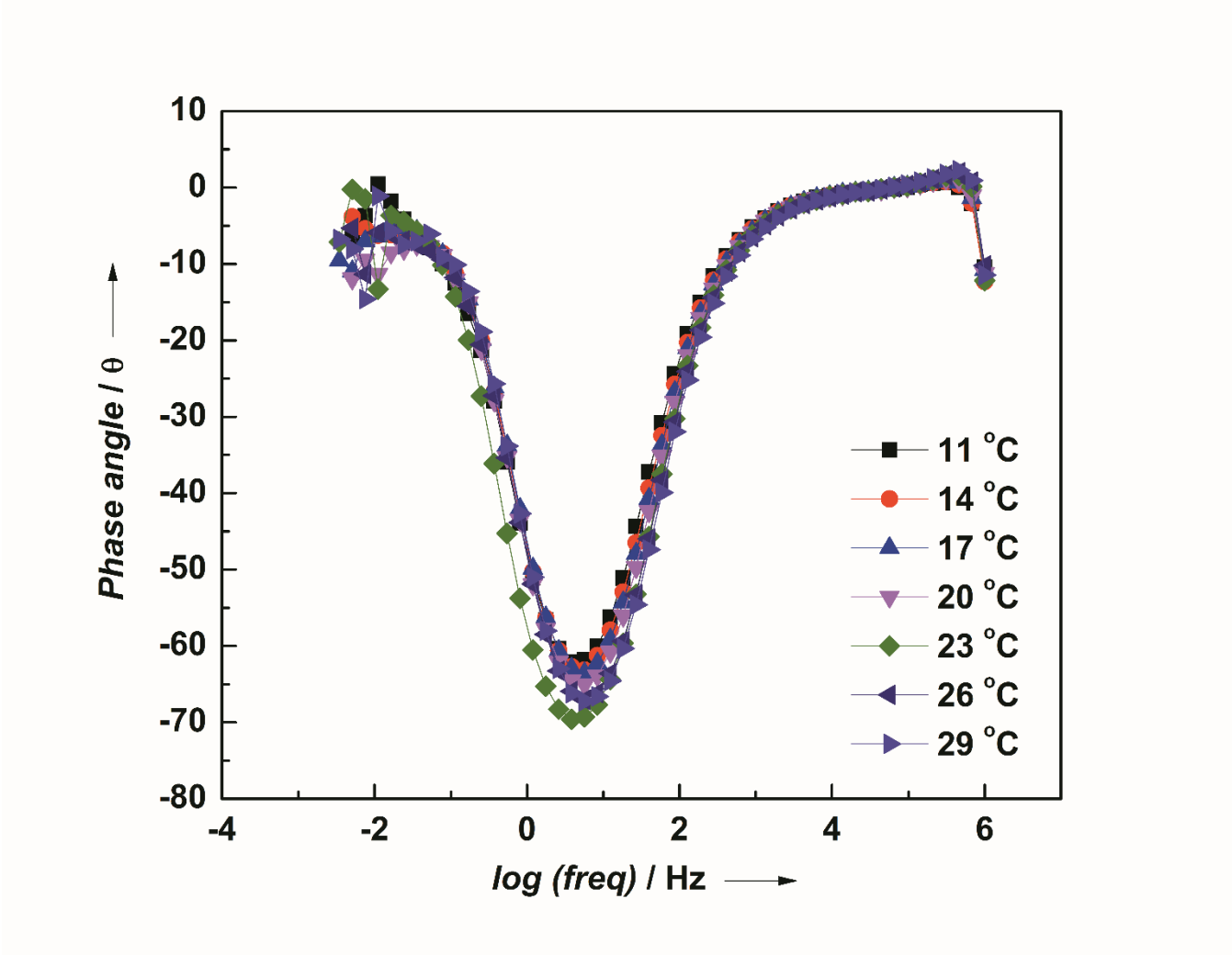

Fig. 14. PEIS Spectroscopic analysis for 50 wt% $HMImPF_6$ in water.

The experiment was carried out in the range 11 °C to 29 °C. There appeared a change in the phase angle in 20 °C (Fig. 14). Hence, this ionic liquid shows LCST at 20 °C.

Various other ionic liquid/ water and ionic liquid/salt solutions were experimented on via EIS and their LCST and UCST were recorded in the Table 2.

Table 2. Different ionic liquids tested by Electrochemical Impedance Spectroscopy

Anion	**R= Hexyl**	**R= Octyl**	**R= Allyl**
Br^-	LCST in water at 5 ^oC UCST with salt between 56 ^oC - 60 ^oC	UCST with salt at 54 ^oC	No phase transition property
PF_6^-	UCST in water between 19 ^oC - 21 ^oC UCST with salt at 2 ^oC	UCST with salt at 1 ^oC	UCST with salt at 0 ^oC

5.2.7 Conclusions- I

Various low molecular weight room temperature ionic liquids were synthesized by the addition of alkyl halide to imidazole - based compound resulting into a thick viscous liquid which was characterized by and Fourier Transformed - Infrared Spectroscopy and ^{1}H-NMR. The FT-IR spectra of all ionic liquids showed no more or less functional group peaks and were in accordance with the expected structure. ^{1}H NMR confirmed the bond formation between 1-methylimidazole and alkyl group of alkyl halide from characteristic peaks obtained in a range of 4 – 4.5 ppm.

The ionic liquid 1-hexyl-3-methylimidazolium bromide HMImBr was studied in detail. Initially, conventional visual, optical and electrochemical techniques were utilized for a system containing 50% w/w ionic liquid in water which demanded a more sophisticated and enhanced technique. Hence, electrochemical impedance spectroscopy was applied to this system for *the first time to study phase transitions*. The electrochemical analysis was done by constructing a 3-electrode cell with working and counter electrodes at platinum and reference electrode as Ag/AgCl. When frequency range of 1 MHz to 0.01 mHz was applied to the cell, bode plots were observed at various temperatures. These graphs showed a sharp change in the phase angle near the transition temperature which aided in the estimation of the LCST and UCST of a system. Also the respective bode plot values for each temperature were fitted well into an equivalent circuit, the physical meaning to which indicated the formation of separate ionic liquid and water layers in the system. Analysis for HMImBr showed that with almost negligible change with concentration, phase separation between ionic liquid and water starts at around -4 ^{o}C and is completed by 5 ^{o}C.

Thus, it is concluded that the need of a diagnostic tool to find LCST and UCST behaviour of different ionic liquids was justified by the use of ELECTROCHEMICAL IMPEDANCE SPECTROSCOPY which not only helped in finding the phase transition temperature of an ionic liquid/water system, but the curve fitting via this technique also estimated about the events occurring inside the electrolytic solution.

PART-B

5.3 Objective – II

Today, researchers are opting for IL in many fields as there are numerous possibilities of different ILs, each showing unique properties. But, when it comes to design a particular IL for a chosen application, with so many possibilities available, it is difficult to pick the right cation and anion which would show desired LCST properties. To continue the use of CST of ILs in existing and on-growing scientific fields, it is vital to comprehend the parameters playing major role in the critical behaviour of ionic liquids. Ohno et al. have explored this field and been rigorously working on mechanistic and fundamental approaches of amino acid-based ionic liquids and their phase separation[25]. Recently, Wang et al. have found out the mechanism of amino-acid based ionic liquids using molecular dynamics (MD) simulations[26]. On the same path to understand transition mechanisms, hereupon imidazolium based ionic liquids[27,28] are analysed with respect to their physical and structural properties using Kamlet-Taft parameter studies.

5.3.1 Kamlet-Taft parameters studies

To appreciate the mechanism in water-like aprotic ionic liquids, various contributing important factors[29,30] like polarity, hydrogen-bonding, chemical potential, VanderWaal's energy and density are systematically evaluated herein.

To study the fundamental approach of critical thermoresponsive behaviour in low molecular weight imidazolium-based ionic liquids, solvatochromic analysis using Kamlet-Taft parameters[31-33] were implemented in this work to understand the fundamental properties and orientation of molecules at critical temperature. UV-Visible spectroscopy was performed with three dyes namely, zwitterionic Reichardt's dye, 4-nitroaniline and *N, N*-diethyl-4-nitroaniline.

5.3.2 Experimental

A solution of appropriate dye in dehydrated methanol was prepared and added in such quantities so that the solution showed absorption between 0.1-0.4. Methanol was evaporated overnight to get dried dye-ionic liquid system with traces/no water content. Absorbance was measured in visible range.

5.3.3 Results and Discussions

To simplify the interpretation, here results are compared for LCST of 1-hexyl-3-methylimidazilum bromide (HMImBr) (Table 3) and UCST of 1-octyl-3-methylimidazolium bromide (OMImBr) (Table 4).

Kamlet-Taft parameter plots for HMImBr:

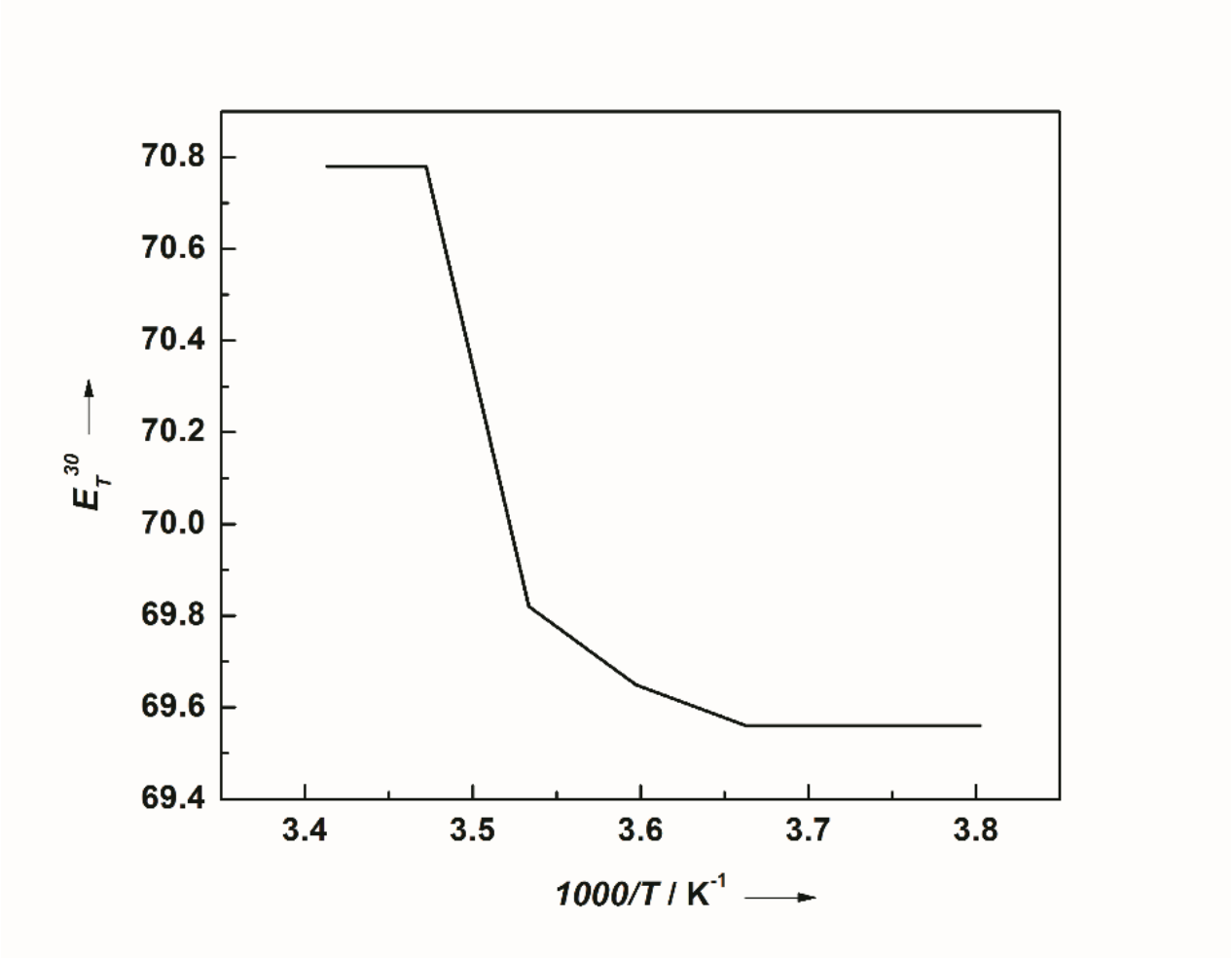

Fig. 15. Graphical representation of E_T^{30} parameter with respect to 1000/T in kelvin for HMImBr.

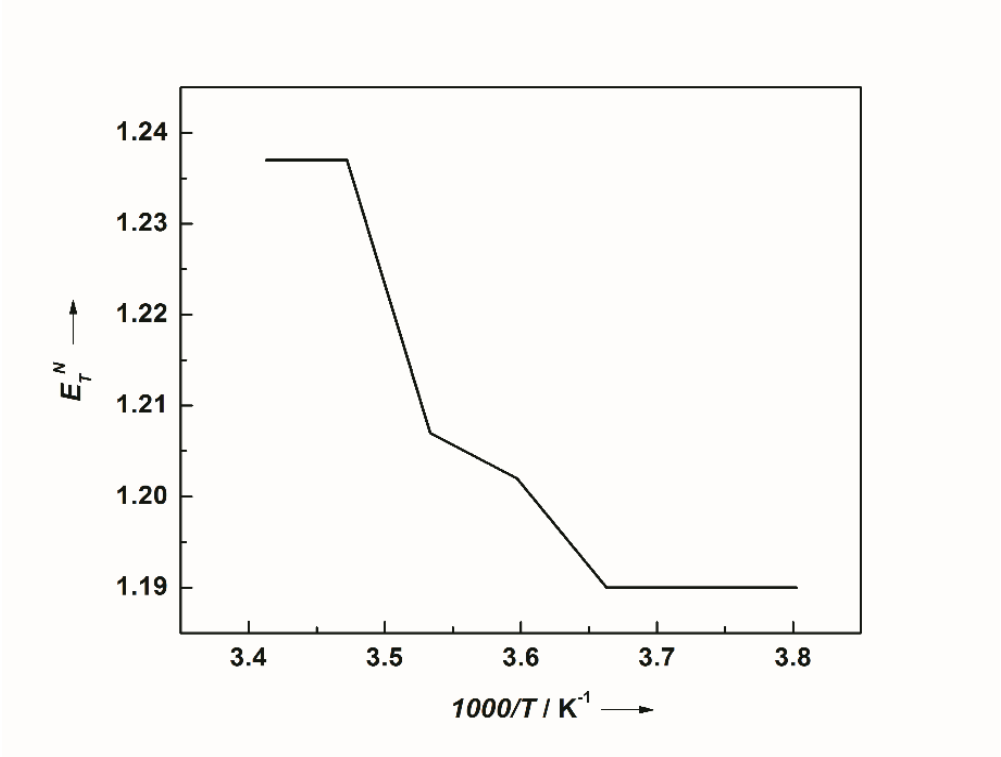

Fig. 16. Graphical representation of E_T^N parameter with respect to 1000/T in kelvin for HMImBr

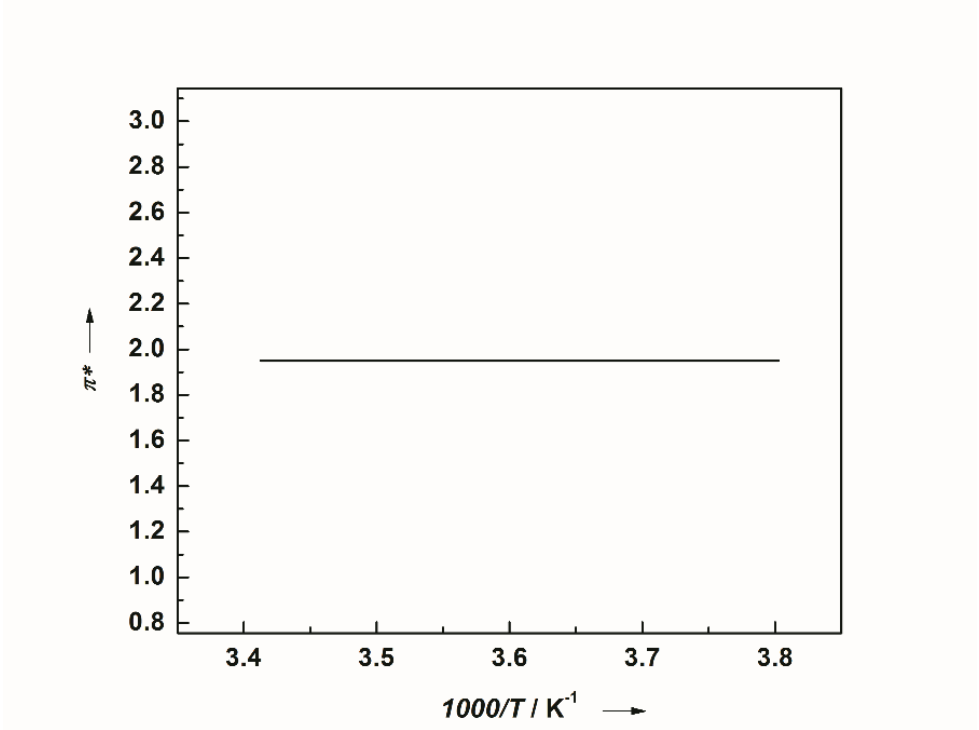

Fig. 17. Graphical representation of π* parameter with respect to 1000/T in kelvin for HMImBr.

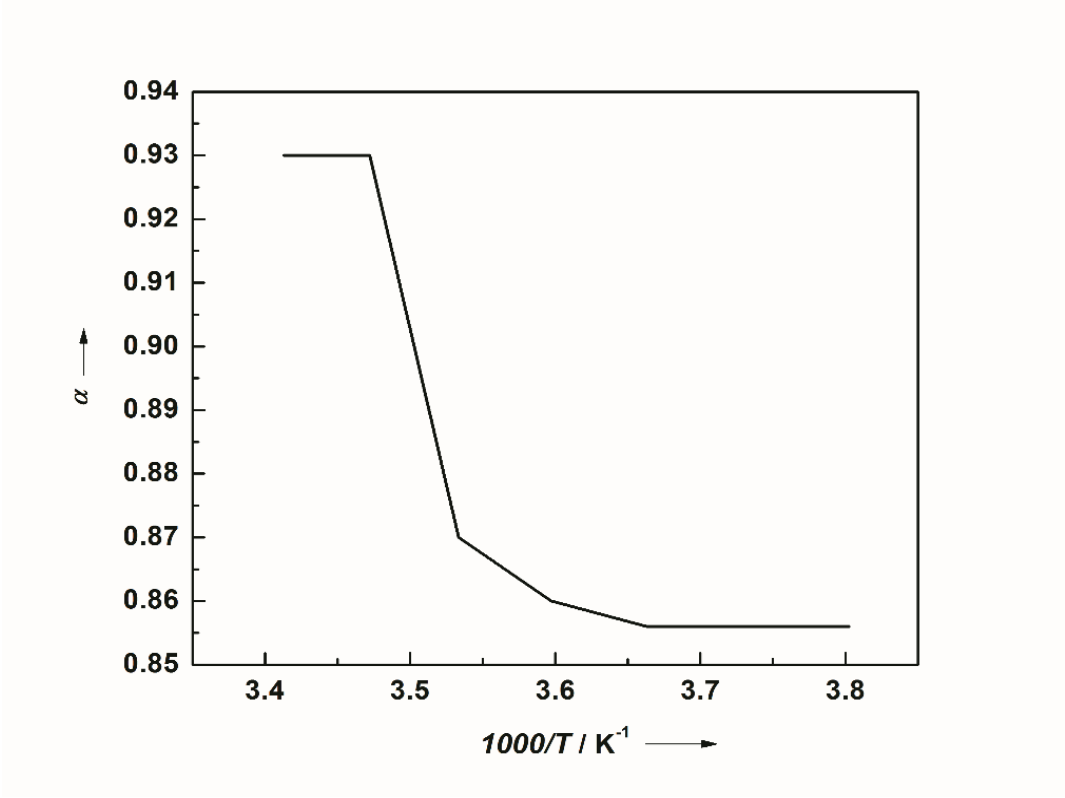

Fig. 18. Graphical representation of α parameter with respect to 1000/T in kelvin for HMImBr.

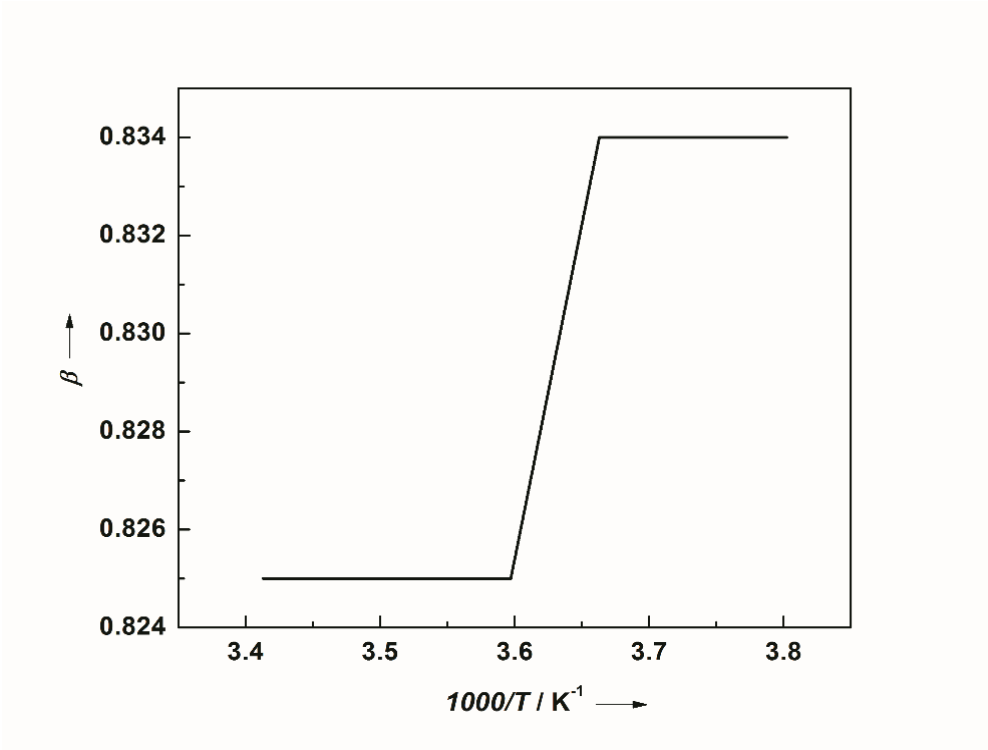

Fig. 19. Graphical representation of β parameter with respect to 1000/T in kelvin for HMImBr.

Table 3. Temperature dependent ET and Kamlet-Taft parameters for HMImBr.

Temperature(°C)	$E_T(30)$	E_T^N	π^*	α	β
-10	69.56	1.199	1.95	0.856	0.834
-5	69.56	1.199	1.95	0.856	0.834
0	69.56	1.199	1.95	0.856	0.834
5	69.65	1.202	1.95	0.862	0.825
10	69.82	1.207	1.95	0.873	0.825
15	70.78	1.237	1.95	0.930	0.825
20	70.78	1.237	1.95	0.930	0.825

It was observed that solvent polarity $E_T(30)$ and normalized polarity E_T^N starts increasing after 0 °C and the system becomes stable after 10 °C. Looking at the graph in Fig. 15. and 16., the trigger starts at 3.66 K^{-1} and the phase transition occurs at ~ 3.62-3.57 K^{-1}. Afterwards, the system achieves stabilization. This phenomenon was as expected, because initially HMImBr molecules are tightly hydrogen bonded with water and solution is in one phase. As the trigger happens, asymmetric imidazolium ring starts to dissociate from water, thereby increasing the polarity due to initiation of two phases. Between 5-10 °C, major part of phase separation occurs and HMImBr-water molecules dissociate to form two corresponding layers suggesting occurrence of LCST. After the stabilization, polarity remains unchanged as IL and water molecules have dissociated completely as the imidazolium ring of HMImBr is free from hydrogen-bonds with water.

This separation is subsequently observed as an increase in hydrogen bond donating ability (α) near the LCST point due to increased *C-2* acidic sites of imidazolium ring, which are free from hydrogen bonding with water. Thus, a decrease is observed in hydrogen bond accepting ability (β) as more of *C-2* hydrogen of ring is free from electrostatic attractions of water.

Kamlet-Taft parameter plots for OMImBr:

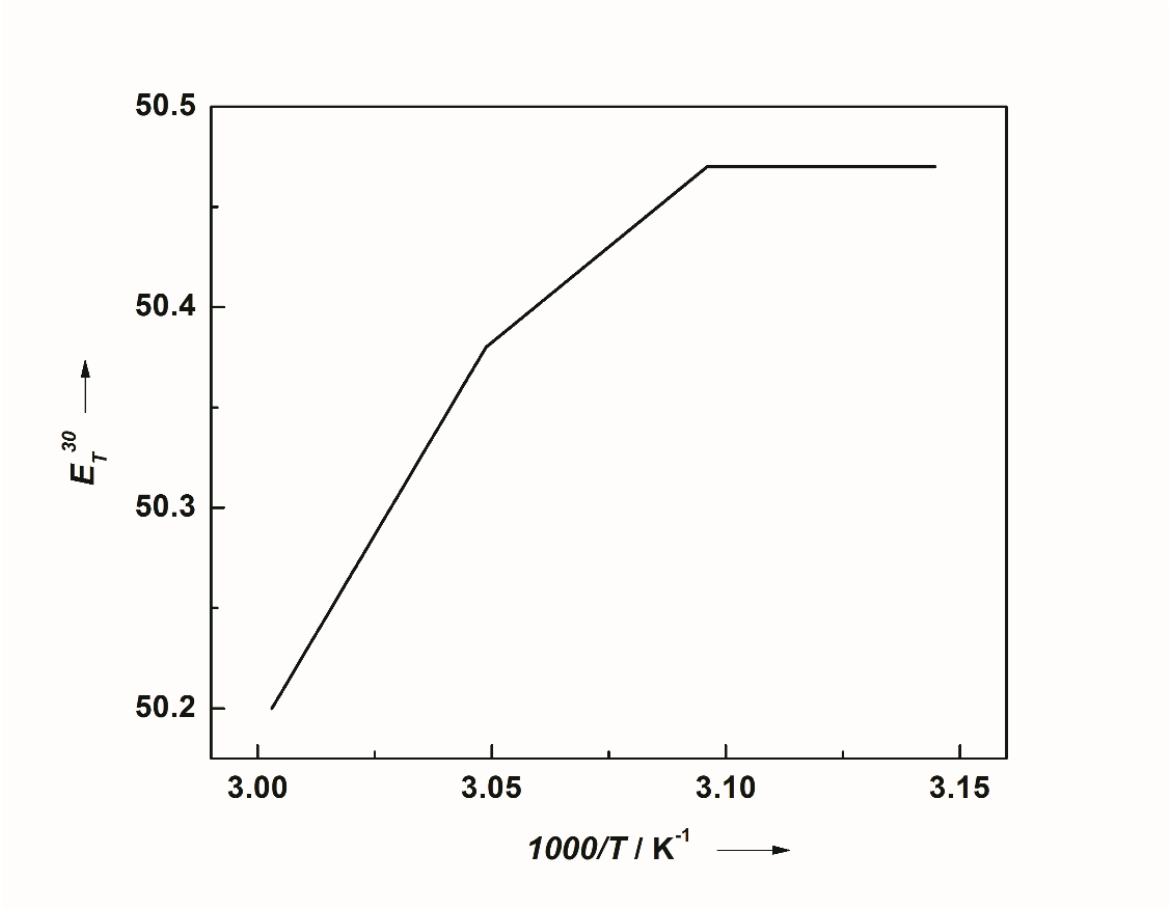

Fig. 20. Graphical representation of E_T^{30} parameter with respect to 1000/T in kelvin for OMImBr.

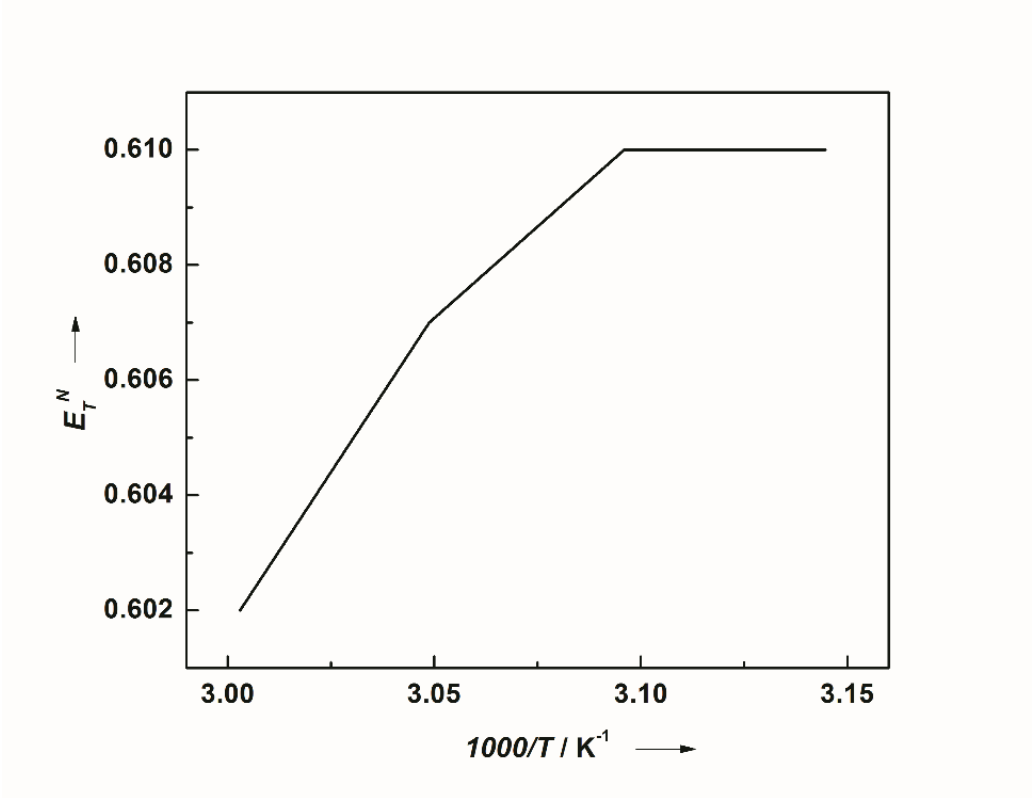

Fig. 21. Graphical representation of E_T^N parameter with respect to 1000/T in kelvin for OMImBr.

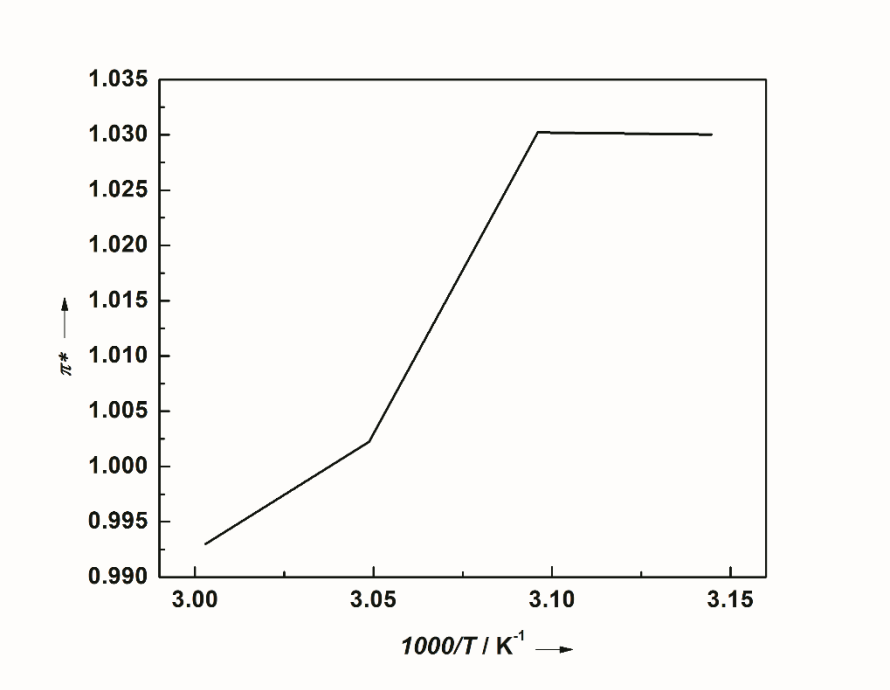

Fig. 22. Graphical representation of π* parameter with respect to 1000/T in kelvin for OMImBr.

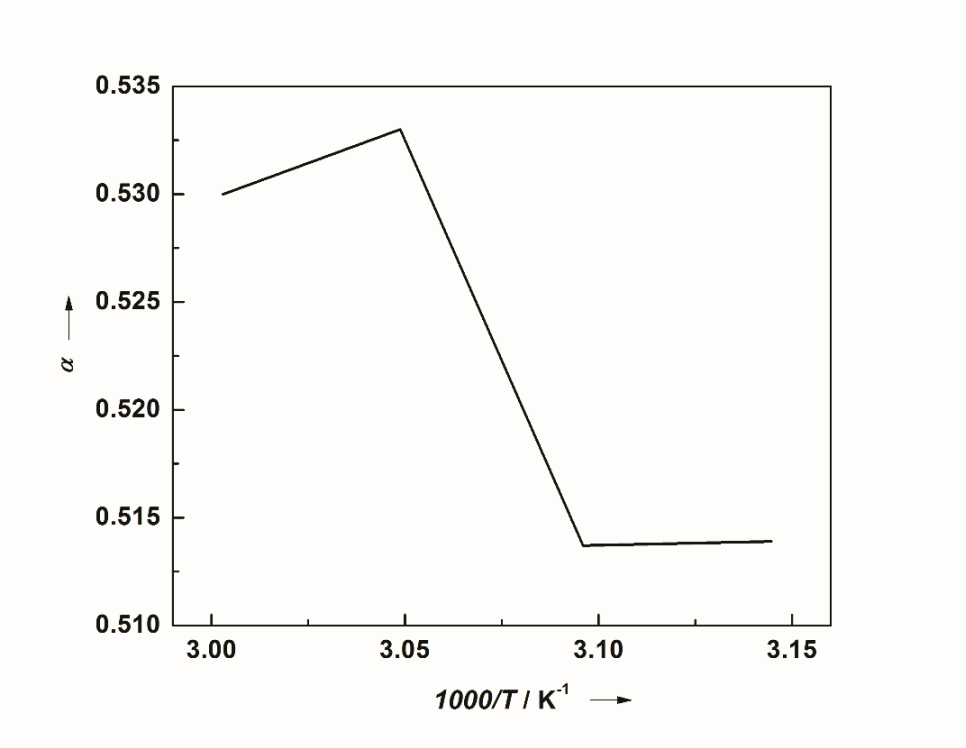

Fig. 23. Graphical representation of α parameter with respect to 1000/T in kelvin for OMImBr.

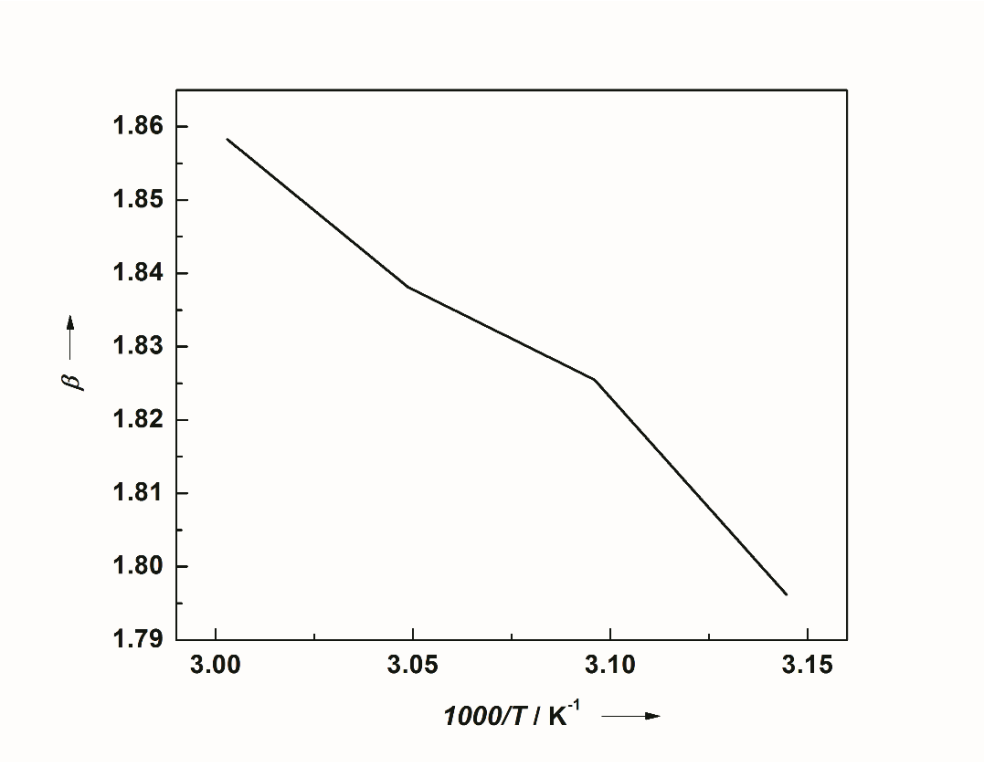

Fig. 24. Graphical representation of β parameter with respect to 1000/T in kelvin for OMImBr.

Table 4. Temperature dependent E_T and Kamlet-Taft parameters for OMImBr.

Temperature (°C)	E^T_N	$E^T_{(30)}$	π^*	α	β
45	50.47	0.610	1.030	0.514	1.796
50	50.47	0.610	1.030	0.514	1.826
55	50.38	0.607	1.002	0.533	1.838
60	50.20	0.602	0.999	0.530	1.858

Comparing the results with OMImBr (Table 2), the solvent polarity E^T_N of OMImBr was decreased with increase in temperature. This can be possible only when the polar sites of the ring are closed or may have bonded with water after phase transition. This suggest that OMImBr shows UCST. The trigger starts at 50 °C and transition occurs at ~55 °C. Before the transition, water and imidazolium ring remains separated. This is seen by a lower β values which suggest that less of hydrogen accepting ability is present in the imidazolium ring. After the transition, *C-2* hydrogen of imidazolium ring is present in electrostatic field of oxygen of water making the β value to increase. Polarity shows a decreasing trend as the two solutes are now in unity via hydrogen-bonding. Hence, it was seen that OMImBr exhibit UCST at 55 °C.

5.3.4 Conclusions- II

Kamlet-Taft parameters studies were done for LCST showing ionic liquids like HMImBr and UCST showing ionic liquids like OMImBr. It was seen that the major factors affecting the critical phase behaviour of these green solvents are solvent polarity, hydrogen bond donating ability and hydrogen bond accepting ability.

For LCST showing ionic liquids, polarity and hydrogen bond donating ability increases at the critical state and the hydrogen-bond accepting ability decreases.

For UCST showing ionic liquids, polarity and hydrogen bond donating ability decreases at the critical state and the hydrogen-bond accepting ability increases.

Hence, I was able to find the dominant factors playing vital roles in the occurrence of CST phenomenon and their mechanistic relationship between them at the phase transitions.

PART-C

5.4 Objective – III

Till date, designing of an ionic liquid with fine-tuned properties is a time-taking and tough method. It becomes hard to pick the right cation and anion which would show desired CST property. Henceforth, it would be rather apt to generalize the concept of transition for these ionic liquids via simulations.

5.4.1 COSMO-RS Simulations

Conductor-like screening model for realistic solvents or COMSO-RS simulations[34,35] are based on a continuum model which treats solute surrounded by the solvent particles as a packet of continuous conductor, allowing the evaluation of the chemical potentials of water-cation-anion ternary mixture and identify the chemical equilibrium point a lot easier and precise. The simulations are superior as compared to ones already being used as it calculates the electrostatic interactions between the solute and the solvent particles. It was introduced by Andreas Klamt[36] in 1995. It acts as a database of unique combination of quantum chemical treatments of solute and solvents under same parameters. Evaluation and identification of liquid-liquid equilibrium using COSMO-RS[37] is proven to be the most reliable and fastest type of calculation available till now.

5.4.2 Experimental

COSMOTherm program is used to compute chemical potential, Gibbs free energies, H-bond energies, van der Waal energies and densities. The cationic imidazolium ring, anion and water were treated as individual components to compose a 50 mol% solution. Obtained values were plotted against temperature. The slopes of the graphs were tabulated to produce a prediction table.

5.4.3 Results and Discussions

For the simulation calculations, parameters like chemical potential, hydrogen bond energies, Van der Waal energies and density were calculated in the transition range for various ionic liquids. Linear profiles were obtained for all graphs, as expected for an increase in temperature. However, scrutinizing the slopes of these lines, a unique and interesting observation was made as tabulated in Table 5. If an IL has high chemical potential (vs *T)* slope (>0.0165), it will either remain soluble or insoluble with water at all temperatures. This means that IL will show neither LCST nor UCST. This is probably because, with such a high increase in chemical potential with temperature, there is no tendency of IL to exhibit any kind of transition. But, if chemical potential of the IL-water system has intermediate values (0.008-0.0165), it can show either LCST or UCST as chemical potential increases with temperature in optimum. Then, the type of transition will be known looking at the values for slopes of H-Bond (vs *T*) and Van der Waal energies (vs *T*) as these are the major factors governing the particular transition. If slope of H-bond energy (vs *T*) is intermediate and slope of Van der Waals energy (vs *T*) is high, then that IL shows LCST. And, if the slope of H-bond energy (vs *T*) is higher but slope of Vander

Waal's energy (vs *T*) is lower, then that IL show UCST behaviour. One valid reasoning behind this observation could be that separation needs a higher slope of VanderWaal's energy. Moreover, for UCST to be shown, ions need to overcome the electrostatic field of water, thus require a higher slope for H-bond energy. Hence, incorporating simulations can aid in prediction of nature of transition exhibited by low-molecular imidazolium based ionic liquids.

Table 5. COSMO-RS simulations representing slopes for chemical potential, hydrogen bond and Van der Waal energies for different ILs.

Ionic Liquid	Short Name	CST property	Slope of μ vs *T / J mol-1*	Slope of H-bond vs *T / J mol-1*	Slope of VdW vs *T / J mol-1*
1-ethyl-3-methylimidazolium bromide	EMImBr	None	0.0169	0.0107	0.0003
1-propyl-3-methylimidazolium chloride	PMImCl	None	0.0191	0.0079	0.0004
1-hexyl-3-methylimidazolium bromide	HMImBr	LCST at 5 ^{o}C	0.0132	0.0163	0.0007
1-hexyl-2,3-dimethylimidazolium bromide	HDMImBr	LCST at 30 ^{o}C	0.0114	0.0162	0.0009

1-butyl-3-methylimidazolium chloride	BMImCl	LCST	0.0133	0.0152	0.0007
1-octyl-3-methylimidazolium bromide	OMImBr	UCST at 54 ^{o}C	0.0097	0.0156	0.0011
1-octyl-3-methylimidazolium hexafluorophosphate	OMImPF_6	UCST at 1 ^{o}C	0.0151	0.0211	0.0002
1-hexyl-3-methylimidazolium hexafluorophosphate	HMImPF_6	UCST at 20 ^{o}C	0.0135	0.0234	0.0004
1-butyl-3-methylimidazolium tetrafluoroborate	BMImBF_4	UCST at 4.4 ^{o}C	0.0149	0.0192	0.0003

5.4.4 Conclusions- III

COSMOTherm proved to be an interesting tool to prepare a prediction table for the CST in ionic liquids. If an IL has high chemical potential, it will either remain soluble or insoluble with water at all temperatures. This means that IL will show neither LCST nor UCST. But if chemical potential of the IL-water system has intermediate values, it can either show LCST or UCST. If slope of H-bond energy vs temp is intermediate and slope of vanderWaals energy is high, then that IL shows LCST. But, if the slope of H-bond energy vs temp is higher but slope of vanderWaals energy is lower, then that IL show UCST

behaviour. So, once we know these values, we can easily predict the nature of any IL, whether it will be an LCST showing, UCST showing or non-CST showing IL.

5.4.5 Chapter conclusions

Fig. 25. Graphical illustration showing high electrochemical aspects of synthesized gel electrolyte.

Focussing together on Kamlet-Taft, impedance studies and COSMO-RS simulations, one can compliment the critical nature of low-molecular weight imidazolium-based ILs in a more comprehensive manner. For ILs which has similar polarity to water (E^T_N near 1), it is seen that chief parameters effecting critical thermoresponsive behaviour of ILs are polarity, chemical potential, hydrogen-bond energy, hydrogen-bond donating and accepting ability and Van der Waal's energy. All these factors correspond to the structural aspects of the imidazolium cation and anion. Together, optimum ratio of hydrophobicity/hydrophilicity is constituted which shows CST. Structure analysis suggests that both cation and anion influence the polarity and Kamlet Taft parameters. For LCST showing IL, polarity, capacitance and α increases and β decreases. Vice-versa happens for UCST showing IL. COSMO-RS results demonstrated that LCST is shown when Vander Waal forces dominate, while UCST is shown when H-Bonding is dominant over other factors. Also, the simulations summarized the rule to predict the nature of CST of low-molecular weight imidazolium based ionic liquids which can be extended further to various other categories of ionic liquids. This will save ample time in synthesizing and help in analyzing the fine-tuned and exclusive ionic liquid with desired and characteristic properties (graphical abstract Fig. 25).

5.4.6 References

[1] Z. Lei, B. Chen, Y.M. Koo, D. R. MacFarlane, *Chem. Rev.* 2017, *117*, 6633–6635.

[2] H.-K. Lim, H. Kim, *Molecules* 2017, *22*, 536-552

[3] P. S. Stayton, T. Shimoboji, C. Long, A. Chilkoti, G. Ghen, J. M. Harris, A. S. Hoffman, *Nature* 1995, *378*, 472–474.

[4] G. Fundueanu, M. Constantin, P. Ascenzi, *Int. J. Pharm.* 2009, *379*, 9- 17.

[5] J. Gorke, F. Srienc, R. Kazlauskas, *Biotechnol. Bioprocess Eng.* 2010, *15*, 40–53.

[6] R. Liu, M. Fraylich, B. R. Saunders, *Colloid Polym. Sci.* 2009, *287*, 627–643.

[7] A. S. Hoffman, *Artif. Organs* 1995, *19*, 458–467.

[8] Y. Kohno, H. Ohno, *Chem. Commun.* 2012, *48*, 7119-7130

[9] E. Choi, A. Yethiraj, *Acs Macro Lett.* 2015, *4*, 799–803.

[10] F. Faridbod, M. Reza, P. Norouzi, S. Riahi, H. Rashedi, Application of Room Temperature Ionic Liquids in Electrochemical Sensors and Biosensors, 2011, pp. 643-660.

[11] H. Passos, A. Luís, J. A. P. Coutinho, M. G. Freire, *Sci. Reports* 2016, *6*, 20276-20282.

[12] G.-R. Zhang, M. Munoz, B. J. M. Etzold, *ACS Appl. Mater. & Interfaces* 2015, *7*, 3562–3570.

[13] J. Flieger, E Grushka, A. C. Żelazko, *Aust. J. Anal. Pharm. Chem.* 2014, 1, 1-8

[14] M. Heskins, J. E. Guillet, *J. Macromol. Sci. Part - Chem.* 1968, *2*, 1441- 1455.

[15] M. Koyama, T. Hirano, K. Ohno, Y. Katsumoto, *J. Phys. Chem. B* 2008, *112*, 10854–10860.

[16] Y. Fukaya, H. Ohno, *Phys. Chem. Chem. Phys.* 2013, *15*, 4066-4072.

[17] Y. Kohno, H. Arai, S. Saita, H. Ohno, *Aust. J. Chem.* 2011, *64*, 1560-1567

[18] S. N. V. K. Aki, J. F. Brennecke, A. Samanta, *Chem. Commun.* 2001, 413–414

[19] S. Shahidi, C. R. Koch, S. Bhattacharjee, M. Sadrzadeh, *Sensors Actuators B: Chem.* 2017, *243*, 460–464.

[20] S. Ghasemi, M. T. Darestani, Z. Abdollahi, V. G. Gomes, *Polym. Int.* 2015, *64*, 66–75.

[21] R. Fortunato, L. C. Branco, C. A. M. Afonso, J. Benavente, J. G. Crespo, *J. Membr. Sci.*

2006, *270*, 42–49.

[22] Lvovich, V. F. *Impedance Spectroscopy: Applications to Electrochemical and Dielectric Phenomena*; John Wiley & Sons, Inc.: Hoboken, NJ, 2012, pp. 1-96.

[23] Ohno, H. *Electrochemical Aspects of Ionic Liquids*; John Wiley & Sons:Hoboken, NJ, 2005, pp. 55-74.

[24] J. Dupont, C. S. Consorti, P. A. Suarez, R. F. de Souza, *Org. Synth.* 2003, 79, 236-243.

[25] K. Fukumoto, M. Yoshizawa, H. Ohno, *J. Am. Chem. Soc.* 2005, *127*, 2398–2399.

[26] Y. Zhao, H. Wang, Y. Pei, Z. Liu, J. Wang, *Phys. Chem. Chem. Phys.* 2016, *18*, 23238–23245.

[27] C. P. Fredlake, J. M. Crosthwaite, D. G. Hert, S. N. V. K. Aki, J. F. Brennecke, *J. Chem. & Eng. Data* 2004, *49*, 954–964.

[28] J. L. Anthony, E. J. Maginn, J. F. Brennecke, *J. Phys. Chem. B* 2001, *105*, 10942–10949.

[29] R. Hayes, S. Imberti, G. G. Ware, R. Atkin, *Angew. Chem*. 2013, 125, 4721 – 4725; *Angew. Chem. Int. Ed*. 2013, 52, 4623 – 4627.

[30] J. M. Slattery, C. Daguenet, P. J. Dyson, T. J. S. Schubert, I. Krossing, *Angew. Chem*. 2007, 119, 5480 – 5484; *Angew. Chem. Int. Ed. Engl*., 46, 5384 – 5388.

[31] M. A. Ab Rani, A. Brant, L. Crowhurst, A. Dolan, M. Lui, N. H. Hassan, J. P. Hallett, P. A. Hunt, H. Niedermeyer, J. M. Perez-Arlandis, et al., *Phys. Chem. Chem. Phys.* 2011, *13*, 16831-168490.

[32] J. M. Lee, S. Ruckes, J. M. Prausnitz, *J. Phys. Chem. B* 2008, *112*, 1473–1476.

[33] D. J. Eyckens, B. Demir, T. R. Walsh, T. Welton, L. C. Henderson, *Phys. Chem. Chem. Phys.* 2016, *18*, 13153–13157.

[34] A. Klamt, F. Eckert, W. Arlt, *Annu. Rev. Chem. Biomol. Eng.* 2010, *1*, 101–122.

[35] R. Anantharaj, T. Banerjee, *Ind. & Eng. Chem. Res.* 2010, *49*, 8705–8725.

[36] A. Klamt, *J. Phys. Chem.* 1995, *99*, 2224–2235.

[37] D. S. Boucher, *Colloids Surfaces A: Physicochem. Eng. Asp.* 2015, *487*, 207–213.

****

Chapter 6

Conclusions

6.1 General Conclusions

Stimuli responsive properties of smart polymers have gained much attention in the recent past. Over the top, thermosensitive materials have already rendered much applications in the field of biomedical and chemistry with highly importance projected in the future than it has ever been in the past. Nowadays, environmentally benign "green" solvents ionic liquids with their enormous database of distinguished cationic and anionic counterparts have enabled the researchers over the globe to invest more time into their future applications. There have been reports about ionic liquids showing thermoresponsive properties as well, in addition to polymers. Considering the vitality of these smart materials, the present research will be addressing synthesis and study of thermoresponsive properties of various polymer-based/ ionic liquid based/ and their copolymer based materials and their tunability over critical solution temperatures.

In **Chapter 1**, the introduction of thermoresponsive property with respect to polymers and ionic liquids are discussed in detail. With a brief introduction about thermoresponsive phase transitions and its types, mechanism to critical solution temperature (CST) and applications corresponding to CST have been discussed. Some of the important literatures which prove the importance of phase tuning of polymers were also reported. The chapter also focuses on, introduction about polyoxazolines as a non-toxic polymer and its advanced applications in biomedical field. And how polyoxazolines can be successful in tuning and creating solid-supported LCST showing materials is provided in brief. Two approaches were studied, one to form organic-inorganic hybrids and second to coat as thin films over silicon substrates. Next, properties, challenges and applications of hydrogels is concentrated upon. Why plasmonic nanoparticles can serves as tuning agents for thermoresponsive polymer matrix and their primary characteristics were looked upon in detail. Finally in the later half, the CST in ionic liquids is focused upon and properties/applications of ionic liquid/water mixtures have been discussed thoroughly. The detailed description of why there is a need for a diagnostic tool to analyze CST in ionic liquids, and major factors affecting CST have also been included in this chapter.

In **Chapter 2**, the research is directed towards improving the tuning of LCST behaviour of oxazoline based thermoresponsive copolymer and creating a solid-supported hybrid materials. In this context, a copolymer of 2-ethyl-2-oxazoline and 2-isopropyl-2-oxazoline was synthesized by ring opening polymerization which showed LCST at 77 °C as detected by DSC. Further, TMOS was chosen as the inorganic precursor to form organic-inorganic hybrids. Samples with varied ratio of copolymer and silicate moiety were prepared and their LCST and tunability were analysed. The LCST of the synthesized hybrid materials could be tuned over a temperature range from 42-58 °C. A typical concave-up type phase diagram was obtained suggesting the dependence of LCST on the copolymer concentration in the hybrid system. (Graphical abstract **Fig. 1**).

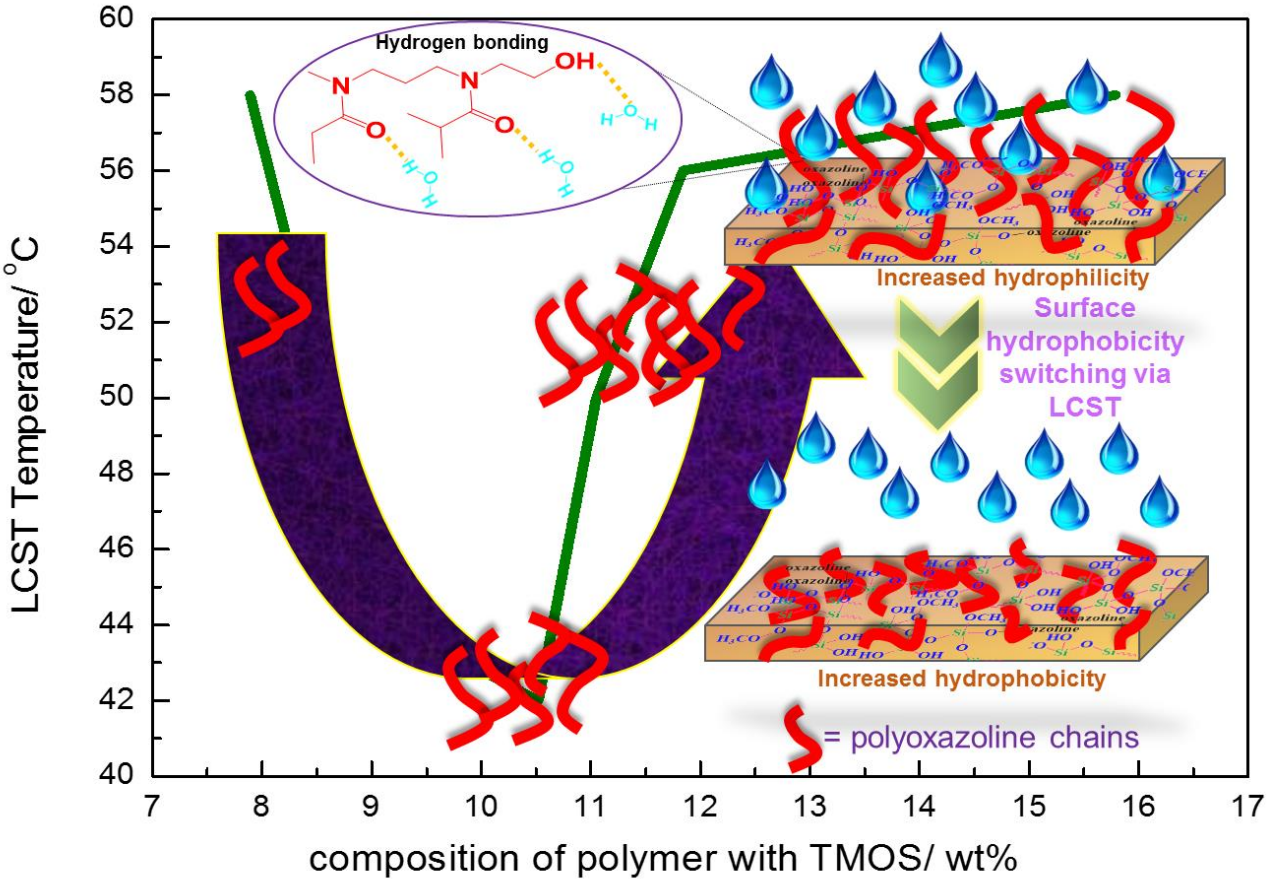

Fig. 1. Graphical illustration of fine-tuning of LCST of polyoxazoline based copolymer using inorganic silicate material.

Chapter 3 describes a yet another method to form solid-supported LCST showing materials utilizing silicon wafers and polyoxazoline as the thermoresponsive material. In this work, silicon wafers were exposed to extreme acidic conditions to covalently bind with the thermosensitive polymer of 2-ethyl-2-oxazoline. The polymer was terminated with triethoxysilyl group to enhance the surface bonding abilities. The formation of self-assembled monolayers of the thermoresponsive polymer was confirmed using FT-IR and XPS analysis. The coated surface become hydrophobic as seen by the contact angle measurements. DSC showed that the LCST of the modified polymer was 75 °C. The system was observed to work as a solid-supported phase gradient (Graphical abstract **Fig. 2.**).

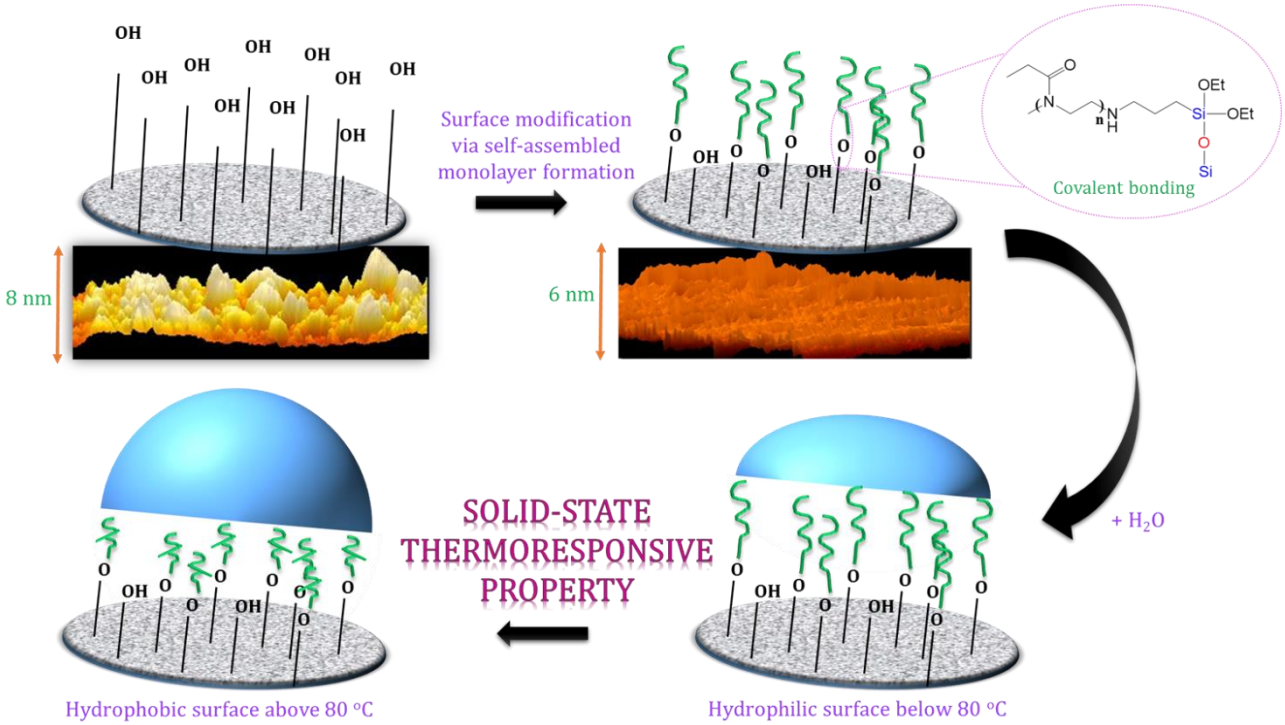

Fig 2. Graphical illustration showing solid-supported thermoresponsive polymer modified silicon wafer for thermal devices.

Chapter 4 includes the synthesis of novel plasmonic nanoparticles (like Au and Ag) embedded thermally sensitive PNIPAM-based hydrogels. In this chapter, imidazolium-based polymerizable ionic liquids solvents as copolymers were used. Synthesis of gold and silver nanoparticles was done using trisodium citrate as the primary reducing and stabilizing agent, and the size was varied from 10 - 45 nm. The hydrogels formed were studied for their factors like size of NPs and effect of ionic liquid structure on its LCST. The results were consistent for both types of nanoparticles. The hydrogels possessed the swelling and shrinking abilities below and above LCST, respectively. The work made the LCST tuning for these hydrogels matrixes over a wide temperature range of 23 – 67 ^{o}C. (Graphical abstract **Fig. 3.**).

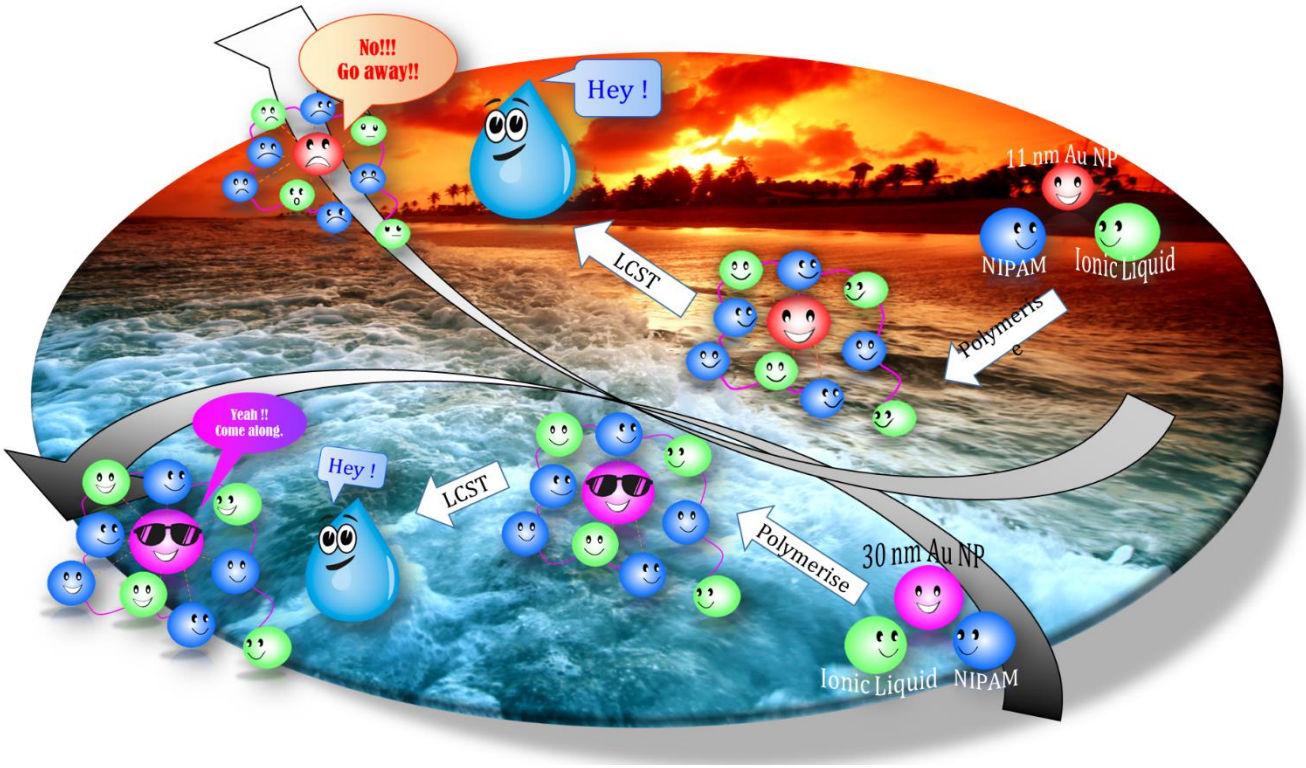

Fig 3. Graphical abstract representing the role of nanoparticle size in the nanoparticles embedded PNIPAM based hydrogels using polymerized ionic liquids.

Lastly, focus was made to study liquid-liquid phase systems. It has been known that some imidazolium-based ionic liquids show LCST in water. However, it became difficult to detect CST in room-temperature low molecular weight imidazolium-based ionic liquids. Therefore, **Chapter 5** deals with the study as to why previous techniques fail in the detection and finding of a diagnostic tool to evaluate LCST and UCST of ionic liquids. A more advance, superior and informative technique which is electrochemical impedance spectroscopy was used as the diagnostic tool to evaluate the phase transition temperature as clear visualization of the separation cannot be observed optically. Major factors affecting the CST in these ionic liquids were also detected by Kamlet-Taft parameter studies. Moreover, a structure-activity relationship table was also constructed based on factors like Gibbs free energy change, hydrogen-bond energy change and van der Waals energy change as scrutinized by COSMO-RS simulations. It helped to foresee the type of the phase transition phenomenon showed by the ionic liquid (Graphical abstract **Fig. 4**).

Hence, This thesis work present various strategies to fine-tune the phase transitions of various thermoresponsive organic-inorganic hybrid systems. In this work, it is seen that phase transitions of thermoresponsive oxazolines can be tuned by modifying them into organic-inorganic hybrids using tetramethylorthosilicate or by forming their self-assembled monolayers over silicon wafer. Thermoresponsive PNIPAM polymer can be fine-tuned using polymerizable ionic liquids and/or metal nanoparticles. Also, the thesis present a diagnostic tool in the form of Electrochemical Impedance spectroscopy to detect phase transitions in imidazolium-based ionic liquids.

Fig 4. Graphical illustration showing factors affecting phase transitions in imidazolium-based ionic liquids.

6.2 Possible future of research

The primary aim of this thesis work was to focus on the thermosensitivity and tunability of various polymer and ionic liquid systems. Literatures have shown the importance of temperature driven phase transitions and their utilization to widespread applications in science via fabrication of thermal devices.

The results shown in the thesis opens up wide range of strategies and aspects to prepare innovative thermoresponsive smart materials with enhanced properties. It also provide with the ability to tune phase transitions of these materials for the fabrication of smart and intelligent thermal devices. Apart from the results reported in this work, there is still a room for improvement and extension. Some of the possible future research interests can be as follows:

1. Formation of TMOS based sol-gel materials using polyoxazoline and their tunability was studied in Chapter 2 by varying the copolymer concentration only. However, studies can also be done with another inorganic materials like various metal oxides or carbon based materials.
2. Silicon wafer modifications as seen in Chapter 3 can be further studied for creation of a high-density monolayer formation with a variety of classes of LCST showing materials such as ionic liquids.
3. The synthesis of novel plasmonic nanoparticles into PNIPAM-co-ionic liquid matrix in chapter 4 open up a whole new avenue of possibilities where these materials can be used. Because of the presence of thermoresponsive properties of PNIPAM, stabilizing and begin ionic liquids and nanoparticles, the applications of these materials bridge between various fields. The work still has the scope to be

studied for other type of pure (copper) or alloy nanoparticles. How chances in the ratio of these three moieties affect the LCST and tunability can be very interesting to note. Synthesis can also be done by different amino-acid based or ammonium based ionic liquids to further enhance the applications of these matrix materials as hydrogels.

4. Detection of estimated/accurate phase transition temperature of room temperature imidazolium-based ionic liquids can also become an interesting but vigorous simulating approach. It will help to create database of future referrals and save ample time and energy for detection of innumerable possible ionic liquids.

List of achievements and presentations at international/domestic conferences

Publications

1. **Surabhi Gupta**, Tomoharu Kataoka, Masao Watanabe, Mamoru Ishikiriyama and Noriyoshi Matsumi, "Fine-Tuning of LCST behavior of oxazoline copolymer based organic-inorganic hybrids as solid-supported sol-gel materials", J. Appl. Polym. Sci. **2019**, *136*, 48163.

Submitted:

[1] **Surabhi Gupta**, Ankit Singh and Noriyoshi Matsumi, "Controlled phase behaviour of thermally sensitive poly(N-isopropylacrylamide/ionic liquid) with embedded Au nanoparticles", submitted.

To be submitted:

[1] **Surabhi Gupta**, Kamiya Jain, Raman Vedarajan, Masaki Watanabe, Mamoru Ishikiriyama and Noriyoshi Matsumi* "Evaluation of phase transitions in imidazolium-based ionic liquid/water system using Impedance Spectroscopy and Kamlet-Taft parameter studies", to be submitted.

Patents

1. **JAPANESE PATENT** [Details: submission ID: 2014-178542; Authors: Masaki Watanabe (TOYOTA), Mamoru Ishikiriyama (TOYOTA), Noriyoshi Matsumi (JAIST), Raman Vedarajan (JAIST), **Surabhi Gupta (JAIST)**, Kamiya Jain (JAIST); Applicants: TOYOTA motor corporation, JAIST; Date of Submission, Sep 2, 2014; Title of invention: Water vapor emitting materials, and analytical methods of LCST behavior.]
2. **UNITED STATES (U.S) PATENT** [Pub No.: US2016/0059212 A1, Date of publication: Mar.3,2016, Title of invention: Water vapor emitting materials, and analytical methods of LCST behavior.]

Awards

1. **Best poster Award**: Energy & Environmental Science Poster Award by RSC, UK while presenting the work: Gold NPs Incorporated Thermo-sensitive Materials Using PNIPAM and Polymerizable Ionic Liquids in ISPE, Yokohama, 2018.

International Conferences

1. **Poster: Surabhi Gupta**, Noriyoshi Matsumi, "Gold NPs Incorporated Thermo-sensitive Materials Using PNIPAM and Polymerizable Ionic Liquids", **The 16th International Symposium on Polymer Electrolytes (ISPE-16)**, Yokohama, Japan, June 2018.
2. **Poster: Surabhi Gupta**, Noriyoshi Matsumi, "Thermo-sensitive chromic materials using thermosensitive polymer and ionic liquid", **255th ACS National Meeting & Exposition**, New Orleans, USA, March 2018.
3. **Oral:** Raman Vedarajan, Kamiya Jain, **Surabhi Gupta**, Masaki Watanabe, Mamoru Ishikiriyama, Noriyoshi Matsumi, "Application of impedance spectroscopy as a tool to identify critical temperature in thermoresponsive materials", ***Pacifichem*** 2015, Honolulu, Hawaii, USA, December 15-20, 2015.

Domestic Conferences

1. **Poster: Surabhi Gupta**, Noriyoshi Matsumi, Effect of Gold Nanoparticles Deposition on LCST Behavior of PNIPAM-Polymerized Ionic Liquid Copolymers, **Chemical Society of Japan (CSJ)**, Toyama, Japan, 2018**.**
2. **Poster**: **Surabhi Gupta,** Noriyoshi Matsumi, "CST Behaviors of Polymerized Ionic Liquids Induced by Metal Nano Particles", **Society of Polymer Science (SPSJ) SPSJ**, Nagoya, Japan, May 2018**.**
3. **Poster**: **Surabhi Gupta**, Noriyoshi Matsumi, "Thermo-sensitive chromic materials using thermosensitive polymer and ionic liquids", **JISMS-2018, JAIST**, Japan, March 2018**.**
4. **Poster**: **Surabhi Gupta**, Raman Vedarajan, Masaki Watanabe, Mamoru Ishikiriyama, Noriyoshi Matsumi, "Studies on Triggering Event of CST by Kamlet-

Taft Parameter Studies and Impedance Studies", **Society of Polymer Science (SPSJ) Fall,** Makuhari Messe, Tokyo, Japan, May 2017

5. **Oral**: **Surabhi Gupta,** Raman Vedarajan, Masaki Watanabe, Mamoru Ishikiriyama, Noriyoshi Matsumi, "Kamlet-Taft Parameter Studies and COSMO-RS Simulations for CST Behavior of Ionic Liquids", **Chemical Society of Japan (CSJ), Yokohama, Japan**, March 2017.
6. **Poster**: **Surabhi Gupta**, Raman Vedarajan and Noriyoshi Matsumi, "Electrochemical Impedance Spectroscopy (EIS) as a Diagnostic Tool to Evaluate LCST Behavior of Ionic Liquids" **Chemical Society of Japan (CSJ)**, University of Toyama, Toyama, Japan, November, 2014.
7. **Poster**: **Surabhi Gupta**, Raman Vedarajan and Noriyoshi Matsumi, "Electrochemical Impedance Spectroscopy (EIS) as a Diagnostic Tool to Evaluate LCST Behavior of Ionic Liquids" **Society of Polymer Science (SPSJ)** Fall, Polymer Preprints, Japan Vol.63, No.2 (2014), Nagasaki, Japan, September 2014.